IMPACT OF ENVIRONMENTAL CONDITIONS ON GEOCHEMICAL PROXIES IN TROPICAL MARINE CALCIFIERS

DISSERTATION

ZUR ERLANGUNG DES DOKTORGRADES DER NATURWISSENSCHAFTEN

(DR. RER. NAT.) AM FACHBEREICH GEOWISSENSCHAFTEN DER UNIVERSITÄT BREMEN

VORGELEGT VON

PETER MÜLLER

BREMEN, JANUAR 2017

The present work was conducted from January 2014 to January 2017 at the Leibniz Centre for Tropical Marine Research (ZMT), Bremen, Germany.

Member of the

Erstgutachterin: **Prof. Dr. Hildegard Westphal**; Leibniz-Zentrum für Marine Tropenforschung Bremen (ZMT) und Universität Bremen

Zweitgutachter: **Prof. Dr. Wolf-Christian Dullo**; Helmholtz-Zentrum for Ozeanforschung Kiel (Geomar) und Christian-Albrechts-Universität zu Kiel

„Wenn die Wissenschaft ihren Kreis durchlaufen hat, so gelangt sie natürlicher Weise zu dem Punkte eines bescheidenen Misstrauens, und sagt, unwillig über sich selbst: Wie viele Dinge gibt es doch, die ich nicht einsehe“.

Immanuel Kant (1724-1804)

I. AFFIRMATION / EIDESSTATTLICHE ERKLÄRUNG

Hiermit versichere ich, dass ich

1. die Arbeit ohne unerlaubte fremde Hilfe angefertigt habe
2. keine anderen als die von mir angegebenen Quellen und Hilfsmittel benutzt habe und
3. die den benutzten Werken wörtlich oder inhaltlich entnommenen Stellen als solche kenntlich gemacht habe.

Bremen, den 16. Januar 2017 _____

II. ABSTRACT

Skeletal structures of marine calcifying organisms have become an important archive of ancient environmental conditions. By the means of ontogenetic geochemical signatures (so-called "proxies"), in particular accretionary calcareous skeletal structures such as corals, bivalve shells or fish otoliths provide sub-seasonally resolved records of modern and ancient climate variability. However, complex physiological and environmental processes can complicate these geochemical signatures and a thorough understanding of these mechanisms is a prerequisite for reliable paleoenvironmental reconstructions. By focusing on proxy incorporation pattern in modern and archeological specimens this thesis aims to extend the applicability of geochemical proxies of calcareous skeletal structures for reliable paleoclimate reconstructions.

First, the influence of water temperature on oxygen isotopes, carbon isotopes as well as Mg/Ca ratios in modern echinoid spines (*Eucidaris galapagensis*) sampled across the natural water temperature gradient of the Galápagos archipelago was studied. Thereby, it was shown that in addition to water temperature, additional physiological or environmental variables affect the incorporation of in particular carbon isotopes and Mg/Ca ratios. Nevertheless, the significant correlation of oxygen isotopes measured in *E. galapagensis* spines and measured water temperatures throughout the Galápagos archipelago indicates their potential for paleoenvironmental reconstructions.

Secondly, this thesis provides new insights into the applicability of mathematical approaches for the conversion of ontogenetically distorted isotope records from fish otoliths and bivalve shells into sub-seasonally resolved time series. Using new simple but traceable linear interpolation approaches as well as more complex growth models from fisheries biology, ontogenetically distorted otolith and bivalve oxygen isotope records were successfully converted into time series and correlated against measured water temperatures. The resulting significant correlations indicate that ontogenetic oxygen isotope records of both skeletal structures represent reliable archives of (paleo-) environmental conditions.

Within a third study, the effect of pre-historic cooking methods on proxy signatures of aragonitic skeletal structures from archeological deposits has been tested using an experimental approach. The results show that all prehistoric cooking methods cause an alteration of the shell chemistry in aragonitic bivalves with regard to the most commonly used geochemical proxy systems even without a conversion of primary aragonite into secondary calcite. However, clumped isotope analysis showed that this proxy system represents a so-far unique

tool to detect and reconstruct certain pre-historic cooking methods and therefore help to avoid erroneous paleoclimate reconstructions from archeological deposits.

Finally, ontogenetic oxygen isotope records of archeological fish otoliths and bivalve shells were used to reconstruct mid- to late Holocene environmental conditions along the Banc d´Arguin, Mauritania, NW Africa. By showing unreasonably low oxygen isotopic compositions, these skeletal structures from a large paleo-estuary indicate consistently the persistence of isotopically lighter monsoon-related freshwater discharge into the coastal zones during the mid-Holocene. Given their deposition a few hundred years after the supposed abrupt aridification of NW Africa, the data questions the hypothesis of an abrupt termination of the African Humid Period.

Aside from showing the potential of geochemical proxies from echinoid spines for paleoenvironmental reconstructions, this thesis underlines the unique potential of ontogenetic oxygen isotope records of modern and archeological otoliths and bivalve shells for sub-seasonally resolved (paleo-) climate reconstructions if the samples are adequately preserved.

III. ZUSAMMENFASSUNG

Schalenstrukturen von kalzifizierenden marinen Organismen haben sich zu einem wichtigen Archiv vergangener Umweltbedingungen entwickelt. Durch ihre geochemischen Signaturen (sog. „Proxies“) beinhalten insbesondere schichtweise geformte karbonatische Skelettstrukturen wie Korallen, Muschelschalen oder Fischotolithe sub-saisonal aufgelöste Informationen bezüglich der Variabilität von Umweltbedingungen heutiger aber auch vergangenen Epochen. Komplexe Stoffwechselprozesse sowie verschiedener Umweltbedingungen können diese geochemischen Signaturen jedoch beeinflussen, so dass ein grundlegendes Verständnis dieser Mechanismen für die verlässliche Rekonstruktion von vergangener Umweltbedingungen unabdingbar ist. Durch die Untersuchung von Proxies in modernen sowie archäologischen Proben erweitert die hier vorgelegte Arbeit daher die Anwendbarkeit dieser geochemischen Signaturen für die verlässliche Rekonstruktion vergangener Umweltbedingungen.

Dazu wurde eine Untersuchung des Einflusses von Wassertemperatur auf Sauerstoffisotope, Kohlenstoffisotope sowie Mg/Ca-Verhältnisse in Seeigelstacheln (*Eucidaris galapagensis*) entlang des natürlichen Temperaturgradienten des Galapagos Archipels vorgenommen. Diese Untersuchung zeigt, dass neben der Wassertemperatur zusätzliche physiologische Mechanismen sowie Umweltfaktoren vor allem die Kohlenstoffisotopie sowie das Mg/Ca-Verhätnis der Stacheln beeinflussen. Die signifikante Korrelation zwischen der Sauerstoffisotopie der Stacheln sowie der gemessenen Wassertemperatur unterstreicht jedoch ihr Potential als mögliche Paläoumweltarchive.

Darüber hinaus enthält diese Arbeit neue Erkenntnisse bezüglich der Anwendbarkeit von verschiedenen mathematischen Modellen zur Umwandlung von ontogenetisch verzerrten Isotopensignaturen aus Fischotolithen und Muschelschalen in sub-saisonal aufgelöste Zeitreihen. Durch die Anwendung simpler jedoch nachvollziehbarer linearer Interpolationen sowie komplexeren Wachstumsmodellen aus der Fischereibiologie konnten ontogenetisch verzerrten Isotopendate eines Fischotolithen sowie einer Muschelschale erfolgreich in Zeitreihen überführt und mit gemessene Wassertemperatur-Daten verglichen werden. Die daraus resultierende signifikante Korrelation zwischen der Sauerstoffisotopie und der Wassertemperatur zeigt, dass beide Skelettstrukturen zur verlässlichen Rekonstruktion von (vergangenen) Umweltbedingungen genutzt werden können.

In einer weiteren Untersuchung wurde der Einfluss von prähistorischen Kochmethoden auf die chemische Zusammensetzung aragonitischer Skeletstrukturen aus archäologischen Proben getestet. Die Ergebnisse zeigen, dass alle getesteten Kochmethoden einen erheblichen Einfluss auf häufig genutzte Proxies innerhalb aragonitischer Muschelschalen haben. Gemessene „*Clumped-isotope*"-Daten weisen jedoch darauf hin, dass dieses Proxy-System die Erkennung sowie die Rekonstruktion prähistorischer Kochmethoden an Hand aragonitischer Schalen in archäologischen Ablagerungen ermöglicht und so helfen kann, fehlerhafte Paläoklimarekonstruktionen aus archäologischen Ablagerungen zu vermeiden.

Abschließend wurden ontogenetische Sauerstoffisotopen-Signaturen von archäologischen Fischotolithen und Muschelschalen genutzt um eine zeitlich hochauflösende Paläoumweltrekonstruktionen des Holozänen Klimawandels der Banc d´Arguin, Mauretanien, NW Afrika, vorzunehmen. Durch auffällig niedrige Sauerstoffisotopien deuten diese Skelettstrukturen aus ehemaligen Ästuar-Gebieten übereinstimmend auf den Abfluss von Monsun-Niederschlägen mit geringerer Sauerstoffisotopie hin. In Anbetracht der Ablagerung dieser Skelettstrukturen einige hundert Jahre nach der bisher angenommenen abrupten Verwüstung NW Afrika stellen diese Daten die bisherige Hypothese eines abrupten Ende der African Humid Period in Frage.

Neben dem Potenzial von Seeigelstacheln für die Rekonstruktion von Umweltbedingungen unterstreicht die hier vorgelegte Arbeit klar das einzigartige Potential von ontogenetischen Isotopen-Signaturen rezenter und archäologischer Fisch-Otolithe und Muschelschalen für sub-saisonal aufgelöste (Paläo-) Umweltrekonstruktionen, vorausgesetzt diese zeigen einen hinreichend guten Erhaltungszustand.

IV. ACKNOWLEDGMENTS

The present thesis would not have been possible without the long-standing support of many different people and organizations. First and most importantly, I want to thank my supervisor Hildegard Westphal for her encouraging supervision of my PhD-project. I am deeply grateful for her faith and willingness to let me follow my own ideas and her guidance along this exciting way.

Many thanks also go to the other members of my PhD-Panel including Simone Kasemann, Matthias Wolff, Henry C. Wu and Claire Reymond for advising me throughout my time as a PhD-candidate and Wolf-Christian Dullo for being part of my thesis committee.

I want to thank the Leibniz Centre for Tropical Marine Research for the funding for this PhD-project and for providing a stimulating interdisciplinary work environment which facilitates the development of new ideas. I thank the Bremen International Graduate School for Marine Sciences (GLOMAR) for valuable courses, guidance and financial support which considerably broadened my personal and scientific scope along this journey. I owe special thanks to Robert Vernet and Jean-Paul Barusseau for providing the archeological samples and for fascinating discussions and valuable contribution to the manuscript of this thesis. Integral parts of my PhD project would not have been possible without their contribution.

I am grateful for the possibility provided by ZMT and GLOMAR to spend three months in 2015 at the Rosenstiel School of Marine and Atmospheric Sciences at the University of Miami in the Stable Isotope Laboratory of Peter K. Swart. I owe thanks to the entire SIL-group consisting of Peter K. Swart, Sean T. Murray, Phillip T. Staudigel, Sevag Mehterian, Sharmilla Giri, Greta Mackenzie, Amel Saied and Chris Kaiser for all their support during my time at your lab. This time was certainly one of the most exhausting but at the same time most fascinating periods of my entire PhD-project.

I would also like to thank my colleagues at the Leibniz Centre for Tropical Marine Research (ZMT) who significantly contributed to the present thesis and in particular Jule Mawik, Dorothee Dasbach and Matthias Birkicht for their support in the labs.

Special thanks go to my co-authors Marc H. Taylor, Henry C. Wu, Julien Michel, André Klicpera, and Claire Reymond. Their support and patience allowed me making my first steps in a safe and professional environment. I owe special thanks to Marc H. Taylor for sharing his extensive knowledge about growth models and for always being open for

developing and applying new interdisciplinary approaches which considerably contributed to my PhD project.

I would also like to thank the entire *Geoecology and Carbonate Sedimentology* working group including Gita Roshni Narayan, Thomas Mann, André Wizemann, André Klicpera, Marleen Stuhr, Natalia Herrán and Sebastian Flotow as well as the Sea level and Coastal Changes group consisting of Alessio Rovere, Daniel Harris and Thomas Lorscheid for manifold support and exciting discussions. Thanks go also to all scientists and crew members of the RV Meteor cruise M129 to the shelf off Mauritania and Senegal in August 2016.

Special thanks go to my good friends Therese and Thomas. It was a pleasure to spend the last years with such exceptional people. I would also like to express my gratitude to Ingo Dressel for being such a good friend since we first met in Hannover. Special thanks go to my bandmates Thilo, Moritz, and Kai who were an integral and particularly loud part of my work-life balance. I would like to express my deepest gratitude to Gila for all the love and hope she gave me during this time. Finally, I would like to thank my family. This thesis would not have been possible without your encouraging and faithful support throughout the last years (and anything before that).

V. TABLE OF CONTENTS

I. Affirmation / Eidesstattliche Erklärung I

II. Abstract III

III. Zusammenfassung V

IV. Acknowledgments VII

V. Table of contents IX

VI. List of figures XIII

VII. List of tables XVI

VIII. Conference contributions XVII

IX. Overview of publications and manuscripts XXI

1. Introduction ..... - 1 -

1.1 Geochemical proxies in skeletal carbonates: Highest-resolution recorders of ancient environmental conditions ..... - 2 -

1.2 Oxygen isotopes in accretionary skeletal carbonates ..... - 3 -

1.3 Element/Calcium ratios in accretionary skeletal carbonates ..... - 6 -

1.4 Clumped isotope thermometry ..... - 8 -

2. Outline of the thesis ..... - 11 -

3. Study areas ..... - 13 -

3.1 The Galápagos archipelago ..... - 14 -

3.2 The Banc d´Arguin, Mauritania, NW Africa ..... - 17 -

4. Methods ..... - 27 -

4.1 Sample preparation and sub-sampling ..... - 27 -

4.2 Scanning electron microscopy ..... - 30 -

4.3 Aragonite/calcite analysis ..... - 30 -

4.4 Radiocarbon dating ..... - 31 -

4.5 Stable isotope analyses ..... - 31 -

4.6 Reconstruction of water temperatures based on skeletal $\delta^{18}O$ data ..... - 31 -

4.7 Clumped isotope analyses and water temperature reconstruction ..... - 32 -

4.8 Element/Calcium ratio analysis ..... - 33 -

4.9 Temporal alignment modeling ..... - 34 -

4.10 Statistical analyses ..... - 34 -

5. Paleoenvironmental proxies in echinoid spines (*Eucidaris galapagensis*, Döderlein 1887) along a natural water temperature gradient ..... - 35 -

Personal contribution to Chapter 5: ..... - 36 -
5.1 Abstract ..... - 37 -
5.2 Introduction ..... - 38 -
5.3 Material and methods ..... - 40 -
5.4 Results ..... - 43 -
5.2 Discussion ..... - 49 -
5.3 Conclusions ..... - 55 -
5.4 Acknowledgements ..... - 56 -
6. Food for thought: Mathematical approaches for the conversion of high-resolution sclerochronological oxygen isotope records into sub-annually resolved time series ..... - 57 -
Personal contribution to Chapter 6: ..... - 58 -
6.1 Abstract ..... - 59 -
6.2 Introduction ..... - 60 -
6.3 Material and Methods ..... - 62 -
6.4 Results ..... - 70 -
6.5 Discussion ..... - 75 -
6.6 Summary and conclusions ..... - 86 -
6.7 Acknowledgements ..... - 87 -
6.8 Supplemental material ..... - 88 -
7. Prehistoric cooking versus paleoclimate proxies in shell-midden constituents ..... - 89 -
Personal contribution to Chapter 7: ..... - 90 -
7.1 Abstract ..... - 91 -
7.2 Introduction ..... - 92 -
7.3 Results ..... - 94 -
7.4 Discussion ..... - 99 -
7.5 Material and methods ..... - 105 -
7.6 Acknowledgements ..... - 108 -
7.7 Supplemental Information ..... - 109 -
8. Otolith and bivalve oxygen isotope records of monsoon precipitation discharge during the mid- to late-Holocene of NW Africa ..... - 115 -
Personal contribution to Chapter 8: ..... - 116 -
8.1 Abstract ..... - 117 -
8.2 Introduction ..... - 118 -
8.3 Material and methods ..... - 119 -

8.4 Results and discussion ..... - 120 -
8.5 Conclusions ..... - 124 -
8.6 Acknowledgments ..... - 124 -
8.7 Supplemental material ..... - 125 -
9. Extended discussion ..... - 129 -
10. Conclusions and outlook ..... - 141 -
11. References ..... - 147 -

VI. LIST OF FIGURES

Figure 1-1: The temperature-dependent fractionation of oxygen isotopes between the precipitating fluid and carbonate minerals ..... -5-

Figure 3-1: Seasonal variability of environmental conditions on the Galápagos archipelago ..... -15-

Figure 3-2: Main ocean currents shaping the hydrology of the Galápagos archipelago with the dominating carbonate facies ..... -17-

Figure 3-3: Schematic illustration of seasonal variation in ocean currents and upwelling intensities along the Banc d'Arguin. ..... -18-

Figure 3-4: Seasonal variability of environmental conditions along on the Banc d`Arguin. ..... -19-

Figure 3-5: Sedimentary facies distribution, grain assemblages, and carbonate factories across the Banc d´Arguin with dominating surface currents (black arrows) and wind directions (white arrows). ..... -21-

Figure 3-6: Holocene paleoclimate records of N Africa ..... -23-

Figure 3-7: Occupation pattern along the Mauritanian and Senegalese coastline from ~22°N to 16°N throughout the mid- to late-Holocene ..... -25-

Figure 4-1: Schematic illustration of the individual sample preparation steps. ..... -28-

Figure 5-1: Map of the Galápagos Archipelago with the five bioregions Elizabeth, West, Central-Southeast, North and Far North changed after Edgar et al. (2004) with sampling sites grouped according to the corresponding bioregion ..... -43-

Figure 5-2: Meso- and microstructure of *Eucidaris galapagensis* spines ..... -45-

Figure 5-3: Measured proxy data from *Eucidaris galapagensis* spines ..... -47-

Figure 5-4: The 2D element map perpendicular to the spine growth axis showing a homogenous element distribution within the dense outer stereom as well as the inner stereom of the *Eucidaris galapagensis* spine ..... -49-

Figure 5-5: Comparison of measured $\delta^{18}O_{Calcite}$ values and modeled seasonal $\delta^{18}O_{Calcite}$ ranges along the natural water temperature gradient for single or combined impact of seasonally varying water temperature and $\delta^{18}O_{Seawater}$ values ..... -53-

Figure 6-1: The Banc d'Arguin in northern Mauritania ..... -63-

Figure 6-2: Exemplary parameterization of the linear interpolation approach using a theoretical annual water temperature cycle (top) and a corresponding theoretical bivalve shell $\delta^{18}O$ record with ontogenetically decreasing increment width (bottom) from Goodwin et al (2003) ....-66-

Figure 6-3: Gulland and Holt plot of annual ($\delta^{18}O$ -derived) *Carlarius heudelotii* otolith growth increment thickness ($\partial L/\partial t$) as a function of mean otolith size (L) and the soVBGF model (line) fitted to time-referenced distances between reconstructed water temperature values (points) for the *Carlarius heudelotii* otolith record ....-69-

Figure 6-4: Measured ontogenetic $\delta^{18}O$ records and reconstructed water temperatures of the *Carlarius heudelotii* otolith (A) and the *Venus crebrisulca* shell (B) ....-71-

Figure 6-5: Ontogenetic growth trajectories for the *Carlarius heudelotii* otolith based on the linear interpolation with winter growth cessations (LI-WGC model), linear interpolation with seasonal growth oscillation (LI-SGO model), seasonally oscillating Von Bertalanffy Growth Function (soVBGF model) as well as the temporal alignment using predicted $\delta^{18}O_{Otolith}$ values (SST/SSS model)....-76-

Figure 6-6: Theoretical seasonal water temperature curve following an idealized sinusoidal wave form and corresponding theoretical ($\delta^{18}O$-based) otolith water temperature records distorted by different ontogenetic and seasonal growth patterns....-79-

Figure 6-7: Theoretical seasonal water temperature curve and theoretical ($\delta^{18}O$ -based) otolith water temperature records of Fig. 6-6 but assuming a equidistant sampling of the otolith record with a sample spacing of 100 μm....-80-

Figure 6-8: Ontogenetic temperature anomaly from reconstructed average water temperature of the *Carlarius heudelotii* otolith and the *Venus crebrisulca* based on the soVBGF model ....-82-

Figure 6-S1: Idealized bivalve shell geometry based on a logarithmic spiral with the spatial relationship between relative distances of theoretical samples along the ventral margin and their distances relative to the umbo....-88-

Figure 7-1: Visual comparison of untreated left valves and the corresponding right valves exposed to the different treatments prior to hydrogen peroxide cleaning ..... -95-
Figure 7-2: Alteration of mineralogy and geochemical proxies in modern *Mercenaria campechiensis* shells by simulated prehistoric cooking methods ..... -96-
Figure 7-3: Clumped and oxygen isotopic composition with corresponding water temperature estimates of mid-Holocene fish otoliths and bivalve shells ..... -98-
Figure 7-4: Ontogenetic oxygen isotope records of three mid-Holocene *Senilia senilis* shells and comparison with modern coastal sea surface temperature (SST) variability of the eastern Banc d`Arguin (Lavaud et al., 2013) ..... -103-
Figure 7-S1: Map of the research area, Mauritania, NW Africa ..... -109-
Figure 8-1: Map of the research area, Mauritania, NW Africa ..... -119-
Figure 8-2: Boxplot of reconstructed modern, late- and mid-Holocene water temperatures using ontogenetic oxygen isotope records of modern and archeological catfish otoliths and bivalve shells ..... -121-
Figure 8-S1: Ontogenetic oxygen isotope records of all catfish otoliths analyzed in this study ..... -125-
Figure 8-S2: Ontogenetic oxygen isotope records of all *Senilia senilis* shells analyzed in this study. ..... -126-
Figure 9-1: Plot of Φ' values of different species groups (Mytilidae (top), Pectinidae (middle)), and species with similar shells shapes (oval shell form (bottom)) against mean annual water temperature (left) and geographic latitude (right) ..... -132-
Figure 9-2: Relationship between the different spatial components of bivalve shell growth ..... -134-
Figure 9-3: Comparison of $\delta^{18}O$-based and conventional growth pattern from literature and their environmental significance. ..... -137-
Figure 9-4: Variation of phi-prime (Φ' and Φ'') values along an environmental and latitudinal gradient. ..... -138-
Figure 11-1: Neolithic shell-midden deposits in the Rass el Sass and Iwik area (Banc d´Arguin, Mauritania) ..... -144-

VII. LIST OF TABLES

Table 5-1: Measured $\delta^{18}O_{Calcite}$, $\delta^{13}C_{Calcite}$, and Mg/Ca ratios from Eucidaris galapagensis spines sampled throughout the Galápagos archipelago.. .....-44-

Table 6-1: Temporal alignment parameters of the otolith and bivalve shell water temperature records using the linear interpolation approach .....-73-

Table 6-2: Temporal alignment parameters for the *Carlarius heudelotii* otolith and the *Venus crebrisulca* shell records using the seasonally oscillating Von Bertalanffy growth function (soVBGF) .....-74-

Table 7-S2: Mineralogy and proxy data of the cooking experiment. Each sample represents a single right valve of a *Mercenaria campechiensis* individual .....-110-

Table 7-S3: Results of the statistical analysis.....-111-

Table 7-S4: Results of the radiocarbon dating and calibration using OxCal 4.2.4.....-112-

Table 7-S5: Mineralogy and proxy raw data of the mid-Holocene samples.....-113-

Table 8-S3: Samples and data used in this study.....-127-

Table 9-1: Growth parameters calculated based on $\delta^{18}O$-signatures of modern and Holocene otoliths of the catfish species *Carlarius heudelotii* and *Carlarius parkii* as well as growth parameters for both species based on fish length from the literature (Conand et al., 1995) .....-135-

Table 9-2: Growth parameters calculated based on $\delta^{18}O$-signatures of modern and Holocene *Senilia senilis* shells (modern data from Lavaud et al., 2013) as well as conventional shell length-based growth parameters for the same species from different latitude from the literature .....-136-

VIII. CONFERENCE CONTRIBUTIONS

The conference contributions listed below were related to the work presented and discussed in the present thesis.

(1) **Peter Müller,** Matthias López Correa, André Klicpera, Robert Vernet, Philippe Tous, Hildegard Westphal (2014) **Oxygen isotope records of archaeological catfish otoliths: Evidences for seasonal monsoon discharge during the mid-Holocene NW Africa**. Geologische Vereinigung Jahrestagung (German Geological Society Annual Meeting); Frankfurt a. M.; Germany.

The Holocene climate change of NW Africa was characterized by a transition from humid conditions during the Early Holocene to the present desert state. However, it is still not clear whether this climate change was either an abrupt or a gradual transition. Sclerochronological approaches can provide important information on climate and oceanographic variability with a sub-seasonal resolution.

Here we present high resolution oxygen isotope data from recent and mid-Holocene catfish otoliths determined as *Arius heudelotii* (Valenciennes, 1840) or *Arius parkii* (Günther, 1864). Both species are associated with estuarine environments in coastal areas of the tropical eastern Atlantic. One recent otolith was removed from a fish caught in the northern part of the Banc d´Arguin (Mauritania). Mid-Holocene otoliths were recovered from a shell midden (~5300 yrs BP) in the central eastern part of the Banc d´Arguin, located at the mouth of an extensive paleo-estuary/wadi system which drained the Early- to mid-Holocene monsoonal precipitation pulses into the coastal area. High resolution otolith sub-sampling was carried out using a Micromill and samples were measured using a Delta V+ Mass- Spectrometer.

Oxygen isotope signatures of recent and Mid- Holocene otoliths show a clear seasonal pattern coinciding with visible annual growth increments. The calculated water temperatures of the recent otolith are in good agreement with remote-sensing derived sea surface temperature data. In contrast, mid-Holocene otoliths show higher year-round water temperatures compared to modern conditions (~4 to 10.5 °C). The oxygen isotope curve of the recent specimen suggests an discontinuation of otolith/fish growth during the cold season, whereas the mid-Holocene otolith signatures show a clear sinusoidal shape indicating a constant year-round otolith growth. Both aspects argue for warmer water temperatures on the Banc d´Arguin during the mid- Holocene.

Moreover, pronounced negative excursions in the oxygen isotope records of mid-Holocene otoliths indicate periods of pulsed monsoon freshwater discharge into the shallow coastal zone. Water temperatures of > 35 °C indicate a decrease of $\delta^{18}O_{Water}$ of about > 1 to 3 ‰ during the monsoon season when compared to modern water temperatures. Thus, monsoon freshwater runoff was still present after the major desiccation event around 5500 yrs BP.

(2) **Peter Müller**, Philip Staudigel, Sean T. Murray, Hildegard Westphal, Peter K. Swart (2016) **Clumped isotopes in shell midden sclerochronology: Prehistoric cooking versus climate signatures?** 5th International Clumped Isotope Workshop; St. Petersburg; FL; USA.

Incrementally banded calcareous components derived from prehistoric shell midden deposits like bivalve shells or fish otoliths provide high-resolution records of multiple paleoenvironmental proxies (e.g. $\delta^{18}O_{Carbonate}$ or element/Ca ratios). Thus, allowing the reconstruction of sub-seasonally resolved environmental conditions, such records became valuable tools to study ancient climate change. However, differing from other common marine paleoenvironmental proxy archives, shell middens were accumulated by the coastal populations, gathering local faunal resources for dietary purposes. Depending on the available technology and regional customs, the midden's constituents could have been exposed to prehistoric cooking prior to deposition. The alteration of such proxy records by prehistoric cooking has poorly been studied so far and is neglected in most paleoenvironmental reconstruction using shell midden constituents.

Here we present experimentally determined clumped isotope, conventional oxygen and carbon isotope as well as element/Calcium data measured in bivalve shells of the hard clam Mercenaria campechiensis exposed to different prehistoric cooking methods. Our data clearly show that pre-depositional heating (i.e. cooking) of aragonitic shells can lead to a considerable alteration of most paleoenvironmental proxies including their clumped isotope signature, even without an apparent reordering of the initial aragonite into secondary calcite. Thus, common methods for assessing the preservation of aragonitic skeletal components (e.g. x-ray diffraction analysis) might fail to detect their potential alteration due to the exposure to pre-depositional cooking methods. However, our data show that clumped isotope thermometry represents a suitable tool for the detection of such pre-depositional heating events and the potential subsequent alteration of paleoenvironmental proxy records. In addition, clumped isotope thermometry also allows the differentiation between certain prehistoric cooking methods and thus appears to be a suitable approach for tracing changes in ancient cooking practices as a consequence of technological advancement throughout human history using shell midden deposits.

(3) **Peter Müller**, Philip Staudigel, Sean T. Murray, Hildegard Westphal, Peter K. Swart (2016) **Impact of prehistoric cooking practices on paleoenvironmental proxies in shell midden constituents**. EGU General Assembly; Vienna; Austria.

Paleoenvironmental proxy records such as oxygen isotopes of calcareous skeletal structures like fish otoliths or mollusk shells provide highest-resolution information about environmental conditions experienced by the organism. Accumulations of such skeletal structures by ancient coastal populations in so called "shell midden" deposits provide us with sub-seasonally resolved paleoclimate records covering time spans up to several millennia. Given their high temporal resolution, these deposits are increasingly used for paleoclimate reconstructions and complement our understanding of ancient climate changes. However, gathered as comestibles, most of these skeletal remains were subject to prehistoric cooking methods prior to deposition. The associated alteration of the chemical proxy signatures as well as the subsequent error for paleoenvironmental reconstructions remained almost entirely neglected so far.

Here, we present clumped isotope, conventional oxygen and carbon isotopes as well as element:Ca ratios measured in modern bivalve shells after exposing them to different prehistoric cooking methods. Our data show that most cooking methods considerably alter commonly used paleoclimate proxy systems which can lead to substantial misinterpretations of ancient climate conditions. Since the magnitude of chemical alteration is not distinguishable from natural temperature variability in most coastal settings, the alteration of shell midden constituents by prehistoric cooking remains likely unnoticed in most cases. Thus, depending on the cooking method, pre-depositional heating might have introduced considerable errors into previous paleoclimate studies. However, our data also show that clumped isotope thermometry represents a suitable diagnostic tool to detect such pre-depositional cooking events and also allows differentiating between the most commonly applied prehistoric cooking methods.

This conference contribution was awarded with the EGU Early Career Scientists Travel Award 2016.

(4) **Peter Müller**, Philip Staudigel, Sean T. Murray, Hildegard Westphal, Peter K. Swart (2016) **Application of clumped isotopes in shell midden sclerochronology**. 4th International Sclerochronology Conference; Portland; ME; USA.

Geochemical analyses of calcareous skeletal structures such as fish otoliths or mollusk shells from archeological sites provide sub-seasonally resolved records of paleoenvironmental conditions. However, many prehistoric settlements were located in coastal or estuarine environments in which biotic or abiotic seawater conditions underwent large seasonal fluctuations (e.g. primary production or salinity/$\delta^{18}O_{Water}$) which complicates the straight forward interpretation of most paleoenvironmental proxies. Carbonate clumped isotope thermometry represents a promising analytical approach as it represents a direct measure of carbonate precipitation temperature independent from the isotopic composition of the ambient water. However, recent studies have shown that in particular aragonite is characterized by fast re-equilibration rates of ^{13}C-^{18}O bonds due to closed systems isotope exchange reactions. Thus, clumped isotope thermometry might be susceptible to short-term heating events such as prehistoric cooking.

To test this hypothesis, we measured the clumped isotopic composition of modern bivalve shells (*Mercenaria campechiensis*) which were experimentally exposed to different prehistoric cooking methods. Our data clearly show that prehistoric cooking causes a considerable alteration of clumped isotopes as a function of exposure time and cooking temperature. However, all cooking methods produced a characteristic clumped isotopic signature primarily dependent on the cooking temperature showing that clumped isotopes can be used to reconstruct prehistoric cooking methods in aragonitic shell midden constituents. This is of particular importance because our data also show that all cooking methods also caused a considerable alteration to other commonly used paleoenvironmental proxies even without any conversion of the initial aragonite into secondary calcite. Thus, clumped isotope thermometry represents a powerful tool to detect and reconstruct prehistoric cooking practices but should also be considered for assessing sample preservation to prevent misinterpretations of ancient climate conditions if samples were altered by prehistoric cooking methods prior to deposition.

The presentation was awarded with the Runner-Up Best Talk award.

(5) **Peter Müller**, Claire Reymond, Philipp Siegel, Hildegard Westphal (2016) **Stable isotopes and Mg/Ca ratios in echinoid spines and their potential as paleoenvironmental archives**. ECSA 56; Bremen; Germany

Geochemical proxies such as oxygen isotopes ($\delta^{18}O$) measured in marine calcareous skeletal structures provide valuable information about environmental conditions experienced during their formation. Thus, oxygen isotope analysis of e.g. foraminifera or corals has become a standard tool to reconstruct ancient oceanographic conditions. In this context, echinoderm skeletons and in particular echinoid spines have gained only limited attention due to so far unknown deviations from the expected equilibrium incorporation of oxygen and carbon isotopes.

In this study, we present oxygen and carbon isotopes, as well as Mg/Ca ratios measured in *Eucidaris galapagensis* (Döderlein, 1887) spines, which were sampled along a strong natural water temperature gradient within the Galápagos archipelago. Using remote sensing sea surface temperature data, we yielded a highly significant negative correlation between water temperature and spine $\delta^{18}O$ values. Our data shows a steeper temperature-$\delta^{18}O_{Carbonate}$ relationship than most other marine calcifiers, which is consistent with previous studies on echinoid skeletons. In contrast, carbon isotopes as well as Mg/Ca ratios are positively correlated with water temperature. This result contradicts the common hypothesis that respiration is driving the simultaneous depletion of oxygen and carbon isotopes. Instead, our data indicate additional processes affecting isotope fractionation in echinoid spines. Nevertheless, our data show that oxygen isotope analysis of *E. galapagensis* spines might provide sub-seasonally resolved water temperature information if spine growth is properly constrained. Since Eucidaris spines are frequently occurring in tropical and subtropical sedimentary record, they potentially represent a new high-resolution archive for reconstructing temporal and spatial environmental change where other commonly used "bio-archives" such as corals do not commonly occur.

IX. OVERVIEW OF PUBLICATIONS AND MANUSCRIPTS

The present cumulative dissertation consists of two manuscripts published in international peer-reviewed journals (Chapters 5 and 6), one submitted manuscript (Chapter 7) and one manuscript in preparation for submission (Chapter 8). These sections are framed by the *Introduction* (Chapter 1), *Outline of the thesis* (Chapter 2), *Study areas* (Chapter 3), *Methods* (Chapter 4), *Extended discussion* (Chapter 9), and a *Conclusions and outlook* chapter (Chapter 10). The personal contribution is identified on the backside of each respective cover page.

Chapter 5: **Müller, P.,** Reymond, C. E., Siegel, P., and Westphal, H., in press, Paleoenvironmental proxies in echinoid spines (*Eucidaris galapagensis*, Döderlein 1887) along a natural water temperature gradient: *Palaeogeography, Palaeoclimatology, Palaeoecology*.

Chapter 6: **Müller, P.,** Taylor, M. H., Klicpera, A., Wu, H. C., Michel, J., and Westphal, H., 2015, Food for thought: Mathematical approaches for the conversion of high-resolution sclerochronological oxygen isotope records into sub-seasonally resolved time series: *Palaeogeography, Palaeoclimatology, Palaeoecology*, Vol. 440, 763-776.

Chapter 7: **Müller, P.,** Staudigel, P. T., Murray, S. T., Vernet, R., Barusseau, J.-P., Westphal, H., Swart, P. K., (under revision) Prehistoric cooking versus paleoclimate proxies in shell-midden constituents. under revision for resubmission to *Nature Scientific Reports*.

Chapter 8: **Müller P.,** Wu, H. C., Barusseau, J.-P., Vernet, R., Westphal, H. (in prep.) Otolith and bivalve $\delta^{18}O$ records of monsoon precipitation discharge during the mid- to late-Holocene of NW Africa. in preparation for submission to *Geology*.

1. INTRODUCTION

The understanding of climate and oceanographic processes is essential for the reliable prediction of future climate change. This, however, requires profound knowledge of present and past climate variability to understand the underlying mechanisms. While existing instrumental records allow the reconstruction of climate variation for the past ~150 years, any information beyond this instrumental era relies on archeological or geological records.

Depending on the desired temporal resolution, various techniques and approaches have been developed in order to extract paleoclimate information from these records. If adequately preserved, long-term climate records can be derived from (usually marine) sedimentary successions, providing information about low-frequency climate variability throughout most of Earth's history. Depending upon regionally varying sediment accretion rates, the temporal resolution of sedimentary records varies greatly and is usually lower than centennial to millennia scales, in particular in deep sea environments (Sadler, 1981; Kemp and Sexton, 2014). Most sedimentary records dating back to the Mesozoic or Paleozoic show much lower temporal resolution as a result of variable sedimentation rates, hiatuses, or post-depositional diagenetic compaction of the strata, all of which complicate the straightforward reconstruction of short-term climate cycles as well as abrupt changes of the ancient climate (Sadler, 1981; Kemp and Sexton, 2014).

For the understanding of steering mechanisms of global climate cycles and in particular for understanding the interaction of stacked cycles such as Milankovitch cycles (eccentricity, obliquity, and precession), paleoclimate records with a higher temporal resolution are required. Continuous records such as sediment successions from depocenters with high sediment-accumulation rates (>mm/decade), ice-cores, speleothems, and tree-ring records can provide higher-resolution paleoclimate records which, however, in most cases do not extend beyond Cenozoic times (<~66 Ma) with sufficient resolution to disentangle multiple superimposed climate cycles. In addition, while ice core records are restricted to polar regions or high altitudes in lower latitudes and tree ring as well as speleothem records are restricted to the terrestrial realm, even exceptional sedimentary records barely exceed a temporal resolution of <100 years. Thus, even though being important for longer-term paleoclimate reconstructions, marine sediment successions usually do not allow for gaining paleoclimate information on a decadal, annual or even seasonal scale. In consequence, additional highest-

resolution (sub-annual) climate archives are required for studying paleoclimate variability including sub-seasonal climate features such as e.g. monsoon precipitation pattern.

1.1 Geochemical proxies in skeletal carbonates: Highest-resolution recorders of ancient environmental conditions

Accretionary formed skeletal structures of calcifying organism preserved within the geological record provide the unique opportunity to extract such highest-resolution (sub-annual) information and thereby broaden our knowledge about ancient climate variability. Similar to the layered growth pattern of trees, many marine calcifying organisms form accretionary skeletal structures with annual growth layers, so called growth increments (Pannella, 1971; Chauvaud et al., 1998; Goodwin et al., 2001; Schöne et al., 2005a; Holcomb et al., 2013; Schöne and Gillikin, 2013). Usually induced by seasonal variations of environmental conditions such as water temperature or food availability, these organisms form clearly confined increments varying in skeletal density or organic matrix content as a result of seasonally enhanced or reduced growth rates (Goodwin et al., 2003; Müller et al., 2015a, Chapter 6 of this thesis). In some cases, even daily or lunar/tidal cycles can be reconstructed by the means of micro-increment analysis of skeletal structures (Goodwin et al., 2001; Reynolds et al., 2007; Lavaud et al., 2013). Among others, the most prominent examples for such incrementally banded skeletal structures are corals, mollusk shells or fish otoliths which all consist of defined increments formed throughout ontogeny of the organisms/colony.

Similar to the approach used in dendrochronology, the relative thickness of growth increments but also their chemical composition provides information about the variability of environmental conditions throughout the lifetime of the organism (Goodwin et al., 2001; Schöne et al., 2003; Schöne et al., 2005b). The analysis of these annual increments in calcified skeletal structures is increasingly used for reconstructing ancient high-resolution climate variability and is usually referred to as the field of 'sclerochronology' (Knutson et al., 1972; Buddemeier et al., 1974; Schöne and Gillikin, 2013). Thereby, in particular long-living marine calcifiers such as corals or high-latitude mollusks such as the bivalve *Arctica islandica* (Linnaeus, 1767) can provide paleoclimate records covering several millennia (Schöne et al., 2005b; Giry et al., 2012).

Despite relative growth rate records based on increment thicknesses, so-called geochemical "proxies" which are incorporated into the shell material provide additional information from the analysis of such skeletal bio-archives. In general, a "proxy" is defined as a "direct or indirect descriptor of a desired (but unobservable) variable such as e.g. temperature, salinity or

nutrient concentrations" (Urey, 1947; Emiliani, 1955; Wefer et al., 1999). In other words, a particular proxy represents the chemical fingerprint of an environmental variable that can be measured throughout the ontogenetic growth record of a given calcareous skeletal structure.

Throughout the last decades, a variety of these physicochemical proxies have been calibrated by correlating measured proxy data obtained from modern calcareous skeletal structures against measured environmental conditions and later successfully applied in paleoclimate or paleoceanographic reconstructions (Kim and O'Neil, 1997; Thorrold et al., 1997; Kasemann et al., 2009; Anagnostou et al., 2012; Füllenbach et al., 2015; Poulain et al., 2015). However, the application of oxygen isotope thermometry on calcareous skeletal structures still represents the most commonly used proxy system for reconstructing water temperatures from biogenic carbonates.

1.2 Oxygen isotopes in accretionary skeletal carbonates

Almost 70 years ago, Urey et al. (1947) proposed the use of calcium carbonate-water isotope thermometry to infer information about precipitation temperature (i.e. water temperature) of marine carbonates. This groundbreaking work initiated the rapid establishment of a new field in marine paleoclimate and paleoceanographic research using oxygen isotopic ratios ($^{18}O/^{16}O$) for reconstructing ancient climate and oceanographic conditions. In general, the difference between the oxygen isotopic composition of seawater and an authigenic carbonate mineral is predominantly a function of water temperature if the carbonate minerals that are precipitated in equilibrium with the ambient seawater following the equation

$$\alpha_{A-B} = \frac{R_A}{R_B} \quad \text{(Eq. 1.1)}$$

where α represents the fractionation factor between the carbonate mineral (A) and the seawater (B) and R their isotopic ratio ($^{18}O/^{16}O$). By convention, the isotopic ratio is reported in the delta (δ) notation which is defined as

$$\delta\ (‰) = 1000\left(\frac{R_x - R_{std}}{R_{std}}\right) = 1000\left(\frac{R_x}{R_{std}} - 1\right) \quad \text{(Eq. 1.2)}$$

where R_x and R_{std} represents the isotopic ratio of the carbonate and the standard, respectively and ‰ is parts per million. Thus, the oxygen isotopic ratio of a given carbonate is expressed as

$$\delta^{18}O\ (‰) = 1000\left(\frac{(^{18}O/^{16}O)_x - (^{18}O/^{16}O)_{std}}{(^{18}O/^{16}O)_{std}}\right) = 1000\left(\frac{(^{18}O/^{16}O)_x}{(^{18}O/^{16}O)_{std}} - 1\right) \quad \text{(Eq. 1.3)}$$

Traditionally, the standards for oxygen isotope data are the *Standard Mean Ocean Water* (SMOW) and *Pee Dee Belemnite* (PDB). SMOW is a water standard with the approximated average isotopic composition of the global seawater whereas PDB is a reference carbonate material derived from the Cretaceous *Pee Dee* formation (South Carolina, USA). However, due to shortage of the original reference material, these standards have been replaced by the new standards called VSMOW (*Vienna Standard Mean Ocean Water*), which is isotopically indistinguishable from its precursor SMOW, and the carbonate standard NBS-19/NBS-20 that is distributed by the International Atomic Energy Agency (IAEA) in Vienna, Austria.

As mentioned above, the fractionation between the seawater isotopic composition and the precipitated mineral is predominantly a function of carbonate formation temperature. In theory, this allows the straightforward reconstruction of ancient water temperatures by analyzing the isotopic composition of carbonate minerals from the geological record. However, minor deviations from the expected fractionation factor of oxygen isotopes occur among and within different calcifying taxa, usually referred to as *kinetic* or *vital effects* (McConnaughey, 1989a; McConnaughey, 1989b). To account for these minor deviations, individual species-specific calibrations of the oxygen isotope thermometer have been developed by correlating the isotopic composition of calcified structures ($\delta^{18}O_{Carbonate}$) grown at a known isotopic ratio of the seawater ($\delta^{18}O_{Seawater}$) against its formation temperature (for an overview see e.g. Grossman, 2012 and reference therein). By doing so, various paleotemperature equations have been developed for a wide range of calcifying organisms. As an example, the equation of Grossman and Ku (1986), defined as

$$T\,[°C] = 21.8 - 4.69(\delta^{18}O_{Aragonite} - (\delta^{18}O_{Seawater} - 0.027)) \qquad \text{(Eq.1.4)}$$

was developed using aragonitic foraminiferal, gastropod, and scaphopod skeletal material. Another example is the equation of Thorrold et al. (1997) who found the $\delta^{18}O$-temperature relationship of marine fish otoliths to follow:

$$1000\,ln(\alpha) = 18.56(10^3 \cdot T^{-1}[K]) - 32.54 \qquad \text{(Eq. 1.5)}$$

These two equations represent the most important equations in the context of this thesis as they provide robust water temperature estimates for the studied skeletal structure. As shown in Fig. 1.1, most calcifying organisms form their shell in, or close to the thermodynamic equilibrium with the ambient seawater. Therefore, if minor, and usually taxon-specific deviations from the expected thermodynamic equilibrium of ~0-3 ‰ are taken into account,

the oxygen isotopic composition of calcareous skeletal components provides reliable paleoclimate information.

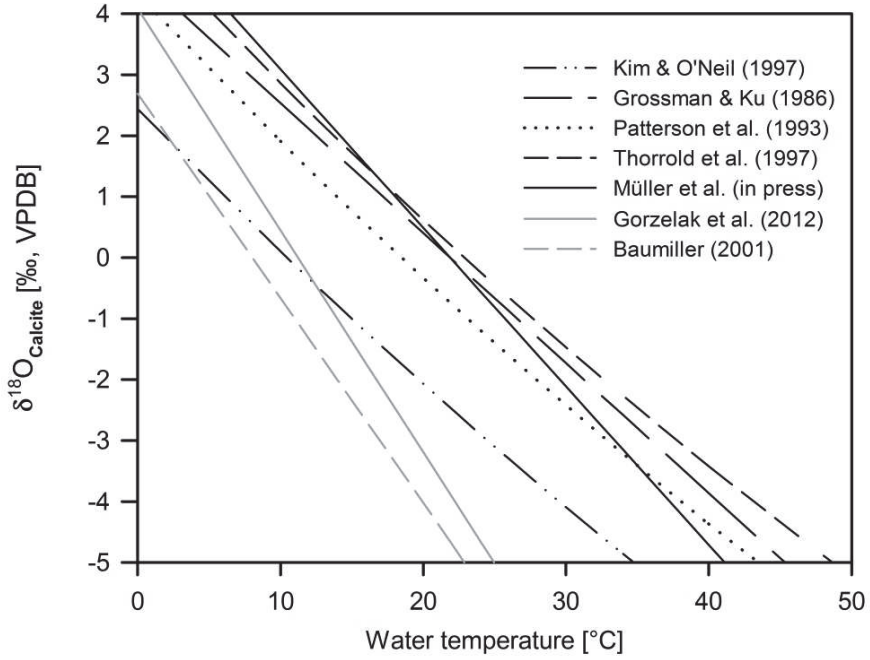

Figure 1-1: The temperature-dependent fractionation of oxygen isotopes between the precipitating fluid and carbonate minerals. The compilation encompasses abiotic calcite (Kim and O'Neil, 1997) and various calcifying marine organisms including aragonitic foraminifera, gastropods and scaphopods (Grossman and Ku, 1986), aragonitic freshwater-associated fish otoliths (Patterson et al., 1993), aragonitic marine fish otoliths (Thorrold et al., 1997), and different calcitic echinoderm tests (Baumiller, 2001; Gorzelak et al., 2012; Müller et al., in press, Chapter 5 of this thesis) calculated assuming a constant $\delta^{18}O_{Seawater}$ of 0.29 ‰ VSMOW. Modified after Müller et al. (in press, Chapter 5 of this thesis).

In practice, however, various uncertainties are encountered when applying oxygen isotope thermometry on marine carbonates (Savin, 1982). Among others, the above mentioned disequilibrium precipitation of biogenic carbonates, the non-constant isotopic composition of global seawater in space and through time, variable ecological and metabolic influences as well as the preservation and diagenetic alteration of carbonates within the geological record represent the main limiting factors for the application of oxygen isotope thermometry on marine carbonates, in particular for deep-time geological units (Urey, 1947; Grossman, 2012). In order to overcome these uncertainties, alternative geochemical proxy systems have been tested in numerous studies. The combination of different proxy systems significantly broadens the information gained from fossil carbonate material. With a so-called *multi-proxy* approach, provided that reliable paleo-water temperature estimates can be deduced from an alternative

proxy system, the oxygen isotopic composition of a carbonate skeletal component can be used to approximate the isotopic composition of the seawater the calcified structure was formed in. Given the usually linear relationship between $\delta^{18}O_{Seawater}$ and seawater salinity, now the paleo-salinity can be estimated based on the oxygen isotopic composition of the calcified structure.

1.3 Element/Calcium ratios in accretionary skeletal carbonates

Previous studies successfully tested and applied paleo-environmental reconstructions using element/Ca ratios measured in calcareous tests of marine organism. Among various calcifying taxa, foraminifera showed one of the most promising relationships between Mg/Ca ratios and ambient water temperature that is predominantly depending on the preferential incorporation of Mg^{+}-ions as impurities in the crystal lattice in particular at higher temperature (Elderfield et al., 2006; Freitas et al., 2006; Yu and Elderfield, 2008). Similar to foraminifera, also the element/Ca ratios of coral skeletons are thought to provide robust information about environmental conditions experienced throughout their growth period. While Mg/Ca ratios in coral skeletons are linked to the general seasonal cyclicity of environmental conditions and have been shown to provide ambiguous information regarding absolute water temperatures (Mitsuguchi et al., 2003; Inoue et al., 2007; Chen et al., 2015), the Sr/Ca ratio is by far the most widely used proxy for paleo-temperature data from coral skeletons (Beck et al., 1992; de Villiers et al., 1995; Inoue et al., 2007; Chen et al., 2015). It is, however, not uniformly applicable among various coral species (Wei et al., 2000). In consequence, if thoroughly proven by calibration studies, these organisms allow the application of such a multi-proxy approach by determining simultaneously their skeletal oxygen isotopic composition and particular element/Ca ratios throughout their growth records. Given the long residence time of Mg in the global oceans, water temperature estimates from foraminiferal Mg/Ca ratios are mostly independent from long-term variation seawater Mg/Ca ratio over geological time scales (Lear et al., 2002) and therefore advantageous compared to water temperature approximations using oxygen isotope thermometry.

While skeletal Mg/Ca and Sr/Ca can be used as independent paleo-water temperature proxies for some marine calcifying organisms such as foraminifera or corals, other calcifying organisms show a more complex incorporation pattern of these elements. In many organisms, the relationship between elemental ratios within the skeletal structure and ambient environmental

conditions usually appears to be more complex, potentially influenced by a wide range of biotic or abiotic factors.

Given the advantages of an alternative water temperature proxy mentioned above, numerous studies investigated element/Ca ratios in bivalve shells to test their potential as reliable paleoenvironmental proxy system. These studies usually focus on elements with similar ionic radii as Ca (e.g. Mg, Sr, Ba, Li or K) as they are preferentially substituted for Ca during the shell formation. For Mg/Ca ratios, some studies found statistically significant relationships between environmental conditions and shell chemistry like e.g. temperature-Mg/Ca relationships (Lazareth et al., 2003; Freitas et al., 2005), whereas other studies found conflicting results regarding the influence of environmental conditions on the incorporation of Mg-ions into bivalve shells (Putten et al., 2000; Freitas et al., 2006). Likewise, some studies showed a significant relationship between bivalve shell Sr/Ca ratios and growth rates (Freitas et al., 2005; Lorrain et al., 2005) while other found a positive correlation between Sr/Ca ratios and water temperature (Freitas et al., 2006) or even no correlation with environmental conditions (Klein et al., 1996; Putten et al., 2000; Lazareth et al., 2003). For Ba/Ca ratios, most studies showed either a direct correlation with seawater Ba concentration (Gillikin et al., 2006) or with primary production (Putten et al., 2000; Lazareth et al., 2003; Lavaud et al., 2013), indicating the potential use of Ba/Ca ratios for paleo-productivity reconstructions. However, even under controlled laboratory conditions, most of the above mentioned studies did not find correlation coefficients exceeding values of >0.6. These results consistently indicate that the incorporation of certain elements into mollusk shells is complex and relies upon various interacting biological and environmental mechanisms.

Based on the persistent problems in reliably linking measured element/Ca ratios of bivalve shells with environmental conditions, rather unconventional element/element ratios are increasingly investigated as potential paleoenvironmental proxies. In this context e.g. Füllenbach et al. (2015) found a significant correlation between shell Sr/Li ratios and water temperature for the marine bivalve *Cerastoderma edule*, indicating the potential of normalized element/element ratios as potential environmental proxy. However, further studies are needed to verify these initial results before reliable paleoclimate information can be obtained from these new proxy systems.

Similar to bivalve shells, fish otoliths show a complex relationship between their chemical composition and environmental conditions (Campana, 1999). Various previous studies showed consistently that the oxygen isotopic composition of fish otoliths is mainly depending

on ambient water temperature and isotopic composition of the seawater (Kalish, 1991; Patterson et al., 1993; Thorrold et al., 1997; Høie et al., 2003). Therefore, equilibrium precipitation with regard to oxygen isotopes allows the reconstruction of water temperatures experienced by individuals based on their ontogenetic isotope record. However, although generally in agreement with other calcifying organisms, previous studies also showed that vital effects need to be taken into account for the reconstruction of absolute water temperature records based on otolith $\delta^{18}O$ records (e.g. Patterson et al., 1993; Thorrold et al., 1997). The potential migration of fish throughout different water masses can complicate the environmental signal within their ontogenetic oxygen isotopic composition, in particular for pelagic fish species (Campana, 1999). However, otoliths from freshwater associated fish species such as catfish can be used to reconstruct freshwater runoff signals (Surge and Walker, 2005).

In contrast to oxygen isotopes, most previous studies showed conflicting results regarding the effect of environmental conditions on element/Ca ratios in fish otoliths (Campana, 1999). While some studies showed a significant effect of e.g. water temperature on Sr/Ca ratios (Bath et al., 2000; Martin and Wuenschel, 2006), other did not find a clear response of otolith Sr/Ca ratios to environmental variables (Elsdon and Gillanders, 2004; de Vries et al., 2005). However, the same studies also showed that the Sr concentrations of the water significantly influenced otolith Ba/Ca ratios. In contrast, other studies found Ba/Ca ratios to be mainly influenced by the Ba concentration of the water (Bath et al., 2000) or seawater salinity (Martin and Wuenschel, 2006). In consequence, while the analysis of oxygen isotopes is a widely accepted tool for reconstructing migration pattern or (ancient) environmental conditions using ontogenetic growth records of (fossil) fish otolith, the applicability of element/Ca ratios of fish otoliths is a matter of controversial debate. Usually, sophisticated statistical tests are required to distinguish different fish stocks or migration pattern based on their element/Ca signature, so far impeding sound interpretations for reliable paleoenvironmental reconstructions.

1.4 Clumped isotope thermometry

Alternative to the oxygen isotopic composition and element/Ca ratios, a new promising proxy system called *clumped isotope thermometry* has recently been developed (Ghosh et al., 2006; Schauble et al., 2006; Eiler, 2007). Conventional oxygen isotope thermometry is based on the temperature-dependent incorporation of one rare oxygen isotope (^{18}O) into the carbonate molecules, a so-called singly-substituted isotopologue. Traditionally, the $^{18}O/^{16}O$ratio of a given carbonate molecule is measured by analyzing CO_2 with a molecular mass of 44 ($^{12}C^{16}O_2$)

against mass 46 ($^{12}C^{16}O^{18}O$) derived from the carbonate molecule via acid digestion. Likewise, the carbon isotopic composition of a carbonate is determined by analyzing the relative abundances of CO_2 with a molecular mass of 44 ($^{12}C^{16}O_2$) against CO_2 with a molecular mass of 45 CO_2 ($^{13}C^{16}O_2$). These three non- or singly-substituted isotopologues with molecular masses of 44, 45 and 46 are by far the most abundant isotopologues accounting for 98.4, 1.11, and 0.4 %, respectively, which sums up to ~99.9 % of the total CO_2 (Eiler, 2007). Therefore, the remaining isotopologues containing more than one rare isotope such as mass 47 (mostly $^{13}C^{18}O^{16}O$), 48 (mostly $^{12}C^{18}O_2$), or 49 ($^{13}C^{18}O_2$) are usually neglected for conventional oxygen or carbon isotope analysis.

Based on principles of quantum mechanics and statistical thermodynamics, multiply-substituted isotopologues (e.g. mass 47, 48 and 49) have lower free energies compared to their singly-substituted equivalents (mass 44, 45, 46) as a result of lower vibrational frequencies and subsequently lower vibrational energy (Eiler, 2007; Dennis et al., 2011). Therefore, multiply-substituted isotopologues are more stable than singly-substituted isotopologues and the deviation between the abundances of multiply-substituted isotopologues in a carbonate molecule and their expected abundances if isotopologues were randomly distributed (the 'stochastic' distribution) is a function of formation temperature ('clumping' of isotopes). This deviation in abundances of multiply substituted-isotopologues from their expected ones is expressed as the Δ-value which is independent of the initial isotopic composition of the precipitation fluid (Eiler, 2007; Huntington et al., 2009; Affek, 2012). Given this strictly temperature-dependent equilibrium within a single phase, this approach theoretically allows the direct reconstruction of carbonate formation temperature (i.e. paleo-water temperatures) using carbonates from the geological record without the need to constrain any (in fact unknown) isotopic composition of ancient seawater (Eiler, 2007).

Similar to other proxy systems, however, previous studies showed that minor deviations from the expected thermodynamic behavior of clumped isotopes occur among different calcifying organisms (Ghosh et al., 2006; Ghosh et al., 2007; Grauel, 2012; Henkes et al., 2013). Despite these apparent vital effects, clumped isotopic signatures of carbonates from the geological record can be re-equilibrated over geological time-scales by solid state diffusion within the crystal lattice, requiring no isotope exchange with the ambient media (i.e. fluids or minerals) (Dennis and Schrag, 2010; Passey and Henkes, 2012; Stolper and Eiler, 2015). While this also allows reconstructing burial histories of carbonate rocks using clumped isotope thermometry, the post-depositional thermal overprinting of the initial clumped isotopic

signature prohibits any reliable water temperature estimation from such geological units (Passey and Henkes, 2012). While the re-ordering of ^{13}C-^{18}O bonds of calcitic carbonates occurs over geological time-scales, aragonitic carbonates might be much more susceptible to clumped isotope reordering involving lower minimum temperatures as well as much higher reordering-rates (Piasecki, 2015; Stolper and Eiler, 2015; Staudigel and Swart, 2016).

The high analytical complexity, the large sample volume required for clumped isotope analysis compared to conventional stable isotope analyses (12-24 mg versus ~50-70 μg carbonate, respectively) (Wacker et al., 2013), analytical uncertainties (and subsequent uncertainties of water temperature estimates of $\sim \pm 2$ °C), and the still small number of species-specific calibration studies still limits the application of clumped isotope thermometry for paleoclimate reconstructions (Affek, 2012). However, considering the steadily increasing analytical precision using progressively decreasing sample volumes and automated sample processing lines (Schmid and Bernasconi, 2010; Petersen and Schrag, 2014), clumped isotope thermometry will most likely become a standard application in paleoenvironmental reconstructions using skeletal carbonates in the future. By providing information about carbonate formation temperature and the simultaneous measurement of conventional oxygen isotopic composition from the same sample, clumped isotope thermometry has the potential to solve the long-standing problem of ancient water chemistry and open the multi-proxy approach also for other calcifying organisms such as mollusk shells or fish otoliths (Ghosh et al., 2007; Henkes et al., 2013).

2. OUTLINE OF THE THESIS

As outlined in Chapter 1, accretionary skeletal carbonates such as fish otoliths or bivalve shells can provide highest-resolution (sub-seasonal) information about environmental conditions experienced by the organisms by the means of ontogenetic proxy records. However, deviations from the expected equilibrium incorporation of elemental or isotopic signatures in many taxa of calcifying organisms are still limiting their straightforward application for paleoenvironmental applications. Furthermore, ontogenetic or seasonal variations of growth (i.e. accretion) rates distort these successive ontogenetic proxy records and thereby complicate their comparability with measured environmental time series.

In the scope of this thesis, oxygen isotopes and element/Ca ratios were studied in different calcifying organisms from tropical regions in order to understand the impact of physiological processes and environmental conditions on proxy incorporation pattern and thereby enhance their applicability for reliable paleoenvironmental reconstructions. The thesis is sub-divided into discrete chapters some of which have been published in international peer-reviewed journals. Thereby, this thesis encompasses many aspects which need to be accounted before proxy data can be used for reliable paleoclimate reconstructions:

Chapter 5 represents a calibration study focusing on oxygen isotopes, carbon isotopes, and Mg/Ca ratios in echinoid spines from the Galápagos archipelago. For this, central segments of sediment-derived spines of the sea-urchin species *Eucidaris galapagensis* were analyzed and the geochemical data ($\delta^{18}O$, $\delta^{13}C$ and Mg/Ca) were correlated against remote-sensing sea surface temperature data that show a clear spatial gradient across the Galápagos archipelago. To test for the potential influence of variation in $\delta^{18}O_{Seawater}$, we modelled the potential contribution of seasonal water temperature variability, seasonal $\delta^{18}O_{Seawater}$ variation and both factors combined.

In **Chapter 6**, new mathematical approaches for the conversion of ontogenetically distorted proxy records into sub-seasonally resolved water temperature time-series are presented. Ontogenetic oxygen isotope records of a modern catfish otolith (*Carlarius heudelotii*) and a modern venerid bivalve shell (*Venus crebrisulca*) were used to demonstrate these methods.

Chapter 7 is an experimental study exploring the potential impact of prehistoric cooking on paleoenvironmental proxies in bivalve shells. By exposing modern bivalve shells to a variety of prehistoric cooking methods, we tested the impact prehistoric cooking practices on oxygen

isotopes, carbon isotopes as well as their clumped isotopic composition. As clumped isotopes can be re-equilibrated by external heating, this might represent a unique tool to detect such heating events if re-ordering rates of ^{13}C-^{18}O-bonds in aragonite are sufficiently high. This potentially allows avoiding erroneous paleoclimate reconstructions if oxygen isotopes are also affected by prehistoric cooking.

In Chapter 8, oxygen isotope thermometry was applied on archeological fish otoliths and bivalve shells from NW Africa to reconstruct local paleoenvironmental conditions during the mid- to late-Holocene. By using sub-seasonally resolved oxygen isotope data from freshwater associated bivalve and fish species, the potential persistence of monsoon freshwater runoff after the supposed aridification event around 5.5 ka BP (deMenocal et al., 2000a) was tested. Thereby, our data might allow to bridge contradictory terrestrial and marine paleoclimate records.

These chapters are followed by the extended discussion (Chapter 9) using yet unpublished data from the aforementioned studies and a recapitulatory chapter summing up the main results of this thesis and highlighting potential future research lines (Chapter 10).

To enhance clarity, the list of all references for the individual chapters are provided at the end of this thesis (page 147).

3. STUDY AREAS

This thesis focuses on the effect of environmental conditions on the incorporation of geochemical proxies into calcareous skeletal structures. For this, samples from the Banc d´Arguin, Mauritania, located in the eastern tropical Atlantic, and the Galápagos archipelago, located in the eastern tropical Pacific were studied. Located in the tropical belt, both areas represent very particular environments as they are both influenced by upwelling of nutrient-rich water masses. These elevated nutrient concentrations along the Banc d`Arguin as well as on the Galápagos archipelago shift the trophic state of both environments towards mesotrophic or even eutrophic conditions and promote high primary production.

The high primary production also controls the abundance and distribution of benthic carbonate producers within both areas. In contrast to most oligotrophic photozoan carbonate factories like e.g. tropical coral reefs, both upwelling systems are dominated by heterotrophic carbonate producers like mollusks, barnacles or bryozoans dominating their carbonate factories (Michel et al., 2011; Klicpera et al., 2015). However, while eutrophic conditions prevail in the main upwelling areas, both areas show a latitudinal transition towards meso- (and oligotrophic) conditions, resulting in distinct facies zonations (Edgar et al., 2004; Klicpera et al., 2015; Reymond et al., 2015).

The Galápagos archipelago shows strong spatial and temporal variations (e.g. seasonal) of upwelling intensity (Houvenaghel, 1978). While the seasonal upwelling is strongest within the south-western area, the northern area is characterized by year-round meso- to oligotrophic conditions. The resulting strong natural gradient in terms of environmental conditions makes this region an ideal study site for *in-situ* analysis regarding the effect of environmental conditions on proxy incorporation in marine skeletal carbonates.

The Banc d`Arguin shows eutrophic conditions in particular in the northern areas with decreasing nutrient concentrations and primary production towards the southern parts. The resulting dominance of heterotrophic carbonates together with the strong seasonal variability of environmental conditions makes this environment a suitable environment for studying the reliability of geochemical proxies in heterotrophic carbonates for (paleo-) environmental conditions. This is of particular importance since the persistence of upwelling along the Banc d`Arguin throughout Holocene times is thought to have promoted the settlement of coastal populations since ~6500 years who extensively exploited marine resources of the adjacent

coastal areas (Barusseau et al., 2007; Barusseau et al., 2010). In consequence, numerous archeological sites all along the Mauritanian coast provide extensive records of calcareous skeletal structures (i.e. fish otoliths and mollusk shells) collected in the coastal environment throughout the Holocene. Once calibrated using their modern analogs, proxy records of these skeletal structures such as oxygen isotopes can provide important information regarding ancient environmental conditions and the climate evolution of NW Africa throughout the Holocene.

3.1 The Galápagos archipelago

3.1.1 Climate and oceanographic conditions

The Galápagos archipelago is located in the Eastern Tropical Pacific in the confluence zone of five major ocean currents causing a high seasonal as well as spatial variability of environmental conditions throughout the archipelago (Houvenaghel, 1978; Eden and Timmermann, 2004). These currents are the eastward flowing Equatorial Under Current (EUC) also known as Cromwell Current (CrC), the westward flowing Equatorial Current (EC), the southwestward flowing Panama Current (PC) as well as the Humboldt Current (HC) that is subdivided into the Peruvian Coastal Current (PCC) and the Peruvian Oceanic Current (POC) (Houvenaghel, 1978; Liu et al., 2014).

During the dry season from June to December, the south-western part of the archipelago is dominated by cold water masses due to topographical upwelling of the eastwards flowing EUC (Houvenaghel, 1978; Eden and Timmermann, 2004; Liu et al., 2014) (see Fig. 3-1). The large seasonal variability results in a strong temperature contrast between the upwelling season (June-December) and the non-upwelling season (January-May) especially along the western side of the largest island *Isabela* and enhanced primary production is promoted by the upwelling of nutrient-rich waters of the EUC. Within the central-eastern part of the archipelago, the cool (~18–~25 °C) and nutrient-rich waters of the EUC mix with warm (~24–~28 °C) and nutrient-poor surface waters of the north/north-east, predominantly supplied by the EC (see Fig. 3-1 and 3-2). The northern area is generally characterized by more stable environmental conditions throughout the year and shows only very limited influence of the upwelling waters (Chavez and Brusca, 1991). The salinity is rather constant throughout the Galápagos archipelago, varying from 33.5 to 35 along a 2°S to1°N transect (Sakamoto et al., 1998). Similar to the small salinity contrast, also the spatial and temporal variability of the seawater oxygen isotopic composition across the Galápagos archipelago is

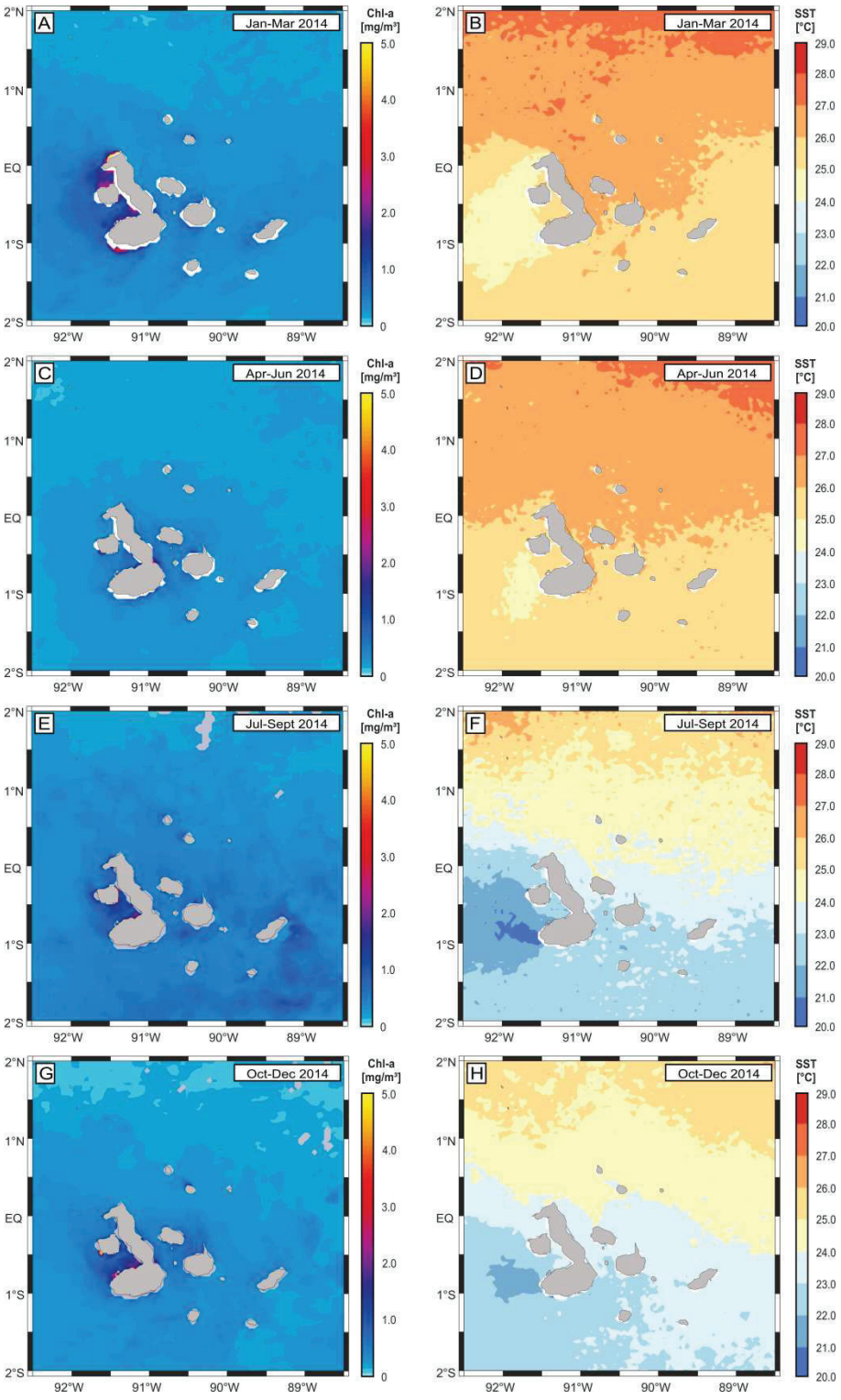

Figure 3-1: Seasonal variability of environmental conditions on the Galápagos archipelago. Quarterly chlorophyll a concentration (A,C,E,G) and sea surface temperatures (B, D, F, H) for the year 2014. Data compiled from NASA Giovanni (MODIS aqua).

small with values ranging from 0.05 to 0.5 ‰ (VSMOW) with an average value of 0.29 ‰ (VSMOW) (Wellington et al., 1996). In consequence, climate reconstructions using oxygen isotopes in coral skeletons showed only a very minor impact of spatially varying $\delta^{18}O_{Seawater}$ values across the Galápagos archipelago that, however, should be considered for sound (paleo-) climate studies using geochemical proxy signatures of calcareous skeletal structures from this region.

Monthly precipitation rates on the Galápagos archipelago vary between almost 0 during the dry season (Jun-Dec) and ~100 mm/month during the wet season (Jan-May), leading to negligible freshwater runoff rates into the coastal zones.

3.1.2 The carbonate factories of the Galápagos archipelago

The transition from the upwelling-dominated southwestern area towards the warmer and more stable northern area generates strong gradients of water temperature, nutrient concentration, and CO_2 concentrations. Due to the effect of these gradients on the marine ecosystems, the Galápagos archipelago has been divided into five main bioregions (named *West, Elizabeth, Central-southeast, North* and the *Far North*) with characteristic water temperatures, nutrient concentrations and CO_2 concentrations (Edgar et al., 2004). The carbonate contents and biogenic components in the sediments reflect this and show a distinct pattern of heterozoan and photozoan carbonate facies along this environmental gradient (Reymond et al., 2015).

While the southern upwelling-dominated area is characterized by a high abundance of filter feeding organisms such as barnacles, the northern area shows a higher abundance of phototrophic calcifiers like e.g. corals, see Fig. 3-1 (Reymond et al., 2015; Humphreys et al., 2016). Grouped into facies types, the southwestern upwelling region shows typical rhodomol and barnamol facies that are typical for highly productive upwelling regions. The eastern parts of the archipelago are characterized by a transitional heterozoan-rhodomol and barnamol facies, consisting predominantly of barnacles and gastropods. In contrast, the northern and far northern bioregion show a barnamol facies type with a considerably higher abundance of phototropic calcifiers such as corals (58 %, 'barnamolcor' *sensu* Reymond et al. (2015)) (Reymond et al., 2015; Humphreys et al., 2016).

Superimposed on local seasonal variation of environmental conditions, the El Niño Southern Oscillation (ENSO) is shaping the benthic carbonate communities across the Galápagos archipelago (Glynn, 1997). Periodically occurring El Niño events cause mortality events of

coral communities of up to >95 % (Glynn, 1997). In contrast, calcifying organisms which are more tolerant to large water temperature variations such as coralline red algae or barnacles are less diminished by El Niño events and subsequently form reef-like accumulations throughout the Galápagos archipelago and therefore dominate the benthic carbonate communities (Fig. 3-2) (Glynn and Wellington, 1983).

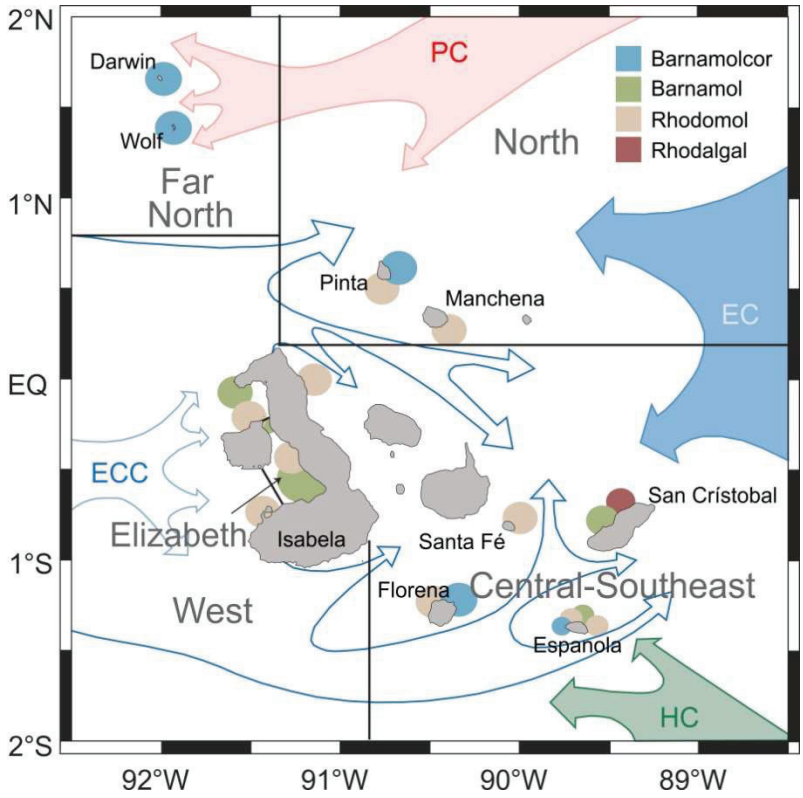

Figure 3-2: Main ocean currents shaping the hydrology of the Galápagos archipelago with the dominating carbonate facies. The distinct bioregions after Edgar et al. (2004) are indicated by the black lines with grey labels. The currents are the Peruvian Current (PC), the Equatorial Current (EC), the Equatorial Counter Current (ECC), and the Humboldt Current (CH). Modified after Reymond et al. (2015).

3.2 The Banc d´Arguin, Mauritania, NW Africa

3.2.1 Modern setting

The Banc d`Arguin represents a shallow epicontinental rimmed platform located in the northern part of the Mauritanian coast. As part of the continental shelf of NW Africa, it stretches over more than 200 km from the Baie du Lévrier in the north (~21.1°N) to Cape Timiris in the south (~19.2°N) and about 150 km in E-W direction, covering a total area of about 15,000 km^2 with water depths of less than 30 m (Mittelstaedt, 1991; Michel et al., 2009).

The climate of Mauritania as well as the hydrology of the adjacent tropical eastern Atlantic is mainly controlled by Canary Current (CC) which is part of the North Atlantic Gyre as well as the seasonally migrating Intertropical Convergence Zone (ITCZ) that determines the prevailing seasonal climate conditions (Mittelstaedt, 1991; Sevrin-Reyssac, 1993). During boreal winter, the ITCZ reaches its southernmost position resulting in the dominance of strong coastal parallel NE trade winds all along the Banc d´Arguin and the subsequent extension of the cold- and nutrient-rich CC further south (see Fig. 3-3) (Van Camp et al., 1991; Martinez et al., 1999). During this time, the entire Banc d`Arguin lies under the influence of strong upwelling resulting from wind-induced Ekman-transport (Van Camp et al., 1991; Cropper et al., 2014). In contrast, during boreal summer when the ITCZ reaches its northernmost position around 15-20°N, coastal parallel NE trade winds occur only north of ~20°C that in turn confines the upwelling area to ~20 - 20.5°N, corresponding to the latitudinal position of Cape Blanc, see Fig. 3-3 (Mittelstaedt, 1991). Due to this strong seasonal variability regarding the local climate and hydrology, year-round upwelling dominates the northernmost part of the Banc d`Arguin whereas seasonal upwelling during boreal winter impacts the central and southern parts (Van Camp et al., 1991). Primary production rates off Mauritania frequently exceeds Chlorophyll-α values (chl-a) of 25 mg/m³ (Fig. 3-4), which is therefore considered to be one of the most productive marine ecosystems in the world (Westphal et al., 2010).

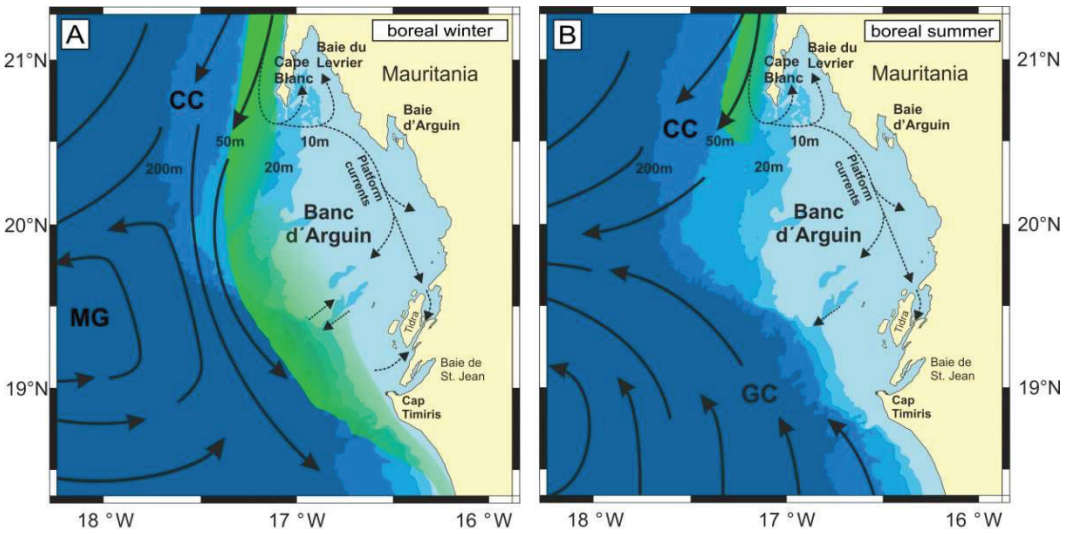

Figure 3-3: Schematic illustration of seasonal variation in ocean currents and upwelling intensities along the Banc d'Arguin. A) Boreal winter with the extension of the southward flowing Canary Current (CC), intensive upwelling (green) along the entire Banc d`Arguin and the Mauritanian Gyre (MG) off the Banc d´Arguin. B) Boreal summer with an extension of the northward flowing Guinea Current (GC), limited influences of the Canary Current and upwelling only north of ~20.5 °N. Modified after Mittelstaedt (1991), Sevrin-Reyssac (1993), and Klicpera (2014).

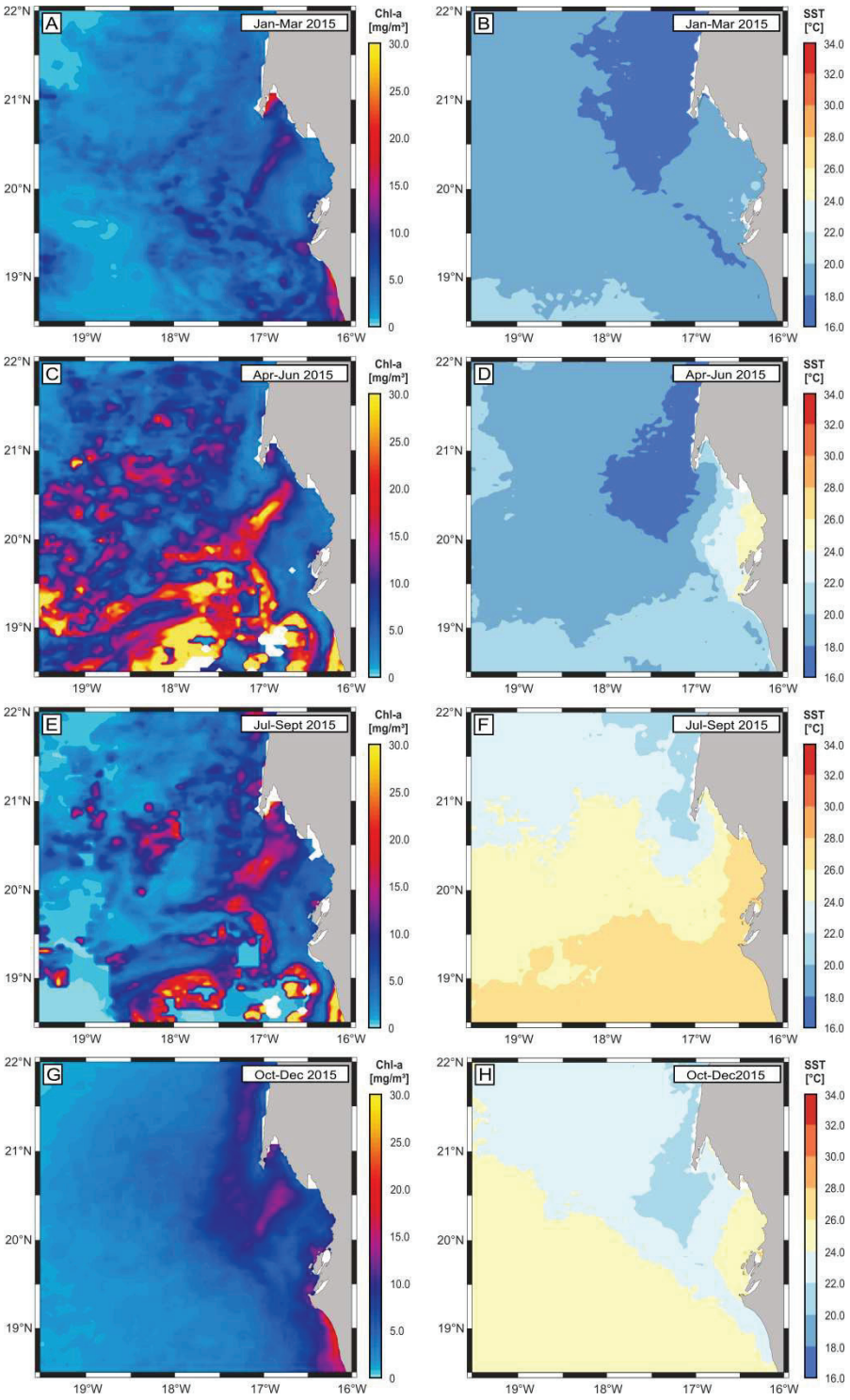

Figure 3-4: Seasonal variability of environmental conditions along on the Banc d`Arguin. Quarterly chlorophyll a concentration (A,C,E,G) and sea surface temperatures (B, D, F, H) for the year 2015. Data compiled from NASA Giovanni (MODIS aqua).

The cold and nutrient-rich waters enter the Banc d`Arguin south of Cape Blanc and are transported southward over the shallow shelf by wind- and tide-driven surface currents (Mittelstaedt, 1991; Sevrin-Reyssac, 1993) (Fig. 3-3). Throughout the transport over the shallow Banc d´Arguin with residence time roughly between 18 and 34 days, the cold water masses warm up to water temperatures exceeding 25 °C, and increase in salinity to values of >39 (Sevrin-Reyssac, 1993). The initially eutrophic water masses decrease in their tropic level to meso- and finally almost oligotrophic nutrient concentration from north to south along the transport trajectory (Berghuis et al., 1993). Lowest nutrient concentrations, highest water temperatures (>30 °C), and highest salinities (>40) are found in the extensive seagrass meadows within the tidal flats of the southern Banc d´Arguin (Lavaud et al., 2013). The water temperatures on the Banc d´Arguin show a clear seasonal cycle varying between ~17.5 and 29 °C with lowest vales during the main upwelling season from January until April and highest values during boreal summer (August/September), see Fig. 3-4. In the main upwelling front south of Cape Blanc, winter water temperature minima and summer water temperature maxima decrease to values of ~15.5 and 26 °C, respectively (Quack et al., 2007), see also Fig. 3-4.

Due to very low annual precipitation in the hyper-arid sub-Saharan hinterland (<50 mm/year in Nouhadibou, (Brahim, 2004)), the Banc d`Arguin is only sporadically influenced by riverine freshwater discharge. Only occasionally, intense rain events re-activate existing wadi-systems along the coast which, however, do not have a considerable impact on predominant marine conditions on the shallow Banc d`Arguin.

3.2.2 The carbonate factories of the Banc d´Arguin

Due to the exceptionally high primary production within the upwelling system off the Banc d´Arguin, the sedimentation system is characterized by heterozoan carbonate producers, which is atypical for tropical carbonates in modern oceans (Westphal et al., 2010). Instead of photozoan calcifying organisms typical for oligotrophic warm water ecosystems of tropical latitudes, filter-feeding organisms dominate in this low-diversity benthic ecosystem.

In particular the northern parts of the Banc d`Arguin including the shallow Baie du Lévrier are characterized by typical heterozoan facies such as barnamol and bimol grain assemblages (Klicpera et al., 2015), see Fig. 3-5. Along the decline in nutrient concentration and primary production from north/west to south/east, the hard bottom community of the northern area and the shelf break changes gradually into a mixed biogenic/siliciclastic facies dominated by

terrestrial (i.e. eolian) sediments (Michel et al., 2011; Klicpera et al., 2015). Within the southern area of the Banc d´Arguin including the extensive intertidal seagrass meadows around Tidra Island, the sedimentation system is dominated by mollusks and terrigenous sediments with a tendency towards silty/muddy siliciclastic material on the shelf edge (Klicpera et al., 2015). On the outer shelf, wedge-like sedimentary bodies (Arguin mud wedge; Timiris mud wedge) are incised by a large submarine canyon system (Hanebuth and Lantzsch, 2008) which acts as sediment and water transportation pathway from the shallow Banc d´Arguin into the abyssal plains resulting in turbiditic sediment successions along the continental slope of the Banc d´Arguin (Hanebuth and Henrich, 2009). This canyon system is related to the large Tamanrasett paleo-estuary which was active during the Pleistocene and early-to mid-Holocene (Skonieczny et al., 2015).

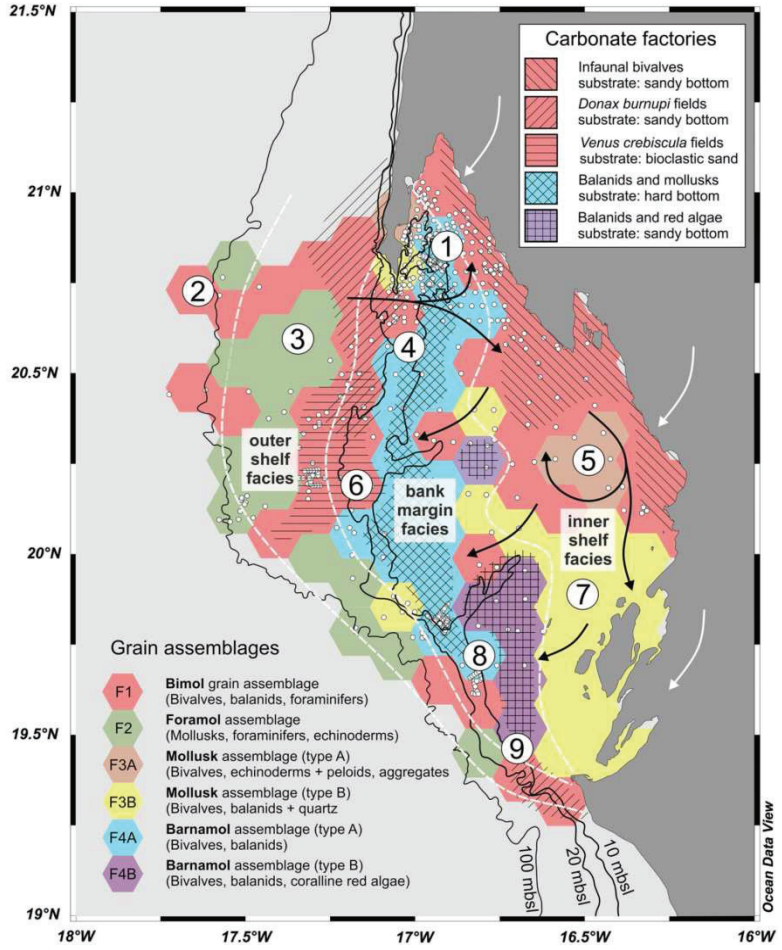

Figure 3-5: Sedimentary facies distribution, grain assemblages, and carbonate factories across the Banc d´Arguin with dominating surface currents (black arrows) and wind directions (white arrows). Figure reprinted from Klicpera et al. (2015) with permission from Springer.

3.2.3 Climate evolution during the Holocene

Differing from the modern hyper-arid state, the hinterland of the Banc d´Arguin experienced phases of much more humid climate conditions since the last glacial maximum (LGM) and intermittently was covered by dense savanna and shrub vegetation. Following predominantly dry and cold conditions during the LGM, the transition towards the so-called African Humid Period (AHP) during the early- and mid-Holocene was characterized by a series of abrupt events alternating between humid and arid episodes (Gasse, 2000). While the long-term climate of NW Africa is known to be mainly controlled by orbital cyclicity, these alternating short episodes of humid and dry conditions indicate additional but complex ocean-land-atmosphere interactions modifying the African climate (Gasse, 2000).

Induced by an increase of insolation due to orbital cycles, humid conditions established throughout most parts of NW Africa around 14.8 ka BP, (deMenocal et al., 2000a). During the AHP, increased monsoon precipitation due to the northward migration of the ITCZ caused a significant expansion of the vegetation in NW Africa by about 500 km towards the north (Gasse, 2000). According to marine paleoclimate records off NW Africa, these humid conditions lasted until ~5.5 ka BP but were punctuated by two prominent dry episodes known as the Younger Dryas and the 8.2 ka event where the latter one is supposed to initialize the transition towards modern arid conditions of NW Africa during the mid- to late-Holocene (deMenocal et al., 2000a; Kuhlmann et al., 2004; Holz et al., 2007), see Fig. 3-6.

While the establishment of humid conditions throughout NW Africa is documented in various marine and terrestrial paleoclimate records, the termination pattern remains a matter of controversial debate. Most marine paleoclimate records (e.g. eolian dust fluxes as a proxy for terrestrial vegetation coverage) indicate an abrupt termination of the AHP around 5.5 ka BP, see Fig. 3-6b (deMenocal et al., 2000a; deMenocal et al., 2000b; Kuhlmann et al., 2004; Adkins et al., 2006; Holz et al., 2007). In contrast many terrestrial paleoclimate records such as lake level data, river discharge records, or archeological evidences indicate a rather gradual transition towards the modern arid following the gradual decrease in insolation throughout the mid- to late-Holocene, see Fig. 3-6f, 3-6g and 3-6i (Vernet and Tous, 2004; Kröpelin et al., 2008; Armitage et al., 2015; Bloszies et al., 2015). Likewise, paleoclimate models show that only complex feedback mechanisms involving e.g. changes in albedo related to vegetation coverage can explain such abrupt decrease in monsoon precipitation during the mid-Holocene (Kutzbach and Liu, 1997; Claussen et al., 1999). However, climate model experiments increasingly fail to reproduce the abruptness of the mid- Holocene aridification

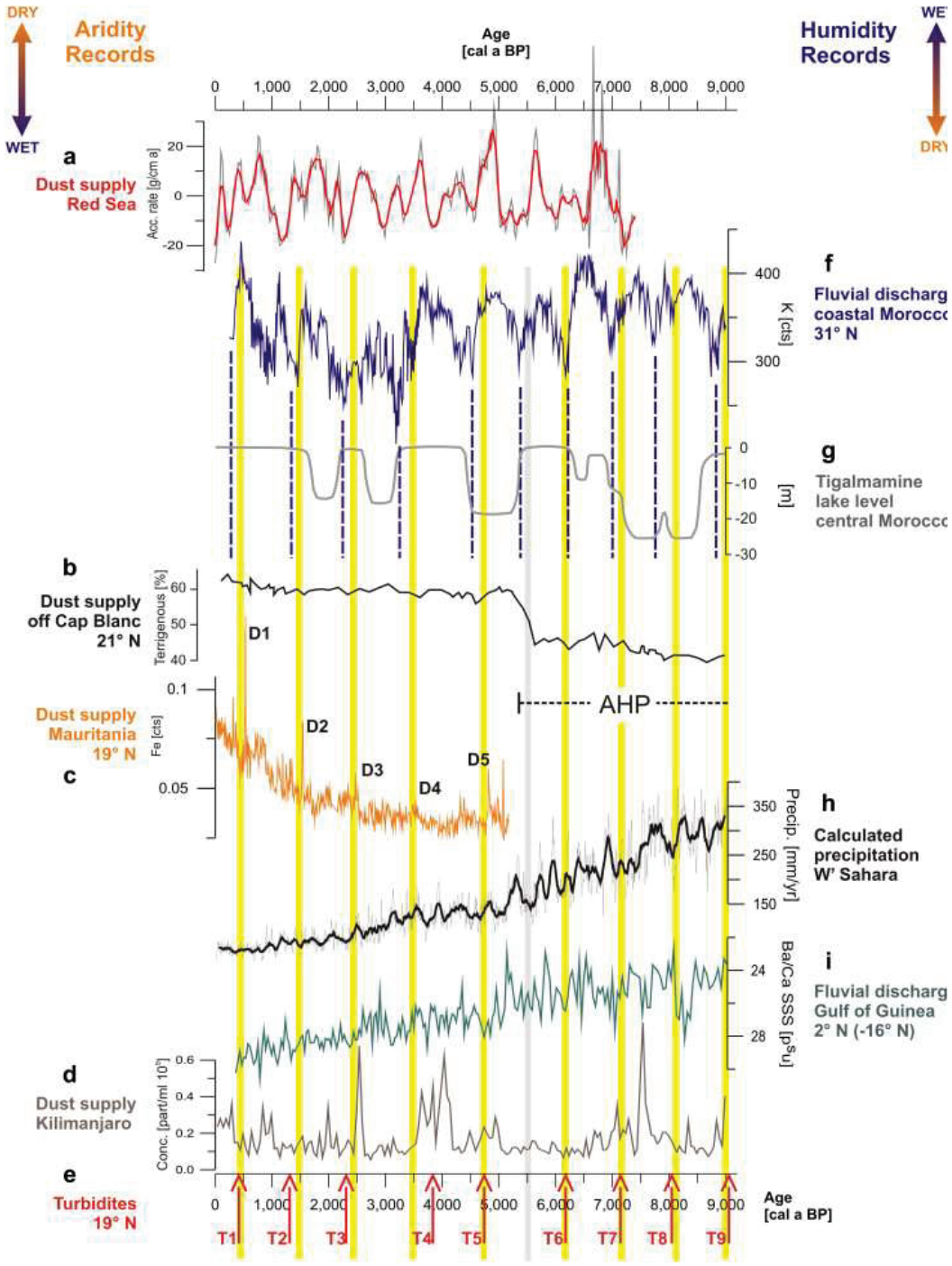

Figure 3-6: Holocene paleoclimate records of N Africa. **a)** Terrigenous sand accumulation rate from the Red Sea (Lamy et al., 2006), **b)** dust supply records from ODP Site 658C off Cape Blanc (Mauritania) (deMenocal et al., 2000a), **c)** iron intensity at site GeoB 9621 (Hanebuth and Henrich, 2009), **d)** dust concentration in a Kilimanjaro ice core (Thompson et al., 2002), **e)** turbidite beds (Zühlsdorff et al., 2008), **f)** potassium intensity off Morocco (Kuhlmann et al., 2004), **g)** Tigalmamine lake level record from central Marocco (Lamb et al., 1995), **h)** decadal precipitation simulation for the West Sahara region (Renssen et al., 2006), **i)** Ba/Ca-based salinity reconstruction for the Gulf of Guinea (Weldeab et al., 2007). Figure reprinted from Hanebuth and Henrich (2009) with permission from Elsevier.

suggested by marine paleoclimate records (Renssen et al., 2006; Liu et al., 2007; Rachmayani et al., 2015; Pausata et al., 2016). In consequence, we still lack a holistic understanding regarding the mechanisms controlling the NW African climate during the Holocene.

3.2.4 Archeological sites along the Banc d`Arguin

Based upon the high primary production along the Banc d´Arguin, hunter and gatherer societies populated most coastal areas along the inner Banc d´Arguin at least from ~6.7 ka BP until today. Due to the post-glacial sea-level rise after the LGM of ~+120 m which reached its high-stand around 6.5 ka BP about 2 to 3 m above the modern sea-level and the associated marine transgression within the coastal zones of the Banc d´Arguin, there are no archeological deposits accessible along the Banc d´Arguin older than ~6.5 ka BP (Vernet and Tous, 2004; Vernet, 2007), see Fig. 3-7. The only exception is the archeological site "Cansado" located at the southern tip of the Cape Blanc peninsula radiocarbon dated to ~6.8 ka BP.

Starting at the end of the post-glacial sea-level rise, the population of coastal zones along the Banc d´Arguin reached its maximum between 6 and 4 ka BP, referred to as the *Nouakchottian* period (Vernet and Tous, 2004). During this time, coastal populations occupied the coastal zones from the northernmost part of the Banc d´Arguin until Nouakchott and the modern Senegal, exploiting efficiently shallow intertidal marine resources by collecting predominantly mollusks (e.g. *Senilia senilis* (bivalvia), local name *Anadara*) as well as intensive fishing of e.g. catfish species (Vernet and Tous, 2004; Barusseau et al., 2007; Vernet, 2007; Barusseau et al., 2010; Dia, 2013). Alongside mid- to late-Holocene decrease in monsoon rainfall intensities over NW Africa and the associated retreat of Savanna vegetation, the occupation pattern along the Banc d´Arguin shows a retreat of coastal populations towards southern areas between 5 and 3 ka BP (Fig. 3-7). Interestingly, Neolithic coastal populations along the Banc d´Arguin disappear between 3.5 and 2.5 ka BP which coincides with the abrupt increase of terrigenous material after 2.5 ka BP observed in the marine paleoclimate record of Hanebuth and Henrich (2009), see Fig. 3-6c.

Depending on their location and local topography, we can find numerous archeological sites along the Banc d´Arguin with ages ranging from ~6.5 to 2.5 ka BP (Dia, 2013). As a consequence of the efficient exploitation of marine resources of the adjacent coastal areas, most archeological sites show large accumulations of calcareous skeletal remains in so-called "shell-midden" deposits. Within this thesis, fish otoliths and bivalve shells from these deposits have been used to infer highest-resolution (sub-seasonal) paleoclimate information (Chapter 7,

8 and 9) in order to bridge so far contradictory evidences from existing marine and terrestrial paleoclimate records.

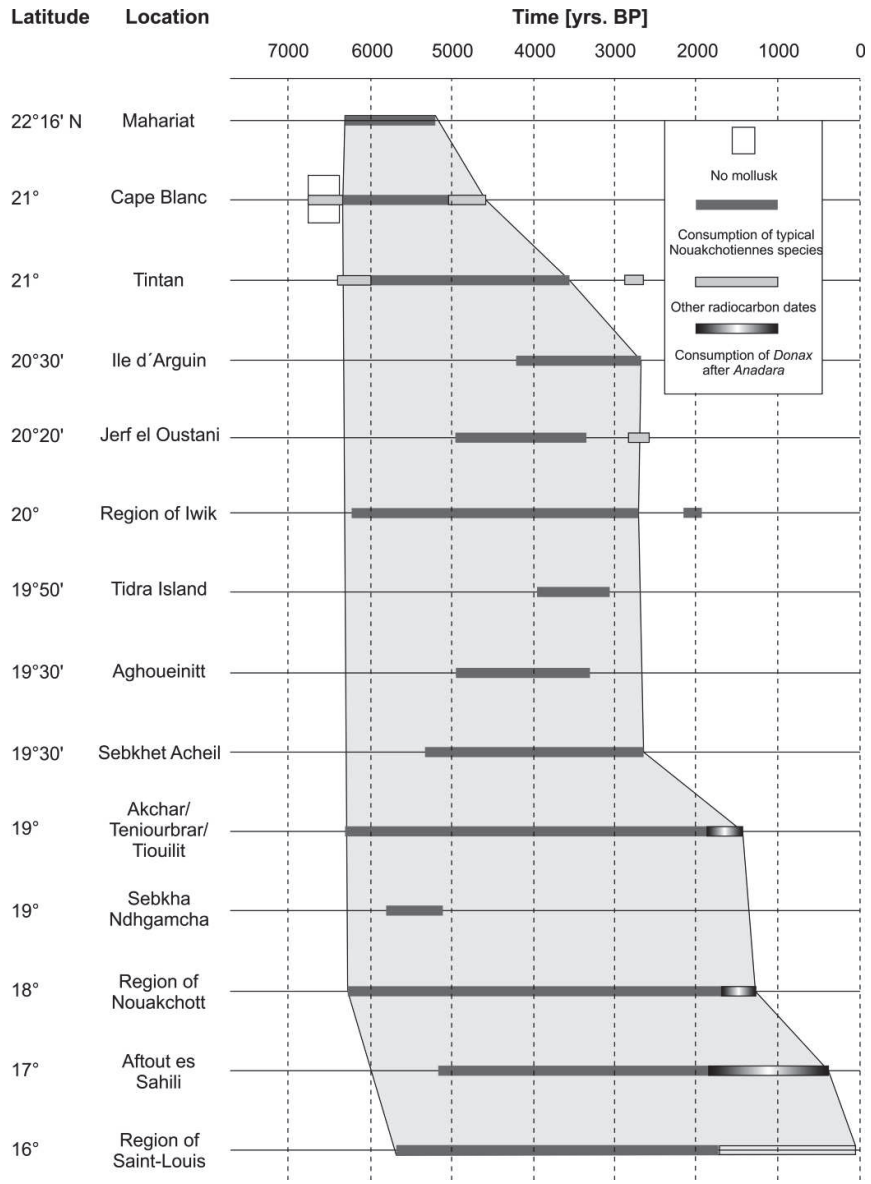

Figure 3-7: Occupation pattern along the Mauritanian and Senegalese coastline from ~22°N to 16°N throughout the mid- to late-Holocene. Modified after Vernet and Tous (2004).

4. METHODS

4.1 Sample preparation and sub-sampling

4.1.1 Thin/thick section preparation

In order to allow highest-resolution micro sampling of modern and archeological skeletal structures as well as optical and scanning electron microscopy, thin (~200 μm) and thick sections (~1 mm) were prepared at the Leibniz Centre for Tropical Marine Research, Bremen, Germany. The individual preparation steps used for the different skeletal structures are schematically shown in Fig. 4-1.

For thin- and thick section preparation, fish otoliths were cut along the transversal plane through the otolith core using a Uniprec® Woko 50 high-precision saw equipped with a 0.6 mm diamond coated blade. After embedding the posterior halves on glass slides ("Gießener"-format) using two-component epoxy resin (Araldite®), the otoliths were sectioned a second time parallel to the first cut. The remaining sections were then grinded close to the final thickness using a highest-precision G&N® MPS2 surface grinding machine in two steps (46 μm and 15 μm diamond diameter) and re-embedded on another glass slide. Afterwards, the initial glass slides were removed by grinding using the G&N® MPS2 surface grinding machine and the sections grinded to the final thickness. If necessary, otolith sections were further polished using a Logitech® PM2A polishing machine to enhance the visibility of the growth increments. Polishing was done using a rotation speed of 24 RPM with a 1.0 and 0.25 μm diamond solution. Thin/thick section preparation of the bivalve shells was done in a similar manner but by initially cutting along the direction of maximum growth perpendicular to the growth increments (see Fig. 4-1).

For optical and scanning electron microscopy as well as geochemical analysis of the echinoid spines, a central spine section of ~1 cm length was isolated by cutting twice perpendicular to the direction of growth using a Uniprec® Woko 50 high-precision saw with a 0.6 mm diamond coated blade. Afterwards, the central spine section was embedded on glass slides using two-component epoxy resin (Araldite®) and cut again perpendicular to the direction of growth to produce a ~ 1 mm thin section. After grinding the spine section to its final thickness (~ 250 μm) using a G&N® MPS2 surface grinding machine, the spine was re-embedded on another object slide and the initial slide was removed by grinding.

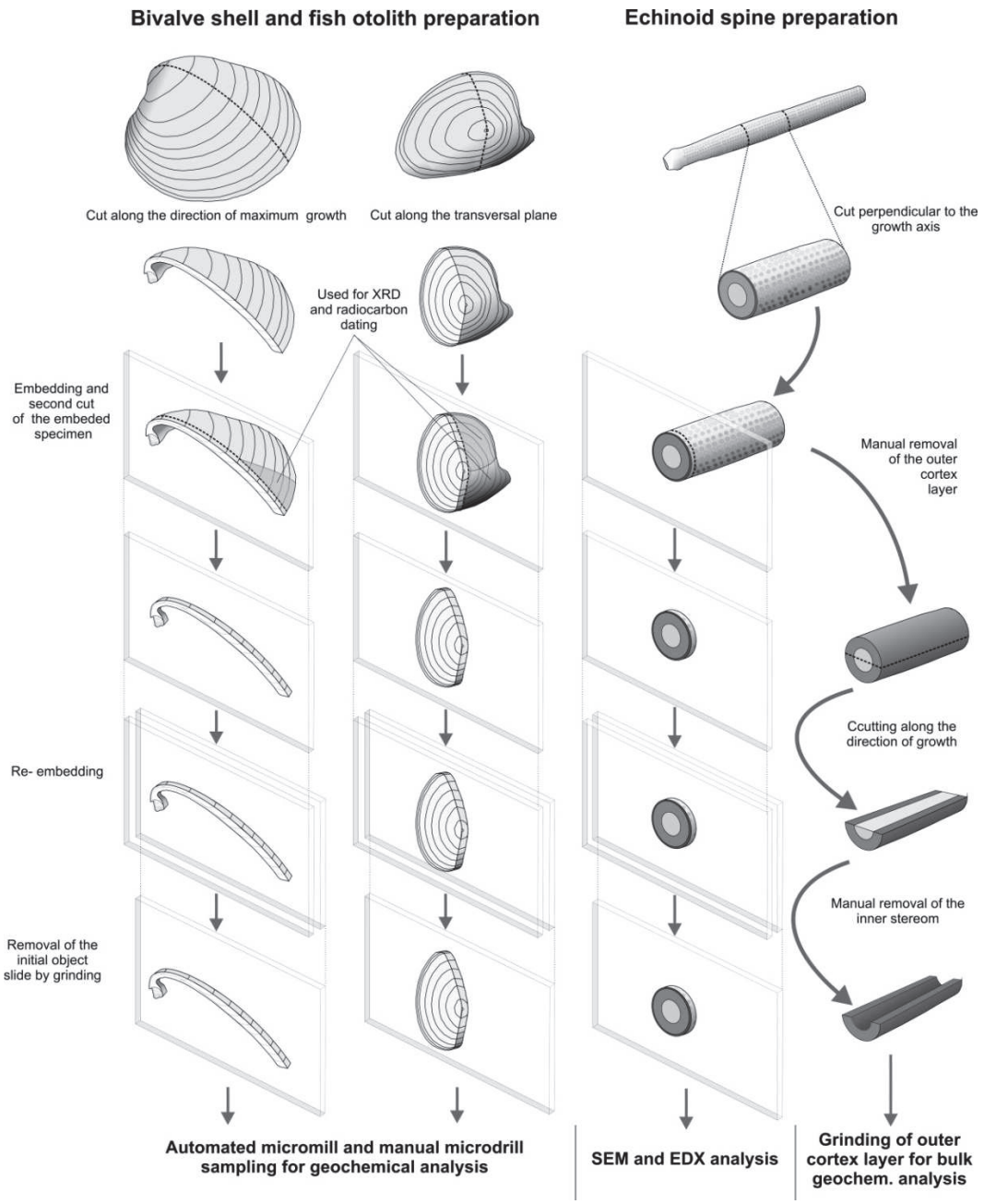

Figure 4-1: Schematic illustration of the individual sample preparation steps. Left: Thin/thick section preparation of bivalve shells along the direction of maximum growth. Middle: Thin/Thick section preparation of the otoliths using the transversal plane. Right: Echinoid spine preparation for SEM/EDX and bulk geochemical analysis of a central spine segment.

4.1.2 Ontogenetic otolith and bivalve shell sub-sampling

To produce ontogenetic proxy records with a sub-seasonal resolution, fish otoliths and bivalve shells were sub-sampled along their ontogenetic growth record using two similar NewWave®/ESI™ Micromill systems at the University of Erlangen-Nürnberg, Erlangen, Germany and the Leibniz Centre for Tropical Marine Research, Bremen, Germany.

Fish otoliths were sub-sampled along core-to-edge transects with an average sample spacing of ~100 µm. Depending on the otolith size, individual sampling tracks were approx. 2-3 mm long, resulting in ~50-80 discrete sub-samples per otolith of approximately 50-100 µg used for $\delta^{18}O$ and $\delta^{13}C$ analysis. Likewise, bivalve shells were sampled along the ontogenetic growth records in the outer shell layer parallel to the visible growth lines. Sample spacing for the bivalve shells was on average ~500 µm along umbo-ventral margin transects. The ~2 mm long sampling tracks for the bivalve shells resulted in discrete powder sub-samples of ~50-80 µg for $\delta^{18}O$ and $\delta^{13}C$ analysis. All sub-samples were stored in sealed polypropylene or glass vials at room temperature until the analyses.

4.1.3 Bulk otolith and bivalve shell samples

For clumped isotope analysis, the posterior halves of the otoliths resulting from the initial cutting step were manually grinded using a ceramic mortar and pestle. Likewise, anterior halves resulting from the second cutting step were prepared in a similar manner to provide powdered bulk otolith material for radiocarbon dating and mineralogical analyses (X-ray diffraction). All powdered samples were stored in sealed polypropylene vials at room temperature until the analyses.

For bulk clumped isotope measurement, mineralogical analysis and radiocarbon dating of the bivalve shells, a powdered and homogenized slice of shell material cut from the ventral margin using a Dremel™ tool equipped with a diamond cutting wheel (Fig. 4-1) has been used. In addition, a bulk sample from the hinge region was sampled for comparative clumped isotope analysis using a U-Power® UP200 hand drill equipped with a 0.8 mm tungsten-carbide dental drill at lowest possible speed (~1000 RPM). Therefore, ~0.5-1.0 cm transects were drilled manually perpendicular to the growth lines of the hinge covering the entire ontogenetic growth record.

4.1.4 Echinoid spine sub-sampling

The remaining part of the central spine section used for thin section preparation was used for geochemical analysis of the echinoid spine material. After manually removing the outer cortex layer using sand paper, the remaining central spine section was cut into two equal halves along the direction of growth and the inner stereom was removed manually using a Dremel™ hand drill at slowest possible drill speed (~5000 RPM), see Fig. 4-1. The remaining outer cortex layer was grinded using an opal mortar and pestle and the remaining powder stored in sealed polypropylene vials at room temperature until the analyses.

4.2 Scanning electron microscopy

To assess the microstructure of the skeletal structures, optical microscopy (Leica® S6D and a Keyence® VHX) as well as SEM analyses (TESCAN® VEGA 3 XMU) were used at the Leibniz Centre for Tropical Marine Research, Bremen, Germany. The microstructure and surface morphology of samples was analyzed using back-scattered electron detector (BSE-SEM) at 10 keV.

4.3 Aragonite/calcite analysis

To assess sample preservation of the archeological specimens (i.e. conversion of primary aragonite into secondary calcite) and potential conversion of aragonite into calcite during the cooking experiments, X-ray diffraction (XRD) has been used to determine the mineralogy of all skeletal structures.

The archeological samples were analyzed at the University of Bremen, Germany using a Philips X´Pert Pro diffractometer equipped with a Cu-tube (kα 1.541, 45 kV, 40.0 mA). Measurements were done using a continuous scan from 3-85° 2Θ with step sizes of 0.016° 2Θ. The Philips software X´Pert HighScore™ was used for data processing. Abundance of aragonite and calcite was determined using the relative peak areas of aragonite (1,1,1) peak (2Θ = 26.1°) and low magnesium calcite (1,0,1) peak (2Θ = 29.6°) against a calibrated standard.

The XRD analyses of the experimental shells were conducted at the Rosenstiel School of Marine and Atmospheric Science of the University of Miami, FL, USA, using a PANalytical X´Pert PRO diffractometer with a Cu-tube (kα 1.541 Å, 45.0 kV, 40.0 mA). Measurements

were done using a continuous scan from 23.0-35.0 2Θ with a step size of 0.005 2Θ and a measuring time of 0.1 seconds per step. Data collection and processing was done using the software X'Pert Data Collector and X'Pert HighScore Plus. Relative abundance of aragonite and calcite was determined using the relative peak areas of aragonite (1,1,1) peak (2Θ = 26.1°) and low magnesium calcite (1,0,1) peak (2Θ = 29.6°) against a calibrated standard.

4.4 Radiocarbon dating

Radiocarbon dating of all archeological samples was done using accelerator mass spectrometry (AMS) at the Poznan Radiocarbon Laboratory, Poznan, Poland. Calibration of conventional radiocarbon ages was done using the software OxCal 4.2.439 and the Marine13 calibration curve (Reimer et al., 2013) and assuming a local reservoir age of ΔR = -300 years, which represents an average estimate for the local mid-Holocene reservoir ages based on several paired terrestrial and marine radiocarbon dates along the Mauritanian coastline throughout the Holocene (J. F. Saliége, unpublished data).

4.5 Stable isotope analyses

The oxygen isotopic composition of individual sub-samples was measured using a Finnigan MAT 251 gas isotope ratio mass spectrometer (IRMS) connected to a Kiel III device at the Center for Marine Environmental Sciences (MARUM), Bremen, Germany, a ThermoFinnigan MAT 253 IRMS connected to a Kiel IV device at ZMT, Bremen, Germany and a ThermoFinnigan Delta V Plus isotope ratio mass spectrometer equipped with a Gasbench II at the University of Erlangen-Nürnberg.

Carbonate samples were routinely measured against certified standards (NBS19) and in-house working standards. Repeated standard measurements (NBS19 and in-house working standards) revealed an external precision (1σ) for all measurements of better than ±0.07‰ VPDB for all $\delta^{18}O_{Carbonate}$ and $\delta^{13}C_{Carbonate}$ analyses.

4.6 Reconstruction of water temperatures based on skeletal $\delta^{18}O$ data

The $\delta^{18}O_{Carbonate}$-based water temperatures for the fish otoliths were calculated using the equation of Thorrold et al. (1997)

$$1000\ln(\alpha) = 18.56 \cdot (10^3 \cdot T^{-1}[K]) - 32.54 \qquad \text{(Eq. 4.1)}$$

where the fractionation factor α is defined as:

$$\alpha = \frac{\delta_{\mathbf{Carbonate}} + 10^3}{\delta_{\mathbf{Seawater}} + 10^3} \quad \text{(Eq. 4.2)}$$

The conversion of $\delta^{18}O_{Carbonate}$ values from the Vienna Pee Dee Belemnite (VPDB) to the Vienna Standard Mean Ocean Water (VSMOW) scale was done using the equation of Gonfiantini et al. (1995):

$$\delta^{18}\mathrm{O}_{\mathbf{Carbonate}}(\mathrm{VSMOW}) = 1.03091 \cdot \delta^{18}\mathrm{O}_{\mathbf{Carbonate}}\,(\mathrm{VPDB}) + 30.91 \quad \text{(Eq. 4.3)}$$

The estimation of $\delta^{18}O_{Carbonate}$-based water temperature for the bivalve shells has been done using the equation of Grossman and Ku (1986):

$$\mathrm{T}\,[°\mathrm{C}] = 21.8 - 4.69 \cdot (\delta^{18}\mathrm{O}_{\mathbf{Carbonate}}[\mathrm{VPDB}] - (\delta^{18}\mathrm{O}_{\mathbf{Seawater}}[\mathrm{VSMOW}] - 0.27)) \quad \text{(Eq. 4.4)}$$

Regional $\delta^{18}O_{Seawater}$ values were taken from literature or estimated using existing regional salinity/$\delta^{18}O_{Seawater}$-equations. For the intertidal seagrass areas of the Banc d`Arguin, Mauritania, Lavaud et al. (2013) reported a local salinity/$\delta^{18}O_{Seawater}$-relationship of

$$\delta^{18}\mathrm{O}_{\mathbf{Seawater}}(\mathrm{VSMOW}) = 0.2692(\pm 0.0126) \cdot \mathbf{Salinity} - 9.1949(\pm 0.4903) \quad \text{(Eq. 4.5)}$$

and an average $\delta^{18}O_{Seawater}$ value of 1.57 ‰ VSMOW which was used for water temperature calculation of the bivalve shell $\delta^{18}O$ data. For the fish otolith-based water temperature reconstructions, monthly resolved remote-sensing salinity data with a spatial resolution of 1° by 1° (Carton and Giese, 2008) and Eq. (4.5) was used to approximate the average $\delta^{18}O_{Seawater}$ value (0.68 ‰ VSMOW) for the more offshore parts of the Banc d`Arguin. For the Galápagos archipelago, a constant $\delta^{18}O_{Seawater}$ value of 0.29 ‰ VSMOW (Wellington et al., 1996) was used.

4.7 Clumped isotope analyses and water temperature reconstruction

Clumped isotope analysis was done at the Stable Isotope Laboratory (SIL) of the Rosenstiel School of Marine and Atmospheric Science (RSMAS), Miami, FL, United States, using the analytical procedure described in Murray et al. (2016). Each sample was analyzed at least twice in a randomized order. All samples were processed on the stainless-steel cryogenic vacuum extraction line evacuated to $< 10^{-6}$ mbar using two turbo-molecular pumps (Balzer TPU 170 and Edwards 50EX). Individual sample aliquots of ~8.0 mg powder were digested for 30

minutes at 90°C in 3.5 ml ~105 % phosphoric acid (H_3PO_4) using a modified "Fairbanks" device (Swart et al., 1991) connected to a common acid bath. Resulting CO_2 was then purified on the cryogenic vacuum extraction line following the protocol described in detail in Murray et al. (2016).

Purified CO_2 was measured using a Thermo Fisher Scientific dual-inlet MAT-253 IRMS. Samples were measured against an in-house working-gas gas standard. Each sample was analyzed at a signal intensity of 12 V on mass-44 over 6 acquisitions of 15 sample-standard measurements. Data reduction and normalization for Δ_{47} and temperature calculations followed the methods of Affek and Eiler (2006) and Huntington et al. (2009). To check for potential contamination, samples were scrutinized based on their offset of δ^{48} and Δ_{48} (Huntington et al., 2009). Precision of clumped isotope analysis is reported using the average 1σ standard errors.

Carbonate $\delta^{13}C$ and $\delta^{18}O$ was measured simultaneously by means of masses 45/44 and 46/44, respectively using a method adapted from Craig (1957) modified for a multi-collector mass spectrometer. Shell and otolith $\delta^{13}C$ and $\delta^{18}O$ values were calibrated using NBS-19 and reported relative to the VPDB scale. External precision of $\delta^{13}C$ and $\delta^{18}O$ analyses was better than ±0.055 and ±0.117 ‰, respectively. All Δ_{47} values were calculated using the method described by Affek and Eiler (2006) and Huntington et al. (2009). Translation into the absolute reference frame (ARF) was accomplished using the method described by Dennis et al. (2011) with 1000, 50 and 25 °C water equilibrated gasses. The equation of Dennis et al. (2011) has been used to convert measured Δ_{47} values into water temperatures:

$$\Delta_{47} = \frac{(0.0636 \pm 0.0049 \cdot 10^6)}{T^2[K]} - 0.0047 \pm 0.0520 \qquad \text{(Eq. 4.6)}$$

4.8 Element/Calcium ratio analysis

Element/Calcium ratios were measured using a Spectro CIROS Vision inductively coupled plasma optical emission spectroscope (ICP-OES) at the Leibniz Centre for Tropical Marine Research, Bremen, Germany. Individual carbonate samples were dissolved in supra pure 0.5 M nitric acid and further diluted with nitric acid according to the expected element concentrations. Instrument calibration solutions were prepared using single element standards in proportion to the expected concentration in the sample material. Triplicate measurements of all samples were done routinely against the international reference standard JLs-1, a coral in-house working standard (ZMT-CM1), and nitric acid blanks. Accuracy for Ca and Mg

measurements of the echinoid spine material was better than 0.63 % and 2.26 %, respectively with a precision of <3 %.

Spatial distribution of Ca and Mg ions within the echinoid spines was measured using a scanning electron microscope (SEM, TESCAN VEGA3) coupled to an Oxford Energy Dispersive X-ray (EDX X-Max SDD) at the Leibniz Centre for Tropical Marine Research (ZMT), Bremen, Germany. Thin sections perpendicular to the direction of growth were used for element mapping in 20 randomly selected spines. Thin sections were sputtered with gold (Cressington Sputter Coater 108 auto) and element mapping was accomplished using the VEGA3 and Aztec software. EDX working parameters were set to a beam voltage of 10 keV, a maximum of 5 million counts with a peak pile-up correction, and a process time of 4 min. Dead time was set to 30-50%.

4.9 Temporal alignment modeling

The temporal alignment models of Chapter 6 were calculated using Microsoft™ Excel 2007® and the R statistical computing language (R Development Core Team, 2013).

4.10 Statistical analyses

All statistical tests used in this study were performed using the software Microsoft™ Excel 2007®, the SigmaStat Statistics-package in SigmaPlot® Version 12.5 and the R statistical computing language (R Development Core Team, 2013).

5. PALEOENVIRONMENTAL PROXIES IN ECHINOID SPINES (*EUCIDARIS GALAPAGENSIS*, DÖDERLEIN 1887) ALONG A NATURAL WATER TEMPERATURE GRADIENT

Peter Müller, Claire E. Reymond, Philipp Siegel, Hildegard Westphal

in press in

Palaeogeography, Palaeoclimatology, Palaeoecology

Palaeogeography, Palaeoclimatology, Palaeoecology xxx (2016) xxx–xxx

Contents lists available at ScienceDirect

Palaeogeography, Palaeoclimatology, Palaeoecology

journal homepage: www.elsevier.com/locate/palaeo

Paleoenvironmental proxies in echinoid spines (*Eucidaris galapagensis*, Döderlein 1887) along a natural water temperature gradient

Peter Müller [a,*], Claire E. Reymond [a], Philipp Siegel [b,1], Hildegard Westphal [a,b]

[a] Leibniz Center for Tropical Marine Ecology (ZMT), Fahrenheitstr. 6, 28359 Bremen, Germany
[b] University of Bremen, Klagenfurter Str. 4, 24359 Bremen, Germany

ARTICLE INFO

Article history:
Received 29 February 2016
Received in revised form 13 June 2016
Accepted 17 June 2016
Available online xxxx

Keywords:
Echinoid spines
Oxygen isotopes
Carbon isotopes
Mg/Ca ratio
Paleoenvironmental proxies
Galápagos archipelago

ABSTRACT

The use of paleoenvironmental proxies such as oxygen isotopes in echinoderm skeletons has been a matter of controversial debate. Many previous studies showed a variety of environmental as well as biological processes causing deviations from equilibrium incorporation of geochemical proxies during the formation of echinoderm skeletons. However, given the global distribution of echinoids, their fast spine growth and their occurrence throughout the entire Phanerozoic, species-specific calibrations of geochemical proxies in echinoid spines can disclose a valuable bio-archive for reconstructing ancient environmental conditions throughout Earth's history if samples are adequately preserved in the sedimentary record.

Here we present data on oxygen isotopes ($\delta^{18}O$), carbon isotopes ($\delta^{13}C$), and Mg/Ca ratios measured in *Eucidaris galapagensis* (Döderlein, 1887) spines, which were sampled along the natural water temperature gradient of the Galápagos archipelago. We found a negative correlation of $\delta^{18}O_{Calcite}$ with ambient water temperature following the equation $1000\ln(\alpha) = 23.03\ (10^3 T^{-1}\ [K]) - 47.90$. We also found $\delta^{13}C_{Calcite}$ be positively correlated with water temperature following the equation $\delta^{13}C_{Calcite}(VPDB) = -47.585 + (0.164 * T[K])$. Mg/Ca ratios also showed a significant correlation with water temperature, however, with a low correlation coefficient. The large scatter of $\delta^{18}O_{Calcite}$ values within the upwelling region indicates higher growth rates during seasons of colder water temperatures. Considering this and the observed steeper slope in the temperature-$\delta^{18}O_{Calcite}$ relationship, our data suggest that the common assumption of respiration affecting oxygen isotope fractionation does not apply for the tropical species *E. galapagensis*. Overall, our data show that *E. galapagensis* spines represent valuable paleoenvironmental archives which might have the potential to provide sub-annually resolved water temperature records if spine architecture and growth pattern are well constrained.

Personal contribution to Chapter 5:

CR (34 %) and HW (33 %) and PM (33%) designed the study; CR (100 %) conducted the fieldwork; PM (50 %), CR (10 %) and PS (40 %) prepared the samples; PM (50 %) and PS (50 %) conducted chemical analysis of the samples; PM (70 %), CR (10 %) and PS (20 %), analyzed the measured proxy data; PM (70 %), CR (20 %), and HW (10 %) wrote the manuscript.

5.1 Abstract

The use of paleoenvironmental proxies such as oxygen isotopes in echinoderm skeletons has been a matter of controversial debate. Many previous studies showed a variety of environmental as well as biological processes causing deviations from equilibrium incorporation of geochemical proxies during the formation of echinoderm skeletons. However, given the global distribution of echinoids, their fast spine growth and their occurrence throughout the entire Phanerozoic, species-specific calibrations of geochemical proxies in echinoid spines can disclose a valuable bio-archive for reconstructing ancient environmental conditions throughout Earth's history if samples are adequately preserved in the sedimentary record.

Here we present data on oxygen isotopes ($\delta^{18}O$), carbon isotopes ($\delta^{13}C$), and Mg/Ca ratios measured in *Eucidaris galapagensis* (Döderlein, 1887) spines, which were sampled along the natural water temperature gradient of the Galápagos archipelago. We found a negative correlation of $\delta^{18}O_{Calcite}$ with ambient water temperature following the equation $1000 \ln(\alpha) = 23.03\ (10^3 * T^{-1}[K]) - 47.90$. We also found $\delta^{13}C_{Calcite}$ to be positively correlated with water temperature following the equation $\delta^{13}C_{Calcite}(VPDB) = -47.585 + (0.164 * T[K])$. Mg/Ca ratios also showed a significant correlation with water temperature, however, with a low correlation coefficient. The large scatter of $\delta^{18}O_{Calcite}$ values within the upwelling region indicates higher growth rates during seasons of colder water temperatures. Considering this and the observed steeper slope in the temperature-$\delta^{18}O_{Calcite}$ relationship, our data suggest that the common assumption of respiration affecting oxygen isotope fractionation does not apply for the tropical species *E. galapagensis*. Overall, our data show that *E. galapagensis* spines represent valuable paleoenvironmental archives which might have the potential to provide sub-annually resolved water temperature records if spine architecture and growth pattern are well constrained.

5.2 Introduction

Reconstructing paleoenvironmental conditions using geochemical proxies from marine calcareous skeletal structures has considerably broadened our understanding of ancient climate and oceanographic processes (e.g. Pelejero et al., 2005; Carre et al., 2014). Based on the fundamental work of Urey (1947), Craig (1953) and Emiliani (1955; 1966), numerous studies have shown the vast applicability of oxygen isotope thermometry among a wide range of calcifying taxa. In particular larger skeletal structures such as corals (Swart, 1983; de Villiers et al., 1995; López Correa et al., 2010), bivalves (Grossman and Ku, 1986; Goodwin et al., 2003; Schöne et al., 2004) and fish otoliths (Surge and Walker, 2005; Vanhove et al., 2012; Müller et al., 2015a) allow the reliable reconstructions of sub-seasonally resolved water temperature records prior to the instrumental era. In this context, echinoderms have only attracted minor attention and our knowledge about proxy incorporation into their skeletons is thus still limited. However, understanding the role of environmental and biological processes on paleoenvironmental proxy signatures in cidaroid spines can disclose a new globally occurring high-resolution paleoenvironmental bio-archive dating back to the Permian (Thompson et al., 2015).

The temperature dependence of isotope fractionation and element incorporation in echinoderm skeletons has been a matter of debate since the early developments of isotope proxies in marine carbonates (Weber and Raup, 1966; Weber, 1973). Previous studies showed, that isotope fractionation in echinoderms is complex and depends on different environmental and biological factors (Weber and Raup, 1966; Weber, 1968; Richter and Bruckschen, 1998; Baumiller, 2001; Gorzelak et al., 2012; Courtney and Ries, 2015). For example, many echinoderm taxa show large isotopic variations across different skeletal compartments within a single individual as well as across individuals grown in the same area (e.g. Gorzelak et al., 2012). Most studies showed a negative correlation between $\delta^{18}O_{Calcite}$ and water temperature, whereas $\delta^{13}C_{Calcite}$ values showed a varying response to water temperature, most likely modified by biological processes such as respiration or kinetic isotope effects (Weber, 1968; Courtney and Ries, 2015). Most echinoderms show depleted oxygen isotopic compositions relative to carbonates precipitated under apparent equilibrium conditions (Baumiller, 2001; Gorzelak et al., 2012). However, Weber (1968) showed that echinoids are closest to oxygen isotope equilibrium fractionation compared to other echinoderm taxa.

Besides isotope proxy systems, previous studies have suggested that Mg/Ca ratios of echinoderm skeletons are a potential indicator of ambient water temperature or seawater Mg/Ca ratio (Chave, 1954; Weber, 1973; Dickson, 2002). Similar to isotope proxies, the incorporation of Mg is not uniform among echinoderm taxa and range from ~3 to ~19 mol% $MgCO_3$ (e.g. Dickson, 2002; Ries, 2004). However, the elemental composition can vary considerably between different skeletal units of echinoderm skeletons, with $MgCO_3$ concentrations reaching up to ~40mol% (protodolomite) in echinoid teeth (e.g. Schroeder et al., 1968; Markel et al., 1971; Weber, 1973). This large range suggests environmental as well as biological processes control element incorporation into echinoderm skeletons. Even though earlier studies suggested water temperature to be the controlling factor for Mg/Ca in echinoderm skeletons (Chave, 1954; Weber, 1973), later studies suggested the seawater Mg/Ca ratio to be the primary influence (Dickson, 2002). Taken together, Mg incorporation into echinoderm skeletons is still not entirely understood, demanding additional experimental or field-based *in-situ* studies.

This study aims to understand the relationship between water temperature, oxygen and carbon isotopic signatures, and Mg/Ca ratios in spines of *Eucidaris galapagensis* (Döderlein 1887) to test their suitability as environmental archives. Therefore, we analyzed *E. galapagensis* spines sampled along the strong natural water temperature gradient of the Galápagos archipelago and correlated the measured proxy data with remote sensing sea surface temperature (SST) data. By analyzing their isotopic as well as elemental composition, we attempt to answer the following questions in order to refine the use of geochemical proxies in echinoid spines:

(1) Are *E. galapagensis* spines reliable archives of environmental conditions such as water temperature?

(2) How are potential deviations from equilibrium incorporation of paleoenvironmental proxies related to environmental conditions throughout the Galápagos archipelago?

(3) Do we see evidence for biological processes causing deviations from equilibrium fractionation of oxygen or carbon isotopes?

5.3 Material and methods

5.3.1 The Galàpagos archipelago

Located in the Eastern Tropical Pacific, the Galápagos archipelago lies in the confluence zone of five major ocean currents causing a high seasonal variability of environmental conditions. In particular the south-western part of the archipelago is dominated by relatively colder SSTs during the dry season from June to December due to topographical upwelling of the eastwards flowing Equatorial Under Current resulting in a larger overall SST variability (Houvenaghel, 1978; Eden and Timmermann, 2004; Liu et al., 2014), see Fig. 5-1. In the central-eastern part of the archipelago, the cool (~18–~28 °C) and nutrient-rich waters of the southwest mix with warm (~24–~28 °C) and nutrient-poor surface waters of the north/north-east, whereas the northern area is generally characterized by more stable environmental conditions throughout the year (Chavez and Brusca, 1991). Seawater salinity varies from 33.5 to 35 along a south to north transect (1°N to 2°S) (Sakamoto et al., 1998). This transition from the seasonally variable upwelling dominated southwestern area towards the warmer and more stable northern area generates a strong gradient of environmental conditions dividing the Galápagos archipelago into five main bioregions (West, Elizabeth, Central-southeast, North and the Far North) differing in terms of water temperature, nutrient and CO_2 conditions (Edgar et al., 2004), see Fig. 5-1. Subsequently, the entire archipelago shows a distinct distribution of heterozoan and photozoan carbonate facies along the environmental gradient (Reymond et al., 2015), with *E. galapagensis* as one of the most abundant carbonate producer within all bioregions (Glynn et al., 1979; Reymond et al., 2015). For clarity reasons, the bioregions West and Elizabeth defined by Edgar et al. (2004) are considered as one bioregion in this study.

5.3.2 Sample collection

In total, 30 *E. galapagensis* spines were sampled between 2011 and 2013 by scuba diving at 17 sites in shallow rocky reefs of 10 islands throughout the archipelago (Fig. 5-1). Water depth of the sites varied between 6 and 15 m. All spines were collected from bulk surface sediment samples which were rinsed with tap water and dried at 40 °C for 48 h. After splitting into individual size fractions, the most pristine *E. galapagensis* spines were selected from the >2 mm fraction.

5.3.3 Spine microstructure and preservation

Metastable high-Mg calcite skeletons of echinoderms are generally susceptible to abrasion, dissolution, disintegration or internal cementation during sediment transportation and diagenesis (Kidwell, Susan and Baumiller, 1990; Gorzelak and Salamon, 2013) which can bias bulk chemical analysis of echinoid skeletal structures. To avoid such potential biases, we investigated spine preservation in thin sections and spine fragments using a petrographic microscope (Keyence® VHX) and a scanning electron microscope (SEM; TESCAN® VEGA3 XMU), respectively. Thin sections were prepared by embedding the spines in epoxy resin to fixate their internal architecture and cutting perpendicular to the spine growth direction using a Uniprec® Woko 50 high precision saw equipped with a diamond coated 0.6 mm blade. Fresh fracture surfaces were manually prepared along the same orientation for SEM analysis. Only pristine spines showing no abrasion or cementations as well as only minor signs of bioerosion were used for chemical analysis.

5.3.4 Sample preparation

For precisely sampling the dense part of the outer stereom, ~1 cm long sections from the center of the spines were isolated, by cutting perpendicular to the direction of growth after manually removing the outer cortex layer. These central sections were then cut into two equal halves along the direction of growth. Afterwards, the inner stereom was carefully removed using a hand drill at lowest possible drill speed (RPM ~ 5000). The remaining outer stereom was cleaned with deionized water in an ultrasonic bath for 10 min to remove potential contaminations, dried for ~24 h at 40 °C and then manually grinded using a mortar and pestle. Powder samples were stored in sealed vials at room temperature until the analysis.

5.3.5 Stable isotope analysis

Stable isotopic composition of spine sub-samples (~80–100 μg) were measured on a Finnigan MAT 251 gas isotope ratio mass spectrometer connected to a Kiel III automated carbonate preparation device at the stable isotope laboratory in the Center for Marine Environmental Sciences (MARUM), University of Bremen, Germany. The long-term standard deviation of the in-house standard (Solnhofen limestone) was 0.04‰ for $\delta^{13}C$ and 0.07‰ for $\delta^{18}O$. Data are reported in the standard delta-notation and all $\delta^{18}O_{Calcite}$ and $\delta^{13}C_{Calcite}$ values are reported in per mil relative to the VPDB reference via the NBS 19 standard.

5.3.6 Ca and Mg concentration and distribution analysis

Calcium and magnesium concentration in the spine stereom material was measured using a Spectro CIROS Vision inductively coupled plasma optical emission spectroscope (ICP-OES) at the Leibniz Center for Tropical Marine Ecology (ZMT), Bremen, Germany. For each spine, ~10 mg of powdered stereom material was dissolved in 2 ml supra pure 0.5 M nitric acid (Carl Roth®). Aliquots of 0.1 ml were further diluted with 0.5 M nitric acid. Instrument calibration solutions were prepared using single element standards in proportion to the *E. galapagensis* spine concentrations. Triplicate measurements of all spine samples were done routinely against the international reference standard JLs-1, a coral in-house working standard (ZMT-CM1), and nitric acid blanks. The Mg/Ca ratio is calculated as (Mg [mol]/Ca [mol]) × 100=Mg/Ca [mol%]). Relative standard deviations of triplicate measurements were 1.74 % for Ca and 3.08 % for Mg. Accuracy for Ca and Mg measurements were better than 0.63 % and 2.26 %, respectively. Analytical uncertainties translate into a maximum error of measured Mg/Ca ratios of <0.35 mol%. Spatial distribution of Ca and Mg ions within the spines were measured using a scanning electron microscope (SEM, TESCAN VEGA3) coupled to an Oxford Energy Dispersive X-ray (EDX X-Max SDD) at the Leibniz Center for Tropical Marine Ecology (ZMT), Bremen, Germany. Thin sections perpendicular to the direction of growth were used for element mapping in 20 randomly selected spines throughout all bioregions. Thin sections were sputtered with gold (Cressington Sputter Coater 108 auto) and element mapping was accomplished using the VEGA3 and Aztec software. EDX working parameters were set to a beam voltage of 10 keV, a maximum of 5 million counts with a peak pile-up correction, and a process time of 4 min. Dead time was set to 30–50 %.

5.3.7 Environmental data and local $\delta^{18}O_{Seawater}$

Average monthly SST values were derived from Moderate Resolution Imaging Spectroradiometer imagery (MODIS-Aqua 4 km, http://disc.sci.gsfc.nasa.gov/giovanni) from April 2012 to March 2013. During this period, the Galápagos archipelago was not influenced by any strong El-Nino Southern Oscillation (ENSO) event. The Southern Oscillation Index (SOI) varied from −10.4 to 10.5 with an average value of −1.5 ± 5.7.

According to Wellington et al. (1996), annual $\delta^{18}O_{Seawater}$ values of the Galápagos archipelago range from 0.05 to 0.5 ‰ (VSMOW) with an average value of 0.29 ‰ (VSMOW), which was used in this study. Potential correlation between water temperature and measured proxy data were tested with a least squares regression analysis (LSRA) using the software

SigmaPlot® 12.5. No transformations were applied to the measured proxy data prior to any statistical test.

To test whether the measured spine $\delta^{18}O_{Calcite}$ variability at in each bioregion is related to temporal and spatial variability in water temperature and/or $\delta^{18}O_{Seawater}$, we calculated theoretical spine $\delta^{18}O_{Calcite}$ range assuming (1) seasonally varying water temperatures using the average SST amplitude of each bioregion calculated from the MODIS aqua data, (2) seasonally varying $\delta^{18}O_{Seawater}$ values using the maximum amplitude reported in Wellington et al. (1996), and (3) co-variation of water temperature and $\delta^{18}O_{Seawater}$. We used average $\delta^{18}O_{Calcite}$ values of *E. galapagensis* spines from each bioregion and the equation of Kim and O'Neil (1997) for the calculation of theoretical $\delta^{18}O_{Calcite}$ values.

5.4 Results

5.4.1 SST record

The MODIS-Aqua data show a strong seasonal difference in average SST as well as the annual SST amplitude along the environmental gradient from southwest towards the Far North (Fig. 5-1, Table 5-1). Due to the seasonal topographic upwelling, sites lying within the southwestern area show the highest seasonal SST amplitude, with water temperatures

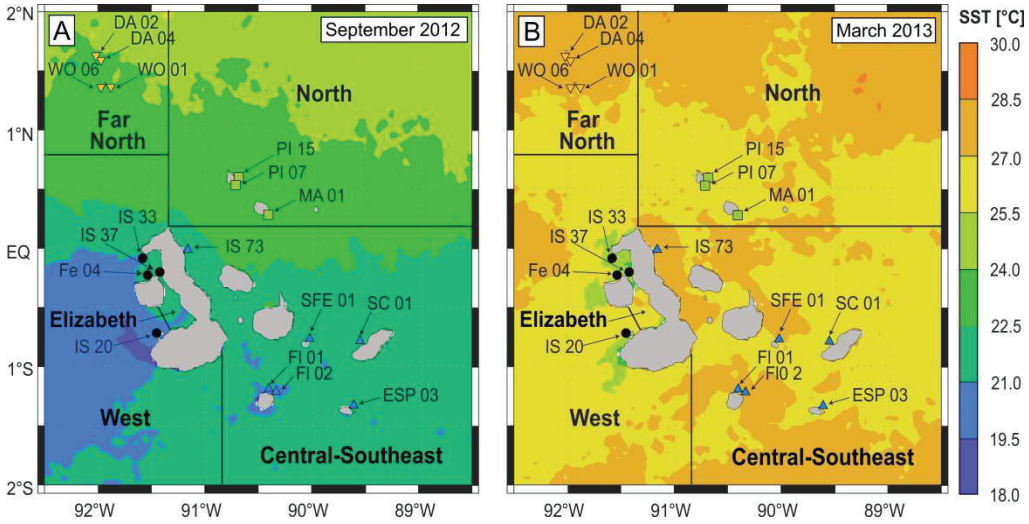

Figure 5-1: Map of the Galápagos Archipelago with the five bioregions Elizabeth, West, Central-Southeast, North and Far North changed after Edgar et al. (2004) with sampling sites grouped according to the corresponding bioregion. **A)** Spatial distribution of MODIS aqua sea surface temperatures throughout the Galápagos Archipelago during the cold dry season in September 2012. **B)** Corresponding sea surface temperature distribution in during the warmer wet season in March 2013.

Table 5-1: Measured $\delta^{18}O_{Calcite}$, $\delta^{13}C_{Calcite}$, and Mg/Ca ratios from *Eucidaris galapagensis* spines sampled throughout the Galápagos archipelago. Average annual water temperatures and annual water temperature amplitudes of each site (April 2012 to March 2013), as derived from the MODIS aqua remote sensing sea surface temperature data set.

Site	Coordinates		$\delta^{18}O_{calcite}$	$\delta^{13}C_{calcite}$	Mg/Ca ratio	Sea Surface Temperature [°C]	
	Latitude	Longitude	[‰VPDB]	[‰VPDB]	[mol%]	Average (±SD)	Annual amplitude
West							
IS 20	0.715850°S	91.34040°W	0.53	0.60	6.51	22.7 (2.60)	7.4
	0.715850°S	91.34040°W	0.51	1.72	5.68		
IS 37	0.267660°S	91.37229°W	0.08	0.77	6.19	23.0 (1.67)	5.1
	0.267660°S	91.37229°W	-0.45	1.21	5.99		
FE 04	0.261942°S	91.44458°W	-0.43	1.23	6.46	22.8 (1.67)	5.3
	0.261942°S	91.44458°W	0.18	1.27	6.79		
IS 33	0.051670°S	91.55880°W	-0.87	1.15	6.34	23.0 (1.66)	5.04
	0.051670°S	91.55880°W	-0.75	0.97	6.39		
Central-southeast							
IS 73	0.01792°S	91.20808°W	-0.48	1.48	6.22	24.4 (2.21)	5.9
	0.01792°S	91.20808°W	0.02	1.24	6.78		
FLO 01	1.22564°S	90.41950°W	-0.37	1.09	6.58	23.6 (2.29)	7.1
FLO 02	1.23299°S	90.42027°W	-0.55	1.47	6.78	23.6 (2.29)	7.1
SF 01	0.80167°S	90.04220°W	-0.90	1.07	6.42	23.7 (2.16)	6.4
	0.80167°S	90.04220°W	0.20	1.26	6.46		
SC 01	0.85469°S	89.56820°W	-0.29	0.97	6.62	23.3 (2.00)	6.3
ESP	1.34813°S	89.63660°W	-1.12	1.27	6.25	24.0 (2.00)	5.3
	1.34813°S	89.63660°W	-0.50	1.16	6.61		
North							
MA 01	0.31283°N	90.40129°W	-0.33	1.54	6.47	24.5 (1.71)	4.9
PI 07	0.54406°N	90.72034°W	-1.37	0.62	6.52	24.6 (1.73)	5.5
	0.54406°N	90.72034°W	-1.33	1.35	6.98		
PI 15	0.54279°N	90.73097°W	-0.59	1.47	6.46	24.6 (1.73)	5.5
	0.54279°N	90.73097°W	-1.09	0.65	6.73		
Far North							
WO 01	1.38696°N	91.81640°W	-0.98	1.13	7.13	25.6 (1.59)	4.8
	1.38696°N	91.81640°W	-0.94	1.53	6.57		
	1.38696°N	91.81640°W	-0.92	1.10	6.61		
WO 06	1.37978°N	91.81830°W	-0.74	1.49	6.44	25.6 (1.59)	4.8
	1.38318°N	91.81110°W	-1.07	1.66	6.21		
DA 02	1.68074°N	91.99950°W	-0.80	2.15	7.06	26.0 (1.57)	4.8
	1.68074°N	91.99950°W	-0.95	2.04	6.33		
DA 04	1.67683°N	92.00752°W	-0.71	2.28	6.93	26.0 (1.57)	4.8

between 19.1 and 26.4 °C and an average value of 22.9 °C. In contrast, locations in the far northern area are characterized by warmer and more stable water temperatures varying between 23.2 and 28.4 °C with an average annual SST of 25.8 °C. For all regions, warmer SSTs occurred during the wet season in January until May and lower SST during the dry season from June to December (Fig. 5-1).

5.4.2 Spine microstructure and preservation

As shown in Fig. 5-2, *E. galapagensis* spines show a typical architecture for cidaroid spines with an outer cortex layer surrounding the inner rectilinear stereom, which can be separated into a denser outer stereom and a less dense inner stereom. All spines showed intact (i.e. non-abraded) outer cortex layers with variable coverage of epibionts or bioerosion (Fig. 5-2A). None of the spines showed apparent signs of disarticulation. Only minor degrees of bioerosion were observed in all bioregions but occurred predominantly in the outer cortex or the central part of the inner stereom which was not used for chemical analysis in this study. We observed no internal cementation within the rectilinear stereom trabeculae of *E. galapagensis* spines independent from the sampling area across the Galápagos archipelago (Fig. 5-2B and C).

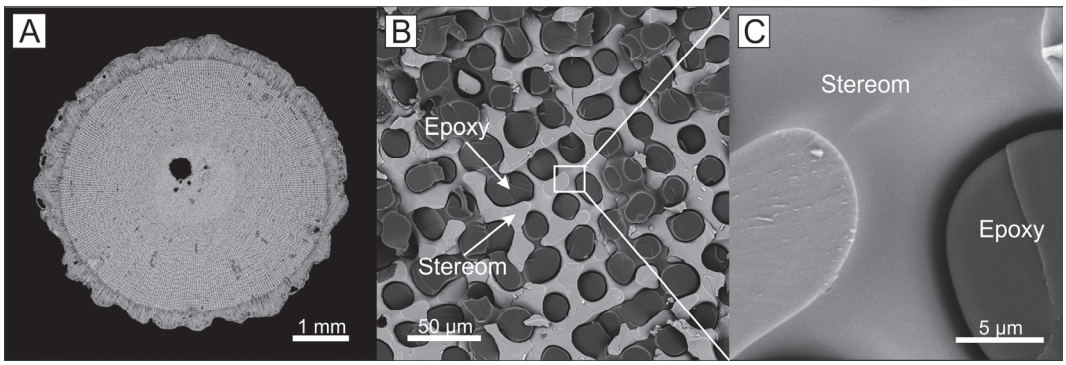

Figure 5-2: Meso- and microstructure of *Eucidaris galapagensis* spines. **A)** Thin section images of a *Eucidaris galapagensis* spine from the Far Northern bioregion (WO-06) sectioned perpendicular to the spine growth axis, seen under transmitted light. **B)** Scanning electron microscope image of the internal spine structure showing the rectilinear structure of the outer stereom (light) filled with epoxy resin (dark) along a fresh fracture surface perpendicular to the spine growth axis. **C)** Close-up of characteristic rectilinear trabeculae with no evident dissolution or cementation.

5.4.3 Oxygen and carbon isotopes

The measured oxygen isotopic composition of the *E. galapagensis* spines varied between −1.37 and +0.53 ‰ with an average isotopic composition of −0.53 ‰ (Table 5-1). Absolute spine $\delta^{18}O_{Calcite}$ values generally agree with other marine calcifying taxa such as mollusks or fish otoliths for the relevant temperature range and do not show the trend

towards strongly depleted $\delta^{18}O_{Calcite}$ values found in previous studies on echinoderm skeletons (Baumiller, 2001; Gorzelak et al., 2012), see Fig. 5-3A. Using the average $\delta^{18}O_{Seawater}$ value of 0.29‰ VSMOW (Wellington et al., 1996), the correlation of measured $\delta^{18}O_{Calcite}$ values against the MODIS-SST data results in a highly significant temperature dependency of the oxygen isotope fractionation factor (α) following the equation

$$1000\ln(\alpha) = 23.03\,(10^3 \cdot T^{-1}[K]) - 47.90 \qquad \text{(Eq. 5.1)}$$

(MS = 2.94, F = 18.102, $p < 0.001$, $R^2 = 0.393$)

where T is the water temperature in kelvin and the fractionation factor (α) is defined as

$$\alpha = \frac{\delta^{18}O_{Calcite} + 1000}{\delta^{18}O_{Seawater} + 1000} \qquad \text{(Eq. 5.2)}$$

The calculated standard error of estimate (SEE) of 0.403 K generally indicates a good accuracy of the $\delta^{18}O_{Calcite}$-based water temperature estimates for *E. galapagensis*. The temperature dependence of the oxygen isotope fractionation in Eq. (5.1) can also be expressed in the $\delta^{18}O_{Calcite} - \delta^{18}O_{Seawater}$ notation as

$$\delta^{18}O_{Calcite}\ (VPDB) - \delta^{18}O_{Seawater}(VSMOW) = 76.377 - (0.26 * T\ [K])$$

(MS = 2.93, F = 18.019, $p < 0.001$, $R^2 = 0.392$) (Eq. 5.3)

The carbon isotopic composition of the spines varied between +0.60 and +2.28 ‰ with an average $\delta^{13}C$ value of 1.30 ‰ VPDB (Fig. 5-3C and Tab. 5-1). We found a significant correlation between $\delta^{13}C_{Calcite}$ and water temperature following the equation

$$\delta^{13}C_{Calcite}(VPDB) = -47.585 + (0.164 * T\ [K]) \qquad \text{(Eq. 5.4)}$$

(MS = 1.174, F = 8.845, $p = 0.006$, $R^2 = 0.240$)

where T is the water temperature in kelvin. Our data do not show a significant correlation between measured $\delta^{13}C$ and $\delta^{18}O$ values of the spine septum (MS = 0.043, F = 0.249, $p = 0.622$, $R^2 = 0.009$), as shown in Fig. 5-3D.

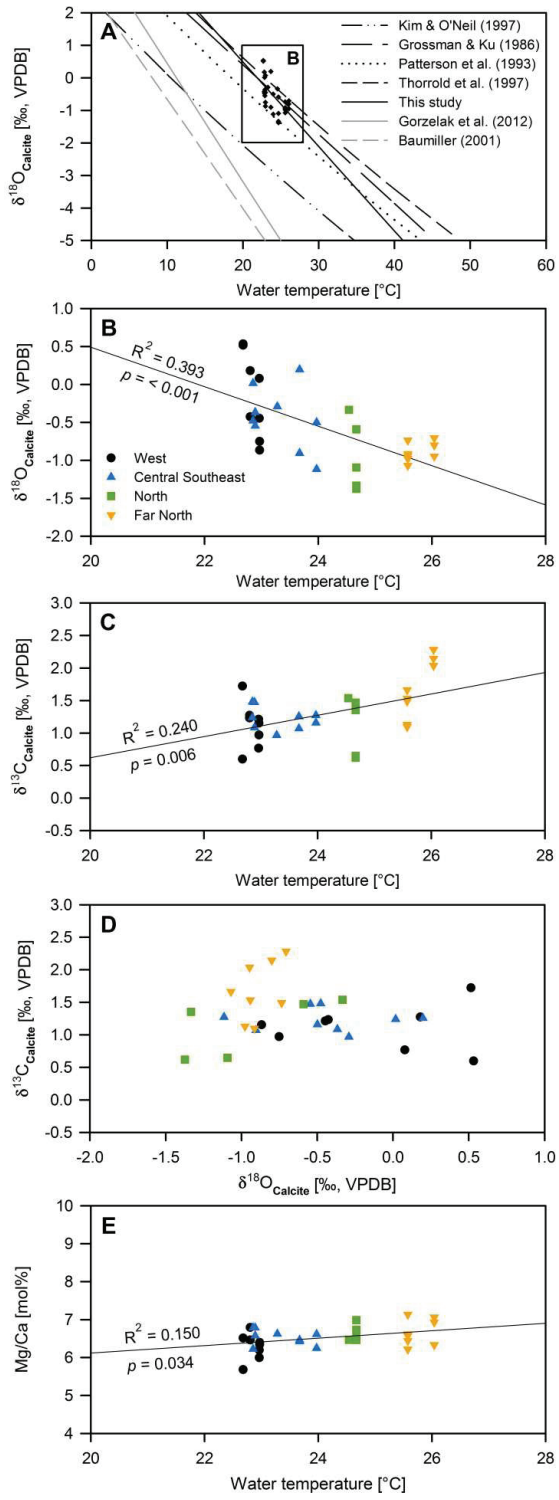

Figure 5-3: Measured proxy data from *Eucidaris galapagensis* spines. **A)** Correlation between measured oxygen isotopic compositions of the spines against average annual water temperature at the sampling sites. Previously determined paleo-temperature curves are plotted for comparison assuming a constant $\delta^{18}O_{Seawater}$ value of 0.29‰ VSMOW. **B)** Close-up of the correlation between measured oxygen isotopic composition against water temperature throughout the Galápagos archipelago. **C)** Measured carbon isotopic composition plotted against water temperature. **D)** Correlation of carbon isotopic composition against oxygen isotopic composition of the individual spines. **E)** Mg/Ca ratios of the septum correlated against average annual water temperatures at the individual sampling sites.

5.4.4 Mg/Ca ratios

Measured Mg/Ca ratios of the *E. galapagensis* spine septum varied between 5.68 and 7.13 mol% with an average value of 6.52 ± 0.31 mol% (Fig. 5-3E and Tab. 5-1). Although the correlation coefficient between Mg/Ca ratios and water temperature is low ($R^2 = 0.150$), LSRA yield statistically significant relation between Mg content and water temperature following the equation

$$\frac{Mg}{Ca}\ [mol\ \%] = 0.0984 * T\ [K] - 22.741 \qquad \text{(Eq. 5.5)}$$

(MS = 0.421, F=4.958, p = 0.034, $R^2 = 0.150$)

where T is the water temperature in kelvin. Measured Mg/Ca ratios from *E. galapagensis* spines do not show a significant relation to oxygen isotopes (MS = 0.239, F = 2.616, p = 0.117, $R^2 = 0.086$). Similarly, we found no significant correlation between Mg/Ca ratios and the carbon isotopic composition of the spines (MS = 0.010, F = 0.105, p = 0.748, $R^2 = 0.004$).

2D element distribution maps of the transversal plane indicate a higher Mg and Ca abundance in the septum compared to the inner stereom (Fig. 5-4) which relates to the lower skeletal density of the stereom (i.e. filling by the epoxy embedding resin). Measured element maps show an even distribution of Mg, Ca, C and O within each skeletal compartment, indicating that bulk Mg/Ca measurements of the septum provides reasonable estimates of average Mg/Ca which are not biased by any spatial inhomogeneity.

5.1.1 Measured versus predicted $\delta^{18}O_{Calcite}$ values

Measured $\delta^{18}O_{Calcite}$ values generally agree with predicted $\delta^{18}O_{Calcite}$ values within the relevant temperature range. However, for samples from the western, central-southeastern as well as northern area, the best agreement between measured and predicted spine $\delta^{18}O_{Calcite}$ ranges is reached when assuming only seasonally varying SST and a constant $\delta^{18}O_{Seawater}$ (see Fig. 5-5A). In contrast, samples from the far northern bioregion show the best agreement between measured and predicted $\delta^{18}O_{Calcite}$ ranges assuming the co-variation of both variables throughout the year (Fig. 5-5C).

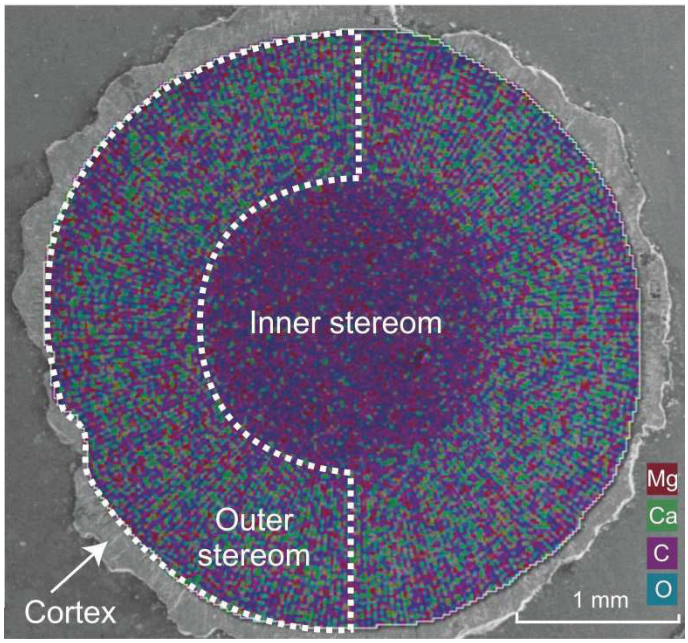

Figure 5-4: The 2D element map perpendicular to the spine growth axis showing a homogenous element distribution within the dense outer stereom as well as the inner stereom of the *Eucidaris galapagensis* spine. Shaded area shows the outer stereom part which was used for stable isotope and Mg/Ca ratio analysis.

5.2 Discussion

5.2.1 Impact of temperature, growth and metabolism on spine $\delta^{18}O$ and $\delta^{13}C$

The measured oxygen isotopic composition of *E. galapagensis* spines shows a highly significant correlation with water temperature which agrees with previous studies on oxygen isotope fractionation in biogenic and synthetic carbonates (Grossman and Ku, 1986; Patterson et al., 1993; Kim and O'Neil, 1997; Thorrold et al., 1997). In contrast to our data, many previous studies on oxygen isotopes in echinoderms showed considerably lower $\delta^{18}O_{Calcite}$ values relative to expected equilibrium values (Weber and Raup, 1966; Weber, 1968; Baumiller, 2001; Gorzelak et al., 2012). Weber (1968) suggested that the primitive respiratory system of echinoderms drives isotope exchange between respiratory CO_2, depleted in ^{13}C and ^{18}O, and thereby result in a simultaneous depletion of the skeletal $\delta^{18}O$ values of echinoderm skeletal structures relative to the theoretical equilibrium values. However, previous studies also reported less depleted or even enriched $\delta^{18}O_{Calcite}$ values in echinoid tests (Weber, 1968; Richter and Bruckschen, 1998; Courtney and Ries, 2015), which is in agreement with our data. Weber (1968) proposed that the more efficient respiratory system of echinoids compared to other echinoderm taxa has a lower impact on isotope fractionation than in other

echinoderm taxa. Therefore, our data support previous studies showing that echinoids have generally the highest potential among previously studied echinoderm taxa and can provide reliable paleoenvironmental proxy signatures by forming their spines close to theoretical oxygen isotopic equilibrium (Weber, 1968; Richter and Bruckschen, 1998; Courtney and Ries, 2015).

Our data show a steeper slope in the temperature-dependence of oxygen isotope fractionation in *E. galapagensis* compared to inorganic calcite or other biogenic calcareous structures such as bivalve shells or fish otoliths (Grossman and Ku, 1986; Kim and O'Neil, 1997; Thorrold et al., 1997) (Fig. 5-3A). In other words, the magnitude of deviation from theoretical equilibrium increases with increasing water temperature, which was also found in previous studies on skeletal structures of different echinoderm taxa (Richter and Bruckschen, 1998; Baumiller, 2001; Gorzelak et al., 2012). Previous authors reasoned that either vital or kinetic isotope effects caused this consistently observed trend in echinoderm skeletons (Baumiller, 2001; Courtney and Ries, 2015). As mentioned above, it has been hypothesized that the increased respiration rates at higher water temperature cause isotope exchange between respiratory CO_2 and seawater HCO^{3-} , causing a simultaneous depletion of oxygen and carbon isotopes with increasing temperature (Weber, 1968; Gorzelak et al., 2012). Alternatively, McConnaughey (1989a; 1989b) suggested that increased growth rates at higher temperatures cause kinetic isotope effects due to CO_2 hydration and hydroxylation, also resulting in a simultaneous depletion of $\delta^{18}O_{Calcite}$ and $\delta^{13}C_{Calcite}$ values in rapidly growing echinoderms (Gorzelak et al., 2012; Courtney and Ries, 2015).

In contrast to most previous studies, we observed an opposing trend for $\delta^{18}O_{Calcite}$ and $\delta^{13}C_{Calcite}$ values which was found to be significantly influenced by water temperature in *E. galapagensis* spines. Thus, our data indicate that oxygen and carbon isotope fractionation in *E. galapagensis* spines is controlled by two different mechanisms or exhibit strong differences regarding the magnitude of the previously suggested mechanism (respiration versus kinetic isotope effects). Thereby, our data allows two different interpretations regarding the effect of respiration and kinetic isotope effects on carbon and oxygen isotope fractionation in *E. galapagensis* spine formation: (1) Higher growth rates at increased water temperatures cause a depletion of only $\delta^{18}O_{Calcite}$ due to kinetic isotope effects whereas higher respiration rates at colder temperatures result solely in a strong depletion of $\delta^{13}C_{Calcite}$ due to the influence of isotopically lighter respirational CO_2. (2) Alternatively, increased respiration rates at higher water temperatures could cause a strong depletion of $\delta^{18}O_{Calcite}$ and only a minor depletion in

$\delta^{13}C_{Calcite}$ while increased growth during the cold but more productive upwelling season causes the predominant depletion of $\delta^{13}C_{Calcite}$ due to kinetic isotope effects.

Previous studies on cidaroid respiration rates showed consistently lower respiration rates than other echinoid taxa (McPherson, 1968; Johnson, 1973), which suggests a generally limited impact of respiration on the isotopic compositions *E. galapagensis* spines. Moreover, McConnaughey (1989a; 1989b) showed a 3–4 times higher impact of kinetic isotope effects on the $\delta^{13}C$ signature of marine calcifiers (~−10 to −15‰) compared to their $\delta^{18}O$ composition (~−4‰). Despite this, our $\delta^{18}O_{Calcite}$ data show an increasing scatter in the colder Western upwelling region, whereas $\delta^{18}O_{Calcite}$ values of spines from the Far Northern bioregion cluster closely together around the average annual water temperature (Figs. 5-3 and 5-5). Assuming year-round spine growth in *E. galapagensis*, a certain section of a fast growing spine most likely provides a relatively more precisely water temperature information than a slow growing spine because it integrates a smaller amount of time into the growth record (e.g. seasonal extrema vs. annual average). Considering the significantly larger scatter of $\delta^{18}O_{Calcite}$ in the Western bioregion whose reconstructed water temperature amplitude almost perfectly agrees with the measured water temperature amplitude, our data suggests faster spine growth of *E. galapagensis* in colder but more productive upwelling areas. Although there are no growth data of *E. galapagensis* available so far, enhanced growth during seasons of increased food supply is commonly observed in other marine heterotrophic calcifiers (Goodwin et al., 2003), in particular for those adapted to highly productive upwelling areas (Müller et al., 2015a). However, the common feeding strategy of sea urchins (grazing on algae and invertebrates) implies only an indirect link between increased primary production in eutrophic upwelling areas and food supply for *E. galapagensis*.

Altogether, generally lower respiration rates in cidaroid sea urchin species (McPherson, 1968; Johnson, 1973), a considerably higher kinetic isotope effect on $\delta^{13}C$ than on $\delta^{18}O$ (McConnaughey, 1989a; McConnaughey, 1989b) and the larger scatter of $\delta^{18}O_{Calcite}$ values from the colder upwelling area, our data support hypothesis (2). Increased growth rates at lower water temperatures which are potentially induced by an indirectly increased food supply due to the higher primary production in the upwelling region cause primarily a $\delta^{13}C_{Calcite}$ depletion due to kinetic isotope effects. In contrast, the suggested simultaneous depletion of $\delta^{18}O_{Calcite}$ and $\delta^{13}C_{Calcite}$ values due to respirational CO_2 has probably only a minor effect on $\delta^{18}O_{Calcite}$ and $\delta^{13}C_{Calcite}$ in *E. galapagensis* spines compared to other echinoid species which, however, might explain the generally lower $\delta^{18}O_{Calcite}$ composition compared to theoretical

equilibrium values, in particular at higher water temperatures (Fig. 5-3). This aspect is further supported by previous studies showing that the temperature dependency of respiration rates in echinoids can also vary over ontogeny (e.g. Greenwood, 1980). However, our data does not allow for thoroughly disentangling the absolute contribution of respirational or kinetic isotope effects on spine $\delta^{18}O_{Calcite}$ and $\delta^{13}C_{Calcite}$ values in *E. galapagensis*. Future laboratory- or field-based studies are needed to understand the absolute contribution of respiration versus kinetic isotope effects on isotope fractionation in *E. galapagensis* spines. Nevertheless, the highly significant correlation between water temperature and spine $\delta^{18}O_{Calcite}$ found in this study suggests that oxygen isotopes from *E. galapagensis* spines can be used as a reliable (paleo-) water temperature proxy.

5.2.2 Seasonal and spatial SST and $\delta^{18}O_{Seawater}$ variability

For equilibrium systems, $\delta^{18}O_{Calcite}$ values are negatively correlated with water temperature at any given isotopic composition of the seawater. Contemporaneously, $\delta^{18}O_{Calcite}$ values are positively correlated with changes in $\delta^{18}O_{Seawater}$ at a given water temperature. Therefore, increasing evaporation during warmer seasons is driving the $\delta^{18}O_{Seawater}$ towards heavier (i.e. more positive) isotopic compositions, partially counteracting the effect of the warmer temperatures on $\delta^{18}O_{Calcite}$. However, seasonal and spatial water temperature variability of the Galápagos archipelago might still introduce considerable seasonal or spatial variations in $\delta^{18}O_{Calcite}$ values of *E. galapagensis* spines (Fig. 5-5A). Likewise, seasonal and/or spatial variations in $\delta^{18}O_{Seawater}$ due to evaporation or changes in dominating ocean currents, precipitation or terrestrial freshwater runoff potentially induce variations in *E. galapagensis* spine $\delta^{18}O_{Calcite}$ values (Fig. 5-5B).

Modeled $\delta^{18}O_{Calcite}$ values show the best agreement with measured $\delta^{18}O_{Calcite}$ values if only seasonal and spatial water temperature variations are considered (Fig. 5-5A–C). Thereby, spines from the colder western, central-southeastern and northern areas provide precise records of annual water temperature amplitudes, whereas $\delta^{18}O_{Calcite}$ values measured in spines from the far northern area consistently underestimate the annual water temperature amplitude assuming a constant $\delta^{18}O_{Seawater}$ of 0.29‰ (VSMOW) (Fig. 5-5A). In contrast, simulated covariation of water temperature and $\delta^{18}O_{Seawater}$ precisely explain the measured amplitude of $\delta^{18}O_{Calcite}$ values for the far northern region but strongly underestimates it for all other regions (Fig. 5-5C).

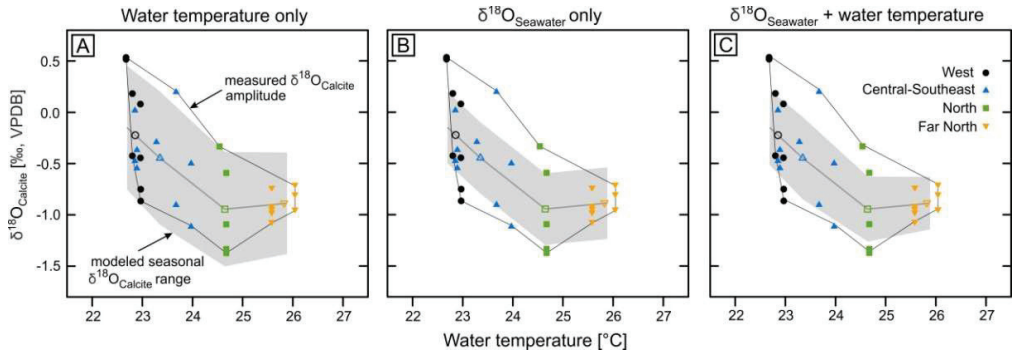

Figure 5-5: Comparison of measured $\delta^{18}O_{Calcite}$ values (closed symbols, surrounded by the black line) and modeled seasonal $\delta^{18}O_{Calcite}$ ranges along the natural water temperature gradient (grey area) for single or combined impact of seasonally varying water temperature and $\delta^{18}O_{Seawater}$ values. **A)** Average isotopic compositions from each bio-region (open symbols, grey line) were used to model seasonal $\delta^{18}O_{Calcite}$ ranges assuming seasonal variation in water temperature and a constant $\delta^{18}O_{Seawater}$ of 0.29‰ VSMOW, **B)** seasonal variation in $\delta^{18}O_{Seawater}$ from 0.05 to 0.5‰ VSMOW as reported by Wellington et al. (1996) and a constant water temperature, and **C)** seasonal co-variation of $\delta^{18}O_{Seawater}$ and water temperature. The equation of Kim and O'Neil (1997) was used to predict spine $\delta^{18}O_{Calcite}$ values.

Wellington et al. (1996) reported a narrow $\delta^{18}O_{Seawater}$ range throughout the Galápagos archipelago with $\delta^{18}O_{Seawater}$ values varying between 0.05 and 0.5 ‰ (VSMOW) and that the influence of $\delta^{18}O_{Seawater}$ variability on the oxygen isotopic composition of corals throughout the Galápagos archipelago is low (< 20%). Furthermore, Wellington et al. (1996) showed that the influence of $\delta^{18}O_{Seawater}$ on skeletal $\delta^{18}O$ values of corals is highest within the western upwelling region (13.2 – 19.1%), decreases towards the central-southeastern area (12.0%), and almost disappears within the northern part of the Central-southeastern bioregion (2.3–9.9%). Thus, it is unlikely to assume that a strong covariation of water temperature and $\delta^{18}O_{Seawater}$ caused the observed $\delta^{18}O_{Calcite}$ pattern in spines from the far northern bioregion because the variation in $\delta^{18}O_{Seawater}$ decreases to negligible values within the central part of the archipelago. Instead, we suggest that water temperature together with variation in spine growth rates cause the observed scatter in $\delta^{18}O_{Calcite}$ of *E. galapagensis* spines. Faster growing spines from the Western bioregion provide more precise water temperature information about seasonal extrema and thereby cover the entire temperature range of the environment (Figs. 5-3 and 5-5). Thereby, our data show the potential of *E. galapagensis* spines to allow the reconstruction of local seasonal water temperature amplitudes. However, further studies on spine growth pattern of *E. galapagensis* are needed to confirm this potential application for reliable reconstructions of seasonal paleo-water temperature amplitudes.

5.2.3 Mg/Ca ratios

Previous studies showed that Mg/Ca ratios of echinoderm skeletons are primarily controlled by water temperature and seawater Mg/Ca ratios (Chave, 1954; Weber, 1973; Richter and Bruckschen, 1998; Dickson, 2002; Dickson, 2004; Ries, 2004). Although Mg/Ca ratios show large differences among different echinoderm taxa, echinoid tests and particularly echinoid spines are characterized by comparably low Mg/Ca ratios of ~3 to ~19 mol% (e.g. Dickson, 2002; Ries, 2004). Although at the lower end of the reported Mg/Ca range in echinoderms, our *E. galapagensis* spine data agrees with previous studies regarding the absolute Mg/Ca ratios in echinoid spines (average measured Mg/Ca ratio of 6.52 ± 0.31 mol%). There is also a good agreement between our data and the low Mg/Ca ratios measured in *Eucidaris tribuloides* (~3–5 mol%) (Ries, 2004), which suggests a consistent trend of relatively low Mg/Ca ratios among species of the genus *Eucidaris*. Despite this variation among different taxa, most studies showed a positive correlation between Mg/Ca ratios and ambient water temperature for echinoid spines which was also found for *E. galapagensis*. However, the correlation coefficient of water temperature versus Mg/Ca ratios for *E. galapagensis* is considerably lower than found for other echinoderm taxa (Weber, 1973; Dickson, 2002). Although Borremans et al. (2009) found salinity to be a main driver influencing variations in Mg/Ca ratios in echinoderms, this is unlikely for *E. galapagensis* as the Galápagos archipelago has a fairly homogenous salinity both spatially and temporally (Wellington et al., 1996; Sakamoto et al., 1998). This indicates that additional biological processes or other environmental factors such as spatial or temporal variation in seawater Mg/Ca ratios modify Mg incorporation in *E. galapagensis* spines.

Previous studies also showed that different biological processes can cause deviations from expected relationship between water temperature and echinoid Mg/Ca ratios. Lavigne et al. (2013) found elemental composition to be invariant among the adult sea urchin *Strongylocentrotus purpuratus* collected from four oceanographically distinct regions along the Californian coast. They hypothesized that geochemical plasticity during early development in contrast to adult stage associated with changes in pCO_2 can cause strong deviations from the expected echinoid test chemistry. Moreover, echinoids are known to incorporate different concentrations of Mg among different skeletal structures as well as within individual skeletal units. For example, within a single spine there is ~2 mol% Mg decrease from the base to the tip (Magdans and Gies, 2004). Differential $MgCO_3$ incorporation processes which can occur on a nanometer-scale (Gorzelak and Salamon, 2013) may resemble a solid solution strengthening mechanism (Magdans and Gies, 2004) and differences in Mg/Ca ratios might

also be attributed to spine ontogeny (Moureaux et al., 2010), secondary infilling of pores, or thickening of the outer septa (Dubois and Ameye, 2001). Alternatively, environmental variability in e.g. water temperature, salinity or seawater Mg/Ca might also explain the measured Mg/Ca ratios (Dickson, 2004; Borremans et al., 2009). As local seawater Mg/Ca values were not available, it was not possible to differentiate between potential environmental and biological processes. However, although statistically significant, the low correlation coefficient between water temperature and Mg/Ca ratios suggests that water temperature does not represent the only mechanism affecting spine Mg/Ca ratios in *E. galapagensis*. Additional controlled laboratory studies are needed to understand the mechanism controlling Mg incorporation in *E. galapagensis* spines, which potentially discloses Mg/Ca ratios in *E. galapagensis* spines as a useful paleoenvironmental proxy system.

5.3 Conclusions

The oxygen isotopic compositions of *E. galapagensis* spines show a significant negative relationship with water temperature throughout the Galápagos archipelago, confirming their potential for paleoenvironmental reconstructions. Spines sampled in the colder upwelling regions show a larger scatter of $\delta^{18}O_{Calcite}$ whereas spines from warmer and more stable areas yield a narrower $\delta^{18}O_{Calcite}$ range. We suggest faster growth rates for individuals occurring in the colder, upwelling-dominated areas and slower growth rates in the warmer northern area causing the observed scatter in spine $\delta^{18}O_{Calcite}$ values. This explanation is supported by a positive correlation of $\delta^{13}C_{Calcite}$ with water temperature, potentially indicating a depletion of $\delta^{13}C_{Calcite}$ due to kinetic isotope effects in particular in colder upwelling areas. Similar to $\delta^{13}C_{Calcite}$, we found a significant correlation between Mg/Ca ratios and water temperature which is, however, potentially confounded by a number of interactive mechanisms.

Considering the steep slope of the $\delta^{18}O_{Calcite}$ –temperature relationship consistent with previous studies on echinoderms and the opposed trend of $\delta^{13}C_{Calcite}$ and $\delta^{18}O_{Calcite}$ with water temperature, our data suggest that processes other than respiration cause the observed deviation from equilibrium fractionation of oxygen isotopes in *E. galapagensis* spines. However, our data do not allow the identification of potential biological mechanisms causing the observed deviation from equilibrium fractionation of oxygen isotopes. Nevertheless, our data show the potential of *E. galapagensis* spines as paleoenvironmental archives, potentially providing sub-seasonal water temperature records if spine architecture and growth patterns can be well constrained.

5.4 Acknowledgements

This project was funded by the Leibniz Center for Tropical Marine Ecology (ZMT) Bremen, Germany. We owe thanks to the editor Dr. Amy Prendergast and two anonymous reviewers for constructive comments which considerably helped improving the manuscript. We also thank Dr. Monika Segl, Dr. Henning Kuhnert (both University of Bremen) and Jule Mawick (ZMT) for help with stable isotope and element analysis, respectively, and Dr. Justin B. Ries for insightful discussions of our data. Special thanks go to the Charles Darwin Research Station, the Charles Darwin Foundation, and the Galápagos National Park authority for helping with logistics in the field. We also acknowledge the MODIS mission scientists and associated NASA personnel for the production of the data used in this study.

6. FOOD FOR THOUGHT: MATHEMATICAL APPROACHES FOR THE CONVERSION OF HIGH-RESOLUTION SCLEROCHRONOLOGICAL OXYGEN ISOTOPE RECORDS INTO SUB-ANNUALLY RESOLVED TIME SERIES

Peter Müller, Marc H. Taylor, André Klicpera, Henry C. Wu, Julien Michel, Hildegard Westphal

Published in

Palaeogeography, Palaeoclimatology, Palaeoecology, 2015. Vol. 440. 763-776

Palaeogeography, Palaeoclimatology, Palaeoecology 440 (2015) 763–776

Contents lists available at ScienceDirect

Palaeogeography, Palaeoclimatology, Palaeoecology

journal homepage: www.elsevier.com/locate/palaeo

Food for thought: Mathematical approaches for the conversion of high-resolution sclerochronological oxygen isotope records into sub-annually resolved time series

Peter Müller [a,*], Marc H. Taylor [a], André Klicpera [a], Henry C. Wu [b], Julien Michel [c], Hildegard Westphal [a,d]

[a] Leibniz Center for Tropical Marine Ecology (ZMT), Bremen, Germany
[b] MARUM, Center for Marine Environmental Sciences, University of Bremen, Germany
[c] Department for Earth Sciences, VU University Amsterdam, The Netherlands
[d] Department of Geosciences, University of Bremen, Germany

ARTICLE INFO

Article history:
Received 28 April 2015
Received in revised form 4 September 2015
Accepted 15 September 2015

Keywords:
Sclerochronology
Bivalve
Otolith
Von Bertalanffy growth function
Growth model
Temporal alignment

ABSTRACT

Oxygen isotope ($\delta^{18}O$) records of incrementally banded marine calcifiers provide high-resolution information about modern and past environmental conditions. However, given their biological origin, these records are often distorted by ontogenetic and seasonal growth pattern. To evaluate their reliability, many studies correlate skeletal $\delta^{18}O$ records with instrumentally measured time series of environmental conditions using a variety of methods to recalculate their temporal framework. Lacking consistency and a limited traceability of many temporal alignment methods underline the need for standardized and flexible method for the temporal alignment of sclerochronological records. Here, two methods for the temporal alignment of sclerochronological data and their application on measured oxygen isotope signatures of a fish otolith and a marine bivalve shell are presented and compared. The first method is a flexible approach using a linear interpolation between carefully selected temporal reference points for recalculating ontogenetic growth effects with an optional extension accounting for seasonal growth oscillations. The second approach uses the seasonally-oscillating Von Bertalanffy growth function parameterized based on the oxygen isotope record to reconstruct the underlying growth model and reconstruct thereby its temporal framework. Using these methods, we re-align $\delta^{18}O$-based water temperature records of a *Carlarius heudelotii* otolith and a *Venus crebrisulca* shell with measured sea surface temperature time series and compare the resulting correlation as well as the different underlying growth models. Our results show that both methods represent useful tools for the temporal alignment of sclerochronological records. However, underlying growth models strongly differ depending on the temporal alignment method and the parameters used for the reconstruction of the temporal framework. This underlines the importance of a careful selection of a particular alignment method depending on the complexity of distortion due to seasonal and ontogenetic growth trajectories. Moreover, we show that both organisms represent reliable paleoenvironmental archives providing sub-seasonally resolved water temperature records.

Personal contribution to Chapter 6:

PM (100 %) designed the study and analyzed the proxy data, PM (30 %) and MHT (70 %) conducted the modelling, PM (70%) and MHT (30 %) interpret the model outputs, PM (50 %), MHT (20 %), AK (10 %), HCW (10%), JM (5 %) and HW (5 %) wrote the manuscript.

6.1 Abstract

Oxygen isotope ($\delta^{18}O$) records of incrementally banded marine calcifiers provide high-resolution information about modern and past environmental conditions. However, given their biological origin, these records are often distorted by ontogenetic and seasonal growth pattern. To evaluate their reliability, many studies correlate skeletal $\delta^{18}O$ records with instrumentally measured time series of environmental conditions using a variety of methods to recalculate their temporal framework. Lacking consistency and a limited traceability of many temporal alignment methods underline the need for standardized and flexible method for the temporal alignment of sclerochronological records. Here, two methods for the temporal alignment of sclerochronological data and their application on measured oxygen isotope signatures of a fish otolith and a marine bivalve shell are presented and compared. The first method is a flexible approach using a linear interpolation between carefully selected temporal reference points for recalculating ontogenetic growth effects with an optional extension accounting for seasonal growth oscillations. The second approach uses the seasonally-oscillating Von Bertalanffy growth function, parameterized based on the oxygen isotope record to reconstruct the underlying growth model and reconstruct thereby its temporal framework. Using these methods, we re-align $\delta^{18}O$-based water temperature records of a *Carlarius heudelotii* otolith and a *Venus crebrisulca* shell with measured sea surface temperature time series and compare the resulting correlation as well as the different underlying growth models. Our results show that both methods represent useful tools for the temporal alignment of sclerochronological records. However, underlying growth models strongly differ depending on the temporal alignment method and the parameters used for the reconstruction of the temporal framework. This underlines the importance of a careful selection of a particular alignment method depending on the complexity of distortion due to seasonal and ontogenetic growth trajectories. Moreover, we show that both organisms represent reliable paleoenvironmental archives providing sub-seasonally resolved water temperature records.

6.2 Introduction

The analysis of incrementally banded calcareous structures of aquatic organisms (e.g. bivalve shells, corals, fish otoliths and others) has become a valuable tool for studying modern as well as ancient climate variability (Andrus, 2011; Schöne and Gillikin, 2013). Using sclerochronological approaches, ontogenetic proxy records such as oxygen isotopes ($\delta^{18}O$) provide high-resolution (sub-daily to sub-seasonal) records of environmental conditions covering time intervals ranging from several months to millennia (Schöne et al., 2004; Surge and Walker, 2005; Schöne et al., 2005b; Hallmann et al., 2008; Lavaud et al., 2013).

To evaluate the reliability of such paleoenvironmental archives, ontogenetic $\delta^{18}O$ records of modern organisms are often compared to and regressed against instrumentally measured environmental variables. However, in order to align these proxy records with instrumental time series, a well-constrained temporal framework throughout the sclerochronological records is required. Besides commonly observed annual growth bands, micro-increments induced by daily or tidal cycles can provide such a temporal framework enabling the conversion of ontogenetic $\delta^{18}O$ records into high-resolution time series (Schöne et al., 2005a; Lavaud et al., 2013). The use of micro-increments for the temporal alignment of sclerochronological data certainly represents the most reliable reconstruction of ontogenetic growth pattern and should be used whenever micro-increments are observable. However, a large number of marine organisms do not provide such well-defined and continuous records of apparent micro-increments. Moreover, seasonal growth variability with growth hiatuses or episodes of enhanced or reduced growth distorts the chronological formation of growth increments in almost every aquatic organism from coastal settings to abyssal depths (Goodwin et al., 2003), complicating the interpretation of measured ontogenetic proxy records in many cases. This distortion is usually further complicated by ontogenetically decreasing growth rates impeding a straightforward conversion of isotope records into a time series.

Many studies on organisms which are lacking apparent micro increments use a variety of approaches to compensate for these issues such as comparing measured $\delta^{18}O_{Carbonate}$ data with modeled theoretical $\delta^{18}O_{Carbonate}$ data based on measured environmental conditions (e.g. Surge et al., 2001; Freitas et al., 2006), applying linear interpolations within the proxy data (e.g. Maier and Titschack, 2010; Welsh et al., 2011), graphic manipulation (stretching or compression) (e.g. Dettman et al., 1999; Versteegh et al., 2012; Bougeois et al., 2014), computation with special software (e.g. Paillard et al., 1996; Walther and Rowley, 2013),

geodesic operations (Nasreddine et al., 2009) or presenting the data without any temporal framework (e.g. Surge and Walker, 2005; Jones et al., 2009; Wang et al., 2013; Gordillo et al., 2015). However, reporting sclerochronological data without any temporal context hampers the direct comparison with measured environmental variables. Other studies using mathematical or graphical approaches often provide little information on important parameters that explain the temporal alignment and impede its replicability. Both aspects clearly underline the need for a flexible and traceable method for temporal alignments when micro-increments are not available.

In response to these shortcomings, we developed two different mathematical approaches for the replicable temporal alignment of sclerochronological data, which cover a wide range of potential applications. Both methods are based on the assumption that characteristic $\delta^{18}O_{Carbonate}$ values throughout the skeletal record can be assigned to corresponding events recorded in the measured environmental variable (e.g. measured $\delta^{18}O$ maxima and minima and corresponding water temperature minima and maxima, respectively). However, this implies that skeletal structures as well as the sampling technique (e.g. micro milling) provide an adequate spatial (i.e. temporal) resolution to ensure the correct identification of such temporal reference points.

The first method uses a simple linear interpolation based on carefully selected reference points throughout the skeletal record (e.g. $\delta^{18}O_{Carbonate}$ maxima/minima) to recalculate the temporal framework. Although linear interpolations have already been used in previous studies, we provide a ubiquitous applicable equation enabling a standardized notation for documenting the temporal alignment of sclerochronological data. This approach allows using an arbitrary number of reference points per year and enables the introduction of growth cessations into the reconstructed time series. The introduction of growth cessations is of particular importance as many calcifying organisms show considerable slowdowns or even growth cessation beyond the upper and/or lower thermal limits (Goodwin et al., 2003). Moreover, we developed an optional extension for the linear interpolation approach which allows the consideration of seasonal growth oscillations throughout the sclerochronological record.

The second method represents the application of an extended version of the Von Bertalanffy growth function (VBGF) (von Bertalanffy, 1934), published by Somers (1988), which models ontogenetic growth trends including a sinusoidal oscillating term accounting for seasonal growth variations. The application of the common VBGF as well as the seasonally-oscillating VBGF (soVBGF) on ontogenetic sclerochronological records is theoretically possible since the

incremental growth of calcified structures mostly corresponds to overall size of an organism (for fish otoliths see e.g. Casselman (1990)) or can directly be related to the same parameter (e.g. shell height in bivalves, see Cloern and Nichols, 1978). By using the distance between selected reference points throughout a sclerochronological record (e.g. local $\delta^{18}O_{Carbonate}$ maxima/minima), and their corresponding timing (e.g. seasonal temperature minima/maxima, respectively), one has all the information needed for an iterative fitting of the soVBGF to individual proxy records.

In this study, we explore the potential of both approaches for the temporal alignment using measured ontogenetic otolith and bivalve shell $\delta^{18}O$ signatures and subsequently calculated water temperature records. The high-resolution $\delta^{18}O_{Carbonate}$ records were measured from one modern Smoothmouth sea catfish otolith (*Carlarius heudelotii*, Valenciennes 1840) and one modern marine bivalve (*Venus crebrisulca*, Lamarck, 1818), sampled on the Banc d'Arguin, Mauritania, NW Africa in November 2011 and March 2008, respectively. The resulting temporal alignments and the underlying growth models are also compared with the most commonly applied temporal alignment method using predicted $\delta^{18}O_{Carbonate}$ time series for the conversion of skeletal records into time series.

Supplemental material includes calculations and raw data of all examples presented in this study and a script for the soVBGF approach based on the R statistical computing language (R Development Core Team, 2013) and are available online (Müller et al., 2015b).

6.3 Material and Methods

6.3.1 C. heudelotii *and* V. crebrisulca *sampling and preparation*

The *C. heudelotii* otolith was removed from an individual caught in November 2011 in the northernmost part of the Banc d'Arguin (central Baie du Lévrier, water depth < 20 m), Mauritania, NW Africa. *C. heudelotii* is a classified as demersal marine–estuarine (ME) species preferring coastal and estuarine environments but reproducing under marine conditions and occurs along the entire West-African coast from Mauritania to Angola (Taylor, 1986; Schneider, 1990).

The *V. crebrisulca* individual used for this study was collected alive in February 2008 on the western central Banc d'Arguin, (20.17°N, 17.10°W) at a water depth of 15 to 20 mbsl (Fig. 6-1). The endobenthic bivalve *V. crebrisulca* occurs in water depth of about 10–30 m along the shelf margin of the Banc d'Arguin (Diop, 1988), which is characterized by intensive upwelling

with the highest upwelling rates during boreal winter months. For details of the study area see Klicpera et al. (2015), Michel et al. (2009) and Sevrin-Reyssac (1993).

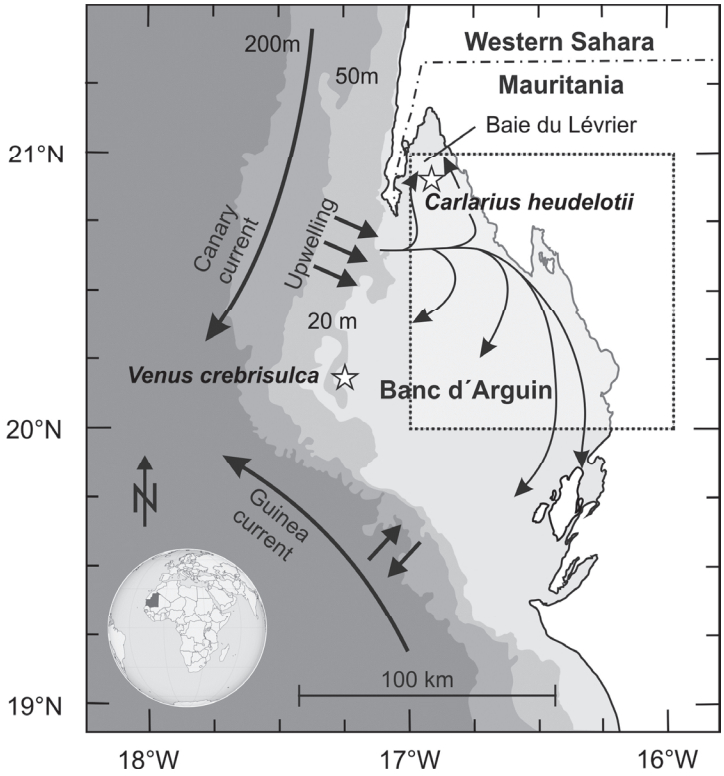

Figure 6-1: The Banc d'Arguin in northern Mauritania. Sampling sites of the *Venus crebrisulca* and *Carlarius heudelotii* individuals are indicated by white stars. Area covered by SST data is indicated by the dotted rectangle.

Otolith thick sections were prepared in the transversal plane through the otolith core (1.0 mm thickness) and for the bivalve shell along the maximum growth direction from the hinge towards the commissure of the left valve (2.0 mm thickness). According to Surge and Walker (2005) for catfish otoliths and Diop (1988) for *V. crebrisulca* shells, age determination of both specimens can be done by counting the prominent dark winter growth bands from the most recent growth band (otolith edge and ventral shell margin, respectively) back through the incremental record toward the ontogenetically youngest growth band. Counting the growth bands revealed an age of 13 years for the *C. heudelotii* and 4.5 years for the *V. crebrisulca* individual, corresponding to 1998 and 2004 as the year of birth/recruitment, respectively.

6.3.2 $\delta^{18}O$ analysis and temperature reconstruction

Sampling for oxygen isotope analysis was accomplished using a Merchantec Micromill equipped with a 150 μm diameter drill bit. The otolith specimen was sampled from the otolith edge towards the core with a constant sample spacing of 100 μm, resulting in 66 discrete

samples. The bivalve shell was sampled along the outer aragonitic shell layer from the hinge towards the ventral margin with a sample spacing of ~500–1500 μm (~585 μm on average), resulting in 50 discrete samples with known distances in between.

Otolith samples (each ~50 μg) were analyzed using a ThermoFinnigan Delta V Plus isotope ratio mass spectrometer equipped with a Gasbench II. Analytical precision of $\delta^{18}O_{Otolith}$ analysis was better than ± 0.08 ‰ VPDB (1σ). Bivalve samples (each ~50-80 μg) were analyzed using a Finnigan MAT 251 isotope ratio mass spectrometer equipped with a Kiel-I device. Repeated standard measurements revealed an analytical precision for $\delta^{18}O_{Bivalve}$ analysis better than ± 0.06 ‰ VPDB (1σ). All $\delta^{18}O_{Carbonate}$ values are reported in per mil with respect to the VPDB standard.

We used the equation of Thorrold et al. (1997) to reconstruct the $\delta^{18}O$-derived water temperatures experienced by the *C. heudelotii* individual ($1000 \ln(\alpha) = 18.56 \cdot (10^3 \cdot T^{-1}[K]) - 32.54$). Conversion of $\delta^{18}O_{Otolith}$ values from VPDB to VSMOW was done using the equation of Gonfiantini et al. (1995). Water temperatures experienced by the *V. crebcisulca* specimen were reconstructed using the equation of Grossman and Ku (1986) corrected for isotopically enrichment of PDB-derived CO_2 of 0.27 ‰ (Gonfiantini et al., 1995) ($T[°C] = 21.8 - 4.69 * (\delta^{18}O_{Aragonite}$ [VPDB] - ($\delta^{18}O_{Seawater}$ [VSMOW] - 0.27))). According to the local salinity/ $\delta^{18}O_{Seawater}$ relationship of Lavaud et al. (2013), we approximated the average $\delta^{18}O_{Seawater}$ (VSMOW) value as 0.68 ‰ and 0.70 ‰ for the periods from 1998 to 2004 (*C. heudelotii* otolith) and 2004 to 2008 (*V. crebrisulca* shell), respectively, using remote sensing SST and SSS data described below.

6.3.3 Environmental data

Weekly resolved Optimal Interpolated Sea Surface Temperature- Version 2 (OI-SST; Reynolds et al., (2002)) and monthly resolved SODA SSS 2.2.4 data (Carton and Giese, 2008) from 1998 to 2008, covering the lifetime of both individuals were used for this study. Both datasets provide a spatial resolution of 1° by 1° (20–21 N, 16–17 W) and provide thereby spatially averaged SST and SSS values for the central and northern Banc d'Arguin including the Baie du Lévrier (Fig. 6-1).

6.3.4 New methods for the temporal alignment of sclerochronological data

6.3.4.1 Linear interpolation with recalculation of seasonal growth oscillation (Method 1)

The linear interpolation approach is based on the assumption that characteristic data points of the skeletal $\delta^{18}O$ record can be assigned to corresponding data points throughout a time series of environmental conditions (e.g. local $\delta^{18}O_{Carbonate}$ minima and maxima corresponding to seasonal water temperature maxima and minima, respectively (Fig. 6-2)). This allows the conversion of sclerochronological records into a time series by using the following equation:

$$t_n = \frac{(d_n - d_{n-1})}{\left(\frac{d^*_n - d^*_{n-1}}{(t^*_n - t^*_{n-1})}\right)} + t_{n-1} \qquad \text{(Eq. 6.1)}$$

where t_n represents the final time of each individual data point in years as a decimal number; d_n is the distance of a data point along the sampling transect (e.g. μm from first data point, see Fig. 6-2); d_n-1 the distance of the previous data point along the measured transect; d^*_n is the distance of the closest next characteristic data point along the measured transect (e.g. next local $\delta^{18}O_{Carbonate}$ maximum or minimum); d^*_n-1 is the distance of the closest previous characteristic data point along the measured transect. The dates for d^*_n and d^*_n-1 are assigned manually by the terms t^*_n and t^*_n-1, which represent the next and the previous corresponding temporal reference points of the measured environmental variable in years as decimal number, respectively (see Fig. 6-2). The term t^*_n-1 is either the calculated time of the previous data point or the manually selected date of a temporal reference point. The identification of characteristic data points (d^*_n) and corresponding temporal reference points (t^*_n) is done by matching characteristic data points of the shell record (e.g. $\delta^{18}O_{Carbonate}$ maxima and minima) and corresponding characteristic seasonal events in measured time series of environmental conditions (e.g. water temperature minima and maxima, respectively). The timing of the very first data point of the proxy record as well as the timing of a data point after an apparent growth cessation is assigned manually based on the observed environmental conditions or the knowledge of the considered organism. In case of more than one apparent growth cessation, an arbitrary number of gaps can be introduced into the temporal alignment. Therefore, temporal reference points defining the end of the growing period needs to be assigned manually (t^*_n). The timing of growth re-initiation corresponding to the following data point is also assigned manually, similar to the very first data point (see examples included in the Supplementary material).

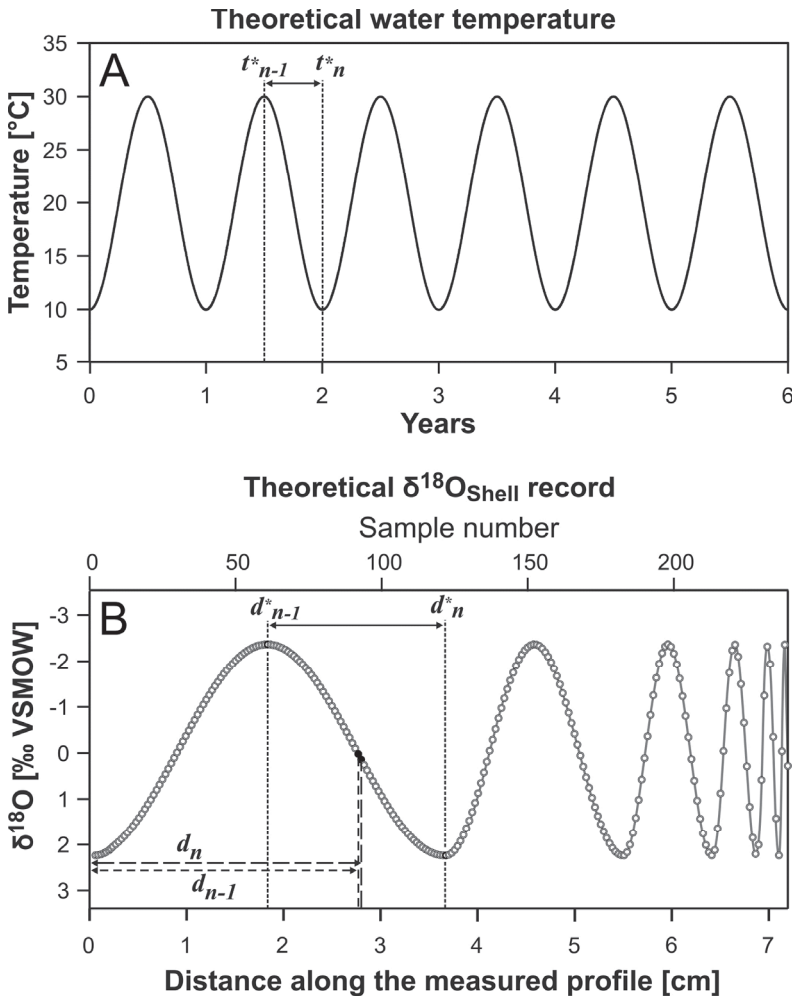

Figure 6-2: Exemplary parameterization of the linear interpolation approach using a theoretical annual water temperature cycle (top) and a corresponding theoretical bivalve shell $\delta^{18}O$ record with ontogenetically decreasing increment width (bottom) from Goodwin et al (2003). By using Eq. (6.1), measured local $\delta^{18}O$ minima/maxima (d^*_n/d^*_n-1) or corresponding reconstructed temperatures maxima/minima are assigned to timing of measured seasonal SST maxima/minima (t^*_n/t^*_n-1). Dashed vertical lines indicate the interval of the theoretical water temperature curve (t^*_n, t^*_n-1) and the intercept between local $\delta^{18}O$ maximum/minimum used for the time-alignment of the exemplarily chosen solid black $\delta^{18}O$ data points (d^*_n/d^*_n-1) and every other data point within this interval.

To incorporate seasonal growth oscillations into the temporal alignment of Eq. (6.1), we developed a sinusoidal correction term based on the soVBGF published by Somers (1988). It allows the correction of the temporal alignment of Eq. (6.1) based on a flexible (i.e. symmetric or asymmetric) sinusoidal growth oscillation following the equation

$$t'_n = t_n \pm \frac{C^*}{2\pi} * \sin\left(\frac{1}{(t^*_n - t^*_{n-1})} * \pi * (t - t^*_{n-1})\right) \qquad \text{(Eq. 6.2)}$$

where t'_n represents the time of each individual data point corrected for seasonal growth oscillation, t_n is the time of each data point resulting from Eq. (6.1), the factor C* modulates the amplitude of seasonal growth oscillation. Thereby, care must be taken to avoid artificial "shrinking" of the organism (in most cases $0 \leq C^* \leq 1$). Similar to Eq. (6.1), $t^*_n - 1$ and t^*_n are defining the (symmetric or asymmetric) time span of the seasonal growth oscillation, such as seasonal maxima/minima of water temperature or food availability.

6.3.4.2 *Application of a seasonally oscillating Von Bertalanffy growth function to sclerochronological records (Method 2)*

Alternatively to Eq. (6.1) and (6.2), we developed a method which emphasizes a more realistic growth model for the temporal alignment by applying the soVBGF (Somers, 1988) on skeletal proxy records to reconstruct individual growth pattern. The soVBGF approach uses characteristic data points of the ontogenetic $\delta^{18}O$ signature for the parameterization of an individual growth function. The resulting growth model then provides the temporal framework for aligning the initial $\delta^{18}O$ record to e.g. an instrumentally measured water temperature record. The temporal alignment using the soVBGF approach is done in three steps. The first step assists in the visual identification of characteristic data points. The second step is a refined iterative fitting of the soVBGF to these characteristic data points. The final step applies a re-estimation of dates for each data point using the prediction of the previously fitted soVBGF. Each step is explained in detail below:

1) The first step is designed to aid in the temporal referencing of data points for later refined fitting. To that end, we start with the simpler non-oscillating form of the VBGF:

$$L_t = L_\infty \left\{1 - e^{-[K(t-t_0)]}\right\} \qquad \text{(Eq. 6.3)}$$

where Lt is the length of the organism (equivalent to the distance along otolith core-edge or shell hinge-to-ventral margin transects) at the age t; t_0 is the theoretical age when $L_t = 0$; L_∞ the asymptotic length (maximum length reached by the mature organism) and K the growth coefficient. According to **Gulland and Holt (1957)**, a plot of growth increments by mean increment length allows for the solving of K and L_∞:

$$\frac{\Delta L}{\Delta t} = \alpha + \beta * \bar{L}_t \qquad \text{(Eq. 6.4)}$$

Where $\partial L / \partial t$ is the change in length (∂L) per change in time (∂t), L_t is the mean length over that increment, and α and β are the regression intercept and slope, respectively (see Fig. 6-3A).

Using the fitted regression parameters, K = -β, and $L_\infty = -\alpha / \beta$. The VBGF can then be rearranged to solve for t:

$$t = \left(\frac{1}{-K}\right) * \log\left(1 - \frac{L_t}{L_\infty}\right) + t_0 \qquad \text{(Eq. 6.5)}$$

where t_0 can be estimated based on an approximate birth/recruitment date of the organism (e.g. by the means of apparent annual growth increments) and provides a base (i.e. starting point) for the alignment of the ontogenetic record with environmental data. Fig. 6-3A shows an example of a Gulland and Holt plot using $\delta^{18}O_{Cabonate}$ derived water temperature maxima/minima for defining annual growth increments for the *C. heudelotii* otolith. Using the fitted values for K and L_∞, and an estimate for t_0 based on the approximate birth/recruitment date of the organism, one can reconstruct a first estimate of sample dates for each sclerochronological (e.g. $\delta^{18}O$) data point, which aids in the identification of temporal-reference points during comparison to environmental time series.

2) Following the identification of temporal-reference points, a refined fitting is accomplished with the soVBGF (Somers, 1988):

$$L_t = L_\infty \left\{1 - e^{-[K(t-t_0) + S_{(t)} - S_{(t_0)}]}\right\} \qquad \text{(Eq. 6.6)}$$

with

$$S_{(t)} = \left(\frac{C*K}{2\pi}\right) * \sin 2 * \pi * (t - t_s) \qquad \text{(Eq. 6.7)}$$

where the term $S_{(t)}$ models the seasonal sinusoidal oscillation of growth whose amplitude is controlled by the parameter C ($0 \leq C \leq 1$) and beginning of the sinusoidal oscillation is defined by t_s. The addition of the term $S_{(t0)}$ in Eq. (6.6) ensures that the soVBGF passes through t_0 when length equals zero. Eq. (6.6) is iteratively fitted to the time-referenced data points. Given the non-linear nature of the VBGF, all parameters must be solved using an optimized algorithm as e.g. a non-linear least squares estimate with the Solver add-in for Microsoft EXCEL or the R function "nls". An example of this fitted model for the *C. heudelotii* otolith $\delta^{18}O$ record is shown in Fig. 6-3B.

3) The third step represents the calculation of a look-up table, consisting of predicted otolith/shell size at a given age/time (L_t) resulting from the fitted soVBGF model (Eq. (6.6)). This lookup-table is necessary in that the soVBGF cannot be rearranged to solve for t given L_t

in the same way that the VBGF can (Eq. 6.5). Using the lookup table, all sclerochronological data points can be assigned a date.

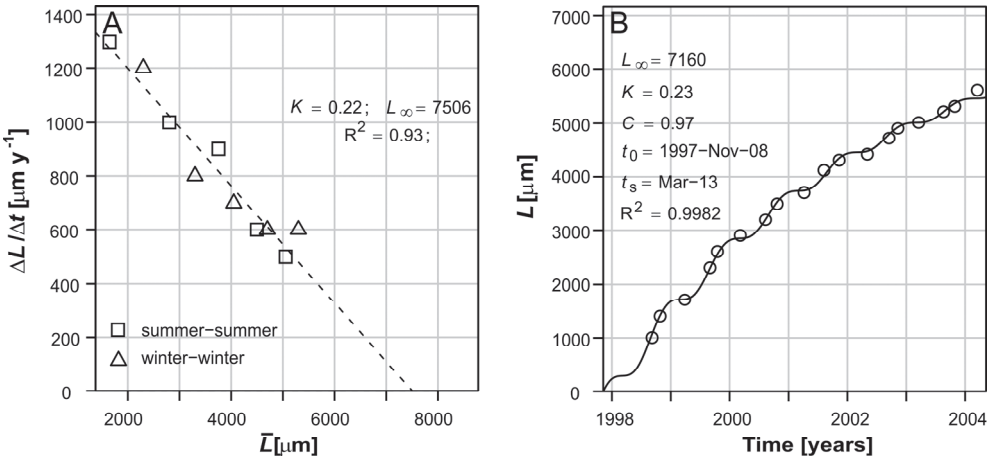

Figure 6-3: A) Gulland and Holt plot of annual ($\delta^{18}O$ -derived) *Carlarius heudelotii* otolith growth increment thickness ($\partial L/\partial t$) as a function of mean otolith size (L). Rectangles and triangles represent consecutive distances between two adjacent local $\delta^{18}O$-based water temperature maxima (summer) and minima (winter), respectively, plotted against their mean distance from otolith core. The linear regression through the data points $\partial L/\partial t = \alpha + \beta$ provides a first estimate of the growth constant, $K = -\beta$, and the infinite otolith size, $L_\infty = -\alpha/\beta$. **B)** soVBGF model (line) fitted to time-referenced distances between reconstructed water temperature values (points) for the *Carlarius heudelotii* otolith record. Time axis tick marks correspond to January 1st of the respective year.

6.3.5 Temporal alignment applied to the otolith and bivalve records

The *C. heudelotii* otolith record was time aligned using the linear interpolation approach assuming winter growth cessations (LI-WGC), the linear interpolation assuming year-round growth with strong seasonal growth oscillations (LI-SGO) and the soVBGF approach assuming year-round growth with season growth oscillations (soVBGF). The *V. crebrisulca* record was converted into a time series using the linear interpolation approach assuming year-round growth (LI) and the soVBGF approach with seasonal oscillations in year-round somatic growth (soVBGF).

In addition to the new methods, we aligned the $\delta^{18}O$ records of the *C. heudelotii* otolith and the *V. crebrisulca* shell with the measured SST record by modelling a theoretical $\delta^{18}O_{Carbonate}$ time series covering the lifetime of both organisms (SST/SSS models). Therefore, we used the SST and SSS data as well as the local Salinity/ $\delta^{18}O_{Seawater}$ relationship published by Lavaud et al. (2013) to predict weekly resolved $\delta^{18}O_{Otolith}$ and $\delta^{18}O_{Shell}$ values from 1998 to 2004 and 2004

to 2008, respectively. Modeling of theoretical $\delta^{18}O_{Carbonate}$ values was done using the same equation as used for the otolith and shell temperature reconstruction but in a reversed manner. The temporal alignment was done by tying the measured $\delta^{18}O_{Carbonate}$ values to the predicted values aiming for the best fit between both records. The underlying growth models were calculated using the position of every sample along the measured transect relative to the reconstructed date of shell/otolith increment formation.

6.3.6 Temporal alignment applied to the otolith and bivalve records

6.3.6.1 Correlation of temporarily aligned otolith and shell records with environmental data

Least squares regression analysis (LSRA) was used to test the correlation between time-aligned otolith and bivalve shell water temperature records and the SST data. Therefore, weekly resolved SST data were further interpolated according to the exact result of the temporal alignments. In case of heteroscedasticity or non-normal distribution of the residuals which impedes a LSRA, reconstructed water temperature values were transformed prior to the LSRA using a log transformation (*C. heudelotii* LI-WGC model, *C. heudelotii* LI-SGO model, *V. crebrisulca* soVBGF model) or a cube transformation (*V. crebrisulca* SST/SSS model).

6.4 Results

6.4.1 Reconstructed water temperature records

6.4.1.1 C. heudelotii water temperature record

The *C. heudelotii* $\delta^{18}O$ record is characterized by a sinusoidal pattern, alternating between absolute maximum and minimum values of +1.43 and −0.85 ‰, respectively, and an average $\delta^{18}O$ value of +0.33 ‰ with a 1σ standard deviation of ± 0.53 ‰ (see Fig. 6-4A). The early juvenile and the late adult part of the otolith water temperature record (<1000 and >5600 μm distance from otolith core) do not show clear seasonal patterns which might bias the temporal alignment. Thus, only the intercept in between showing clear seasonal cycles were used for the temporal alignment. After excluding early juvenile and late adult parts of the record, the remaining late juvenile to early adult $\delta^{18}O$ record varies between +1.43 and −0.51 ‰, with an average $\delta^{18}O$ composition of +0.45 ± 0.46 ‰. Using the equation of Thorrold et al. (1997) and assuming a constant $\delta^{18}O_{Seawater}$ value of +0.68 ‰VSMOW for the period from 1998 to 2004, the measured $\delta^{18}O_{Otolith}$ values translate into water temperatures ranging from 17.4 to 26.5 °C with an average water temperature of 22.0 ± 2.14 °C. The

reconstructed water temperature values are in very good agreement with measured SST ranging from 17.6 to 26.4 °C with an average SST of 21.2 ± 2.29 °C between 1998 and 2004.

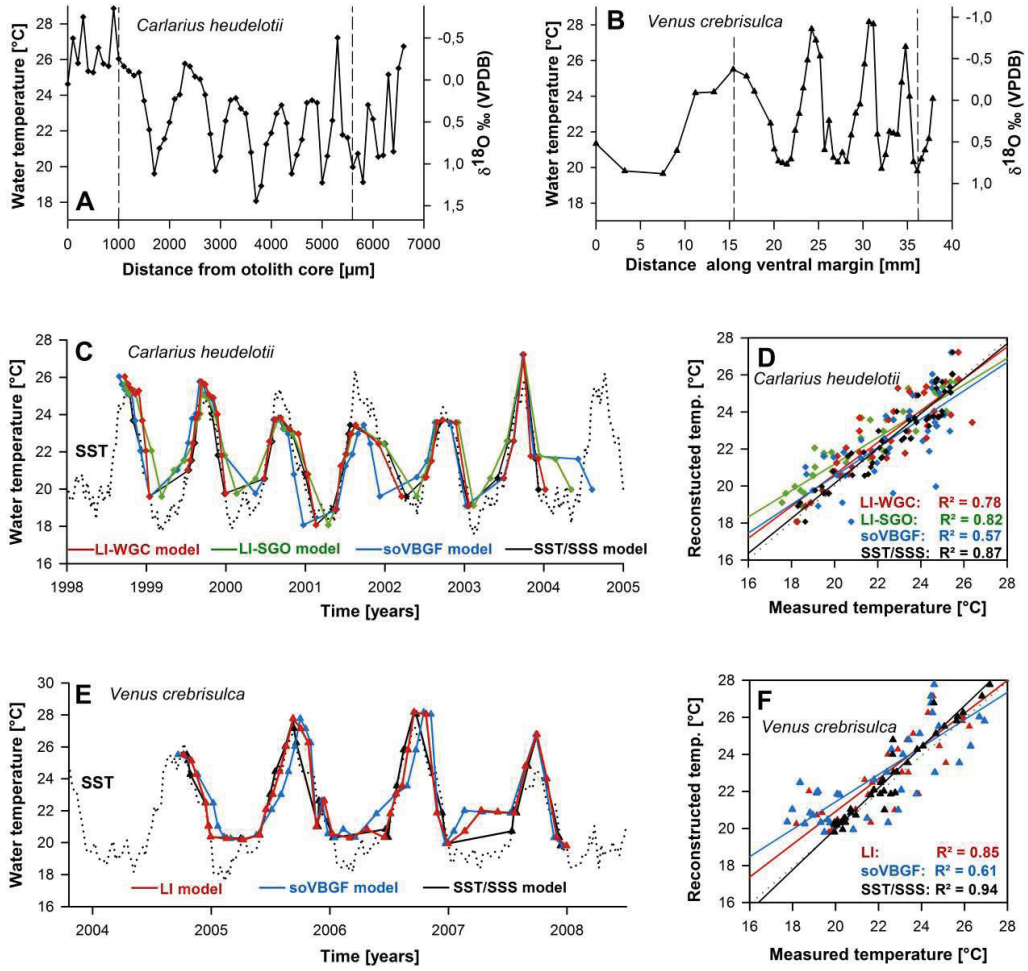

Figure 6-4: A and **B)** Measured ontogenetic $\delta^{18}O$ records and reconstructed water temperatures of the *Carlarius heudelotii* otolith (A) and the *Venus crebrisulca* shell (B). Dashed vertical lines confine the intercepts with clear seasonal oscillations used for the time-alignment. **C)** Optimal Interpolated Sea Surface Temperature (SST) and the temporal alignments of the time-aligned *Carlarius heudelotii* water temperature record using the linear interpolation with winter growth cessations (LI-WGC model), the linear interpolation with seasonal growth oscillation (LI-SGO model), the seasonally oscillating Von Bertalanffy growth function (soVBGF model) and the temporal alignment using the predicted $\delta^{18}O_{Otolith}$ record (SST/SSS model). **D)** Correlation between time-aligned *Carlarius heudelotii* water temperature record and OI-SST data. **E)** OI-SST (SST) and temporal alignments of the *Venus crebrisulca* water temperature records using a linear interpolation (LI model), the seasonally oscillating Von Bertalanffy growth function (soVBGF model) and the temporal alignment using the predicted $\delta^{18}O_{Shell}$ record (SST/SSS model). **F)** Correlation between the time-aligned *Venus crebrisulca* water temperature record and OI-SST data.

6.4.1.2 V. crebrisulca *water temperature record*

The measured *V. crebrisulca* $\delta^{18}O$ profile shows a sinusoidal pattern with absolute maximum and minimum values of +0.89 and −0.92 ‰, respectively and an average $\delta^{18}O$ composition of +0.24 ± 0.53 ‰ (see Fig. 6-4B). Applying the Grossman and Ku (1986) equation assuming a constant $\delta^{18}O_{Seawater}$ of +0.7 ‰ VSMOW, these $\delta^{18}O$ values translate into water temperatures ranging between 19.65 and 28.17 °C with an average water temperature of 22.73 ± 2.49 °C (see Fig. 6-4B). The reconstructed water temperature range and the average water temperature are in very good agreement with the SST data from 2004 until 2008 (17.6 to 27.3 °C, average SST = 21.4 ± 2.58 °C).

6.4.2 *Temporal alignment*

6.4.2.1 C. heudelotii *otolith records*

For the LI-WGC model, we used the linear interpolation of Eq. (6.1) assuming a growth cessation during the cold upwelling season in winter/spring. Seasonal otolith temperature maxima (d^*_2), seasonal otolith temperature minima (d^*_3) and the first data points following the water temperature minima (d^*_1) were used as reference points throughout the otolith temperature record, corresponding to observed summer water temperature maxima(t^*_2), onset of the winter upwelling season (t^*_3) and termination of the winter upwelling season (t^*_1), respectively (see Table 6-1). Since the onset as well as the duration of the upwelling season is variable, temporal reference points confining the upwelling season (d^*_1 and d^*_3) were adjusted for every year based on the measured SST data (see Table 6-1). The resulting time-aligned otolith water temperature reconstruction accurately reproduces the seasonal SST cycle of the OI-SST dataset between 1998 and 2004 (Fig. 6-4C). LSRA shows a highly significant correlation ($p < 0.001$) between reconstructed and measured SST with an R^2 of 0.78 ($F = 156.36$, $df = 10$). The mean absolute error (MAE) indicates a precision of the otolith water temperature reconstruction of ± 0.84 °C (see Fig. 6-4C and D).

Alternatively, Eq. (6.1) and Eq. (6.2) were applied for modeling year round otolith growth with seasonal growth oscillation (LI-SGO model). Seasonal otolith maximum and minimum temperatures were used as reference points (d^*_1 and d^*_2), corresponding to the measured winter SST minimum (t^*_1) and summer SST maximum (t^*_2), respectively (see Tab. 6-1). After the first temporal alignment, temporal reference points corresponding to the winter minima (t^*_1) were re-fitted to increase the match of reconstructed and measured water temperature records. Similarly, the ontogenetically decreasing amplitude of seasonal growth oscillations was

approximated by iteratively fitting of annual C* values, matching up reconstructed and measured water temperature records. Thereby, we re-modeled an increase in otolith growth rates during summer and a decrease in otolith growth rates during winter with an ontogenetically decreasing magnitude (see Tab. 6-1). The resulting LI-SGO-model water temperature record is in very good agreement with measured SST time series between 1998 and 2004 (Fig. 6-4C). LSRA yielded a highly significant correlation ($p < 0.001$) with a R^2 of 0.82 ($F = 200.74$, $df = 45$). The MAE indicates a precision of the temperature reconstruction of ± 1.08 °C (see Fig. 6-4C and D).

Table 6-1: Temporal alignment parameters of the otolith and bivalve shell water temperature records using the linear interpolation approach. **Top)** *Carlarius heudelotii* linear-interpolation with winter growth cessation model (LI-WGC model). **Middle)** *Carlarius heudelotii* linear-interpolation with seasonal growth oscillation (LI-SGO model). **Bottom)** *Venus crebrisulca* linear interpolation with year-round growth (LI model).

# Year	Growth period	Ann. Inc. width [cm]	# Days	# Samples	% First year growth	Temporal reference points t^*_1	t^*_2	t^*_3	C^*
***C. heudelotii* (LI-WGC model)**									
1	23 Sept-04 Feb*	0.08	133	8	-	1998.52**	1998.73	1999.04*	-
2	09 Jun-31 Dec	0.12	176	12	100	1999.52	1999.69	2000.00	-
3	24 May-16 Feb*	0.08	238	8	67	2000.48	2000.69	2001.13*	-
4	17 May-17 Mar*	0.07	303	7	58	2001.38	2001.63	2002.21*	-
5	09 Jul-22 Jan*	0.06	197	6	50	2002.52	2002.73	2003.06*	-
6	01 Jun-04 Jan*	0.06	187	6	50	2003.50	2003.75	2004.01*	-
***C. heudelotii* (LI-SGO model)**									
1	23 Sept –31 Dec	0.07	99	8	-	-	1998.73	-	0.9
2	Full Year	0.12	365	12	100	1999.19	1999.69	-	0.9
3	Full Year	0.08	365	8	67	2000.13	2000.69	-	0.9
4	Full Year	0.07	365	7	58	2001.29	2001.63	-	0.2
5	Full Year	0.06	365	6	50	2002.40	2002.73	-	0
6	Full Year	0.06	365	6	50	2003.12	2003.75	-	0
7	-	-	-	-	-	2004.34	-	-	-
***V. crebrisulca* (LI model)**									
1	Full Year	0.753	-	3	-	-	-	-	-
2	Full Year	2,050	365	11	100	2004.44**	2004.77	2005.00*	-
3	Full Year	0.616	365	13	30.05	2005.40	2005.69	2006.02*	-
4	Full Year	0.540	365	11	26.34	2006.46	2006.71	2007.00*	-
5	Full Year	0.402	365	9	19.61	2007.56	2007.75	2008.00*	-

*) Following year; **) Date was used for the calculation of annual growth rates, not for time alignment

For the soVBGF model, we used the end of spring warming, the onset of autumn cooling (confining the visible summer high-temperature plateaus in the otolith record) and the winter minimum (i.e. the middle of the upwelling season) as temporal reference points. All

parameters used for the soVBGF model derived from the iterative fitting (see Fig. 6-3B) are reported in Tab. 6-2. Using the soVBGF approach, reconstructed water temperatures also reproduce the observed seasonal SST cycle from summer 1998 until winter 2003/2004. The correlation between the resulting otolith-derived water temperature time series and the measured SST time series is highly significant ($p < 0.001$) with an R^2 of 0.57 ($F = 59.66$, $df = 45$) with an MAE of ± 1.16 °C, (see Fig. 6-4C and D).

The SST/SSS model also results in a very good agreement between reconstructed and measured water temperature. The correlation between reconstructed otolith temperature record and the measured water temperature record from 1998 to 2004 is highly significant ($p < 0.001$) with an R^2 of 0.88 ($F = 340.47$, $df = 45$) with an MAE for temperature reconstruction of 0.65 °C (see Fig. 6-4C and D).

Table 6-2: Temporal alignment parameters for the *Carlarius heudelotii* otolith (top) and the *Venus crebrisulca* shell records using the seasonally oscillating Von Bertalanffy growth function (soVBGF). Significance levels: *<0.05, **<0.01, ***<0.001

Parameter	Estimate	Std. Error	*t* value	*p*-value
C. heudelotii				
L_∞	7160	237.5	30.148	$2.04*10^{-13}$***
K	0.2324	0.01615	14.387	$2.31*10^{-9}$***
C	0.9715	0.2478	3.92	0.00176**
t_0	27.87	0.04004	696.031	$2*10^{-16}$***
t_s	0.195	0.02445	7.975	0.0000231***
V. crebrisulca				
L_∞	47280	4219	11.206	0.0000101***
K	0.309	0.07096	4.354	0.00334***
C	0.6051	0.3165	1.912	0.09748
t_0	33.37	0.6217	53.679	$2.04*10^{-10}$***
t_s	0.3931	0.08927	4.404	0.00314***

6.4.2.2 V. crebrisulca *shell record*

Similar to the otolith, only the intercept of the *V. crebrisulca* shell record with clearly identifiable seasonal water temperature cycles was used for the temporal alignment (15.4 - 37.8 mm distance from hinge, see Fig. 6-4B). We applied the linear interpolation of Eq. (6.1), assuming year-round growth, to convert the water temperature record into a time series. To align the reconstructed water temperatures with the measured SST, we used seasonal

temperature maxima (d^*_2), the first data point of a relative long cold period (d^*_3) and the last data point of this cold period (d^*_1) as reference points. These reference data points correspond to the measured annual summer SST maximum (t^*_2), onset of the winter upwelling season (t^*_3) and termination of the winter upwelling season (t^*_1), respectively (Tab. 6-1). The resulting time series of the reconstructed water temperature is in very good agreement with the measured SST for the entire lifespan of the *V. crebrisulca* individual (see Fig. 6-4E). LSRA revealed a highly significant correlation ($p < 0.001$) between reconstructed and measured SST with an R^2 of 0.76 ($F = 119.94$, $df = 37$) and an MAE of ± 1.10 °C (see Fig. 6-4E and F).

The parameterization of the soVBGF approach was done using the reconstructed seasonal water temperature maxima and one centered data point for each cold season as temporal reference points. These points correspond to seasonal SST maxima and the middle of the upwelling season, respectively. All parameters of the soVBGF are reported in Tab. 6-2. The time-aligned *V. crebrisulca* water temperature record reproduces the measured seasonal SST cycle between 2004 and 2008 (see Fig. 6-4E). LSRA yielded a highly significant correlation ($p < 0.001$) with an R^2 of 0.62 ($F = 60.43$, $df = 37$). The MAE indicates a precision of the temperature reconstruction of ±1.41 °C (see Fig. 6-4E and F).

The temporal alignment of the SST/SSS model of the *V. crebrisulca* shell record also reproduces to the measured SST time series for the lifetime of the organism (2004 to 2008). The correlation between reconstructed and measured water temperature is highly significant ($p < 0.001$) with an R^2 of 0.94 ($F = 551.11$, $df = 37$) and a MAE of the temperature reconstruction of 0.48 °C (see Fig. 6-4E and F).

6.5 Discussion

6.5.1 Fidelity of temporal alignments and underlying growth models

All methods yield highly significant correlations between the $\delta^{18}O$-derived water temperature reconstructions of the *C. heudelotii* otolith and *V. crebrisulca* shell record with measured SST data (Fig. 6-4). Hence, all four temporal alignment methods (simple linear interpolation, linear interpolation with seasonal growth oscillation, soVBGF and the SST/SSS model) are generally useful approaches for the conversion of ontogenetic records into time series. However, reconstructing the temporal framework of sclerochronological records implies the reconstruction of the underlying growth models. This in turn enables the visualization,

assessment and potential modification of these growth models in order to evaluate and improve the fidelity of the reconstructed time series (Fig. 6-5A and B). Although the ontogenetic growth trends calculated by the different methods look generally similar (Fig. 6-5A and B), the reconstructed seasonal growth pattern strongly differ depending on method and model parameters (Fig. 6-5C–D).

For the LI-WGC otolith growth model, daily growth rates for the warm season vary between 1.5 and 6.5 μm/day with an ontogenetically decreasing trend. These values translate into a theoretical temporal resolution of the water temperature record of 15–66 days/sample, decreasing over the lifetime of the organism. Similarly, daily growth rates during the cold season vary between 1.6 and 5.4 μm/day which corresponds to a temporal resolution of 19–

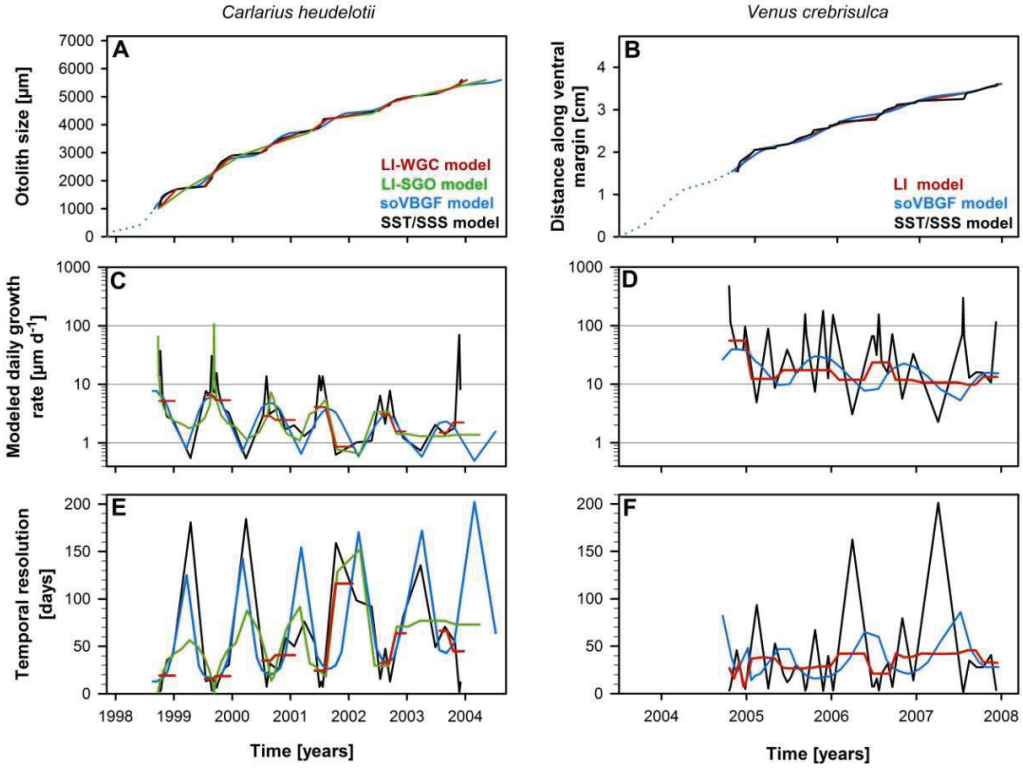

Figure 6-5: A and B) Ontogenetic growth trajectories for the *C. heudelotii* otolith based on the linear interpolation with winter growth cessations (LI-WGC model), linear interpolation with seasonal growth oscillation (LI-SGO model), seasonally oscillating Von Bertalanffy Growth Function (soVBGF model) as well as the temporal alignment using predicted $\delta^{18}O_{Otolith}$ values (SST/SSS model) and the *V. crebrisulca* shell (B) using the linear interpolation (LI model), seasonally oscillating Von Bertalanffy Growth Function (soVBGF model) and the temporal alignment using the predicted $\delta^{18}O_{Otolith}$ shell record (SST/SSS model). **C** and **D)** Modelled daily growth rates of the different growth models for the *Carlarius heudelotii* otolith (left) and the LI and sVBGF model for the *Venus crebrisulca* shell (right). Note the logarithmic scale of the axis of ordinate. **E** and **F)** Theoretical temporal resolution of the water temperature reconstructions based on the growth models of the *Carlarius heudelotii* otolith (left) and the *Venus crebrisulca* shell (right).

116 days/sample with an ontogenetically decreasing trend. Although the LI-WGC model provides realistic estimate of ontogenetic growth trajectories (Fig. 6-5A), it is not able to account for seasonal growth oscillations which are, however, indicated by the initial otolith water temperature record. In contrast, if seasonal growth oscillations are apparently low, as it is the case for the *V. crebrisulca* specimen, linear interpolations represent a more reliable method for recalculating ontogenetic as well as seasonal growth trajectories. Using the LI-model, the *V. crebrisulca* record is described by daily growth rates of 10–55 and 10–13 μm/day, corresponding to a theoretical temporal resolution of 20–43 days/sample and 36–42 days/sample during the warm season and the upwelling season, respectively (see Fig. 6-4E and F and Fig. 6-5D).

The LI-SGO model is based on Eq. (6.1) and (6.2), where Eq. (6.2) is introducing seasonal growth oscillations into the linear interpolation growth model. Using this approach, we modeled an asymmetrical acceleration of otolith growth during the warm season followed by a slowdown of otolith growth during the cold season, as indicated by the course of the initial $\delta^{18}O$ record. This approach yields an improved seasonal growth model and also increases the correlation coefficient between the temporarily aligned *C. heudelotii* otolith record and the measured SST (see Figs. 6-4 and 6-5). Thereby, the LI-SGO model is characterized by daily growth rates of 1.4–100.8 μm/day during the warm season, corresponding to a temporal resolution of 1–72 days/sample. During the cold season, daily growth rates are 1.1–1.7 μm/day, translating into a theoretical sampling resolution of 57–152 days/sample. Similar to the LI-WGC otolith growth model, annual growth rates show a consistent decrease with increasing age, reducing the temporal resolution of the water temperature record over time.

Using the soVBGF approach, modeled daily growth rates of the *C. heudelotii* individual are 0.1–0.8 μm/day for the cold season and 3–8 μm/day for the warm season. Reconstructed daily growth rates of the *V. crebrisulca* individual indicate faster growth of 5–10 μm/day during the warm season and 15–40 μm/day during the cold season. These growth rates translate into a theoretical temporal resolution for the *C. heudelotii* otolith record of 10–35 days/sample during the warm season and 125–170 days/sample during the cold season. In contrast, relatively faster and more constant growth of the *V. crebrisulca* individual provides a similar temporal resolution of the skeletal proxy record (15–28 days/sample for the cold season and 45–90 days/sample for the warm season) using a sample spacing of only 585 μm on average (see Fig. 6-5). While the *C. heudelotii* otolith growth pattern is characterized by almost an entire shutdown of growth during the cold season (C= 0.97), the seasonal variability of *V.*

crebrisulca shell growth is less pronounced (C=0.61) with the period of maximum growth during the onset of the cold season (see Tab. 6-2 and Fig. 6-5B and D).

The temporal alignments using the SST/SSS approach result in the best correlation between reconstructed and measured water temperature for both organisms (Fig. 6-4). This result is generally not surprising as every data point of the reconstructed water temperature records is tied to the measured SST data, not considering a realistic growth model rather than aiming for the best match between both records. For the *C. heudelotii* otolith, modeled daily growth rates using the SST/ SSS approach vary between 0.5–0.8 μm/day for the cold season and 7.8–37.5 μm/day for the warm season. This corresponds to temporal resolution of the otolith of 54.6–186.3 days/sample during the cold season and 2.7–49.2 days/sample for the warm season. Thereby, the overall otolith growth model provides realistic estimates for seasonal otolith growth variations with a remarkable similarity to the soVBGF model but with a slightly less pronounced ontogenetic decrease in annual growth rates (Fig. 6-5C and E). However, in contrast to the *C. heudelotii* otolith, the SST/SSS model for the *V. crebrisulca* shell shows strongly fluctuating growth rates of 2.3–299.0 μm/day during the cold season and 16.1–462.7 μm/day during the warm season. This translates into a theoretical temporal resolution of 1.5–201.2 and 3.2– 28.0 days/sample during the cold and warm seasons, respectively.

All temporal alignment methods predicted relatively constant year round growth with no apparent growth cessations for the *V. crebrisulca* individual during a certain period of the year. This is in agreement with a previous study on growth pattern of *V. crebrisulca* for this region (Diop, 1988). However, in contrast to the LI and SST/SSS growth models which show the highest growth rates during the warm season, Diop (1988) found the highest accretion rates around the onset of winter upwelling in November. Although resulting in the lowest correlation coefficient, the soVBGF growth model accurately reproduces the growth pattern found by Diop (1988) by predicting slowest growth rates during spring warming and the highest growth rates during the onset of the cold upwelling season (see Fig. 6-5D).

Generally, temporal alignments using linear interpolations or predicted $\delta^{18}O_{Carbonate}$ records represent straightforward methods for recalculating ontogenetic growth trends and thereby fitting almost any kind of proxy record to a given time series of environmental conditions. However, both methods emphasize the relevance of the measured time series, rather than a realistic growth model. While these approaches can provide reasonable growth estimates for organisms where somatic growth is primarily controlled by the underlying time series (e.g. water temperature for the *C. heudelotii* otolith), it is most likely less applicable for organisms

where somatic growth is controlled by multiple interfering environmental variables (e.g. water temperature and food availability for *V. crebrisulca* growth). In any case, both methods require

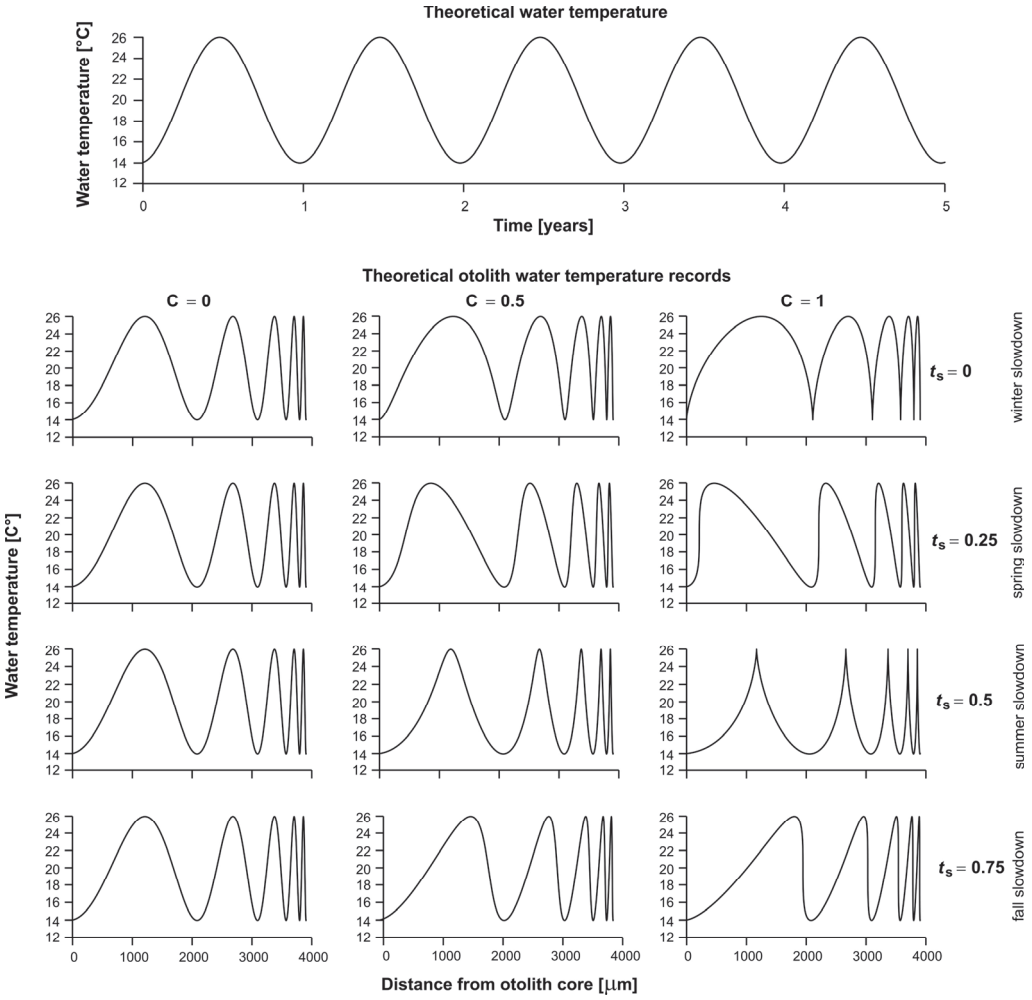

Figure 6-6: Theoretical seasonal water temperature curve following an idealized sinusoidal wave form and corresponding theoretical ($\delta^{18}O$-based) otolith water temperature records distorted by different ontogenetic and seasonal growth patterns. Otolith temperature signatures were modeled using the sVBGF approach with different combinations of seasonal growth oscillation strength (C=0, C=0.5, C=1) and time of the year when the oscillation cycle begins ("summer point", t_s). Strongest growth oscillations occur when C=1 (far right plots), which result in a complete shutdown in growth during part of the year.

well constrained seasonal cycles within the proxy record to avoid potential miss-alignments as a consequence miss-interpreting skeletal proxy records. Furthermore, these approaches do not consider seasonal growth oscillations which might lead to considerable miss-alignments for skeletal records derived from organisms inhabiting ecosystems which are characterized by strong seasonal variations of environmental conditions. To include seasonal growth oscillations, a higher number of temporal reference points can be introduced throughout a seasonal cycle in order to increase the fidelity of growth models. Alternatively, Eq. (6.2) can be used to

iteratively fit the temporal alignment to a given time series of environmental conditions and thereby considerably increase the reliability of the underlying growth model.

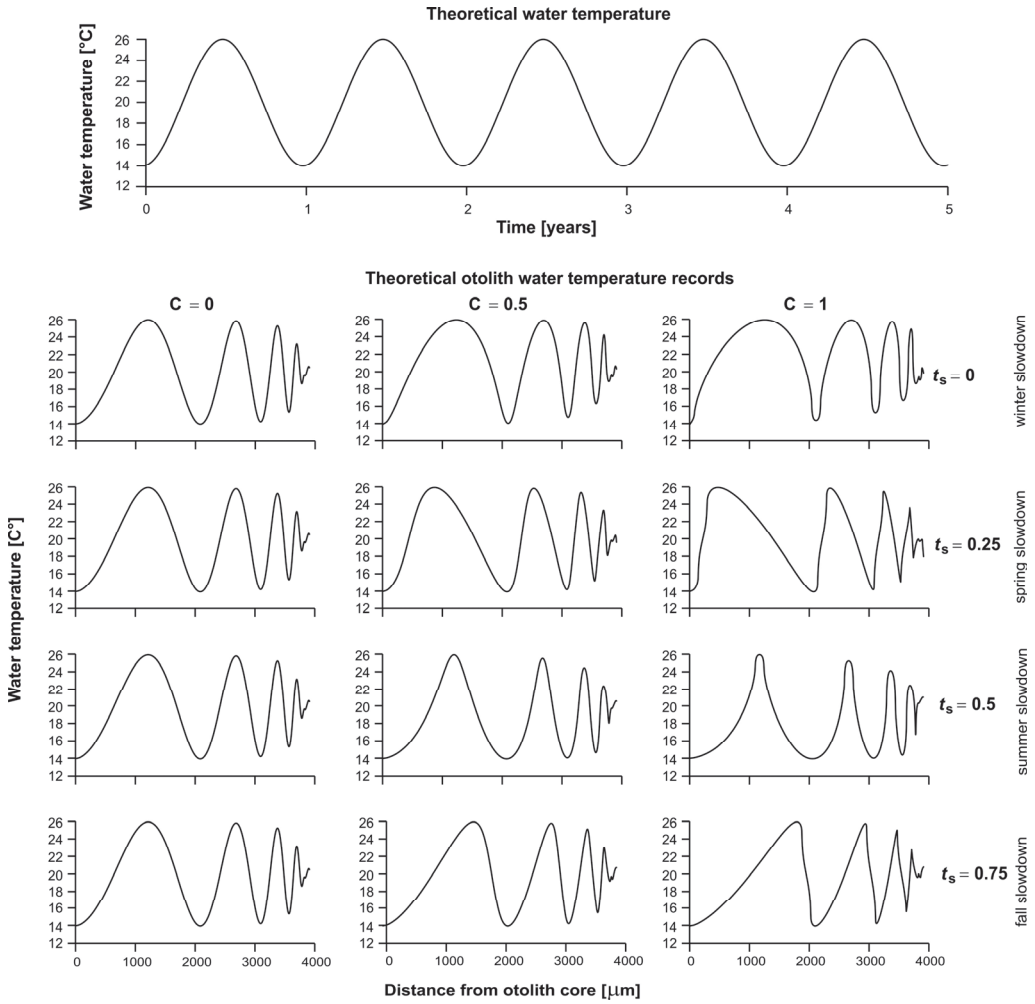

Figure 6-7: Theoretical seasonal water temperature curve and theoretical ($\delta^{18}O$ -based) otolith water temperature records of Fig. 6-6 but assuming a equidistant sampling of the otolith record with a sample spacing of 100 μm. Note the loss of amplitude, as also predicted by the theoretical results of Goodwin et al. (2003) for bivalve shells underlying ontogenetically decreasing annual increment thicknesses.

In contrast, the soVBGF approach does not force the ontogenetic record to mimic the environmental conditions time series but rather emphasizes a realistic growth model for the temporal alignment. However, while the linear interpolation with correction for seasonal growth oscillation allows introducing an asymmetrical (skewed) correction for seasonal growth oscillation (e.g. right-skewed as a consequence of relatively longer spring warming and short autumn cooling), the soVBGF model assumes a symmetrical sinusoidal oscillation of growth throughout the year. This explains the lower correlation coefficient of the soVBGF models as data points corresponding to the shorter cooling phase of the year might be slightly misaligned.

Due to the lack of flexibility of the soVBGF, anomalous growth events (e.g. exceptionally high/low food availability and/or high/low water temperatures) outside the predicted sinusoidal seasonal pattern cannot be considered. In case of strong seasonal growth oscillations, slow growing seasons (e.g. winter/spring months in the *C. heudelotii* individual) are particularly susceptible to minor deviations from the predicted growth pattern, resulting in potential miss-alignments for these intercepts (Fig. 6-4C and D). This in turn limits its applicability for the temporal alignment of strongly and irregularly distorted ontogenetic proxy records caused by e.g. aperiodically varying environmental conditions. Furthermore, the soVBGF approach is less well-suited to describe early juvenile growth. For early juvenile fish, somatic growth has been shown to be almost linear in many cases and thereby deviate from the predicted sinusoidal oscillating growth pattern (Campana and Jones, 1992). This might lead to potential miss-alignments for the ontogenetically youngest part of skeletal proxy records, as also shown by the underestimation of the spawning date by the *C. heudelotii* soVBGF model (see t_0 in Fig. 6-3). Thus, the soVBGF approach is most suitable for temporal alignments of continuous sinusoidal proxy records showing a clear ontogenetic growth trend covering the late juvenile and adult intercept of a skeletal record.

Alternative growth models (e.g. Winsor, 1932; Richards, 1959; Tanaka, 1982; Tanaka, 1988) might be applicable for temporal alignments of sclerochronological data. However, the comparably simple soVBGF model allows the reconstruction of a wide variety of different growth patterns found in marine organisms. Many growth patterns and subsequent theoretical bivalve shell $\delta^{18}O$ records provided in Goodwin et al. (2003) can be reproduced using the soVBGF model (Fig. 6-6). Besides that, the soVBGF approach enables modeling the loss of annual amplitude within $\delta^{18}O$ records as a consequence of ontogenetically decreasing increment thickness similar to the theoretical models of Goodwin et al. (2003), as shown in Fig. 6-7. Our theoretical model shows a stronger ontogenetic decrease in annual temperature amplitude within the otolith record than the theoretical model of Goodwin et al. (2003). This can be related to lower theoretical sampling resolution of 100 μm in our model, which is, however, closer to sampling-reality for most organisms.

6.5.2 Analogy of so VBGF parameters of sclerochronological records with common VBGF parameters

For fish, VBGF models usually describe somatic growth over time by using the total length of the fish rather than otolith size. The appearance of a linear relationship between both parameters has been debated for decades (Campana and Jones, 1992). While some studies

suggest a quasi linear relation between otolith size and fish length (e.g. Warburton, 1978; McGurk, 1984), others found non-linear and ontogenetically variable relationships (e.g. Marshall and Parker, 1982; Secor and Dean, 1989; Casselman, 1990). It has also been shown that water temperature can modulate otolith growth (Gutierrez and Morales-Nin, 1986), inducing otolith growth even if water temperature exceeds the maximum temperature for somatic growth of some species (Mosegaard et al., 1988). In case of a non-linear relationship between otolith size and fish length, the estimation of the growth coefficient K based on otolith-derived $\delta^{18}O$ records for a temporal alignment is possible but impedes the comparability of both growth coefficients ($K_{Total\ length}$ vs. $K_{Otolith\ Size}$). In consequence, it is not necessarily possible to use previously determined K or C values (e.g. derived from body size/age analysis) for estimating K and C in the context of temporal alignments of sclerochronological data and vice versa. For catfish otoliths, Warburton (1978) showed a linear

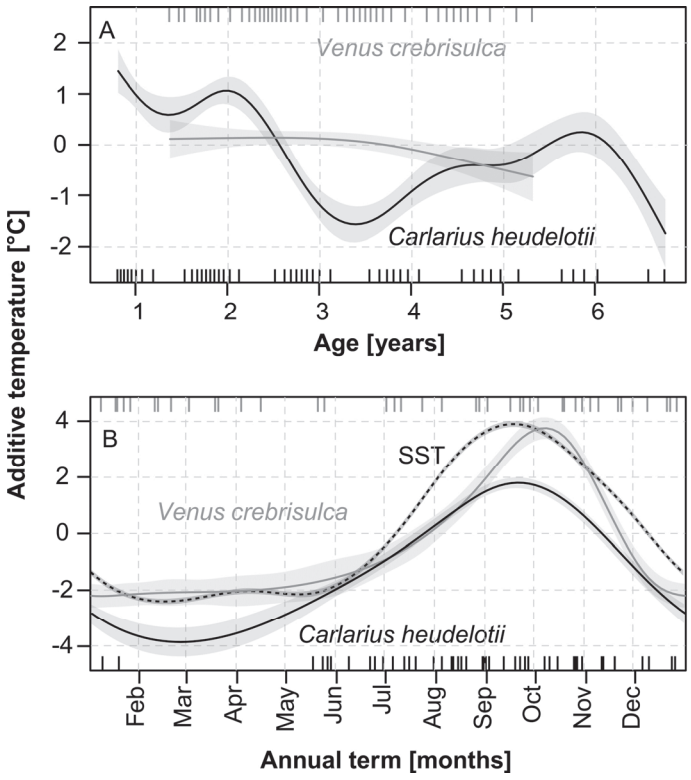

Figure 6-8: Top: Ontogenetic temperature anomaly from reconstructed average water temperature of the *Carlarius heudelotii* otolith and the *Venus crebrisulca* based on the soVBGF model. **Bottom:** Average seasonal water temperature anomaly of the otolith (six year record), the bivalve (four year record) from the measured SST. Shaded area represents the 95% confidence interval of the generalized additive model (GAM) model used for calculation. Tick marks at the top and bottom of each sub-figure indicate calculated timing of oxygen isotope samples within the soVBGF models.

relationship between otolith length and total fish length for the catfish species *Ariopsis guatemalensis* (Günther, 1864), suggesting that both measures are directly comparable but, to the best of our knowledge, such growth data are not available for *C. heudelotii* so far.

In most studies on bivalve shells, sampling for stable isotope analysis is carried out by sampling the outer shell layer along the ventral margin. This approach provides a complete ontogenetic growth record starting at the hinge/umbo (i.e. the ontogenetically youngest sample) towards the commissure (i.e. ontogenetically oldest sample). Thereby, the sample locations along the profile are usually reported relative to their distance along the ventral margin or as the distance from umbo. When using the soVBGF approach, growth coefficients (K) and seasonal growth oscillation coefficients (C) derived from these measures are not directly comparable to commonly determined VBGF parameters which are usually referring to shell height. However, given the typical bivalve shell geometry of a logarithmic spiral, the distance along the ventral margin is almost linearly related to the shell height enabling the translation of distance along the ventral margin into shell height (see supplemental material) enabling the application of the soVBGF approach for the temporal alignment of bivalve shell proxy records. If the soVBGF approach is used to compare growth parameters with commonly determined VBGF parameters from the literature, we suggest measuring the locations of the samples along the ontogenetic transect relative to the intersection point of the commissural plane and the umbo (i.e. shell height, see supplemental material). This approach provides reasonable estimates of individual ontogenetic and seasonal growth pattern in modern or fossil bivalve shells and also enables their comparison with modern VBGF parameters from the literature.

6.5.3 C. heudelotii and V. crebrisulca as (paleo-) environmental archives

6.5.3.1 C. heudelotii *otolith*

Our data show that ontogenetic $\delta^{18}O$ records of *C. heudelotii* otoliths can provide high-resolution records of water temperatures experienced by the organism, which is in agreement with previous studies on the $\delta^{18}O$ composition of fish otoliths (Patterson et al., 1993; Thorrold et al., 1997; Høie et al., 2004). However, in contrast to our study, Surge and Walker (2005) found robust agreement between otolith $\delta^{18}O$-derived water temperature estimates and measured SST for the hardhead catfish *Ariopsis felis* (Linneaus, 1766) by using the equation of Patterson et al. (1993). By having the same slope but a constant temperature offset, the equation of Thorrold et al. (1997) results in approximately 4.5 °C higher water temperatures estimates than the equation of Patterson et al. (1993). For *C. heudelotii*, the equation of

Patterson et al. (1993) results in unreasonably low water temperatures, which can potentially be explained by different habitats of both species. While the equation of Thorrold et al. (1997) was experimentally developed using the marine species *Micropogonias undulates* (Linnaeus, 1766), the equation of Patterson et al. (1993) was empirically determined using multiple species derived from freshwater lakes. Being an anadromous species, the strong association of *A. felis* with brackish- to freshwater conditions (Yáñez-Arancibia and Lara-Domínguez, 1988) might explain the suitability of the continental water temperature equation of Patterson et al. (1993). However, as mentioned above, *C. heudelotii* is classified as marine–estuarine species that enters estuaries but reproduce in marine environments (Taylor, 1986; Schneider, 1990). Although the underlying mechanisms causing the differences in isotope fractionation between both species remain unknown, the application of the equation of Thorrold et al. (1997) for the temperature estimation of *C. heudelotii* provides reasonable water temperature reconstructions.

Due to the likely inhabitation of shallow marine coastal nursery areas during the juvenile phase of *C. heudelotii* (0–3300 μm; spring 1998 – winter 1999/2000), reconstructed water temperatures agree with the remote sensing surface water temperature data set. However, reconstructed otolith summer water temperatures underestimate measured summer SST maxima by 2.5 °C for the late juvenile to early adult phase (3300–5600 μm, corresponding to winter 1999/2000 – winter 2003/2004). Rather than a potential ontogenetic variation in oxygen isotope fractionation, we suggest that ontogenetic migration into deeper areas of the Banc d'Arguin caused the observed underestimation of summer water temperature. This interpretation is based on the general ecology of *C. heudelotii* being a demersal species (Schneider, 1990) and the fact that the underestimation of 2.5 °C coincides with the observed local water temperature gradient from surface to bottom waters of approximately 2–3 °C in the central areas of the Baie du Lèvrier and the adjacent Banc d'Arguin (Westphal et al., 2014). After reaching sexual maturity with an age of about 4 years (2002–2003), a return-migration to coastal nursery areas for reproduction might explain the observed re-increase of reconstructed summer water temperatures (see Fig. 6-8).

As a consequence of ontogenetically decreasing annual increment width and constant otolith sub-sampling, saw-toothed seasonal water temperature oscillation can be observed with systematically increasing trend after 5600 μm from core (corresponding to winter 2003/2004). Although the general increase in reconstructed water temperature can potentially be explained by a migration into warmer coastal areas, we suggest an ontogenetically diminution of the

growing season towards the environmental optimum (i.e. summer) during the late adult stage. This effect was similarly observed in skeletal records of other marine organisms (Goodwin et al., 2003).

6.5.3.2 V. crebrisulca *shell*

The sub-seasonally resolved *V. crebrisulca* water temperature record covers four seasonal cycles. Differing from the *C. heudelotii* otolith record, the sub-seasonal water temperature record indicates relatively constant growth rates throughout the entire year with an increase in somatic growth during the cold (upwelling) season. Although water temperature has also been reported as an important factors controlling somatic growth of marine mollusks (Goodwin et al., 2001), the soVBGF growth model as well as the growth pattern found by Diop (1988) suggests that phytoplankton concentration (i.e. food availability) represent the most important environmental variable controlling somatic growth of *V. crebrisulca*. The adaptation of *V. crebrisulca* to temporarily cold but highly productive upwelling conditions is also indicated by its biogeographic distribution in the main upwelling areas where the highest primary production occurs during the winter upwelling season (Diop, 1988; Sevrin-Reyssac, 1993; Goudswaard et al., 2007).

The SST and SSS data sets used for the correlation and the calculation of the SST/SSS growth models do not exactly cover the sampling site of the *V. crebrisulca* individual. However, according to Sevrin-Reyssac (1993), the sampling location can be considered as part of the hydrological system of the shallow Banc d'Arguin. Thereby, this region is mainly influenced by shelf water masses, entering the shallow shelf in the northern part of the Banc and are transported southwards by wind induced surface currents (see Fig. 6-1). This hydrological model is supported by the general shelf morphology, the surface current system controlling the seasonal water temperature pattern on the Banc d'Arguin (Dobrovine et al., 1991) and the local carbonate facies resulting from the upwelling of nutrient-rich water masses showing a clear succession of different heterozoan carbonate associations from north to south along the Banc d'Arguin (Michel et al., 2009; Michel et al., 2011; Klicpera et al., 2015). Thus, environmental data with the abovementioned spatial coverage represent reliable measures of environmental conditions at the *V. crebrisulca* sampling site. However, remote sensing SST and SSS values might slightly overestimate the absolute values as a consequence of higher water temperatures and subsequently stronger evaporation in shallow coastal areas. This could also explain the slight overestimation of summer maximum and winter minimum temperatures within the *V. crebrisulca* temperature reconstruction (see Fig. 6-4E and F).

Nevertheless, the good agreement with measured SST values throughout the lifetime of the organism demonstrates the reliability of *V. crebrisulca* $\delta^{18}O$ records as a paleotemperature archives without remarkable salinity effect for this region (Fig. 6-8).

6.6 Summary and conclusions

We explored the applicability of different mathematical approaches for the conversion of skeletal proxy records into sub-annually resolved water temperature time series. Based on $\delta^{18}O$-derived water temperature records of a *C. heudelotii* otolith and a *V. crebrisulca* shell, we demonstrate that our new mathematical methods that are based on an improved linear interpolation and a modified version of the seasonally oscillating Von Bertalanffy growth function can be used for aligning proxy records to instrumentally measured time series. We also demonstrate that both methods can be applied over a wide range of seasonal and ontogenetic growth features found among carbonate secreting taxa. Higher correlation coefficients were found when sclerochronological proxy records were fitted to a given time series of water temperature based on linear interpolations integrating seasonal growth oscillations. In contrast to that, the application of the seasonally oscillating Von Bertalanffy Growth Function for the temporal alignment provided more realistic growth models which, however, resulted in lower correlation coefficients as a consequence of deviations from the predicted growth pattern. Nevertheless, all temporal alignments resulted in highly significant correlations between reconstructed and measured water temperature.

Generally, when selecting a suitable method for the temporal alignment of a given sclerochronological record, emphasis should be given to the complexity of the distortion (i.e. amplitude of seasonal growth oscillations and/or ontogenetic reduction of annual growth rates). Furthermore, we advocate for the detailed description and reporting of all relevant parameters if mathematical approaches are used for the temporal alignment of sclerochronological data within future studies.

Despite a slight bias in the *C. heudelotii* otolith record, most likely caused by individual ontogenetic migration pattern and a strong seasonal oscillation of otolith growth, the $\delta^{18}O$-derived sub-seasonal water temperature reconstruction is precise within ±0.65–1.16 °C, depending on the temporal alignment method. The *V. crebrisulca* shell is characterized by a relative constant growth throughout the entire year and its ontogenetic $\delta^{18}O$ record provides a precise sub-seasonally resolved water temperature record with a precision of ± 0.48–1.41

°C. Thus *C. heudelotii* otoliths as well as *V. crebrisulca* shells can be considered as reliable recorders of (paleo-) water temperatures with a sub-seasonal resolution.

6.7 Acknowledgements

Funding for this work was provided by the Leibniz Center for Tropical Marine Ecology (ZMT), Bremen, Germany. We gratefully acknowledge constructive comments of three anonymous reviewers which considerably improved the manuscript. We thank the following people and organizations for their assistance and support: Philippe Tous (Oceanic Development/SRFC, France) for providing *C. heudelotii* otolith samples; Kees Goudswaard (IMARES, Wageningen, The Netherlands) for providing *V. crebrisulca* samples; Sebastian Flotow (ZMT, Bremen, Germany) for sample preparation; Michael Joachimski (University of Erlangen-Nürnberg, Germany) and Henning Kuhnert (University of Bremen, Germany) for oxygen isotope analysis; Matthias López Correa (University of Erlangen-Nürnberg, Germany) for support with the Micromill sampling; the Bremen International Graduate School for Marine Sciences (GLOMAR) and in particular Rebecca Rendle-Bühring (University of Bremen, Germany) for discussion and support in the preparation of the manuscript.

6.8 Supplemental material

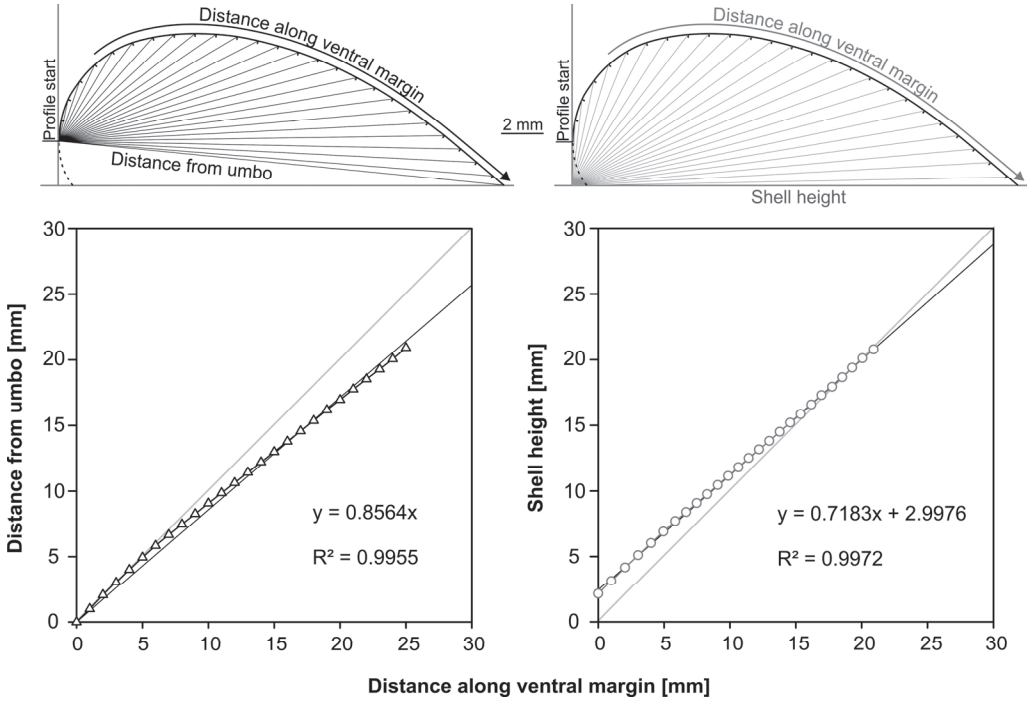

Figure 6-S1: Left: Idealized bivalve shell geometry based on a logarithmic spiral with the spatial relationship between relative distances of theoretical samples along the ventral margin and their distances relative to the umbo. **Right:** The same idealized shell geometry with the spatial relationship between distances along the ventral margin and the relative distances to the intersection of the commissural plane and the umbo (i.e. simplified shell height). Linear regressions show a quasi-linear relationship between both measures whose deviation is, however, depending on the shell curvature.

7. PREHISTORIC COOKING VERSUS PALEOCLIMATE PROXIES IN SHELL-MIDDEN CONSTITUENTS

Peter Müller[1,*], Philip T. Staudigel[2], Sean T. Murray[2], Robert Vernet[3], Jean-Paul Barusseau[4], Hildegard Westphal[1,5], Peter K. Swart[2]

[1]Leibniz Centre for Tropical Marine Research, 28359 Bremen, Germany.

[2]Rosenstiel School of Marine and Atmospheric Science, University of Miami, Miami, FL, 33149, USA.

[3]Institut Mauritanien de Recherches Scientifiques, Nouakchott, Mauritania.

[4]Centre de Formation et de Recherche sur les Environnements Méditerranéens, University of Perpignan Via Domitia, Perpignan, France.

[5]Department of Geosciences, University of Bremen, Bremen, Germany.

[*]Corresponding author: Peter Müller, Fahrenheitstraße 6, 28359 Bremen, Germany, phone +49 421 23800 178, email peter.mueller@leibniz-zmt.de

Under revision for resubmission to *Nature Scientific Reports*

Personal contribution to Chapter 7:

PM (100 %) conceived the experiment, PM (85 %), PTS (5 %), STM (5 %) and PKS (5 %) accomplished the experimental work; RV (50 %) and JPB (50 %) provided archeological samples; PM (40 %), PTS (40 %), STM (10 %) and PKS (10 %) accomplished the proxy analyses; PM (50), PTS (10 %), STM (5 %), RV (5 %), JPB (5 %), HW (10 %) and PKS (15 %) contributed to data interpretation and wrote the manuscript.

7.1 Abstract

The reconstruction of pre-depositional cooking treatments used by prehistoric coastal populations for processing aquatic faunal resources is often difficult in archeological shell-midden assemblages. However, besides limiting our knowledge about social, cultural, economic and technological aspects, unknown pre-depositional cooking techniques can cause large errors in paleoclimate reconstructions as they can considerably alter the geochemical proxy signatures in calcareous skeletal structures such as bivalve shells or fish otoliths.

Based on experimental and archeological data, we show that carbonate clumped isotope thermometry can be used to detect and reconstruct prehistoric processing methods in aragonitic skeletal structures from archeological shell-midden assemblages. Given the temperature-dependent re-equilibration of clumped isotopes in aragonitic carbonates, this allows differentiating between specific processing, cooking or trash dispersal strategies such as boiling, roasting, or burning. Besides allowing the detailed reconstruction of cultural or technological aspects of shell-midden formation, this also allows to avoid erroneous paleoclimate reconstructions as all shells that were subjected to pre-historic cooking methods show a clear alteration of their initial oxygen isotopic composition.

7.2 Introduction

Many prehistoric populations exploited faunal resources of adjacent aquatic environments (Richards and Hedges, 1999; Richards et al., 2005). Thereby, skeletal structures such as mollusk shells or fish otoliths were often accumulated in the vicinity of prehistoric settlements in so-called shell-midden deposits. Their composition, internal structure or spatial and temporal distribution represent a valuable source of information regarding human dispersal, site-specific occupation pattern, human subsistence strategies, associated dietary preferences or fishing and foraging seasonality (Waselkov, 1987; Balbo et al., 2011; Thomas, 2015b). Moreover, mollusk shells or fish otoliths derived from shell-midden provide sub-seasonally resolved proxy records such as oxygen isotopes and thereby provide highest-resolution paleoclimate data from ancient coastal environments (Andrus et al., 2002; Surge and Walker, 2005; Walker and Surge, 2006; Carré et al., 2014; Thomas, 2015a). Thus, shell-midden deposits are increasingly used for archeological as well as paleoclimate studies and significantly broaden our understanding of cultural evolution, ancient environmental change as well as human-environment interactions (Surge and Walker, 2005; Andrus, 2011; Disspain et al., 2015; Thomas, 2015a).

As subsistence was the primary reason for exploiting aquatic faunal resources for many prehistoric cultures, most shell-midden constituents were most-likely subjected to certain processing or cooking techniques prior to deposition (Waselkov, 1987). In particular mollusks, where the comparably small amount of edible flesh is protected by tightly closed valves or the operculum require sophisticated processing strategies for the efficient extraction of the small edible portion (Waselkov, 1987; Balbo et al., 2011). However, evidences for certain processing or cooking techniques such as pottery- and tool fragments or blackened/burned stones are often sparse in shell-midden deposits or allow a variety of potential interpretations regarding specific cooking or processing strategies. This is in particular the case if shell-middens were accumulated at transitory preparation sites near fishing or shellfish gathering grounds rather than in close proximity of prehistoric settlements.

While usually unknown processing methods limit our understanding of various cultural, economic as well as technological aspects of shell-midden formation, processing or cooking methods involving heating (i.e. cooking) most likely alter proxy records of calcareous skeletal remains and thereby may introduce large uncertainties into paleoclimate reconstructions (Andrus and Crowe, 2002; Larsen, 2015; Milano et al., 2016). Hence, the reliable

reconstruction of prehistoric processing methods is crucial for avoiding erroneous paleoclimate reconstructions using geochemical proxies in shell-midden constituents.

In this study, we tested the potential application of carbonate clumped isotope thermometry on aragonitic skeletal structures such as mollusk shells or fish otoliths for the detection and reconstruction of specific prehistoric cooking methods. Carbonate clumped isotope thermometry is based on the preferential formation of ^{13}C-^{18}O bonds ("clumping") in the carbonate molecule with decreasing carbonate formation temperature, independent from the isotopic composition of the precipitating fluid (Ghosh et al., 2006; Schauble et al., 2006; Dennis et al., 2011). Therefore, clumped isotope thermometry is considered a promising paleo-water temperature proxy as it circumvents uncertainties in conventional oxygen isotope thermometry which commonly derive from unknown ancient water chemistry (Ghosh et al., 2006; Eiler, 2007; Dennis et al., 2011). In addition, clumped isotope thermometry allows the reconstruction of thermal histories of carbonate rocks as the relative abundance of ^{13}C-^{18}O bonds can be re-equilibrated during post-formational heating (Dennis and Schrag, 2010; Huntington et al., 2011). Thereby, rate and magnitude of ^{13}C-^{18}O bond re-ordering is a function of temperature and exposure time and can occur even in closed systems without any isotope exchange with ambient media (Dennis and Schrag, 2010; Huntington et al., 2011; Passey and Henkes, 2012). While re-equilibration in calcite occurs over geological time scales, aragonite shows much higher re-ordering rates, resetting the clumped isotopic signature within minutes to hours (Staudigel and Swart, 2016). Thus, clumped isotope thermometry might represent the ideal tool for detecting pre-depositional heating of aragonitic shell-midden constituents and might also allow differentiating between certain processing or cooking practices.

In order to test this hypothesis, we exposed the right valves of modern hard clams (*Mercenaria campechiensis*, Gmelin 1791) cultured in the Gulf of Mexico to a variety of prehistoric cooking methods. Our experiment comprised untreated shells (corresponding to manually opened shells and serving as controls), shells boiled in seawater (~100 °C), roasted over charcoal (174 ± 13 °C) and directly burned in charcoal (554 ± 95 °C). For all treatments, exposure times ranged from 15 minutes to 6 hours. Afterwards, we measured the bulk clumped isotopic composition (Δ_{47}), oxygen and carbon isotopes ($\delta^{18}O$ and $\delta^{13}C$, respectively) as well as the potential conversion of the primary aragonite into secondary calcite.

In addition, we measured bulk $\delta^{18}O$ and Δ_{47} values of mid-Holocene shell-midden constituents excavated in the northern part of the Mauritanian coast (Banc d'Arguin), radiocarbon dated to 5,020 – 5,320 cal. yrs. BP. These samples comprised four catfish otoliths (Ariidae) and seven bivalve shells (*Senilia senilis*, Linnaeus 1758). Besides measuring bulk $\delta^{18}O$ and Δ_{47} values, we also analyzed additional samples drilled from the hinge region of each bivalve shell as well as high-resolution ontogenetic oxygen isotope records of three exemplary shells.

7.3 Results

7.3.1 Experimental shells

Depending upon the cooking temperature, variable changes in shell mineralogy, visual appearance and outer shell structure occurred within the different cooking treatments (Fig. 7-1). Boiling and roasting of the shells caused bleaching and blackening of the outer organic layer, respectively. While the cooked shells showed consistently a pristine outer shell structure, some but not all roasted shells exhibited small cracks (<0.5 mm) perpendicular to the ventral margin. Despite these sporadically occurring cracks, overall shell integrity remained pristine, not allowing a clear differentiation from uncooked control shells. Bleaching and blackening of the cooked and roasted shells' periostracum entirely disappeared after the removal of the periostracum using hydrogen peroxide. Direct burning of the shells resulted in blackening of the outer surface, whitening of the inner shell layer, and was accompanied by an immediate loss of structural integrity and the conversion of the solid shell structure into brittle and chalky fragments. Boiling and roasting did not cause any conversion of initial aragonite into secondary calcite (Fig. 7-2a) while the burned shells showed a generally increasing conversion of primary aragonite to secondary calcite over the time of exposure.

The exposure of bivalve shells to different cooking practices caused a rapid alteration of their clumped isotopic composition (Δ_{47}). Thereby, re-ordering rates in aragonite were high enough to cause an immediate reduction in Δ_{47} where the magnitude is a function of cooking temperature and exposure time. Boiling at 100 °C caused only a minor reduction in the Δ_{47} values which is not significantly different from the control shells. This agrees with the thermodynamic model for clumped isotope re-ordering in aragonite at 100 °C (Staudigel and Swart, 2016), showing that the exposure time of several hours to temperatures ~100 °C is not sufficient to cause a significant decrease in Δ_{47} values. In contrast, roasting and burning

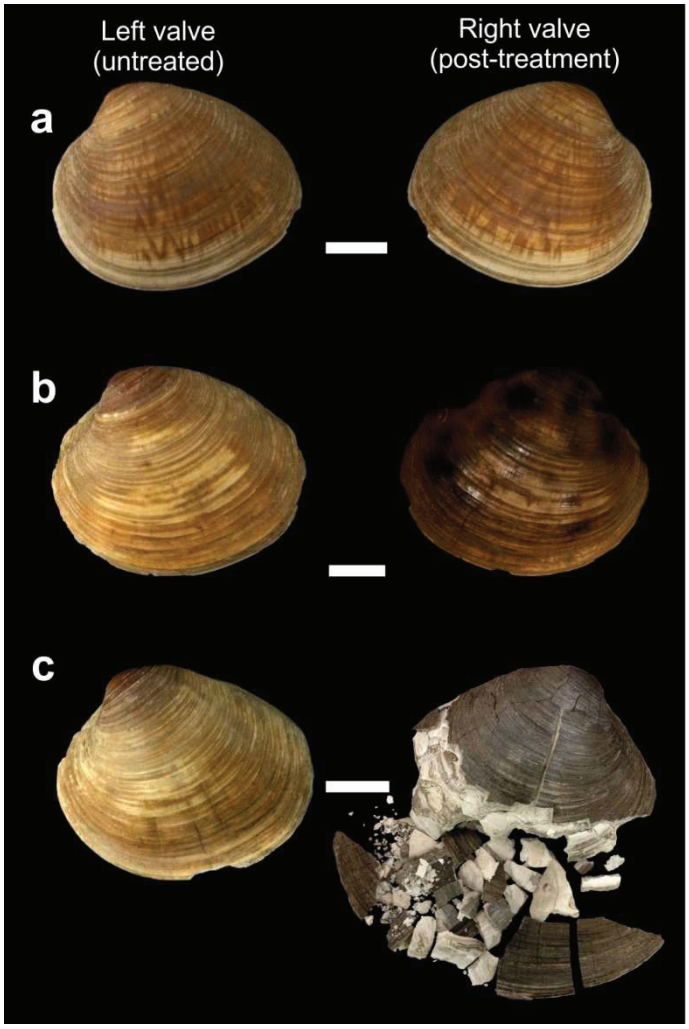

Figure 7-1: Visual comparison of untreated left valves and the corresponding right valves exposed to the different treatments prior to hydrogen peroxide cleaning. **a)** Boiling for 40 minutes. **b)** Roasting for 240 minutes. **c)** Burning for 240 minutes. Scale bars represent 1.0 cm.

caused an immediate decrease in Δ_{47} to values ranging from 0.501 to 0.605 ‰, and 0.324 to 0.411 ‰, respectively. As shown in Fig. 7-2b and c, experimental lowering of shell Δ_{47} values within the roasting and burning treatments are in good agreement with thermodynamic models for the relevant temperatures over the time of exposure (Staudigel and Swart, 2016).

Independent from cooking temperature or exposure time, all cooking treatments resulted in a statistically significant lowering of bulk $\delta^{18}O_{Shell}$ values, diminishing their potential for reliable water temperature reconstructions (Fig. 7-2C and D). The maximum decrease of $\delta^{18}O_{Carbonate}$ values was –0.60 ‰ (VPDB) for boiling, –0.53 ‰ (VPDB) for roasting, and –0.90 ‰ (VPDB) for the burning treatment. Using the equation of Grossman and Ku (1986), the

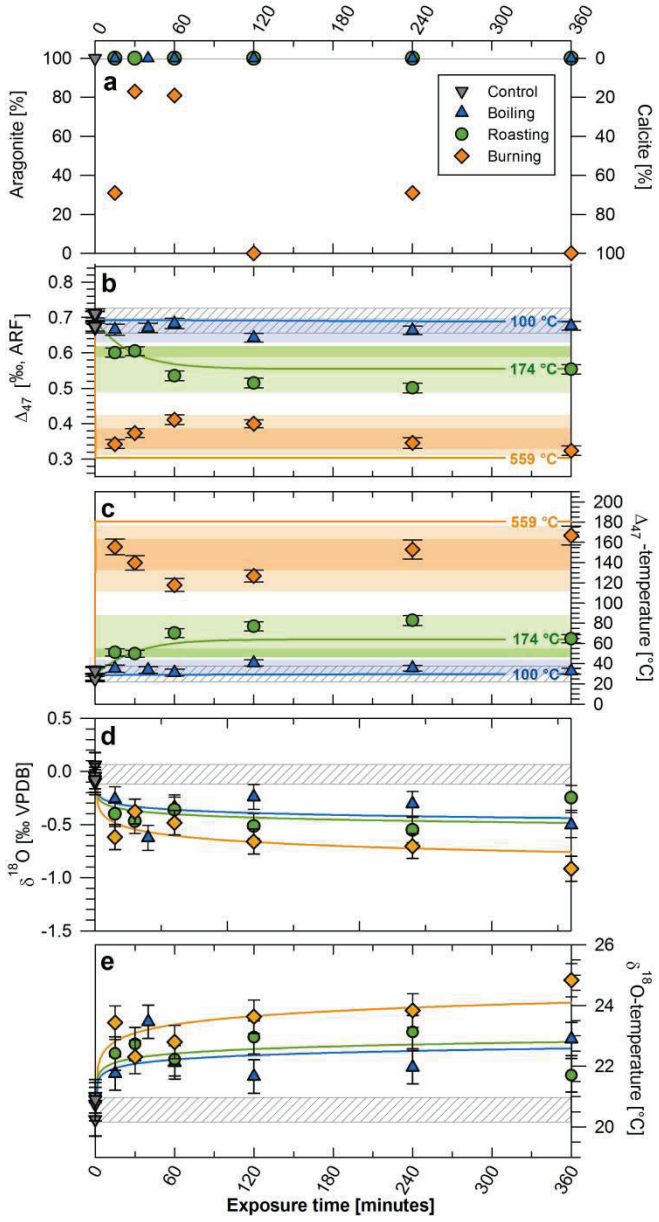

Figure 7-2: Alteration of mineralogy and geochemical proxies in modern *Mercenaria campechiensis* shells by simulated prehistoric cooking methods. Untreated (grey triangles and grey striped areas), boiled (blue triangles), roasted (green circles), and burned shells (orange diamonds). **a)** Conversion of primary aragonite into secondary calcite. **b)** Clumped isotopic composition (Δ_{47}) reported in the absolute reference frame (ARF) defined by Dennis et al. (2011) of the bivalve shells after exposure to the different cooking methods. Solid lines represent predicted Δ_{47} values using the Arrhenius model of Staudigel and Swart (2016) for each experimental temperature. Error bars represent mean standard errors of the individual measurements. Grey striped area represents the range of untreated control shells (n=5). Shaded areas represent the characteristic Δ_{47} windows for each cooking treatment over the entire experiment duration (light) and realistic cooking durations of <30 minutes (dark). **c)** Calculated Δ_{47}-based water temperature estimated using the equation of Dennis et al. (2011) and corresponding theoretical Δ_{47}-based water temperature estimates

predicted by the thermodynamic model of Staudigel and Swart (2016). Similar to panel B), light and dark blue/yellow areas represent the characteristic Δ_{47}-windows translated into water temperature values using the equation of Dennis et al. (2011). **d)** Change in $\delta^{18}O_{Shell}$ over time of exposure for the different cooking methods. Solid lines represent exponentially fitted curves highlighting the overall trend towards lower $\delta^{18}O_{Shell}$ values. **e)** Calculated $\delta^{18}O_{Shell}$-based water temperatures using the equation of Grossman and Ku (1986) and assuming a constant $\delta^{18}O_{Seawater}$ of 0.0 ‰ (VSMOW).

decrease in $\delta^{18}O_{Carbonate}$ values translates into water temperature overestimations of 2.8, 2.5 and 4.2 °C, respectively. While $\delta^{18}O_{Carbonate}$ values of all treatments were significantly different from the control shells, there was no significant difference in between the different cooking treatments. We observed no statistically significant alteration trend with respect to shell $\delta^{13}C_{Carbonate}$ values among the different treatments. However, the variability in $\delta^{13}C_{Carbonate}$ values of the treated shells exceeds the range measured in the control shells, indicating that isotope exchange reactions also affected shell $\delta^{13}C_{Carbonate}$ values.

7.3.2 Archeological samples

Mid-Holocene otolith Δ_{47}-values (0.657 to 0.708 ‰) largely agree with predicted values based on modern water temperature observations (Lavaud et al., 2013; Müller et al., 2015a, Chapter 6 of this thesis). In contrast, mid-Holocene bivalve shells show highly variable Δ_{47} values ranging from 0.597 to 0.709 ‰, considerably lower than expected for natural environments. Noteworthy, bulk samples of the shells show higher variations in Δ_{47} and tend towards lower Δ_{47} values (0.597-0.709 ‰) than corresponding samples from the hinge region of the same individuals (0.639-0.689 ‰). Subsequently, Δ_{47}-based water temperature reconstructions using the bulk shell samples result in unreasonably high paleo-water temperature estimates (25.5-52.4 °C). In contrast, the samples drilled from the hinge region of the same shells provide more realistic water temperature estimates for coastal intertidal environments (29.7-41.2 °C).

Mid-Holocene bulk $\delta^{18}O_{Carbonate}$ values are consistent amongst all otoliths and bivalve shells, ranging from –0.29 to +1.13 ‰ (VPDB) (Fig. 7-3). Assuming mid-Holocene $\delta^{18}O_{Seawater}$ values of +0.68 and +1.57 ‰ (VSMOW) for the otoliths (Müller et al., 2015a, Chapter 6 of this thesis) and bivalve shells (Lavaud et al., 2013), respectively, reconstructed water temperatures are only slightly higher during the mid-Holocene than observed today. Measured ontogenetic bivalve $\delta^{18}O$ records show a clear sinusoidal cyclicity which covers time-spans of three to six years of growth. Measured $\delta^{18}O_{Carbonate}$ values range from –1.8 to +1.5 ‰ VPDB, translating into mid-Holocene water temperatures ranging from 21.1 to 36.2 °C.

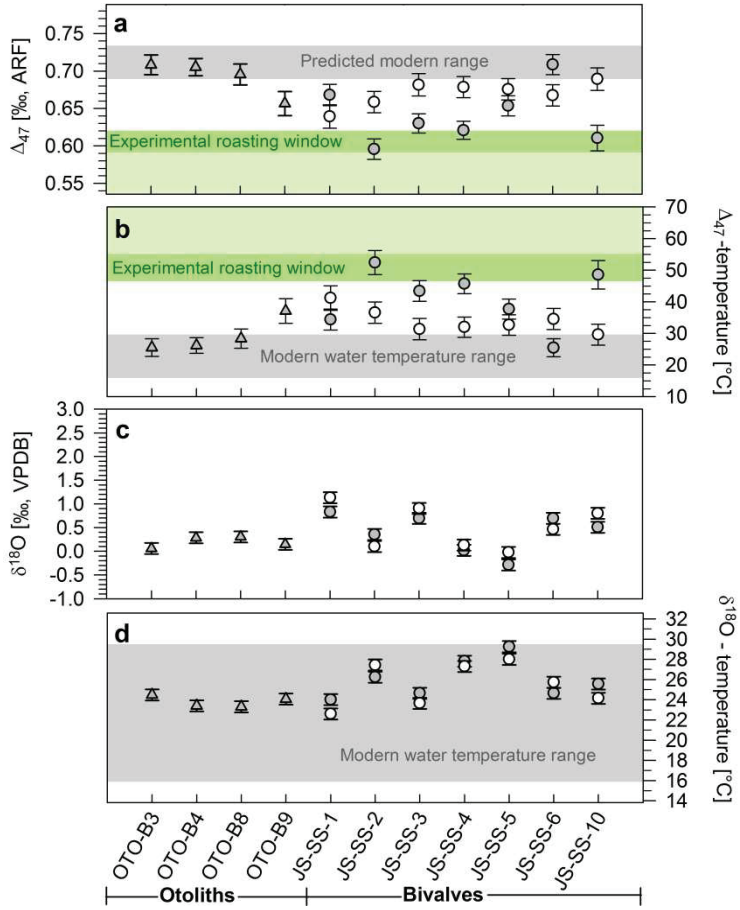

Figure 7-3: Clumped and oxygen isotopic composition with corresponding water temperature estimates of mid-Holocene fish otoliths and bivalve shells. **a)** Clumped isotopic composition (Δ_{47}) reported in the absolute reference frame (ARF) defined by Dennis et al. (2011) of bulk otoliths (grey triangles), bulk bivalve shells (grey circles) and hinge samples from the bivalve shells (open circles). Error bars represent mean standard errors of the individual measurements. The grey area represents the theoretical Δ_{47}-range based on modern local water temperature data (Lavaud et al., 2013) translated into Δ_{47}-values using the equation of Dennis et al. (2011). The shaded green area represent the experimentally determined Δ_{47}-window for roasting at 174±13 °C for 6 hours (light) and only realistic cooking duration of >30 minutes (dark). **b)** Δ_{47}-based water temperature reconstruction using the equation of Dennis et al. (2011) with modern water temperature data (Lavaud et al., 2013). Shaded green areas represent the experimentally determined Δ_{47}-window of the roasting treatment translated into water temperature estimates using the equation of Dennis et al. (2011) for 6 hours (light) and realistic cooking duration of >30 minutes (dark green). **c)** Oxygen isotopic composition of bulk fish otoliths, bulk bivalve shells and hinge samples from the bivalve shells. **d)** Oxygen isotope-based water temperature reconstructions for the otoliths using the equation of Thorrold et al. (1997) assuming a constant $\delta^{18}O_{Seawater}$ value of +0.68 ‰ (VSMOW) (Müller et al., 2015a, Chapter 6 of this thesis) and oxygen-isotope based water temperature reconstructions for the bivalve shell samples using the equation of Grossman and Ku (1986) assuming a constant modern $\delta^{18}O_{Seawater}$ value of +1.57 ‰ (VSMOW) (Lavaud et al., 2013) with the modern local water temperature range (Lavaud et al., 2013).

7.4 Discussion

Previous studies on the effect of prehistoric cooking on mollusk shells simulated cooking temperatures ranging from 100 to 500 °C (Larsen, 2015; Milano et al., 2016). Our data agrees with these studies in that they also observed a conversion of primary aragonite to secondary calcite at temperatures > 300 °C, and is also consistent with experimental studies showing that 300 - 400 °C is the minimum temperature for the conversion of biogenic aragonite into calcite (Wardecki et al., 2008; Stolper and Eiler, 2015). Based on their experimental results, Milano et al. (2016) proposed the use of crystal microstructure for the detection of pre-depositional heating in shell-midden deposits. However, they only observed clear changes in crystal microstructure along with a conversion of primary aragonite into secondary calcite. Considering the pristine aragonitic shell mineralogy in the roasting treatment of this study, our data indicate that mineralogical or shell microstructure analyses most likely fail to detect pre-depositional heating if cooking temperatures are below 300 - 400 °C. The deviation from the expected linear conversion trend in the burned shells was presumably caused by spatial and temporal variability in treatment temperature along with potential variations in absolute temperature maxima experienced by the individual shells. Although burning causes a clear conversion of the primary aragonite into secondary calcite in all shells and would thereby easily identifiable in shell-midden deposits, the preservation of burned shells in shell-midden deposits is questionable considering their brittle shell structure.

The observed minor overshooting of modelled Δ_{47} values in the roasting treatment was most likely caused by short term temperature spikes (>200 °C) which were also measured during the experiment. In contrast, the observed undershooting of theoretical equilibration temperatures by the burning treatment could have been caused by several different mechanisms including: 1) disorder-to-order re-equilibration during cooling to ambient air temperature after the experiment, 2) a steep temperature gradient between the charcoal surfaces and the shells, 3) complex interplays of re-ordering processes as a consequence of aragonite/calcite transitions during the experiments or 4) spatial and temporal temperature variability of the burning treatment. It appears unlikely that cooling to ambient air temperature caused the observed underestimation of temperature as disorder-to-order re-equilibration occurs over considerably longer time scales (Passey and Henkes, 2012). We also did not measure a sufficient temperature gradient between the charcoals and the shells to explain the observed Δ_{47} pattern. Instead, we suspect that the conversion of aragonite into calcite causes the deviation from the thermodynamic model which has also been shown by experiments of

Stolper and Eiler (2015) and Piasecki (2015), involving at least three different mechanism of clumped isotope re-ordering during the aragonite/calcite conversion. These mechanisms are 1) a sharp decrease in Δ_{47} during the initial heating of the primary aragonite (annealing) followed by 2) a partial conversion of aragonite into calcite causing a re-increase in Δ_{47} and 3) a second re-ordering phase of the secondary calcite resulting in a decrease in Δ_{47} values with considerably lower re-equilibration rates. This complex model of clumped isotope re-ordering during the transition of aragonite into calcite is supported by our data as the measured trajectory of Δ_{47} alteration within the burning treatment exactly follows the pattern described by Piasecki (2015). However, our experiment was designed to precisely simulate (spatially and temporarily heterogeneous) prehistoric cooking practices and has thus only limited validity regarding the underlying thermodynamic mechanisms of clumped isotope re-ordering during the aragonite/calcite transition.

Regardless of experimental uncertainties, the lower Δ_{47} values of the shells in the roasting and burning treatments are significantly different from the control as well as from each other. In particular, if only considering those shells which were heated for realistic shellfish processing/cooking durations of less than 30 minutes, the decreases in Δ_{47} values result in a confined Δ_{47}/temperature window for each cooking treatment. Thus, our experimental data strongly support the aforementioned hypothesis that clumped isotope thermometry in aragonitic skeletal remains represents a suitable diagnostic tool for detecting and differentiating between certain prehistoric cooking techniques in shell-midden deposits.

The measured alterations of $\delta^{18}O_{Carbonate}$ values generally agree with previous studies in terms of magnitude, however, differ regarding minimum temperature required for a measurable alteration of oxygen isotopes by prehistoric cooking practices. Andrus and Crowe (2002) reported no alteration of $\delta^{18}O_{Otolith}$ values at temperatures up to ~200 °C for fish otoliths, and only detected changes in isotopic signatures of otoliths burned directly in hot (~800 °C) coals (Andrus and Crowe, 2002). In contrast, Milano et al. (2016) showed only a clear decrease in the $\delta^{18}O_{Shell}$ values of mollusk shells at temperatures of >300 °C. We suggest that the difference of our data as well as the data of Milano et al. (2016) to those of Andrus and Crowe (2002) is related to the direct exposure of the mollusk shells to the cooking medium while Andrus and Crowe (2002) exposed entire fish to the different cooking treatments with otoliths protected from direct heat inside the vestibular system. This hypothesis is supported by the general agreement between our data and those data of Milano et al. (2016) who also observed similar decrease in $\delta^{18}O$ values of mollusk shells at temperatures between 300 and

700 °C. The experiment of Milano et al. (2016), however, did not include relevant roasting temperatures between 100 and 300 °C which most likely represent the temperature window where a decrease in the $\delta^{18}O_{Carbonate}$ values occurs without a conversion of primary aragonite into secondary calcite.

The different magnitudes of $\delta^{18}O_{Shell}$ alteration between this study and Milano et al. (2016) at lower temperatures (<300 °C) indicates that experimental design plays a key-role for assessing the impact of prehistoric cooking practices on paleoclimate proxy signatures of shell-midden constituents. While controlled oven experiments are a suitable approach for studying the underlying processes of aragonite-calcite conversion and for identifying isotope exchange mechanisms, the realistic simulation of prehistoric cooking practices using coal fire provides more reliable estimates about the absolute alteration of paleoenvironmental proxies in shell-midden assemblages. The stronger alteration at lower temperatures found in this study is probably related to the presence of water in the boiling treatment, high-frequency temperature variability in the roasting and burning experiment accompanied by higher gas fluxes as well as generally higher CO_2 and CO concentrations compared to closed oven setups of Milano et al. (2016). Such factors are likely to facilitate isotope exchange reaction between the carbonate mineral and the ambient cooking medium and can thus explain the higher alteration magnitude found in this study with respect to $\delta^{18}O_{Carbonate}$ values at lower cooking temperatures. Together with naturally occurring temperature fluctuations throughout realistic roasting and burning experiments, such processes might also explain the observed non-linearity of $\delta^{18}O$ alteration within the different treatments. However, independent from experimental uncertainties, our data show that $\delta^{18}O_{Shell}$ signatures do not allow distinguishing between different pre-depositional processing or cooking techniques in shell-midden deposits. Considering the magnitude of alteration among all treatments, it remains questionable whether such lowering of $\delta^{18}O_{Shell}$ values in archeological shell-midden constituents can be distinguished from natural (spatial or temporal) variation in water temperature or $\delta^{18}O_{Seawater}$ in ancient environments.

Given the apparent alteration of shell $\delta^{13}C$ values, potential alteration of ^{14}C signatures and subsequent uncertainties in measured radiocarbon ages obtained from archeological shell-midden constituents have to be expected. This hypothesis is supported by previous experiments showing that radiocarbon dates measured from food crusts on prehistoric pottery fragments can also be subjected to alteration during cooking by e.g. a reversed old-wood

effect (Philippsen, 2012). However, detailed future studies are needed to quantify the effect of pre-depositional heating on radiocarbon signatures in shell-midden constituents.

Although absolute mid-Holocene water temperature reconstructions using clumped isotope thermometry might be imprecise as a result of small but unknown deviation from theoretical equilibrium precipitation (i.e. "vital effects"), measured Δ_{47} values of the mid-Holocene bivalve shells are considerably lower than expected for natural environments. We therefore presume that these shells were heated prior to deposition. The difference in Δ_{47} values between bulk and hinge samples of the same bivalve shells suggests that the outer shell surface of most shells experienced considerably higher temperatures than the corresponding hinge region. The overlap of Δ_{47} values measured in the mid-Holocene shell with the experimentally determined Δ_{47}-window of the roasting treatment (see Fig. 3) suggests that the articulated shells were placed on heated surfaces to cause heat-related muscle relaxation which predominantly affected the outer shell surface. This might imply that not all of the excavated valves show heat-related Δ_{47} alterations, which is supported by our data (Fig. 7-3).

An alternative explanation for the post-mortem alteration of clumped isotopic signatures in the mid-Holocene bivalve shells might be the long-term sub-aerial exposure with increased soil temperatures as a consequence of high solar insolation in this sub-Sharan region. However, assuming a potential re-equilibration due to surface exposure throughout the Holocene, one would also expect a similar alteration magnitude among different bivalve shells, similar Δ_{47} values within individual shells (hinge versus bulk samples) as well as similar Δ_{47} values of the otoliths and bivalves excavated from the same shell-midden. Thus, it appears unlikely to us that the exposure to increased sediment surface temperatures caused the observed trend in the clumped isotopic signature of the mid-Holocene samples.

Although the clumped isotopic signatures of the bivalve shells show strong evidences for pre-depositional roasting, the bulk oxygen isotopic composition provides reasonable water temperature estimates for coastal regions during the mid-Holocene (Fig. 7-3). Likewise, high-resolution ontogenetic oxygen isotope records show clear seasonal water temperature signals which indicate slightly higher water temperatures during the mid-Holocene than observed today in this region (Fig. 7-4). However, whether the measured bulk $\delta^{18}O_{Carbonate}$ values or high-resolution ontogenetic $\delta^{18}O_{Carbonate}$ records of the mid-Holocene samples provide correct measures of absolute water temperatures or if they overestimate ancient water temperatures due to a pre-depositional alteration remains speculative. Given the uncertainty in absolute cooking temperatures as well as unknown durations of cooking, the absolute alteration of the

mid-Holocene bivalve shell $\delta^{18}O$ values cannot be corrected in order to reconstruct their initial oxygen isotopic composition.

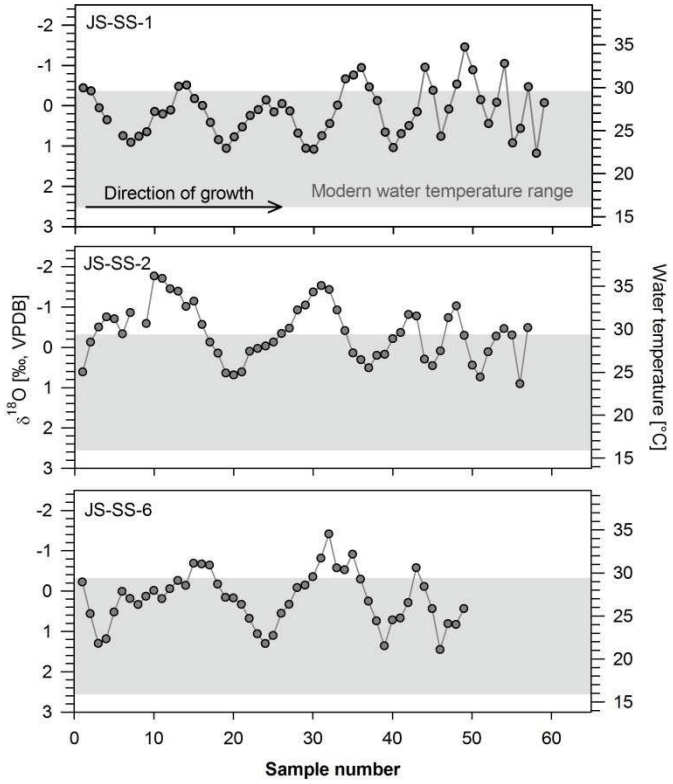

Figure 7-4: Ontogenetic oxygen isotope records of three mid-Holocene *Senilia senilis* shells and comparison with modern coastal sea surface temperature (SST) variability of the eastern Banc d`Arguin (Lavaud et al., 2013). Water temperature reconstruction was done using the equation of Grossman and Ku (1986), assuming a $\delta^{18}O_{Seawater}$ value of +1.57 ‰ (VSMOW) (Lavaud et al., 2013). Error bars for the measured $\delta^{18}O_{Carbonate}$ values and related water temperature estimates are smaller than the symbol size.

7.4.1 Implications for shell-midden sclerochronology

Our data clearly shows that prehistoric cooking significantly alters oxygen isotopic signatures of aragonitic skeletal structures even without a conversion of primary aragonite into secondary calcite. Thereby, the magnitude of oxygen isotope alteration is most likely indistinguishable from natural environmental variability and can thus cause substantial misinterpretations of ancient environmental conditions. Potential changes in cooking practices over time as a consequence of technological advancement can thus result in temporarily variable alteration of shell-midden deposits and - if not considered - lead to spurious indications of abrupt ancient climate changes. However, although shell-midden constituents which were subjected to pre-

depositional heating should not be used for the reconstruction of absolute ancient water temperatures, sub-seasonally resolved ontogenetic isotope records can be preserved and subsequently still provide important information such as fishing and foraging seasonality or site occupation pattern.

As shown by our experimental data, the temperature-dependent magnitude of clumped isotope reordering makes this proxy system a unique diagnostic tool for detecting but also differentiating between certain prehistoric cooking practices. Thereby, clumped isotope thermometry can provide new insights into social, cultural as well as technological aspects during shell-midden formation. Despite evidences of human behavior (e.g. ritualistic versus nutrition purposes of shellfish foraging or particular subsistence strategies) (McNiven and Wright, 2008; Makarewicz and Sealy, 2015; Thompson and Andrus, 2016) and new information about the function of particular sites (e.g. processing sites, dinner-time camps or residential locales) (Bird and Bird, 1997), the reconstruction of specific cooking methods also helps to test the validity of modern analogues of shell-midden formation from ethnographic or ethnohistoric observations (Hardy et al., 2016). Detailed information about specific processing techniques will broaden our understanding of prehistoric trading activities as the use of processing methods which prevent spoiling is a prerequisite for the long-term transportation of the edible portion of marine mollusks (Waselkov, 1987). Moreover, potential seasonal differences in shellfish processing techniques can contribute to our understanding of fishing and foraging seasonality and can provide a better understanding of environmental pressure induced by ancient climate changes on prehistoric coastal populations (Hastorf and DeNiro, 1985). In particular for long-term shell-midden assemblages deposited over several millennia, the reconstruction of specific processing techniques enables tracing the technological advancement over time of shell-midden accretion. Thereby, clumped isotope analysis of shell-midden constituents potentially provides information about contact of prehistoric populations with foreign cultures and the subsequent introduction of new technologies used for the efficient processing of marine faunal resources.

With regard to geochemical proxy records of shell-midden constituents, our mid-Holocene data suggest that geochemical proxy signatures of fish otoliths are generally less susceptible regarding the alteration by pre-depositional cooking practices which agrees with the experimental data of Andrus and Crowe (2002). Either the protection from external heat inside the vestibular system or the removal of fish heads prior to food preparation might have preserved their initial proxy signatures. In consequence, fish otoliths might represent more

robust sources of paleoclimate data and should preferentially be analyzed if clumped isotope thermometry cannot be used for assessing the thermal history of shell-midden constituents. However, the opening of bivalves using a heated surface was probably a widespread technique in many prehistoric cultures and was reported in many ethnographic observations (Waselkov, 1987). Consequently, if this technique can be identified using clumped isotope thermometry, the upper valves which were not altered by high temperatures might still provide reliable paleoclimate information and thereby valuable paleoclimate data.

7.5 Material and methods

7.5.1 Modern Mercenaria campechiensis shells

In total, 23 sub-adult *M. campechiensis* individuals were cultured by *Southern Cross Sea Farms*®, at Cedar-Key, FL, USA (N29° 08' 32.09662" W83° 00' 19.66703"). All individuals had the same age (14 months), similar size (~3.52 ± 0.24 cm shell height) and were reared in the same water masses throughout ontogeny. All individuals were sampled on 30 April 2015 and shipped overnight to RSMAS and sacrificed on 01 May 2015 immediately after arrival. Shells were manually cleaned with tap water, dried at room temperature and stored at ~ 20° C until the experiment. In each treatment, right valves of six shells were exposed for 15 to 360 minutes. Treatments were (1) boiling in seawater at ~100 °C, (2) roasting over charcoal at ~174 ± 13 °C and (3) burning in charcoal at 554 ± 95 °C while five untreated shell were used as control. Afterwards, all shells were cleaned for 24 hours with 60 ml ultrapure 10 % hydrogen peroxide buffered to a pH of ~8.2 with NaOH following the protocol of Bastidas and Garcìa (1999) at room temperature to remove the periostracum and other organic compounds and grinded using a ceramic pestle and mortar. Powdered bulk samples were stored in sealed glass vials at room temperature.

7.5.2 Mid-Holocene samples

Mid-Holocene specimens were excavated from a shell-midden in the Ras el Sass area, Mauritania, NW Africa. For details of the study area and spatial distribution of shell-midden deposits see Barusseau et al. (2007) and the map provided in the supplementary information (Suppl. Fig. 7-S1). All shells and otoliths were ultrasonically cleaned in deionized water and dried at 40 °C for 48 hours. Shells were cut along the direction of maximum growth and otoliths along the transversal plane using a tap water-cooled UniPrec WOCO 50 saw with a 0.6 mm thick diamond blade. The hinge region of each shell was sampled using a U-Power®

UP200 hand drill equipped with a 0.8 mm tungsten-carbide dental drill at lowest possible RPM (RPM ≈ 1000). Thick sections (~2 mm) were prepared along the direction of maximum growth and were sampled in the outer shell layer using a NewWave/Merchantec Micromill system. Posterior halves of the shells and otoliths were ground using a ceramic pestle and mortar. Powdered samples were stored in sealed glass vials at room temperature until chemical analysis. The anterior halves of the otoliths were ground in a similar manner and aliquots of ~50 mg each were used for mineralogical analyses and radiocarbon dating. Similarly, a piece of each shell was prepared for mineralogical analysis and radiocarbon dating by cutting a slice of shell material from the ventral margin of the anterior halves using a Dremel™ tool equipped with a diamond cutting wheel.

7.5.3 Mineralogical analyses

Mineralogy of the experimental shells was measured using a PANalytical X´Pert PRO diffractometer with a Cu-tube (kα 1.541 Å, 45.0 kV, 40.0 mA) at RSMAS, Miami, FL, USA. Measurements were done using a continuous scan from 23.0-35.0 2Θ with a step size of 0.005 2Θ and a measuring time of 0.1 seconds per step. Data collection and processing was done using the software X'Pert Data Collector and X'Pert HighScore Plus, respectively. Relative abundance of aragonite and calcite were determined using the relative peak areas of aragonite (1,1,1) peak (2Θ = 26.1°) and low magnesium calcite (1,0,1) peak (2Θ = 29.6°) against a calibrated standard. Archeological XRD-samples were analyzed with a Philips X´Pert Pro diffractometer equipped with a Cu-tube (kα 1.541, 45 kV, 40.0 mA) at the University of Bremen, Germany. Measurements were done using a continuous scan from 3-85° 2Θ with step sizes of 0.016° 2Θ. We used the Philips software X´Pert HighScore™ for data processing. Abundance of aragonite and calcite was determined using the relative peak areas of aragonite (1,1,1) peak (2Θ = 26.1°) and low magnesium calcite (1,0,1) peak (2Θ = 29.6°) against a calibrated standard. Mineralogical data of the experimental and mid-Holocene samples are reported in the supplementary information (Suppl. Tab. 7-S2 and 7-S5).

7.5.4 Radiocarbon dating

Radiocarbon dating of four otoliths and three bivalve shells was done at the Poznan Radiocarbon Laboratory, Poznan, Poland using a standard protocol for accelerator mass spectrometry. Calibration of conventional radiocarbon ages was done with OxCal 4.2.4 (Bronk Ramsey, 2009) using the Marine13 calibration curve (Reimer et al., 2013) and assuming a local reservoir age of ΔR = -300 yrs., which represents an average estimate for

the local mid-Holocene reservoir ages based on several paired radiocarbon dates along the Mauritanian coastline throughout the Holocene (J. F. Saliége, unpublished data) which is also supported by radiocarbon dates from this archeological site. Raw as well as calibrated radiocarbon ages are reported in the supplementary information (Suppl. Tab. 7-S4).

7.5.5 Clumped isotope analysis

Clumped isotope analysis of the powdered bulk samples were performed at the Stable Isotope Laboratory of the Rosenstiel School of Marine and Atmospheric Science (RSMAS), Miami, FL, United States, using the analytical procedure described in Murray et al. (2016). Each sample was analyzed at least two times in a randomized order. All samples were processed on the stainless-steel cryogenic vacuum extraction line at RSMAS, evacuated to $<10^{-6}$ mbar using two turbo-molecular pumps (Balzer TPU 170 and Edwards 50EX). Individual sample aliquots of ~8.0 mg powder were digested for 30 minutes at 90°C in 3.5 ml ~105 % phosphoric acid (H_3PO_4) using a modified "Fairbanks" device (Swart et al., 1991) connected to a common acid bath. Resulting CO_2 was then purified on the cryogenic vacuum extraction line following the protocol described in detail in Murray et al. (2016).

Purified CO_2 was measured at RSMAS using a dual-inlet MAT-253 gas source isotope ratio mass spectrometer (Thermo Fisher Scientific, Bremen, Germany). Samples were measured against an in-house working-gas gas standard. We analyzed each sample at a signal intensity of 12 V on mass-44 over 6 acquisitions of 15 sample-standard measurements. Data reduction and normalization for Δ_{47} and temperature calculations followed the methods of Affek and Eiler (2006) and Huntington et al. (2009). To check for potential contamination, samples were scrutinized based on their offset of δ48 and Δ_{48} (Huntington et al., 2009). Precision of clumped isotope analysis is reported using the average 1σ standard errors.

We measured $\delta^{13}C$ and $\delta^{18}O$ of the samples by means of masses 45/44 and 46/44, respectively using a method adapted from Craig (1957) modified for a multi-collector mass spectrometer. Shell and otolith $\delta^{13}C$ and $\delta^{18}O$ values were calibrated using NBS-19 and reported relative to Vienna Pee Dee Belemnite (VPDB). External precision of $\delta^{13}C$ and $\delta^{18}O$ analyses was better than ±0.055 and ±0.117 ‰, respectively. All Δ_{47} values were calculated using the method described by Affek and Eiler (2006) and Huntington et al. (2009). Translation into the absolute reference frame (ARF) was accomplished using the method described by Dennis et al. (2011) with 1000, 50 and 25 °C water equilibrated gasses. All isotope data are reported in the supplementary information (Suppl. Tab. 7-S2 and 7-S5).

Recent publications of Schauer et al. (2016) and Daëron et al. (2016) have suggested a small difference between the correction protocols proposed by Santrock et al. (1985) and Brand et al. (2010) leading to differences in the calculated $\delta^{13}C$, $\delta^{18}O$ and Δ_{47} values. These differences are small (~0.02 ‰) for $\delta^{13}C$ and $\delta^{18}O$ and generally within the external precision of the analytical method. For Δ_{47}, the suggested changes were more significant and dependent upon the $\delta^{13}C$ value of the material being analyzed. These differences increased from essentially no changes for a sample with a $\delta^{13}C$ value close to 0 ‰ to 0.04‰ for a sample with a $\delta^{13}C$ value of -40 ‰. We compared our method of calculating $\delta^{13}C$ and $\delta^{18}O$ values modified from Craig (1957) and found the difference between our method and that proposed by Brand et al. (2010) to show only a 0.03 ‰ difference for samples with a $\delta^{13}C$ difference of -40 ‰. This decreases to less than 0.01 ‰ for $\delta^{13}C$ values of samples analyzed in this study. Hence, based on the range of $\delta^{13}C$ values of the samples measured in this study we conclude that the artefacts noted by Schauer et al. (2016) and Daëron et al. (2016) do not significantly impact the results presented here.

7.5.6 Ontogenetic oxygen isotope records

Sub-samples drilled from the outer shell layer (~80–100 μg) were measured on a Finnigan MAT 251 isotope ratio mass spectrometer connected to a Kiel III automated carbonate preparation device at the stable isotope laboratory in the Center for Marine Environmental Sciences (MARUM), University of Bremen, Germany. The long-term standard deviation of the in-house standard (Solnhofen limestone) was better than 0.06 ‰ for $\delta^{18}O$.

7.5.7 Statistical analysis

We used a one way analysis of variances (ANOVA) with a Bonferroni-corrected t-test as post hoc test. The assessment of equal variances and normal distributions was done using a Levene's test and a Shapiro-Wilk test, respectively. In case of non-normal distributed data (mineralogy), we used a Kruskal-Wallis one way ANOVA on ranks and the Dunn's method as post hoc test. The significant levels for all statistical test were set to $\alpha = 0.05$. Results of the statistical analyses are reported in the supplementary information (Suppl. Tab. 7-S3).

7.6 Acknowledgements

Funding for this work was provided by the Leibniz Centre for Tropical Marine Research (ZMT), Bremen, Germany and the Bremen International Graduate School for Marine

Sciences (Glomar), Bremen, Germany. We thank the following people and organisations for their assistance and support: Southern Cross Sea Farms, Cedar Key, FL, USA for providing the samples. Christopher Kaiser (RSMAS) and Christoph Vogt (University of Bremen) for help with the XRD analyses, Sharmila Giri, and Amel Saeid (both University of Miami) for assistance with the lab work and Hanno Müller (ZMT) for support with the statistical analysis.

7.7 Supplemental Information

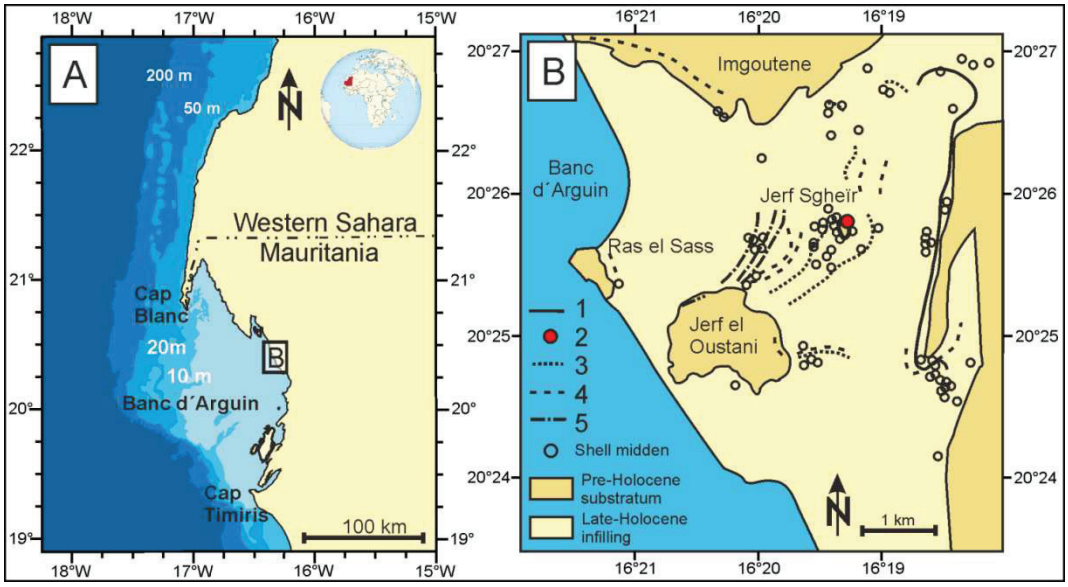

Figure 7-S1: Map of the research area, Mauritania, NW Africa. **A)** Mauritanian/Western Sahara coastline with the shallow shelf area of the Banc d´Arguin, modified from Müller et al. (2015a, Chapter 6 of this thesis). **B)** Close-up of the study site in the hinterland of Ras el Sass in the mouth of a large paleo-estuary. The location of shell-midden alignments and beach ridges show the human occupation pattern following the coastal progradation throughout the mid- to late-Holocene: 1: >5000 years BP according to archeological evidences; 2: Jerf Sgheïr shell-midden of this study (5,320-5,020 cal. yrs. BP); 3: Tintan group (4600-4000 uncal. yrs. BP); 4: Last Neolithic groups (3300 uncal. yrs. BP) 5: Copper Age groups, (2700-2600 uncal. yrs. BP), modified from Barusseau et al. (2007).

Table 7-S2: Mineralogy and proxy data of the cooking experiment. Each sample represents a single right valve of a *Mercenaria campechiensis* individual. Contamination of the initial aragonitic mineralogy within the control shells are related to the sporadic but clearly visible incorporation of dolomite grains within the inner layer of the shell originating from the dolomite catchment area of the adjacent estuaries.

Sample / Treatment	Exp. time [min]	Δ_{47} [‰, ARF]	SE (±) [‰, ARF]	$\delta^{18}O$ [‰, VPDB]	$\delta^{13}C$ [‰, VPDB]	Aragonite [wgt %]	Calcite [wgt %]	Dolomite [wgt %]
Control								
MC-1R	0	0.7038	0.0127	0.06	-3.80	99.0	0.0	1.0
MC-2R	0	0.7043	0.0134	0.06	-3.87	97.0	0.0	3.0
MC-3R	0	0.7117	0.0127	-0.10	-3.88	100.0	0.0	0.0
MC-4R	0	0.6699	0.0140	-0.05	-3.86	100.0	0.0	0.0
MC-5R	0	0.6747	0.0130	-0.08	-3.93	100.0	0.0	0.0
Boiling								
SW-15	15	0.6652	0.0157	-0.26	-4.02	100.0	0.0	0.0
SW-15	40	0.6703	0.0135	-0.62	-4.07	100.0	0.0	0.0
SW-15	60	0.6829	0.0144	-0.34	-3.84	100.0	0.0	0.0
SW-120	120	0.6424	0.0125	-0.24	-3.73	100.0	0.0	0.0
SW-240	240	0.6639	0.012	-0.31	-3.76	100.0	0.0	0.0
SW-240	360	0.6764	0.0127	-0.50	-3.83	100.0	0.0	0.0
Roasting								
R-15R	15	0.6003	0.0129	-0.40	-3.94	100.0	0.0	0.0
R-30R	30	0.605	0.0125	-0.47	-3.86	100.0	0.0	0.0
R-60R	60	0.5349	0.0135	-0.36	-3.77	100.0	0.0	0.0
R-120R	120	0.5146	0.0134	-0.51	-4.07	100.0	0.0	0.0
R-240R	240	0.5008	0.0136	-0.55	-3.89	100.0	0.0	0.0
R-360R	360	0.5534	0.0133	-0.25	-3.55	100.0	0.0	0.0
Roasting								
B-15R	15	0.3424	0.0122	-0.62	-3.93	31.0	69.0	0.0
B-30R	30	0.3739	0.0126	-0.38	-3.83	83.0	17.0	0.0
B-60R	60	0.4113	0.0132	-0.48	-3.74	81.0	19.0	0.0
B-120R	120	0.3999	0.0112	-0.66	-4.15	100	0.0	0.0
B-240R	240	0.3458	0.0149	-0.70	-3.89	31.0	69.0	0.0
B-360R	360	0.3241	0.0134	-0.92	-4.20	0.0	100.0	0.0

Table 7-S3: Results of the statistical analysis. The significant levels for all statistical test were set to $\alpha = 0.05$. Bold numbers indicate significant differences between two treatments.

Treatments	Δ_{47}	$\delta^{18}O$	$\delta^{13}C$	Mineralogy*
Control vs. boiling	>0.05	**<0.05**	>0.05	>0.05
Control vs. roasting	**<0.001**	**<0.001**	>0.05	>0.05
Control vs. burning	**<0.001**	**<0.001**	>0.05	>0.05
Boiling vs. roasting	**<0.001**	>0.05	>0.05	>0.05
Boiling vs. burning	**<0.001**	**<0.05**	>0.05	**<0.05**
Roasting vs. burning	**<0.001**	>0.05	>0.05	**<0.05**

*) ANOVA on ranks

Table 7-S4: Results of the radiocarbon dating and calibration using OxCal 4.2.4. Radiocarbon dates of three bivalve shells and four otoliths excavated from the Ras el Sass area, Mauritania, NW Africa. Radiocarbon ages were calibrated with OxCal 4.2.4 (Bronk Ramsey, 1995) using the Marine13 calibration curve (Reimer et al., 2013) with a local ΔR value of -300 yrs. (J.-F. Saliège, unpublished data) which is supported by the analysis of paired terrestrial/marine samples (Ash-1/OTO-BX), providing a local estimate for the ΔR value of ~-330 yrs.

Sample	Material	Lab Code	^{14}C age [yrs BP]	Uncertainty [^{14}C yrs]	ΔR [yrs.]	cal. yrs. BP from	cal. yrs. BP to	Median	Uncertainty + [yrs]	Uncertainty - [yrs]
Layer 1										
JS-SS-1	Bivalve	Poz-69422	4830	35	-300	5270	4990	5130	140	140
JS-SS-2	Bivalve	Poz-69424	4770	35	-300	5210	4880	5020	190	140
JS-SS-3	Bivalve	Poz-69425	4845	35	-300	5280	5020	5150	130	130
Layer 2										
Ash-1	Ashy soil	Pa2344	4900	40						
OTO-B3	Otolith	Poz-60777	4920	30	-300	5330	5070	5260	70	190
OTO-B4	Otolith	Poz-60778	4970	30	-300	5430	5250	5320	110	70
OTO-B8	Otolith	Poz-71188	4920	35	-300	5390	5060	5260	130	200
OTO-B9	Otolith	Poz-71189	4970	35	-300	5440	5240	5320	120	80

Table 7-S5: Mineralogy and proxy raw data of the mid-Holocene samples. Clumped isotopic composition, conventional oxygen and carbon isotope as well as mineralogical raw data of the mid-Holocene samples excavated from a shell-midden at the northern Mauritanian coast, NW Africa. Minor occurrences of primary calcite within catfish otoliths from Mauritania was also found in modern fish otoliths (<2 % calcite).

Sample	Organism	Sample type	Δ_{47} [‰, ARF]	SE (±) [‰, ARF]	$\delta^{18}O$ [‰, VPDB]	$\delta^{13}C$ [‰, VPDB]	Aragonite [wgt %]	Calcite [wgt %]
Shell-midden layer 1								
JS-SS-1	Bivalve	Bulk	0.6681	0.0142	0.83	-0.16	100.0	0.0
	Bivalve	Hinge	0.6392	0.0157	1.13	-0.35	-	-
JS-SS-2	Bivalve	Bulk	0.5956	0.0137	0.35	-0.53	100.0	0.0
	Bivalve	Hinge	0.6585	0.0142	0.10	-0.87	-	-
JS-SS-3	Bivalve	Bulk	0.6300	0.0130	0.69	0.79	100.0	0.0
	Bivalve	Hinge	0.6815	0.0149	0.91	0.03	-	-
JS-SS-4	Bivalve	Bulk	0.6208	0.0120	0.02	0.10	100.0	0.0
	Bivalve	Hinge	0.6784	0.0141	0.13	-0.19	-	-
JS-SS-5	Bivalve	Bulk	0.6535	0.0134	-0.29	0.03	100.0	0.0
	Bivalve	Hinge	0.6754	0.0142	-0.02	-0.29	-	-
JS-SS-6	Bivalve	Bulk	0.7086	0.0134	0.69	0.13	100.0	0.0
	Bivalve	Hinge	0.6675	0.0144	0.46	0.64	-	-
JS-SS-10	Bivalve	Bulk	0.6104	0.0170	0.51	0.52	100.0	0.0
	Bivalve	Hinge	0.6891	0.0149	0.80	0.12	-	-
Shell-midden layer 2								
OTO-B3	Otolith	Bulk	0.7082	0.0132	0.06	-1.42	98.0	2.0
OTO-B4	Otolith	Bulk	0.7052	0.0115	0.28	-0.58	96.0	4.0
OTO-B8	Otolith	Bulk	0.6954	0.0140	0.30	-0.75	100.0	0.0
OTO-B9	Otolith	Bulk	0.6565	0.0161	0.15	-1.78	100.0	0.0

8. Otolith and bivalve oxygen isotope records of monsoon precipitation discharge during the mid- to late-Holocene of NW Africa

Peter Müller[1*], Henry C. Wu[2, 3], Jean-Paul Barusseau[4], Robert Vernet[5], Hildegard Westphal[1,6]

[1]Leibniz Centre for Tropical Marine Research, 28359 Bremen, Germany.

[2] Institut de Recherche pour le Développement, France Nord, LOCEAN, 32 Avenue Henri Varagnat, 93143 Bondy, France

[3] Laboratoire des Sciences du Climat et de l'Environnement, LSCE/IPSL, CEA-CNRS-UVSQ, Université Paris-Saclay, 91198 Gif-sur-Yvette, France

[4] Centre de Formation et de Recherche sur les Environnements Méditerranéens, University of Perpignan Via Domitia, Perpignan, France.

[5] Institut Mauritanien de Recherches Scientifiques, Nouakchott, Mauritania.

[6] Department of Geosciences, University of Bremen, Bremen, Germany.

[*]**Corresponding author:** Peter Müller, Fahrenheitstraße 6, 28359 Bremen, Germany, phone +49 421 23800 178, email peter.mueller@leibniz-zmt.de

In preparation for submission to *Geology*

Personal contribution to Chapter 8:

PM (80 %) and HW (20 %) conceived the study, RV (50 %) and JPB (50 %) provided archeological samples; PM (100 %) accomplished the proxy analyses; PM (50), HCW (30 %), HW (10 %), RV (5 %), JPB (5 %), contributed to data interpretation and wrote the manuscript.

8.1 Abstract

The aridification pattern of NW Africa during the mid-Holocene still represents a matter of controversial debate. While most marine paleoclimate records indicate a rather abrupt aridification around ~5.5 ka BP, terrestrial paleoclimate records suggest a spatially and temporally heterogeneous transition from the African Humid Period towards the modern arid state. To bridge these conflicting marine and terrestrial paleoclimate data, we analyzed highest-resolution (sub-seasonal) ontogenetic $\delta^{18}O$ records of bivalve shells and catfish otoliths from an archeological site within a large paleo- estuary system along the Banc d`Arguin, Mauritania, NW Africa close to ODP Site 658C. By strongly overestimating modern water temperatures, our mid Holocene (~5.1 ka BP) $\delta^{18}O$-based water temperature reconstructions give strong evidences for isotopically lighter monsoon discharge even after the supposed 5.5 ka BP aridification event but also show that fully marine conditions were established by ~3.4 ka BP. Thereby our data support the hypothesis of a rather gradual aridification of the Mauritanian hinterland that, however, concluded the modern arid state by ~3 ka BP. Hence, the abruptly increasing terrigenous dust export after 5.5 ka BP may be attributed to rather distal source areas of terrigenous material which does not necessarily include the adjacent coastal zones.

8.2 Introduction

Previous studies showed consistently that large parts of the present-day Sahara and Sahel region were dominated by dense savanna and shrub vegetation between ~15 to ~5 ka BP, the so-called African Humid Period (AHP) (Ritchie et al., 1985; deMenocal et al., 2000a; Kuhlmann et al., 2004; Holz et al., 2007; Kröpelin et al., 2008; Roberts, 2014). However, the termination of the AHP and the transition to the modern arid state is still a matter of controversial debate (Kröpelin et al., 2008; Claussen et al., 2014; Pausata et al., 2016). Many marine records indicate an abrupt aridification around 5.5 ka BP potentially triggered by feedback mechanisms amplifying the gradually declining insolation during the mid- to late-Holocene (deMenocal et al., 2000a; Kuhlmann et al., 2004; McGee et al., 2013). In contrast, many terrestrial and archeological deposits indicate spatially as well as temporally variable changes during the mid- to late-Holocene and generally a more gradual transition towards the present-day arid climate (Kröpelin et al., 2008; Armitage et al., 2015; Bloszies et al., 2015). Despite conflicting evidences from different proxy records, many climate models experiments fail to reproduce the suggested abruptness of the mid-Holocene climate evolution (Liu et al., 2007; Rachmayani et al., 2015; Pausata et al., 2016). In consequence, we are still lacking a holistic understanding of the temporal and spatial aridification pattern of NW Africa during the Holocene and subsequently of the underlying mechanisms controlling the intensity and spatial extend of the West African Monsoon (WAM). This in turn hampers reliable predictions regarding the response of the WAM to future climate changes.

In this study, we used ontogenetic oxygen isotope ($\delta^{18}O$) records of modern and archeological catfish otoliths and *Senilia senilis* (Bivalvia) shells from the Rass el Sass area, Mauritania, NW Africa for paleoenvironmental reconstructions. Several studies showed that sub-seasonally resolved ontogenetic $\delta^{18}O$ records of catfish otoliths represent reliable recorders of environmental conditions (Surge and Walker, 2005; Müller et al., 2015a, Chapter 6 of this thesis). Likewise, *S. senilis* shells have been shown to provide precise records of water temperature in intertidal environments along the NW African coast (Azzoug et al., 2012b; Lavaud et al., 2013). Previous studies also showed that these $\delta^{18}O$ records represent reliable recorders of seasonal monsoon discharge (Surge and Walker, 2005; Azzoug et al., 2012b) as a consequence of negative excursion in ambient $\delta^{18}O_{Seawater}$ values caused by isotopically lighter monsoon precipitation discharge. Therefore, if isotopically lighter precipitation was drained into the Ras el Sass area during the mid-Holocene our data are likely to show a combined signal of seasonal water temperature and seasonal monsoon discharge.

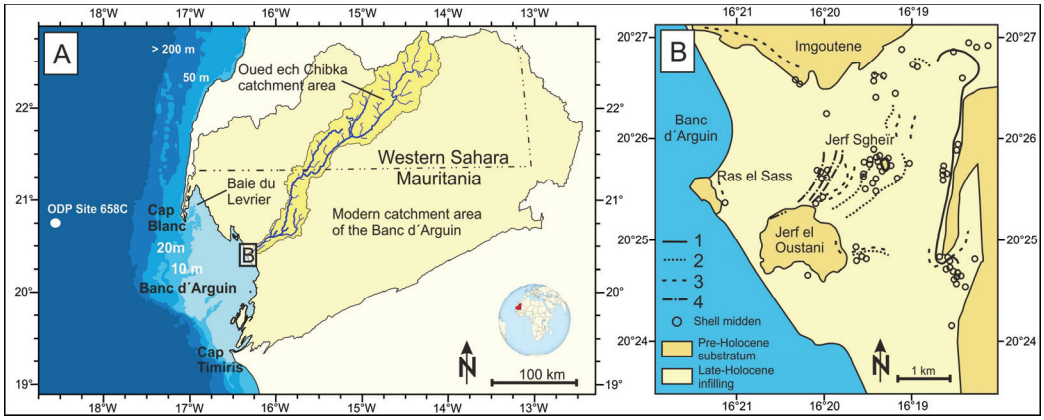

Figure 8-1: Map of the research area, Mauritania, NW Africa. **A)** Overview map with the modern catchment of the Oued ech Chibka wadi system which is part of the ancient Tamanrasett estuary (Skonieczny et al., 2015). The catchment area was calculated using the SCALGOLive software (www.scalgo.com) and the World SRTM base map. **B)** Close-up of the working area on the Jerf Sgheïr paleo-island with multiple shell-midden deposits inside the mouth of the Tamanrasett paleo-estuary. The location of shell-midden alignments and beach ridges showing human occupation following the coastal progradation during the mid-Holocene: 1: No ^{14}C ages; ages but according to archaeology >5000 years BP; 2: Tintan group radiocarbon dated to 4600-4000 uncal. yrs. BP; 3: Last Neolithic groups radiocarbon dated to 3300 uncal. yrs. BP; 4: Copper Age groups radiocarbon dated to 2700-2600 uncal. yrs. BP. Maps modified after Barusseau et al. (2007) and Müller et al. (under revision, Chapter 7 of this thesis.).

8.3 Material and methods

We measured high-resolution ontogenetic oxygen isotope records of one modern *Carlarius parkii* otolith, six archeological catfish otoliths (*Carlarius* spp.), and four archeological *S. senilis* shells from then inner Banc d`Arguin, Mauritania, NW Africa. The archeological samples were excavated from a succession of midden deposited in the vicinity of the paleo-island Jerf Sgheïr (Fig. 8-1). Individual radiocarbon dating of the otoliths and bivalve shells resulted in a consistent age range from 3.4 to 5.3 cal. yrs BP, covering the main aridification period of NW Africa during the Holocene. These data sets were combined with previously published high-resolution $\delta^{18}O_{Carbonate}$ records of a modern catfish otolith (*Carlarius heudelotii* from Müller et al. (2015a, Chapter 6 of this thesis)), three modern bivalve shells (*S. senilis* from Lavaud et al. (2013)), and three mid-Holocene bivalve shells (*S. senilis* from Müller et al., under revision, Chapter 7 of this thesis.).

Thick section preparation and sub-sampling of the modern and archeological fish otoliths and bivalve shells was done using a Merchantec® Micromill following the protocol described in Müller et al. (2015a, Chapter 6 of this thesis). The oxygen isotopic composition of individual sub-samples (~50 μg) was determined using a Finnigan MAT 251 gas isotope ratio mass

spectrometer (IRMS) connected to a Kiel III device at the Center for Marine Environmental Sciences (MARUM), University of Bremen, Germany and a ThermoFinnigan MAT 253 IRMS connected to a Kiel IV device at ZMT, Bremen, Germany. Repeated standard measurements (NBS19 and in-house working standards) revealed an external precision (1σ) for all measurements of better than ±0.06‰ for all $\delta^{18}O_{Carbonate}$ analyses. Reconstruction of modern and Holocene water temperature was done using the equations of Thorrold et al. (1997) and Grossman and Ku (1986) assuming a constant $\delta^{18}O_{Seawater}$ composition of 0.68 ‰ VSMOW (Müller et al., 2015a, Chapter 6 of this thesis) and 1.57 ‰ VSMOW (Lavaud et al., 2013) for the fish otoliths and bivalve shells, respectively. We only used oxygen isotope data from the first 4-6 years of otolith growth that show a clear seasonal cyclicity (see supplemental Fig. 8-S1 and 8-S2).

8.4 Results and discussion

Previous studies showed that *S. senilis* shells are precipitated in or close to isotopic equilibrium with the ambient seawater, resulting in accurate sub-seasonally resolved $\delta^{18}O_{Carbonate}$-based water temperature records with a mean absolute error (MAE) of ≤ 1.5 °C (Lavaud et al., 2013). For the inner Banc d'Arguin, the maximum range of $\delta^{18}O_{Carbonate}$-based water temperature reconstructions using *S. senilis* shells (16.0 to 29.5 °C) was found to be in very good agreement with measured temperature ranges (15.9 to 29.5 °C) (Lavaud et al., 2013).

Similar to *S. senilis* shells, catfish otoliths have been shown to represent reliable recorders of ambient water temperature, in particular during the early-life stages where growth rates are the highest (Surge and Walker, 2005; Müller et al., 2015a, Chapter 6 of this thesis). Similar to the modern *C. heudelotii* otolith $\delta^{18}O$ record published in Müller et al. (2015a, Chapter 6 of this thesis), the $\delta^{18}O$ record of the modern Guinean sea catfish (*C. parkii)* otolith shows a clear seasonal cyclicity varying between -0.45 and +1.47 ‰ VPDB with an average $\delta^{18}O_{Carbonate}$ composition of +0.32 ‰ VPDB. Assuming a constant $\delta^{18}O_{Seawater}$ of +0.68 ‰ VSMOW, the values translate into water temperatures ranging from 18.0 to 27.0 °C with an average value of 23.4 °C, which is in good agreement with measured water temperature variations throughout the year (see supplemental Fig. 8-S1).

Today, the two catfish species *C. heudelotii* and *C. parkii* occur on the shallow Banc d´Arguin whose otoliths can hardly be distinguished from each other in archeological deposits (Dirk Nolf; Philippe Tous; pers. comm.). Both demersal species are generally similar in terms of

maximum length (approx. 750 mm and 760 mm for *C. heudelotii* and *C. parkii*, respectively) but slightly differ in terms of preferred habitat (Marceniuk and Menezes, 2007). While *C. parkii* prefers marine and brackish environments, *C. heudelotii* is more commonly associated with brackish and freshwater ecosystems along the NW African coast (Schneider, 1990; Marceniuk and Menezes, 2007). Given the preferential occurrence of both species in freshwater-associated environments, otolith-based water temperature reconstructions for the mid- and late-Holocene are likely to be biased towards higher water temperatures if isotopically lighter monsoon precipitation was drained onto the Banc d´Arguin during the mid- to late-Holocene. Considering the shallow water depth of < 20 m in most parts of the Banc d´Arguin, a generally well-mixed water column (Westphal et al., 2014) and the existence of paleo-estuaries all along its coastline (see Fig. 8-1) (Cuq, 1993; Skonieczny et al., 2015), monsoon-related variations in $\delta^{18}O_{Seawater}$ during the mid- to late-Holocene are likely to be visible even in more offshore areas of the Banc d´Arguin.

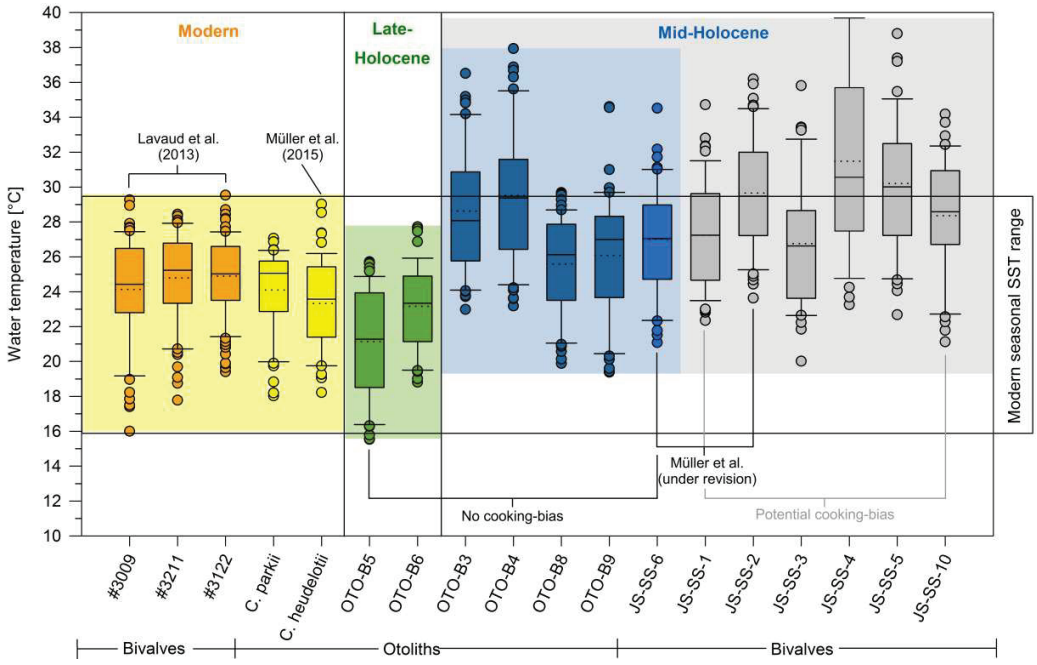

Figure 8-2: Boxplot of reconstructed modern, late- and mid-Holocene water temperatures using ontogenetic oxygen isotope records of modern and archeological catfish otoliths and bivalve shells, plotted against the measured local modern water temperature range (Lavaud et al., 2013) for intertidal coastal areas in the eastern inner Banc d`Arguin. The box and whispers correspond to the 65 and 95 % confidence intervals, respectively. Individual points represent outliers. Solid and dotted horizontal lines inside the box show the median and average reconstructed water temperature values, respectively. Yellow and green areas represent maximum modern and late-Holocene SST variation. The grey area represents mid-Holocene SST variations based on all mid-Holocene samples. The blue are represents mid-Holocene SST variation considering only samples which do not show any evidence for pre-depositional heating (Müller et al., under revision, Chapter 7 of this thesis).

The late-Holocene otoliths (3.4 to 3.5 ka BP) show a clear seasonal cycle within their ontogenetic oxygen isotope records. Measured $\delta^{18}O_{Carbonate}$ values vary between -0.59 and +2.03 ‰ VPDB which translates into water temperatures ranging from 15.5 to 27.8 °C (see supplemental Fig. 8-S2). Average $\delta^{18}O_{Carbonate}$ values are +0.83 and +0.44 ‰ VPDB, translating into average water temperatures of 20.9 and 23.0 °C, respectively, which is slightly lower then observed today in the coastal areas of the inner Banc d'Arguin (Lavaud et al., 2013), see Fig. 8-2. However, considering the uncertainty of modern otolith temperature reconstructions (MAE ≤ 1 °C, (Müller et al., 2015a, Chapter 6 of this thesis)) our water temperature reconstructions are in agreement with alkenone based SST estimates for the late-Holocene which also show similar (± 1 °C) water temperatures as observed today (Zhao et al., 2000; Adkins et al., 2006; Kim et al., 2007). Thereby, our data do not show any evidence for isotopically lighter monsoon - freshwater discharge at ~3.5 ka BP that would lead to considerable water temperature overestimations. This is consistent with previous paleoclimate reconstructions that showed arid conditions were fully established by ~3.5 ka BP in most parts of NW Africa (deMenocal et al., 2000a; Kröpelin et al., 2008).

The mid-Holocene *S. senilis* shells show a clear sinusoidal oxygen isotope signature varying between minimum and maximum $\delta^{18}O$ values of -3.3 and +1.7 ‰ VPDB (see supplemental Fig. 8-2). Assuming a constant $\delta^{18}O_{Seawater}$ value of 1.57 ‰ VSMOW these values translate into sub-seasonally resolved water temperature records varying between 20.0 and 43.5 °C with average water temperatures between 27.0 and 31.5 °C (see Fig. 8-2). Thereby, the mid-Holocene *S. senilis* shells strongly overestimate modern average seasonal water temperature minima and maxima by +6.1 and +7.7 °C, respectively.

The mid-Holocene otoliths also show a clear seasonal cyclicity within their ontogenetic $\delta^{18}O$ records similar to the modern and late-Holocene samples. However, their measured $\delta^{18}O_{Carbonate}$ values are considerably lower than modern and late-Holocene equivalents, varying between -2.61 and +1.18 ‰ VPDB with average values between -0.7 and 0.0 ‰ (see supplemental Fig. 8-S2). These $\delta^{18}O_{Carbonate}$ values translate into reconstructed water temperatures ranging from 19.4 to 37.9 °C and average values between 25.2 and 28.5 °C (see Fig. 8-2). The average seasonal minimum temperature was found to be 21.4 °C and an average seasonal maximum temperature is 34.7 °C, which is +5.5 and +5.2 °C warmer than observed today during the cold and warm season, respectively (see Fig. 8-2).

These consistent high mid-Holocene water temperatures among several otoliths and bivalve shells are in opposition to mid-Holocene SST estimates from different climate models (~+0.4

to +1.5 °C) (Kutzbach and Liu, 1997; Kim et al., 2007) as well as marine paleoclimate proxy records from the same latitude (~±0 °C) (Chapman et al., 1996; Elderfield and Ganssen, 2000; Henderiks and Bollmann, 2004). Likewise, foraminifera $\delta^{18}O$ record of the eastern tropical Atlantic was found to be rather stable during this period, indicating only a very minor tendency towards lower $\delta^{18}O_{Seawater}$ values during the mid- to late-Holocene (Kim et al., 2007). Neither the relative small changes in water temperatures nor the small tendency towards lower $\delta^{18}O_{Seawater}$ values throughout the mid- to late-Holocene can explain the high water temperatures found consistently among various skeletal components.

Müller et al. (under revision, Chapter 7 of this thesis) showed that six out of seven *S. senilis* shells analyzed in this study may have been subjected to pre-depositional heating (i.e. cooking) while all otoliths appear to be pristine. These pre-depositional heated samples might be biased towards lower isotopic values (i.e. higher temperatures) mimicking the effect of potential freshwater runoff. However, there is a very good agreement between the reconstructed water temperatures among the bivalve shells (cooked vs. uncooked) and in particular between the supposably cooked bivalve shells and the pristine fish otoliths (Fig. 8-2), indicating no or only a very minor alteration of shell $\delta^{18}O$ values. Even if assuming a potential pre-depositional alteration, the magnitude of modern and presumably mid-Holocene water temperature overestimations by the ontogenetic $\delta^{18}O_{Shell}$ records are considerably larger than any experimentally determined magnitude of $\delta^{18}O$ alteration by a variety of prehistoric cooking methods (< 4.2 °C) (Müller et al., under revision, Chapter 7 of this thesis). We therefore presume that also the measured *S. senilis* $\delta^{18}O$ records provide robust information regarding the paleoenvironmental conditions during the mid-Holocene.

We therefore argue that isotopically lighter monsoon discharge caused considerable changes in coastal $\delta^{18}O_{Seawater}$ values that finally lead to a strong overestimation of ancient water temperatures. Using the equation of Grossman and Ku (1986), a lowering of the estuarine $\delta^{18}O_{Seawater}$ by about 2 ‰ VSMOW during the WAM season in Senegal, representing the modern analog of the Banc d´Arguin during the mid-Holocene (Azzoug et al., 2012b) results in a water temperature overestimation of ~9.4 °C. This is in good agreement with the average overestimation of modern water temperatures of 6.9 °C by the mid-Holocene *S. Senilis* shells and further supports the aforementioned hypothesis.

8.5 Conclusions

By providing evidence for monsoon discharge at 5.1 ka BP at ~20.5°N, our data support the hypothesis of Liu et al.(2007) suggesting a decoupling of vegetation collapse and decrease of monsoon precipitation over NW Africa during the mid- to late Holocene. Their coupled global atmosphere-ocean-land model suggests an abrupt change in vegetation throughout NW Africa around 5 ka BP while the monsoon precipitation was found to decrease more gradually. This allows to explain the contrasting evidence for an abrupt change in vegetation deduced from adjacent marine dust records (deMenocal et al., 2000a) and the evidence for the persistence of coastal monsoon precipitation after the 5.5 ka BP by our data. Thereby, our data support the results of Liu et al. (2007) questioning the importance of feedback mechanisms for the climate evolution of NW throughout the mid- to late-Holocene. However, our data also support the establishment of arid conditions at ~20.5°N at 3.5 ka BP, which is in agreement with most paleoclimate records as well as most climate models (deMenocal et al., 2000a; Gasse, 2000; Kröpelin et al., 2008).

8.6 Acknowledgments

Funding for this study was provided by the Leibniz Centre for Tropical Marine Research (ZMT), Bremen, Germany. We gratefully acknowledge the helpful discussions with Matthias López-Correa and André Klicpera. We thank the following people for their assistance and support: SCLAGOlive (www.scalgo.com) for providing the catchment area data, Philippe Tous for providing modern otolith samples, Sebastian Flotow (ZMT) for sample preparation, Dr. Henning Kuhnert (University of Bremen) and Dorothee Dasbach (ZMT) for support with the oxygen isotope analysis.

8.7 Supplemental material

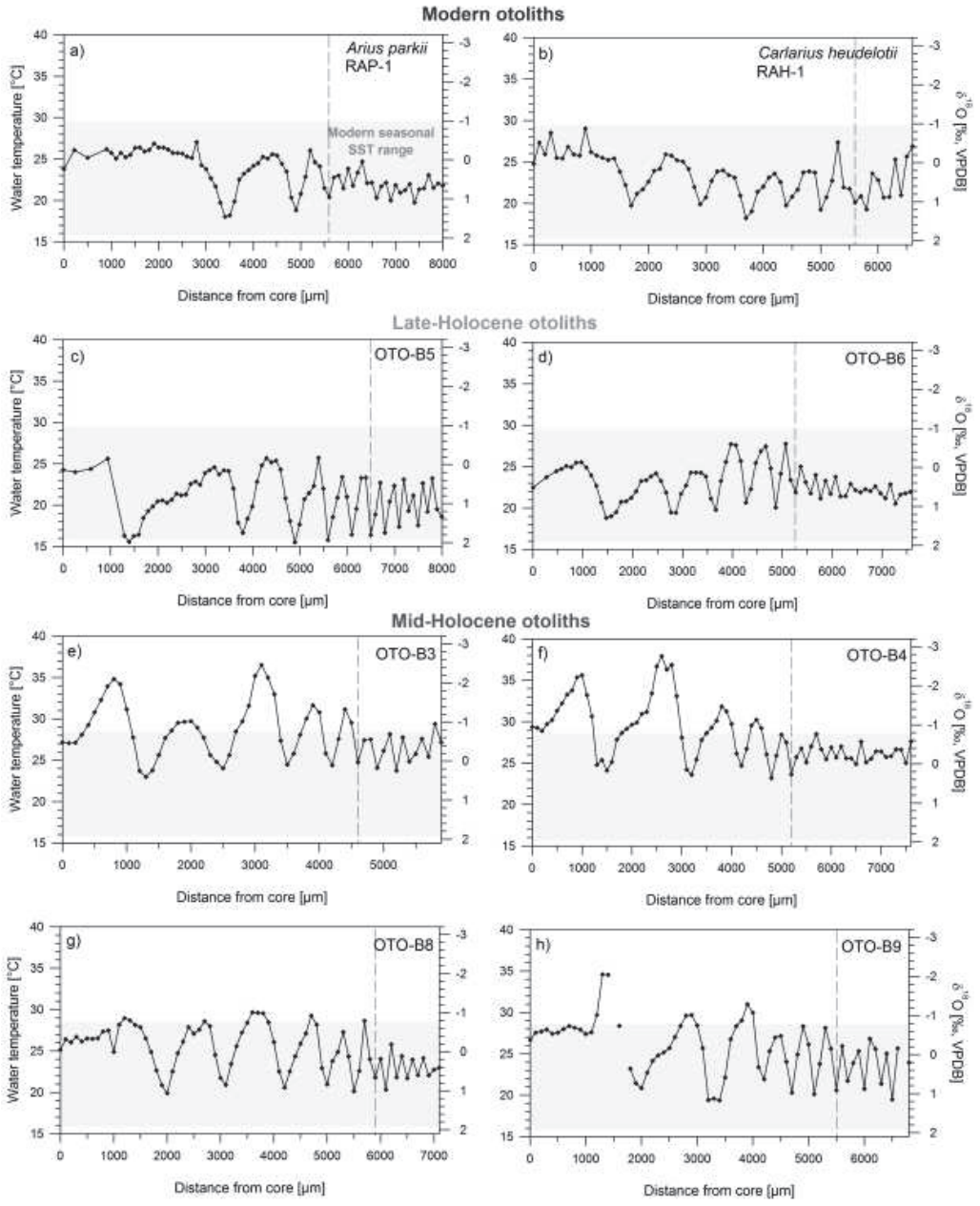

Figure 8-S1: Ontogenetic oxygen isotope records of all catfish otoliths analyzed in this study and from Müller et al. (2015a, Chapter 6 of this thesis) (modern *Carlarius heudelotii, panel* b) with estimated water temperatures using the equation of Throrrold et al. (1997) assuming a constant $\delta^{18}O_{Seawater}$ value of +0.68 ‰ (VSMOW) (Müller et al., 2015a, Chapter 6 of this thesis). The dashed vertical line indicates the boundary between a clear sub-annual resolution of the isotope records during earlier life stages (left) and insufficiently coarser resolution due to ontogenetically decreasing annual growth rates (right). Only the sub-seasonally resolved intercepts of the isotope records have been used in this study.

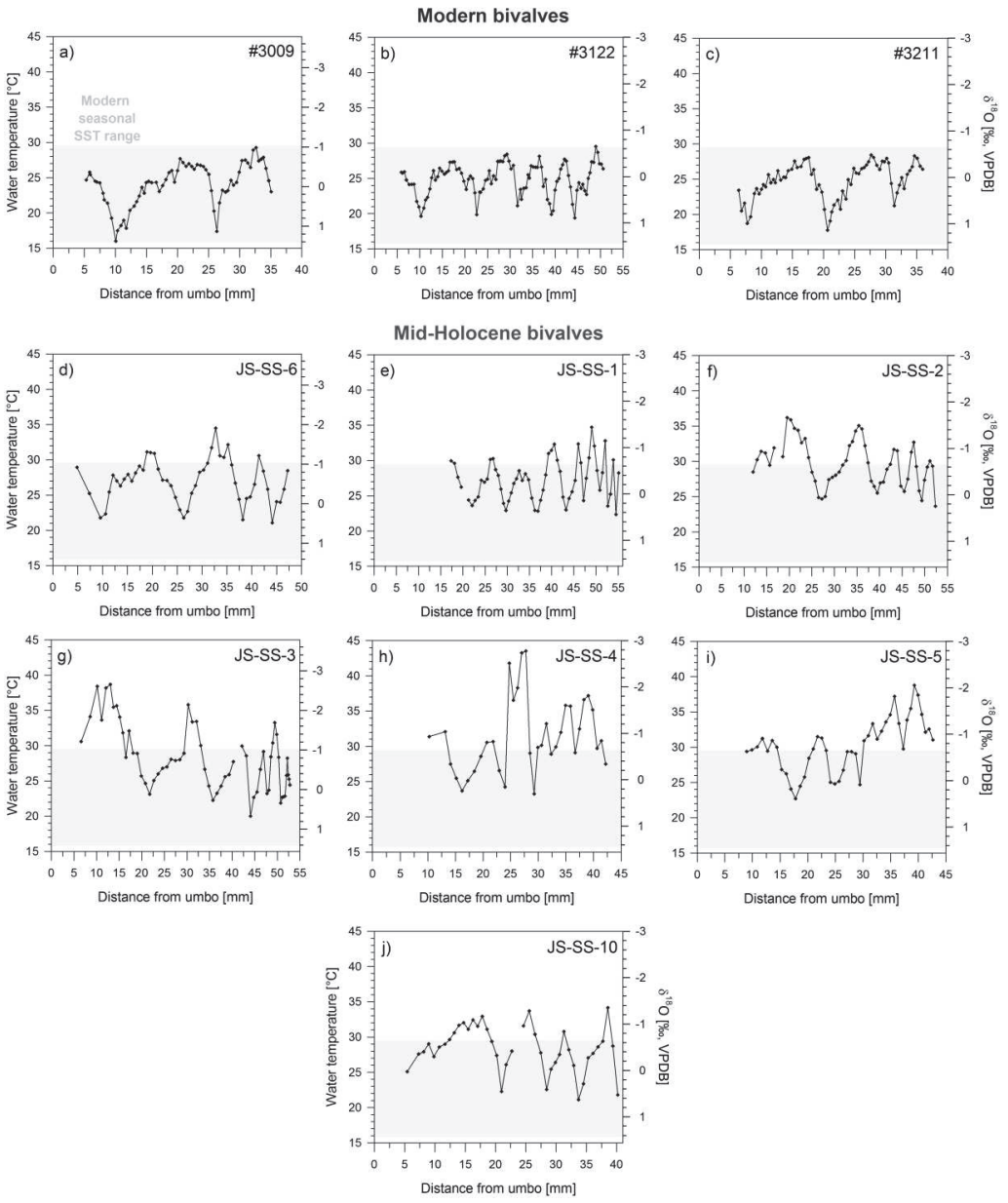

Figure 8-S2: Ontogenetic oxygen isotope records of all *Senilia senilis* shells analyzed in this study and from Lavaud et al. (2013) (modern *Senilia senilis* shells, panels a, b, and c), from Müller et al. (in revision, see Chapter 7 of this thesis, panels d, e, and f) with estimated water temperatures using the equation of Grossman and Ku (1986) and assuming a constant $\delta^{18}O_{Seawater}$ value of +1.57 ‰ (VSMOW) (Lavaud et al. 2013). The dashed vertical line indicates the boundary between a clear sub-annual resolution of the isotope records during earlier life stages (left) and insufficiently coarser resolution due to ontogenetically decreasing annual growth rates (right). Only the sub-seasonally resolved intercepts of the isotope records have been used in this study.

Table 8-S3: Samples and data used in this study.

Samples	Age [cal. ka BP]	Sample ID	Organism	Location	Reference
Fish otolith	modern	RAH1	*Carlarius heudelotii*	Baie du Lévrier	Müller et al. (2015a)
Fish otolith	modern	RAP1	*Carlarius parkii*	Baie du Lévrier	This study
Bivalve shell	modern	#3009 #3122 #3211	*Senilia senilis*	Iwik	Lavaud et al (2013)
Fish otolith	3.4	OTO-B5	*Carlarius* spp.	Jerf Sgheïr	This study
	3.5	OTO-B6			
	5.3	OTO-B3			
	5.3	OTO-B4			
	5.3	OTO-B8			
	5.3	OTO-B9			
Bivalve shell	5.1	JS-SS-1	*Senilia senilis*	Jerf Sgheïr	Müller et al. (in revision, Chapter 7 of this thesis)
	5.0	JS-SS-2			
	5.2	JS-SS-3			
Bivalve shell	-	JS-SS-4	*Senilia senilis*	Jerf Sgheïr	This study
	-	JS-SS-5			
	-	JS-SS-6			
	-	JS-SS-10			

9. EXTENDED DISCUSSION

Numerous previous studies showed that the oxygen isotopic composition of a broad range of skeletal structures from marine calcifying organisms is in or close to the thermodynamic (i.e. isotopic) equilibrium with the ambient seawater (e.g. Swart, 1983; Grossman and Ku, 1986; Patterson et al., 1993; Thorrold et al., 1997; Candelier et al., 2013). However, previous studies showed consistently that calcareous skeletal structures of echinoderms exhibit remarkable deviations from the expected isotopic equilibrium and tend to lower oxygen isotopic compositions (e.g. Weber, 1968; Baumiller, 2001; Gorzelak et al., 2012). This thesis generally confirms these previous studies in showing that spines of the echinoid species *Eucidaris galapagensis* tend towards lower isotopic compositions as expected under equilibrium conditions (Müller et al., in press, Chapter 5 of this thesis). In particular the measured carbon isotopic composition of the *E. galapagensis* spines indicates that additional metabolic or environmental mechanisms are affecting the proxy incorporation into the spine calcite. Even though our data generally indicate that the oxygen isotopic composition of *E. galapagensis* spines can provide meaningful reconstructions of (ancient) water temperature, additional studies are needed to further explore the impact of physiological processes on proxy incorporation in echinoderm skeletons in order to improve their applicability for paleoenvironmental reconstructions.

A wide range of previous studies showed consistently that in particular incrementally banded mollusk shells or fish otoliths bear the potential to provide sub-seasonally resolved paleoenvironmental information (Andrus et al., 2002; Surge and Walker, 2005; Schöne et al., 2005b; Surge et al., 2008; Versteegh et al., 2012; Lavaud et al., 2013). This thesis generally confirm these previous studies in showing that sub-seasonally resolved water temperature reconstructions can be obtained from ontogenetic oxygen isotope records of modern and archeological catfish otoliths and bivalve shells (Müller et al., 2015a, Chapter 6 of this thesis; Müller et al., under revision, Chapter 7 of this thesis; Müller et al., in prep., Chapter 8 of this thesis),

In particular shells of the bivalve *Senilia senilis* have a high potential as a reliable, sub-seasonally resolved archive of past environmental conditions by the means of ontogenetic oxygen isotope records (Lavaud et al., 2013). Despite information about ancient water temperature, its strong association with intertidal, estuarine environments makes it a promising 'bio-recorder' of seasonal monsoon discharge in West Africa (Azzoug et al., 2012a; Azzoug et al., 2012b). This

is related to the different oxygen isotopic compositions of freshwater relative to isotopic composition of seawater which can finally lead to distinct excursions within the isotopic signature of the *S. senilis* shells towards lighter values during the monsoon season (Azzoug et al., 2012b). Similarly, ontogenetic oxygen isotope signatures of otoliths from freshwater associated catfish species can provide similar indications for (paleo-) freshwater runoff signatures throughout the Holocene (Müller et al., in prep., Chapter 8 of this thesis; Surge and Walker, 2006).

Both, *S. senilis* shells and catfish (*Carlarius* spp.) otoliths occur frequently in archeological shell-midden deposits along the NW African coast. As most of these shell-middens were deposited by Neolithic hunter- and gatherer societies in paleo-estuarine environments (Vernet and Tous, 2004; Barusseau et al., 2007; Vernet, 2007), these proxy archives bear a high potential for broadening our knowledge of the mid- to late-Holocene aridification pattern of NW Africa (Lavaud et al., 2013; Müller et al., 2015a, Chapter 6 of this thesis). However, similar to other paleoenvironmental reconstructions using geochemical proxy signatures of marine calcifiers, the unknown isotopic composition of mid-Holocene freshwater runoff as well as mid-Holocene seawater complicate their interpretation and limit the reliability of absolute water temperature estimates (Müller et al., in prep., Chapter 8 of this thesis). The contemporaneous occurrence of seasonal water temperature maxima and potential monsoon precipitation discharge pulses during boreal summer impedes a thorough disentanglement of their superimposed effect on the isotopic composition. This interactive effect of temperature and $\delta^{18}O_{Seawater}$ (i.e. salinity) has already been observed in other studies on fish otoliths (Surge and Walker, 2005) and bivalve shells (Azzoug et al., 2012b) and has been shown to limit the reliability of absolute water temperature estimations using skeletal structures originating from coastal environments such as the Banc d`Arguin. Thus, additional paleoenvironmental proxies are desired to thoroughly disentangle the individual contribution of water temperature and freshwater discharge in particular for the mid-Holocene of NW Africa.

As mentioned in Chapter 1, alternative geochemical proxy systems such as element/Ca ratios or clumped isotopes are either not fully understood due to a variety of interdigitated biological or environmental processes or still constricted by a limited number of available calibrations and comparably large analytical uncertainties, respectively. However, reconstructed individual growth pattern based on ontogenetic isotope records of calcareous skeletal structures may provide such additional (paleo-) environmental information since growth pattern of many marine organisms are also controlled by ambient environmental conditions such as e.g. water

temperature, food availability or salinity (Müller et al., 2015a, Chapter 6 of this thesis). Using the VBGF-approach described in Müller et al. (2015a, Chapter 6 of this thesis), ontogenetic $\delta^{18}O$ records of fish otoliths or bivalve shells can be used for the straightforward reconstruction of the theoretical maximum length of an otolith or a bivalve shell (L_∞), the growth coefficient (K) which represents a factor enunciating the time until L_∞ is reached, and for seasonally oscillating growth, the factor C determining the seasonal growth oscillation following a sinusoidal oscillation. The relative changes in these growth parameters in modern and ancient bivalve shells or fish otoliths may contain additional information about relative changes in environmental conditions over time.

However, previous studies showed considerable variation of these growth parameters within individuals from the same environment but also among populations from different areas (Munro, J.; Pauly, 1983). In consequence, the parameters L_∞ and K have most likely only a limited validity for inferring changes in growth parameter induced by environmental changes over time. Based on this observation, the same authors proposed a normalized measure of growth performance (phi-prime, Φ') which based on the relationship between the growth coefficient (K) and the asymptotic maximum weight of an organism (W_∞). Given the mostly linear relationship between fish weight and maximum length, Pauly and Munro (1984) also defined length-based growth performance equation following

$$\Phi' = Log_{10}k + 2Log_{10}L_\infty \qquad \text{(Eq. 9.1)}$$

where Φ' represent the species-specific growth performance based on the asymptotic maximum length L_∞ and the growth coefficient K of a given organism. This usually normally distributed species-specific growth performance **Φ'** allows an improved comparison of growth pattern among individuals from e.g. different habitats (Pauly and Munro, 1984). Using either a simple Gulland and Holt plot (see Fig. 6-3) or for more precise results the (so)VBGF approach described in Müller et al. (2015a, Chapter 6 of this thesis), one can easily calculate the $\delta^{18}O$-based growth parameters L_∞ and K and subsequently the growth performance **Φ'** for any accretionary structure of a given organisms (e.g. a bivalve shell or a fish otolith). The isotope-based growth performance will be referred to as **Φ''** in the following in order to avoid confusion with the traditional phi-prime index (Φ') relating to growth in body length.

By comparing the frequency distribution of Φ' values of 66 bivalve species, Vakily (1992) showed that they generally cluster in narrow range for species-groups but in particular for certain species. Subsequently, the Φ' concept is commonly used to test for consistency within

growth data sets obtained from literature. Despite this, Vakily (1992) also showed significant correlations of estimated bivalve Φ'-values against average annual water temperature for various bivalve species groups (e.g. Mytilidae and Pectinidae) as well as for bivalve species with similar shell shapes (oval shell form) (see Fig. 9-1), which has later been supported by other studies on marine bivalves (e.g. Stern-Pirlot and Wolff, 2006). Interestingly, the goodness of fit further increases when correlating Φ' values against the geographic latitude for the above mentioned species/shape groups (Vakily, 1992), indicating that the latitudinal water temperature change plays a major role in determining growth parameters among a wide range of bivalve species (see Fig. 9-1). Similarly, previous studies on the variability of fish growth performance also showed a strong latitudinal (i.e. water temperature) gradient (Pörtner et al., 2001).

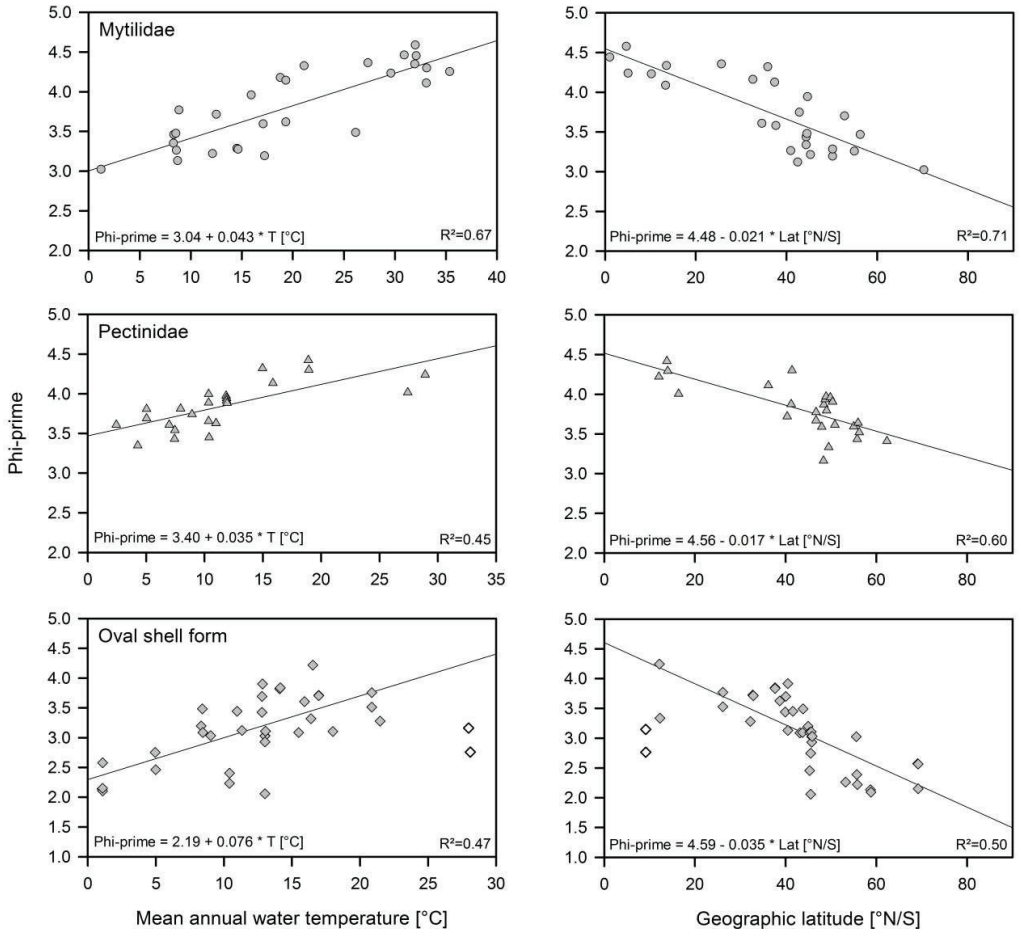

Figure 9-1: Plot of Φ' values of different species groups (Mytilidae (top), Pectinidae (middle)), and species with similar shells shapes (oval shell form (bottom)) against mean annual water temperature (left) and geographic latitude (right). The open symbols in the lower panel have been omitted from the linear regression. Redrawn from **Vakily (1992)**.

These consistent observations of predominantly temperature-dependent variation of growth performances among marine organisms have important implication for the potential application

of the Φ'-concept on isotope-based growth parameters in a paleoenvironmental context: Firstly, by calculating Φ'' values from a given set of modern bivalve shells or fish otoliths, the reliability of isotope-based growth parameters can be assessed by comparing among individuals and with conventionally estimated growth parameters from the literature. Secondly, the application of the Φ'-concept on isotope-based growth data may provide additional information about relative changes in environmental conditions in a certain environment over time and therefore serve as an alternative 'soft' proxy extending the use of geochemical proxies in accretionary skeletal structures for paleoenvironmental reconstructions.

To test this assumption, individual oxygen isotope-based growth parameters (L_∞, K and Φ'') were calculated for modern, late- and mid-Holocene catfish otoliths as well as the modern and mid-Holocene bivalve shells from the Banc d`Arguin, Mauritania. Therefore, ontogenetic oxygen isotope data of two modern catfish otoliths from Müller et al. (2015a, Chapter 6 of this thesis) and Müller et al. (in prep., Chapter 8 of this thesis), and mid- to late-Holocene oxygen isotope data from Müller et al. (in prep., Chapter 8 of this thesis) were used. For the comparison of *Senilia senilis* growth, we used modern oxygen isotope records of three *S. senilis* individuals published in Lavaud et al. (2013) and mid-Holocene oxygen isotope records of six shells from Müller et al. (in prep., Chapter 8 of this thesis). All growth parameters were calculated using a modified version of the R-script provided in Müller et al. (2015a; 2015b) and Eq. (9.1). We only used the first three to five seasonal cycles (i.e. years) of the oxygen isotope records which show a clear sub-seasonal resolution (see Fig. 8-S1 and 8-S2). The approximate modern summer temperature maxima on September 1st and the winter temperature minima on February 1st were used as temporal anchor points for the reconstructed $\delta^{18}O$-based water temperature maxima and minima, respectively. All calculated growth parameters are given in Tab. 9-1 and 9-2.

The $\delta^{18}O_{Otolith}$-derived growth parameter of modern and Holocene otoliths were compared with fish-length-based growth parameters of Conand et al. (1995) for *Carlarius heudelotii* and *Carlarius parkii* from coastal water off Guinea. The $\delta^{18}O_{Shell}$-derived growth parameters of modern and mid-Holocene *S. senilis* shells were compared with measured growth parameters from Banc d´Arguin, Mauritania (Wolff et al., 1987; Van der Geest, 2013) as well as three independent studies from Sierra Leone (Ndomahina, 1975; Okera, 1976; Ansa and Sikoki, 2005). The absolute growth parameters of Wolff et al. (1987) were extracted from Stern-Pirlot and Wolff (2006).

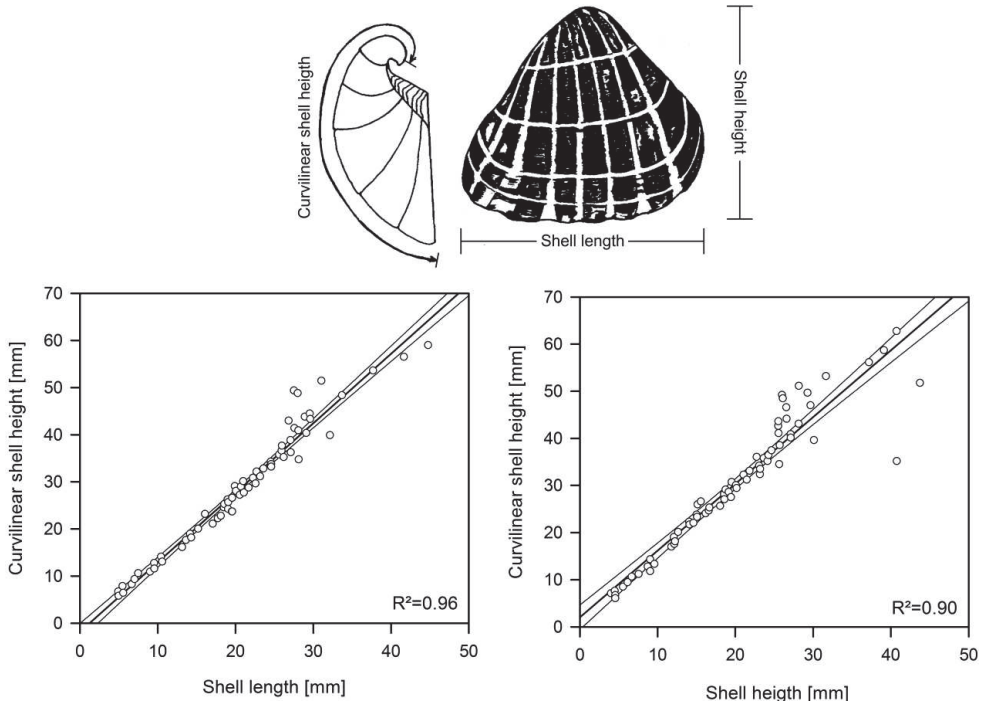

Figure 9-2: Relationship between the different spatial components of bivalve shell growth. Modified after Okera (1976) and Ndomahina (1975).

As mentioned in Müller et al. (2015a, Chapter 6 of this thesis), the comparison between literature-derived bivalve growth parameters but also between conventional and isotope-derived growth parameters can be hampered by inconsistent shell size measurements referring to different spatial components of shell growth. Absolute shells growth can either be measured referring to the shell length (anterior-posterior distance), the linear shell height (dorsal-ventral distance) or the curvilinear shell height (dorsal-ventral distance including the shell curvature), see Fig. 9-2. Even though all parameters are linearly related and should therefore show the same trend for a given cohort, minor differences impede a reliable direct comparison. However, similar to the theoretical data provided in the supplemental material of Müller et al. (2015a, Chapter 6 of this thesis), Ndomahina (1975) found a linear relationship between the different spatial components for *S. senilis* shells following the equation

$$Curvilinear\ shell\ heigth = 1.3555 \cdot Shell\ length - 0.3335 \qquad \text{(Eq. 9.2)}$$

and

$$Curvilinear\ shell\ height = 1.3333 \cdot Shell\ height + 3.3489 \qquad \text{(Eq. 9.3)}$$

with all measured distances in millimeter [mm], see Fig. 9-2. Therefore, if necessary, all shell growth parameter from the literature were converted into curvilinear shell height using

equation (9.2 and 9.3). (see Tab. 9-2), which is the common reference scale used for sampling of ontogenetic isotope signatures ((curvilinear) distance from umbo).

Table 9-1: Growth parameters calculated based on $\delta^{18}O$-signatures of modern and Holocene otoliths of the catfish species *Carlarius heudelotii* and *Carlarius parkii* as well as growth parameters for both species based on fish length from the literature (Conand et al., 1995).

	L_{inf} [mm]	K	t_0	Φ' / Φ''
Modern ($\delta^{18}O_{Otolith}$-based)				
C. heudelotii (RAH1)	6.705	0.28	0.38	7.11
C. parkii (RAP1)	8.000	0.48	0.14	7.48
Average	7.353	0.38	0.26	7.30
Standard deviation	±0.92	±0.14	±0.17	±0.26
Modern (fish length-based) after Conand et al. (1995)				
C. heudelotii	700	0.14		2.84
C. parkii	612	0.17		2.81
Average	656	0.16		2.83
Standard deviation	±62	±0.02		±0.03
Late Holocene (*Carlarius* spp. $\delta^{18}O_{Otolith}$ -based)				
OTO-B5	8.490	0.28	0.28	7.31
OTO-B6	7.570	0.21	0.13	7.09
Average	8.030	0.25	0.205	7.20
Standard deviation	±0.65	±0.05	±0.11	±0.16
Mid-Holocene (*Carlarius* spp. $\delta^{18}O_{Otolith}$ -based)				
OTO-B3	5.955	0.31	0.47	7.05
OTO-B4	7.600	0.27	0.25	7.19
OTO-B8	7.300	0.31	0.23	7.22
OTO-B9	6.800	0.31	0.11	7.15
Average	6.914	0.30	0.27	7.15
Standard deviation	±0.72	±0.02	±0.15	±0.07

As shown in Fig. 9-3, the estimated Φ'' values of the modern as well as Holocene otoliths are in very good agreement with each other. This generally supports the assumption that ontogenetic $\delta^{18}O$ data can be used to calculate reasonable growth parameters. However, the comparison of estimated modern Φ'' values with conventionally determined Φ' values based on fish length-based (Conand et al., 1995) shows considerable differences whose magnitude can not only be explained by potentially different environmental conditions (Fig. 9-3). As already hypothesized in Müller et al. (2015a, Chapter 6 of this thesis), the different scales (otolith size versus fish length) impede a direct comparison of $\delta^{18}O_{Otolith}$-based growth data and

conventional fish length-based growth data. However, given the predominantly linear relationship between otolith size and total fish length (Warburton, 1978), this approach may still provide reliable growth data and subsequently additional (paleo-) environmental information. Nevertheless, future studies on the variability of Φ'' values derived from single-species $\delta^{18}O_{Otolith}$ records are needed to confirm this hypothesis before reliable conclusions regarding its actual applicability can be drawn.

Table 9-2: Growth parameters calculated based on $\delta^{18}O$-signatures of modern and Holocene *Senilia senilis* shells (modern data from Lavaud et al. (2013)) as well curvilinear shell height-based growth parameters for the same species from different latitude from the literature.

	L_∞ [mm]	K	t_0	Φ' / Φ''	Lat [°N]	Temp. [°C]
Modern ($\delta^{18}O_{Shell}$-based; data from Lavaud et al. (2012))						
Senilia senilis (#3009)	51.25	0.45	0.45	3.08	19.5	23.0
Senilia senilis (#3122)	64.29	0.25	0.31	3.02	19.5	23.0
Senilia senilis (#3211)	47.57	0.42	0.59	2.98	19.5	23.0
Average	54.37	0.37	0.45	3.03	19.5	23.0
Standard deviation	±8.79	±0.11	±0.14	±0.05		
Modern Mauritania						
Van der Geest (2013)	106.01*	0.06		2.84	19.5	23.0
Wolf et al. (1987)	106.01*	0.09		3.00	19.5	23.0
Modern Sierra Leone						
Ansa and Sikoki (2005)	66.30**	0.46		3.31	7	27.0
Ndomahina (1975)	58.90	0.55		3.35	7	27.0
Okera (1976)	88.68***	0.31		3.39	7	27.0
Mid-Holocene Mauritania ($\delta^{18}O_{Shell}$-based)						
JS-SS-1	68.65	0.20	0.18	2.97	20.2	
JS-SS-2	54.48	0.57	0.88	3.23	20.2	
JS-SS-3	57.94	0.50	0.16	3.22	20.2	
JS-SS-4	42.64	0.34	0.60	2.79	20.2	
JS-SS-5	42.65	0.35	0.66	2.80	20.2	
JS-SS-6	64.89	0.32	0.48	3.13	20.2	
JS-SS-10	87.32	0.11	0.67	2.92	20.2	
Average	55.21	0.38	0.49	3.01	20.2	
Standard deviation	15.76	0.16	0.27	0.19		

*) Converted from linear shell-height into curvilinear shell-height using the equation Eq. (9.2).
**) Converted from linear shell-length into curvilinear shell-height using the equation Eq. (9.3).
***) Converted from shell-length into curvilinear shell-height using equation provided in the same study.

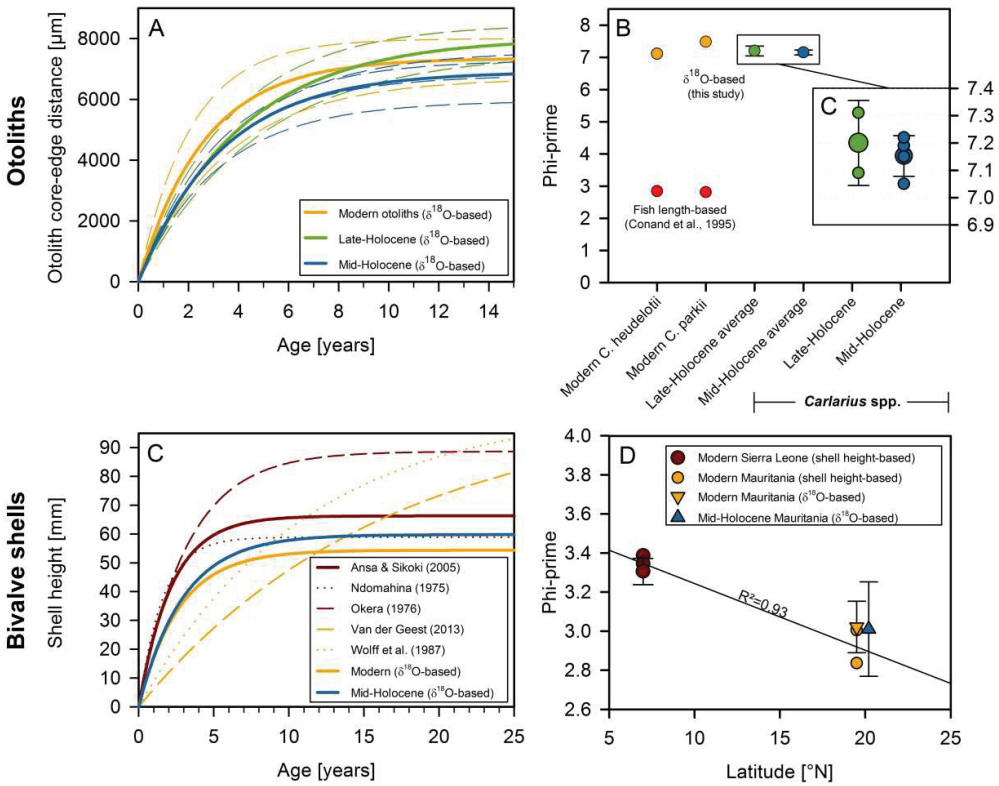

Figure 9-3: Comparison of $\delta^{18}O$-based and conventional growth pattern from literature and their environmental significance. To increase the comparability, the spawning time (t_0) was always set to 0. **A)** Comparison of modern, late-, and mid-Holocene growth parameters for *Carlarius* spp. otoliths based on their $\delta^{18}O$ signatures. The solid lines represent average values, the dashed lines individual otolith curves. **B)** Comparison of the $\delta^{18}O$-based Φ'' values with fish length-based Φ' values of *Carlarius heudelotii* and *Carlarius parkii*. **C)** Comparison of $\delta^{18}O$-based and conventional curvilinear shell height-based growth parameters for *Senilis senilis* from different environments. **D)** All $\delta^{18}O$-based Φ'' values and (curvilinear) shell height-based Φ' values of *Senilis senilis* plotted against geographical latitude (error bars represent the 1σ standard deviation).

For the *S. senilis* shells, there is a very good agreement between the conventionally determined growth performance estimates among studies from the same latitude. All studies from Sierra Leone resulted in very consistent Φ' values ranging from 3.31 to 3.39. For the Banc d´Arguin, calculated Φ' values also show a good agreement with values ranging from 2.84 to 3.00. The differences between Φ' estimates using the data of Wolff et al. (1987) and those of Van der Geest (2013) for the Banc d´Arguin might be related to the fact that the growth coefficient (K) measurement of Van der Geest (2013) was done during a comparably short period in winter which is the season of reduced growth of *S. senilis* on the Banc d´Arguin (Lavaud et al., 2013). A year-round measurement of K would have resulted most likely in slightly higher K-values and subsequently higher Φ'-estimates. Nevertheless, there is a clear latitudinal gradient of Φ' values for *S. senilis* along the NW African coast (see Fig. 9-3D) explaining 93 % of the variation in growth performances. Although the available data set does

not allow testing the impact of other environmental conditions such as salinity of primary production, the very good agreement of this data set with the general temperature-dependency of Φ' found in other bivalve species groups by Vakily (1992) indicates that water temperature is a major driver of growth in *S. senilis*.

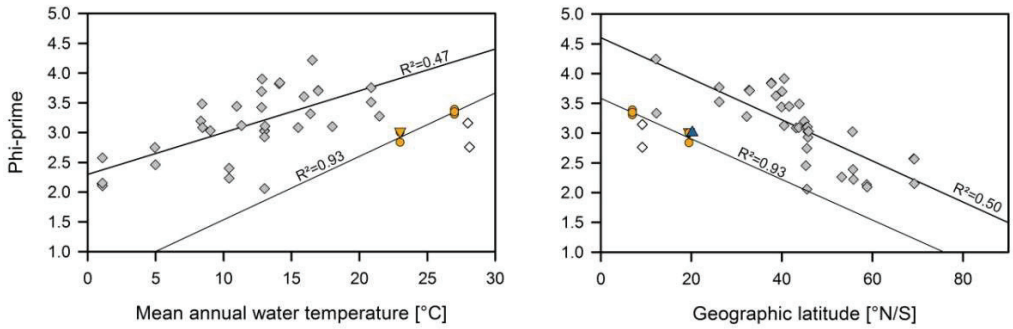

Figure 9-4: Variation of phi-prime (Φ' and Φ'') values along an environmental and latitudinal gradient. **Left:** Correlation of curvilinear Φ' and Φ'' values against mean annual water temperature for various species with an oval shell form from based on shell height measurements from Vakily (1992) (grey diamonds), modern *Senilia senilis* shells based on shell height measurements (yellow circles) and modern *Senilia senilis* shells based on their ontogenetic oxygen isotope signature (yellow triangles). **Right:** Correlation of curvilinear Φ' and Φ'' values against latitude (°N and °S), also including the average Φ'' value of the mid-Holocene *Senilia senilis* shells from the Banc d´Arguin (blue triangles).

In contrast to the otolith data, estimated Φ'' values of *S. senilis* shells should be comparable to conventional Φ' values as they all refer to curvilinear shell height. As shown in Fig. 9-3D, there is a very good agreement between estimated modern Φ'' and Φ' values for *S. senilis* from the Banc d´Arguin. Even though there are apparent difference regarding the growth coefficients (K) as well as the theoretical maximum sizes (L_∞) (see Fig. 9-3C), the similarity of estimated Φ'' values with literature-based Φ' estimates confirms the general applicability of the Φ''-concept on ontogenetic bivalve shell $\delta^{18}O$ signatures.

The estimated Φ''–values of the mid-Holocene shells are in very good agreement with their modern equivalents as well as conventional Φ' estimates of modern shells from the Banc d´Arguin. Considering the latitudinal gradient of Φ' values for *S. senilis* similar to the slope found by Vakily (1992) (Fig. 9-4) which indicates that temperature is a major driver of growth in *S. senilis*, one would expect significantly higher Φ'' values for the mid-Holocene if water temperatures were substantially higher during that time as indicated by the absolute $\delta^{18}O_{Shell}$ values (Müller et al., in prep., Chapter 8 of this thesis). The isotope-based water temperature reconstructions of the mid-Holocene *S. senilis* shells indicate on average ~6.9 °C warmer water temperature on the Banc d´Arguin during the mid-Holocene than observed today,

which could have either been caused by a higher absolute water temperature during the mid-Holocene or isotopically lighter freshwater runoff (Müller et al., in prep., Chapter 8 of this thesis). Considering the temperature-dependency of the Φ' values found in modern *S. senilis* shells (Fig. 9-3 and 9-4), this temperature difference would theoretically result in ~0.74 higher Φ'' values for the mid-Holocene. However, our calculated mid-Holocene Φ'' values are similar to the modern values, indicating rather similar water temperature conditions if water temperature represents the dominating environmental control of shell growth. This supports the interpretation made in Chapter 8 (Müller et al., in prep., Chapter 8 of this thesis) that the consistent overestimation of modern water temperatures by mid-Holocene fish otoliths and bivalve shell was mainly caused by mixing of isotopically lighter freshwater runoff in the estuarine environments rather than a ~+7 °C higher water temperature. However, future studies are needed to extend the modern calibration data set and in particular for assessing the impact of other environmental variable such as salinity or primary production on growth performance in *S. senilis*.

Despite its potential applicability for tracing freshwater runoff pattern of NW Africa throughout the mid- to late-Holocene, this approach might also be useful for deep-time applications where the reliability of absolute water temperature reconstructions is limited by unknown ancient seawater chemistry. Also independent from diagenetic alteration (i.e. recrystallization) and subsequently imprecise absolute water temperature estimates, this approach might allow inferring relative changes in growth parameters whenever the seasonal oscillation of environmental conditions is preserved in ontogenetic isotope or element/Ca ratios records of a given skeletal structure. In theory, this approach is even applicable without any chemical proxy measurements if annual growth rates can be inferred from visible annual growth increments of a given fossil specimen.

Provided that its applicability has been further tested using modern specimens (e.g. using existing isotope records from *Arctica islandica*), this approach might allow studying periods of profound environmental changes throughout earth history where other proxy records are sparse. By studying relative changes in growth pattern through time, it may allow distinguishing between gradual processes or abrupt events causing massive environmental changes and associated mass extinction events such as e.g. the Cretaceous-Paleogene (C-Pg) boundary.

For this particular example, previous studies suggested an abrupt mass extinction of terrestrial and marine organisms as a consequence of a bolide impact at the C-Pg boundary (Alvarez et al., 1980; Hildebrand et al., 1991; Swisher et al., 1992). However, using clumped isotope

thermometry in terrestrial bivalve shells, a more recent study questioned the abruptness of this mass extinction event by measuring a decrease in water temperature or ~8 °C throughout the last 300 ka of the Cretaceous (Tobin et al., 2014). This might have caused a destabilization of terrestrial and marine ecosystems prior to the C-Pg boundary and thereby increased their susceptibility to an additional abrupt event such as the hypothesized bolide impact at the C-Pg boundary (Tobin et al., 2014). Such a decrease in water temperature by 8 °C is likely to have caused considerable changes in growth characteristics of many aquatic calcifiers. Therefore, studying relative changes in growth performance over this time period by either using stable isotopic signatures or shell micro-growth increments might allow test this assumption and thereby broadening our understanding of the underlying mechanisms causing one of the largest mass extinction events in earth history.

Such potential deep-time applications are, however, restricted to periods which are short enough to prohibit any evolutionary adaptation to environmental changes. Furthermore, geological units need to provide an adequate temporal resolution and a high number of samples to increase the fidelity of reconstructed changes in overall growth pattern through time. In any case, future studies are needed to confirm the hypothesis that application of the phi-prime concept on oxygen isotope-based growth parameters provide reliable information about environmental conditions experienced by these organisms.

10. CONCLUSIONS AND OUTLOOK

Ontogenetic geochemical proxy signatures of accretionary calcareous skeletal structures such as corals, mollusk shells or fish otoliths can provide sub-seasonally resolved paleoenvironmental information. By complementing long-term records derived from e.g. sedimentary successions, these high-resolution proxy records can considerably broaden our understanding of climate evolution throughout the earth's history. However, the reliable reconstruction of ancient environmental conditions using geochemical proxy signatures of these 'bio-archives' requires understanding the interplay of physiological processes and environmental conditions affecting these proxy systems. Therefore, this thesis aims to broaden our knowledge regarding the effect of various biological, environmental, and *post-mortem* processes affecting geochemical proxy signatures of accretionary skeletal structures of marine calcifiers.

The analysis of oxygen and carbon isotopes as well as Mg/Ca ratios in spines of the echinoid species *Eucidaris galapagensis* collected from sediment samples throughout the Galápagos archipelago shows the strong influence of both in- and extrinsic variables on proxy incorporation pattern. The oxygen isotopic composition of the analyzed spines was found to be significantly negatively correlated with water temperature and lays thereby close to the expected thermodynamic equilibrium. In contrast, a significant positive correlation of carbon isotopes with water temperature indicates additional physiological processes affecting isotope fractionation during spine formation because this is in contradiction with previous studies which suggested a simultaneous depletion of oxygen and carbon isotopes due to respiratory CO_2. Likewise, even though Mg/Ca ratios show a significant positive correlation with water temperature, the low correlation coefficient also suggests additional mechanisms other than water temperature influencing the Mg incorporation into the spine calcite. The variation of the spine oxygen isotopic composition within the different sub-regions is in good agreement with the individual seasonal water temperature amplitude measured in these regions. This suggests that *E. galapagensis* spine might provide sub-seasonally resolved water temperature records by the means of ontogenetic oxygen isotope records. However, spine growth needs to be thoroughly understood in order to prove this hypothesis.

To extend the applicability of echinoid spines for reliable paleoclimate reconstructions, future research should focus on laboratory experiments under precisely controlled conditions for studying e.g. the temperature-dependency of the aforementioned proxies. The periodic

Calcein staining of the spine material throughout such an experiment would also allow gaining a better understanding of spine growth pattern and the impact of growth rates on oxygen isotope incorporation due to physiological and kinetic isotope effects. Complemented by buoyant weight- and respiration rate measurements, this would allow testing the reliability of oxygen isotope records derived from modern and fossil echinoid spines and in particular their potential for providing ontogenetic proxy records measured throughout their ontogenetic growth record.

In contrast to the still ambiguous growth pattern of echinoid spines, most other accretionary skeletal structure of marine calcifying organisms show clear successions of defined growth increments providing a good temporal framework of ontogenetic proxy signatures. However, ontogenetically decreasing growth rates are a common phenomenon and the subsequently distortion of proxy records in many bivalve shells and fish otoliths complicate their straightforward interpretation. Mathematical approaches developed in this thesis can help to convert such ontogenetically distorted proxy records back into time series using simple linear interpolations or the von Bertalanffy growth model and thereby help to assess the reliability of ontogenetic proxy records. Future studies could test the applicability of existing alternative growth models for an improved fitting of ontogenetic proxy records to environmental time series. These studies should particularly focus on measured proxy records from organisms which form clear micro-increments (e.g. on a tidal base) to further test the results obtained from such mathematical methods for the temporal alignment of ontogenetic proxy signatures.

To illustrate the potential of the aforementioned methods, ontogenetic oxygen isotope records of a catfish otolith (*Carlarius heudelotii*) and a bivalve shell (*Venus crebrisulca*) from the Banc d´Arguin, Mauritania, were converted into sub-seasonally resolved time series and correlated against measured water temperature records within this thesis. The obtained significant correlations of the ontogenetic oxygen isotope records of both skeletal structures with measured water temperature underline their high potential for reliable sub-seasonally resolved water temperatures reconstructions. Given the extensive occurrence of catfish otoliths and bivalve shells in Neolithic (i.e. Holocene) shell-midden deposits along the entire Mauritanian coast, these deposits bear a high potential for broadening our understanding of the Holocene climate change of NW Africa.

Before reliable paleoenvironmental reconstructions can be obtained from shell-midden derived skeletal structures, their preservation and subsequently the reliability of their ontogenetic proxy records needs to be assessed. Despite diagenetic alteration of their

chemical composition by recrystallization of e.g. primary aragonite into secondary calcite, in particular pre-depositional processing methods such as heating (i.e. cooking) may cause additional geochemical alteration. By exposing modern bivalve shells to different prehistoric cooking practices, clumped isotope thermometry has been identified as a so far unique tool for the detection of pre-depositional heating of aragonitic shell-midden constituents. Based on the rapid re-equilibration of clumped isotopes in aragonitic shells during secondary heating, this approach allows the identification of potential heating-related geochemical alteration. Moreover, the temperature-dependent alteration magnitude of the clumped isotopic composition allows reconstructing specific prehistoric cooking methods in archeological shell-midden assemblages. This is of particular importance as this experimental study also confirms results of previous studies by showing a clear alteration of the oxygen isotopic composition of bivalve shells due to prehistoric cooking. However, differences regarding the alteration magnitude as well as the minimum temperature required for a conversion of aragonite into calcite compared to previous studies reveal that the experimental setup is crucial for the assessment of potential cooking-related alterations of shell-midden constituents. Future studies should focus on the underlying mechanisms of chemical alteration by using controlled oven-experiments as well as the exposure to realistic cooking practices across the relevant temperature range from 100-400 °C. Next to the impact on oxygen and clumped isotopes, the experimental data from this study also indicate the apparent alteration of the carbon isotopic composition of the aragonitic bivalve shells by prehistoric cooking. Even though the underlying mechanism is unclear, this implies that also the ^{14}C-signature and subsequently radiocarbon dates obtained from 'cooked' shell-midden constituents may be affected by pre-depositional heating, leading to errors in absolute dating of archeological deposits. Future studies on the effect of pre-depositional heating on the chemical composition of shell-midden constituents should therefore also include this important aspect to avoid erroneous radiocarbon dating of archeological deposits.

The analysis of clumped isotopes in mid- to late-Holocene catfish otoliths and bivalve shells from archeological deposits along the Banc d´Arguin, Mauritania revealed pre-depositional heating of some but not all bivalve shells whereas all catfish otoliths appear to be pristine. In consequence, the ontogenetic oxygen isotope records of pristine bivalve shells and fish otoliths can provide reliable records of environmental conditions throughout the Holocene.

Based on these data, ontogenetic oxygen isotope records of six archeological catfish otoliths and seven bivalve shells were used to reconstruct the climate evolution of NW Africa

throughout the mid- to late-Holocene. By showing unreasonably low oxygen isotopic compositions, fish otoliths and bivalve shells dated to 5.3-5.0 ka BP indicate the persistence of isotopically lighter freshwater runoff into the coastal zone and thereby question the hypothesis of an abrupt aridification of NW Africa around 5.5 ka BP. Ontogenetic oxygen isotope signatures of otoliths dated to 3.5-3.4 ka BP indicate the establishment of arid conditions between 5.0 and 3.4 ka BP. However, despite the first results of this thesis, long-term reconstructions of Holocene climate change throughout NW Africa using archeological shell-midden constituents such as fish otoliths or bivalve shells are still lacking so far.

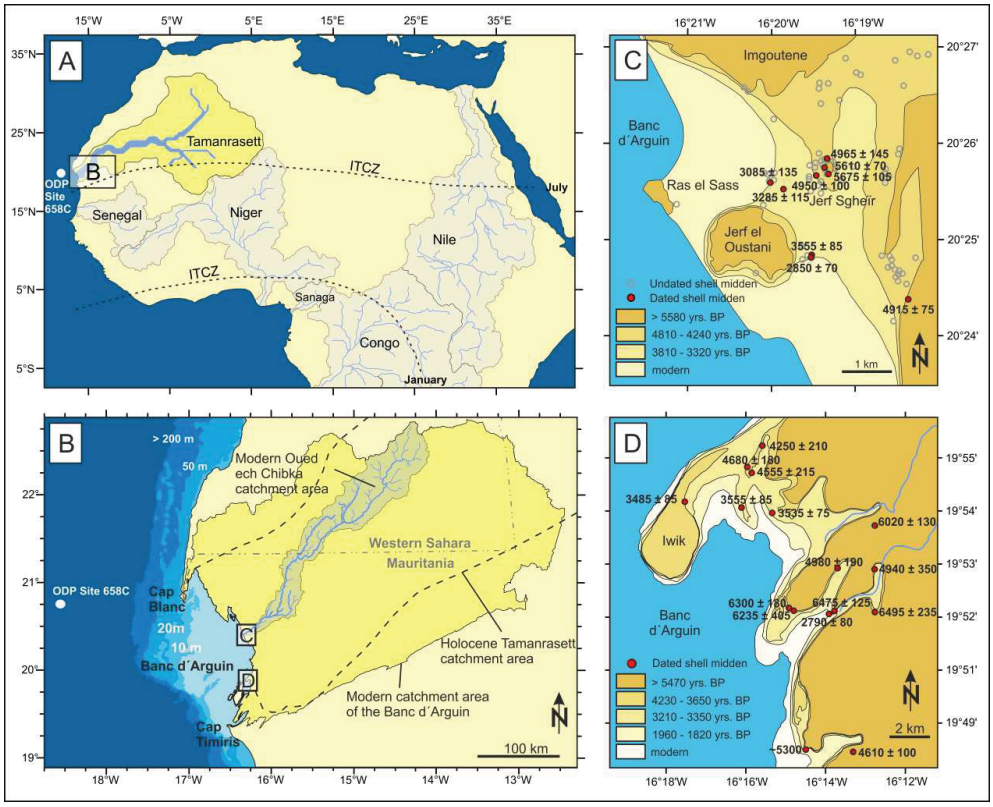

Figure 11-1: Neolithic shell-midden deposits in the Rass el Sass and Iwik area (Banc d´Arguin, Mauritania). **A)** Overview map of NW Africa including the extensive Tamanrasett paleo-river system (Skonieczny et al., 2015). **B)** Overview map of the Banc d´Arguin and the northern Mauritanian hinterland with the mouth of the Tamanrasett paleo-estuary (modified after Skonieczny et al., 2015) and the modern catchment areas (modified after Müller et al., in prep., Chapter 8 of this thesis). **C)** and **D)** Distribution of shell-midden deposits in the Rass el Sass area Iwik area, respectively (modified from Barusseau et al. (2007) and Dia (2013)).

As a result of the long occupation period of the coastal areas of the Banc d´Arguin by Neolithic hunter-gatherer communities (approx. from 6.5 to 2.5 ka BP), the existing shell-midden successions along the northern Mauritanian coast bear a high potential to generate such long-

term records of sub-seasonally resolved paleoclimate information. Shell-midden constituents from the interface of the terrestrial and the marine realm (i.e. the coastal- and paleo-estuarine zones) may allow tracing monsoon-related freshwater discharge pattern and thereby the aridification history of NW Africa throughout the mid- to late-Holocene. The Rass el Sass area and the area east of the Iwik peninsula are located in a large paleo-estuary which drained Holocene monsoon precipitation into the coastal zone of the Banc d'Arguin and can provide such long-term successions of shell-midden deposits (see Fig. 11-1) covering the major aridification period. Using these exceptional archeological deposits, future work should expand the existing sub-seasonally resolved paleoclimate reconstruction in order to broaden our understanding of the Holocene climate evolution of NW Africa. Additional radiocarbon dating of individual shell-midden constituents will complement previous results and the resulting improved age-model help to study the occupation history of both study areas. Future studies should also use X-ray diffraction (aragonite/calcite conversion) and clumped isotope thermometry to assess shell/otolith preservation and potential alteration due to pre-depositional heating. Given adequate sample preservation, the measurement of ontogenetic oxygen isotope signatures of individual otolith and bivalve shell specimens can be used to generate a long-term record of seasonal variation of environmental conditions throughout the supposed aridification period of NW Africa similar to the approach used in Carré et al. (2014).

Beyond extending Holocene paleoclimate records using these shell-midden deposits, future work should also focus on the variation of ontogenetic oxygen isotope signatures in modern catfish otoliths and bivalve shells (preferably *S. senilis*) along the West African coast. The analysis of modern samples along such a latitudinal gradient would further increase the confidence regarding the impact of monsoon precipitation discharge on ontogenetic isotope records. Thereby, in particular samples from the Senegal which represents the modern analog of the Banc d´Arguin during the AHP are of special interest.

Generating ontogenetic oxygen isotope records along this latitudinal gradient also allows testing the applicability of the phi-prime (Φ') concept (Chapter 9 of this thesis) to expand the paleoenvironmental significance of the shell-midden derived proxy data. The comparison of conventional (shell height/otolith size-based) phi prime data (Φ') with isotope-derived phi-prime estimates (Φ'') from the same individuals along the West African coast enables testing the deviation between conventional and isotope-based growth parameters as well as their coupling to environmental variables such as water temperature, salinity or primary production.

Sampling of modern fish otoliths and bivalve shells along the latitudinal gradient of the West African coast would also allow single-species calibrations of the clumped isotope thermometer. This does not only enlarge the number of available clumped isotope calibrations among mollusk shells and fish otoliths but also provides better constrains on paleoclimate conditions by allowing the reconstructions of ancient seawater isotopic compositions using the clumped isotope data of archeological specimens.

Beyond the approaches used and developed in this thesis, Sr isotopic signatures of modern and archeological otoliths and bivalve shells may represent another promising approach to better constrain Holocene monsoon rainfall and discharge pattern. Previous studies showed that due to the conservative mixing of the riverine and marine Sr inventories and the subsequently linear relationship between the water Sr isotopic composition and salinity, the Sr isotopic composition of biogenic calcareous structures can be used as a reliable paleo-salinity proxy (Ingram and Sloan, 1992). While previous studies using the salinity-dependency of Sr isotopes in fish otoliths focused mainly on the identification of nursery habitats and fish migration pattern (e.g. Hobbs et al., 2010 and references therein), the application of Sr isotopes on Holocene shell-midden constituents can provide additional insights into the climate evolution of NW Africa throughout the Holocene by tracing freshwater runoff pattern. This, however, also requires the validations of this assumption using modern otolith and bivalve shell samples along the environmental gradient of the NW African coast.

In summary, this thesis underlines the potential of shell-midden constituents for providing surpassingly high-resolution paleoclimate information. Considering their comparably easy accessibility along the Banc d´Arguin and the rather low analytical costs compared to conventional marine paleoclimate records which demand ship-born sampling missions and extensive laboratory analyses, future studies on archeological deposits along the Banc d´Arguin can effectively complement the existing paleoclimate records of NW Africa. By broadening our understanding of the underlying mechanisms shaping the NW African climate in the past, future studies on shell-midden-derived paleoclimate records can thereby help to improve future predictions regarding the susceptibility of the NW African climate with regard to the ongoing global climate change.

11. REFERENCES

Adkins, J., deMenocal, P., and Eshel, G., 2006, The "African humid period" and the record of marine upwelling from excess 230Th in Ocean Drilling Program Hole 658C: *Paleoceanography*, v. 21, no. 4, p. 1–14, doi: 10.1029/2005PA001200.

Affek, H.P., 2012, Clumped isotope paleothermometry: Principles, applications, and challenges: *The Paleontological Society Papers*, v. 18, no. c, p. 101–114.

Affek, H.P., and Eiler, J.M., 2006, Abundance of mass 47 CO_2 in urban air, car exhaust, and human breath: *Geochimica et Cosmochimica Acta*, v. 70, no. 1, p. 1–12, doi: 10.1016/j.gca.2005.08.021.

Alvarez, L.W., Alvarez, W., Asaro, F., and Michel, H. V, 1980, Extraterrestrial cause for the Cretaceous Tertiary extinction: *Science*, v. 208, no. 4448, p. 1095–1108, doi: 10.1126/science.208.4448.1095.

Anagnostou, E., Huang, K.-F., You, C.-F., Sikes, E.L., and Sherrell, R.M., 2012, Evaluation of boron isotope ratio as a pH proxy in the deep sea coral *Desmophyllum dianthus*: Evidence of physiological pH adjustment: *Earth and Planetary Science Letters*, v. 349–350, p. 251–260, doi: 10.1016/j.epsl.2012.07.006.

Andrus, C.F.T., 2011, Shell midden sclerochronology: *Quaternary Science Reviews*, v. 30, no. 21–22, p. 2892–2905, doi: 10.1016/j.quascirev.2011.07.016.

Andrus, C.F.T., and Crowe, D.E., 2002, Alteration of otolith aragonite: Effects of prehistoric cooking methods on otolith chemistry: *Journal of Archaeological Science*, v. 29, no. 3, p. 291–299, doi: 10.1006/jasc.2001.0694.

Andrus, C.F.T., Crowe, D.E., Sandweiss, D.H., Reitz, E.J., and Romanek, C.S., 2002, Otolith $\delta^{18}O$ record of mid-Holocene sea surface temperatures in Peru: *Science*, v. 295, no. 5559, p. 1508–11, doi: 10.1126/science.1062004.

Ansa, E.J., and Sikoki, F.D., 2005, Growth studies on the population of benthic bivalves in the Andoni flats, Niger delta, Nigeria, *in* 20th Annual Conference of the Fisheries Society of Nigeria, p. 204–206.

Armitage, S.J., Bristow, C.S., and Drake, N.A., 2015, West African monsoon dynamics inferred from abrupt fluctuations of Lake Mega-Chad: *Proceedings of the National Academy of Sciences*, v. 112, no. 28, p. 8543–8548, doi: 10.1073/pnas.1417655112.

Azzoug, M., Carré, M., Chase, B.M., Deme, A., Lazar, A., Lazareth, C.E., Schauer, A.J., Mandeng-Yogo, M., Simier, M., Thierno-Gaye, A., and de Morais, L.T., 2012a, Positive precipitation–evaporation budget from AD 460 to 1090 in the Saloum Delta (Senegal) indicated by mollusk oxygen isotopes: *Global and Planetary Change*, v. 98–99, p. 54–62, doi: 10.1016/j.gloplacha.2012.08.003.

Azzoug, M., Carré, M., and Schauer, A.J., 2012b, Reconstructing the duration of the West African Monsoon season from growth patterns and isotopic signals of shells of *Anadara senilis* (Saloum Delta, Senegal): *Palaeogeography, Palaeoclimatology, Palaeoecology*, v. 346–347, p. 145–152, doi: 10.1016/j.palaeo.2012.06.001.

Balbo, A., Madella, M., Godino, I.B., and Álvarez, M., 2011, Shell midden research: An interdisciplinary agenda for the Quaternary and Social Sciences: *Quaternary International*, v. 239, no. 1–2, p. 147–152, doi: 10.1016/j.quaint.2011.03.032.

Barusseau, J.P., Certain, R., Vernet, R., and Saliège, J.F., 2010, Late Holocene morphodynamics in the littoral zone of the Iwik Peninsula area (Banc d'Arguin — Mauritania): *Geomorphology*, v. 121, no. 3–4, p. 358–369, doi: 10.1016/j.geomorph.2010.05.006.

Barusseau, J.-P., Vernet, R., Saliège, J.-F., and Descamps, C., 2007, Late Holocene sedimentary forcing and human settlements in the Jerf el Oustani - Ras el Sass region (Banc d'Arguin, Mauritania): *Géomorphologie : relief, processus, environnement*, v. 7, p. 7–18.

Bastidas, C., and García, E., 1999, Metal Content of the Reef Coral *Porites astreiode*s: an Evaluation of River Influence and 35 Years of Chronology.: *Marine Pollution Bulletin*, v. 38, no. 10, p. 899–907.

Bath, G.E., Thorrold, S.R., Jones, C.M., Campana, S.E., McLaren, J.W., and Lam, J.W.H., 2000, Strontium and barium uptake in aragonitic otoliths of marine fish: *Geochimica et Cosmochimica Acta*, v. 64, no. 10, p. 1705–1714.

Baumiller, T.K., 2001, Light stable isotope geochemistry of the crinoid skeleton and it's use in biology and paleobiology, *in* Barker, M.F. ed., Echinoderms 2000: Proceedings of the 10th International Conference, Dunedin, 31 January-4 February 2000, p. 107–112.

Beck, J.W., Edwards, R.L., Ito, E., Taylor, F.W., Recy, J., Rougerie, F., Joannot, P., and Henin, C., 1992, Sea-surface temperature from coral skeletal strontium/calcium ratios.: *Science*, v. 257, no. 5070, p. 644–7, doi: 10.1126/science.257.5070.644.

Berghuis, E.M., Duineveld, G.C.A., and Hegeman, J., 1993, Primary production and distribution of phytopigments in the water column and sediments on the upwelling shelf off the Mauritanian coast (Northwest Africa): *Hydrobiologia*, v. 258, no. 1–3, p. 81–93, doi: 10.1007/BF00006188.

von Bertalanffy, L., 1934, Untersuchungen über die Gesetzlichkeit des Wachstums - I. Teil: Allgemeine Grundlagen der Theorie; mathematische und physiologische Gesetzlichkeiten des Wachstums bei Wassertieren: Wilhelm Roux' Archiv für Entwicklungsmechanik der Organismen, v. 131, p. 613–652, doi: 10.1007/BF00650112.

Bird, D.W., and Bird, R.L.B., 1997, Contemporary shellfish gathering strategies among the Meriam of the Torres Strait islands, Australia: Testing predictions of a central place foraging model: *Journal of Archaeological Scienc*e, v. 24, p. 39–63, doi: 10.1006/jasc.1995.0095.

Bloszies, C., Forman, S.L., and Wright, D.K., 2015, Water level history for Lake Turkana, Kenya in the past 15,000years and a variable transition from the African Humid Period to Holocene aridity: *Global and Planetary Change*, v. 132, p. 64–76, doi: 10.1016/j.gloplacha.2015.06.006.

Borremans, C., Hermans, J., Baillon, S., André, L., and Dubois, P., 2009, Salinity effects on the Mg/Ca and Sr/Ca in starfish skeletons and the echinoderm relevance for paleoenvironmental reconstructions: *Geology*, v. 37, no. 4, p. 351–354, doi: 10.1130/G25411A.1.

Bougeois, L., de Rafélis, M., Reichart, G.J., de Nooijer, L.J., Nicollin, F., and Dupont-Nivet, G., 2014, A high resolution study of trace elements and stable isotopes in oyster shells to estimate central Asian middle Eocene seasonality: *Chemical Geology*, v. 363, p. 200–212, doi: 10.1016/j.chemgeo.2013.10.037.

Brahim, K., 2004, Ecologie et biologie de l'émissole lisse *Mustelus mustelus* (Linné, 1758) sur les côtes de Mauritanie: Université de Bretagne Occidentale, 202 p.

Brand, W. A., Assonov, S.S., and Coplen, T.B., 2010, Correction for the ^{17}O interference in $\delta(^{13}C)$ measurements when analyzing CO_2 with stable isotope mass spectrometry (IUPAC Technical Report): *Pure and Applied Chemistry*, v. 82, no. 8, p. 1719–1733, doi: 10.1351/PAC-REP-09-01-05.

Bronk Ramsey, C., 2009, Bayesian analysis of radiocarbon dates: *Radiocarbon*, v. 51, no. 1, p. 337–360, doi: 10.2458/azu_js_rc.v51i1.3494.

Bronk Ramsey, C., 1995, Radiocarbon calibration and analysis of stratigraphy: The OxCal Program: *Radiocarbon*, v. 37, no. 2, p. 425–430, doi: 10.2458/rc.v37i2.1690.

Buddemeier, R.W., Maragos, J.E., and Knutson, D.W., 1974, Radiographic studies of reef coral exoskeletons: Rates and patterns of coral growth: *Journal of Experimental Marine Biology and Ecology*, v. 14, no. 2, p. 179–199, doi: 10.1016/0022-0981(74)90024-0.

Van Camp, L., Nykjaer, L., Mittelstaedt, E., and Schlittenhardt, P., 1991, Upwelling and boundary circulation off Northwest Africa as depicted by infrared and visible satellite observations: *Progress in Oceanography*, v. 26, no. 4, p. 357–402, doi: 10.1016/0079-6611(91)90012-B.

Campana, S.E., 1999, Chemistry and composition of fish otoliths: Pathways, mechanisms and applications: *Marine Ecology Progress Series*, v. 188, p. 263–297, doi: 10.3354/meps188263.

Campana, S.E., and Jones, C.M., 1992, Analysis of otolith microstructure data, *in* Stevenson, D.K. and Campana, S.E. eds., Otolith microstructure examination and analysis, p. 73–100.

Candelier, Y., Minoletti, F., Probert, I., and Hermoso, M., 2013, Temperature dependence of oxygen isotope fractionation in coccolith calcite: A culture and core top calibration of the genus *Calcidiscus*: *Geochimica et Cosmochimica Acta*, v. 100, p. 264–281, doi: 10.1016/j.gca.2012.09.040.

Carré, M., Sachs, J.P., Purca, S., Schauer, A.J., Braconnot, P., Falcon, R. a., Julien, M., Lavallee, D., Carré, M., Sachs, J.P., Purca, S., Schauer, A.J., and Braconnot, P., 2014, Holocene history of ENSO variance and asymmetry in the eastern tropical Pacific: *Science*, v. 345, no. 6200, p. 1045–1048, doi: 10.1126/science.1252220.

Carton, J.A., and Giese, B.S., 2008, A reanalysis of ocean climate using simple ocean data assimilation (SODA): *Monthly Weather Review*, v. 136, no. 8, p. 2999–3017, doi: 10.1175/2007MWR1978.1.

Casselman, J.M., 1990, Growth and relative size of calcified structures of fish: *Transactions of the American Fisheries Society*, v. 119, p. 673–688, doi: 10.1577/1548-8659(1990)119<0673:GARSOC>2.3.CO;2.

Chapman, M.R., Shackleton, N.J., Zhao, M., and Eglinton, G., 1996, Faunal and alkenone reconstructions of subtropical North Atlantic surface hydrography and paleotemperature over the last 28 kyr: *Paleoceanography*, v. 11, no. 3, p. 343, doi: 10.1029/96PA00041.

Chauvaud, L., Thouzeau, G., and Paulet, Y.-M., 1998, Effects of environmental factors on the daily growth rate of *Pecten maximus* juveniles in the Bay of Brest (France): *Journal of Experimental Marine Biology and Ecology*, v. 227, no. 1, p. 83–111, doi: 10.1016/S0022-0981(97)00263-3.

Chave, K.E., 1954, Aspects of the biogeochemistry of Magnesum 1. Calcareous marine organisms: *The Journal of Geology*, v. 62, no. 3, p. 266–283.

Chavez, F.P., and Brusca, R.C., 1991, The Galápagos Islands and their relation to oceanographic processes in the tropical Pacific, *in* James, M. ed., Galápagos Marine Invertebrates, Plenum, New York, New York, p. 9–33.

Chen, T., Yu, K., Zhao, J., Yan, H., Song, Y., Feng, Y., and Chen, T., 2015, Testing coral paleothermometers (B/Ca, Mg/Ca, Sr/Ca, U/Ca and $\delta^{18}O$) under impacts of large riverine runoff: *Acta Oceanologica Sinica*, v. 34, no. 8, p. 20–26, doi: 10.1007/s13131-015-0705-9.

Claussen, M., Bathiany, S., Brovkin, V., and Kleinen, T., 2014, Abrupt or not abrupt - biodiversity affects climate-vegetation interaction at the end of the African Humid Period [abs.]: EGU General Assembly 2014, v. 16, p. 13398.

Claussen, M., Kubatzki, C., Brovkin, V., Ganopolski, A., Holzmann, P., and Pachur, H.-J., 1999, Simulation of an abrupt change in Saharan vegetation in the mid-Holocene: *Geophysical Research Letters*, v. 26, no. 14, p. 2037–2040.

Conand, F., Camara, S.B., and Domain, F., 1995, Age and growth of three species of Ariidae (Siluriformes) in coastal waters of Guinea: *Bulletin of Marine Science*, v. 56, no. 1, p. 58–67.

Courtney, T., and Ries, J.B., 2015, Impact of atmospheric pCO_2, seawater temperature, and calcification rate on the $\delta^{18}O$ and $\delta^{13}C$ composition of echinoid calcite (*Echinometra viridis*) : *Chemical Geology*, v. 411, p. 228–239, doi: 10.1016/j.chemgeo.2015.06.030.

Craig, H., 1957, Isotopic standards for carbon and oxygen and correction factors for mass spectrometric analysis of carbon dioxide: *Geochimica et Cosmochimica Acta*, v. 12, no. 1–2, p. 133–149, doi: http://dx.doi.org/10.1016/0016-7037(57)90024-8.

Craig, H., 1953, The geochemistry of the stable carbon isotopes: *Geochimica et Cosmochimica Acta*, v. 3, no. 2–3, p. 53–92, doi: 10.1016/0016-7037(53)90001-5.

Cropper, T.E., Hanna, E., and Bigg, G.R., 2014, Spatial and temporal seasonal trends in coastal upwelling off Northwest Africa, 1981-2012: *Deep-Sea Research Part I: Oceanographic Research Papers*, v. 86, p. 94–111, doi: 10.1016/j.dsr.2014.01.007.

Cuq, F., 1993, Remote sensing of sea surface and coastal features in the area of the Golfe d'Arguin, Mauritania: *Hydrobiologia*, v. 258, no. 1–3, p. 33–40, doi: 10.1007/BF00006184.

Daëron, M., Blamart, D., Peral, M., and Affek, H.P., 2016, Absolute isotopic abundance ratios and the accuracy of Δ_{47} measurements: *Chemical Geology*, v. 442, p. 83–96, doi: 10.1016/j.chemgeo.2016.08.014.

deMenocal, P., Ortiz, J., Guilderson, T., Adkins, J., Sarnthein, M., Baker, L., and Yarusinsky, M., 2000a, Abrupt onset and termination of the African Humid Period : rapid climate responses to gradual insolation forcing: *Quaternary Science Reviews*, v. 19, p. 347–361.

deMenocal, P., Ortiz, J., Guilderson, T., and Sarnthein, M., 2000b, Coherent high- and low-latitude climate variability during the Holocene warm period: *Science*, v. 288, no. 5474, p. 2198–2202, doi: 10.1126/science.288.5474.2198.

Dennis, K.J., Affek, H.P., Passey, B.H., Schrag, D.P., and Eiler, J.M., 2011, Defining an absolute reference frame for "clumped" isotope studies of CO_2: *Geochimica et Cosmochimica Acta*, v. 75, no. 22, p. 7117–7131, doi: 10.1016/j.gca.2011.09.025.

Dennis, K.J., and Schrag, D.P., 2010, Clumped isotope thermometry of carbonatites as an indicator of diagenetic alteration: *Geochimica et Cosmochimica Acta*, v. 74, no. 14, p. 4110–4122, doi: 10.1016/j.gca.2010.04.005.

Dettman, D.L., Reische, A.K., and Lohmann, K.C., 1999, Controls on the stable isotope composition of seasonal growth bands in aragonitic fresh-water bivalves (Unionidae): *Geochimica et Cosmochimica Acta*, v. 63, no. 7/8, p. 1049–1057, doi: 10.1016/S0016-7037(99)00020-4.

Dia, A., 2013, Les plateformes littorales des marges stables désertiques: Etude sédimentologique, stratigraphique et morphologique des unités fini-holocènes du Band d´Arguin (Mauritanie): PhD-thesis, University of Perpignan Via Domitia, 203 p.

Dickson, J.A.D., 2004, Echinoderm skeletal preservation: Calcite-aragonite seas and the Mg/Ca ratio of phanerozoic oceans: *Journal of Sedimentary Research*, v. 74, no. 3, p. 355–365, doi: 10.1306/112203740355.

Dickson, J.A.D., 2002, Fossil echinoderms as monitor of the Mg/Ca ratio of phanerozoic oceans: *Science*, v. 298, no. 5596, p. 1222–1224, doi: 10.1126/science.1075882.

Diop, M.S., 1988, Biologie et dynamique des populations de praires (*Venus rosalina*) a l'ouest du Banc d'Arguin (Mauritanie): PhD-thesis, Université de Bretagne Occidentale, Brest, 191 p.

Disspain, M.C.F., Ulm, S., and Gillanders, B.M., 2015, Otoliths in archaeology: Methods, applications and future prospects: *Journal of Archaeological Science*: Reports, doi: 10.1016/j.jasrep.2015.05.012.

Dobrovine, B., Ould Mohamed, M., and Ould Sidina, D., 1991, Atlas hydrologique des eaux superficielles du Banc d´Arguin: *Bulletin Scientifique du CNROP*, v. 24, p. 1–24.

Dubois, P., and Ameye, L., 2001, Regeneration of spines and pedicellariae in echinoderms: a review: *Microscopy research and technique*, v. 55, no. 6, p. 427–37, doi: 10.1002/jemt.1188.

Eden, C., and Timmermann, A., 2004, The influence of the Galápagos Islands on tropical temperatures, currents and the generation of tropical instability waves: *Geophysical Research Letters*, v. 31, no. 15, p. L15308, doi: 10.1029/2004GL020060.

Edgar, G.J., Banks, S., Farina, J.M., Calvopina, M., and Martinez, C., 2004, Regional biogeography of shallow reef fish and macro-invertebrate communities in the Galapagos archipelago: *Journal of Biogeography*, v. 31, no. 7, p. 1107–1124, doi: 10.1111/j.1365-2699.2004.01055.x.

Eiler, J.M., 2007, "Clumped-isotope" geochemistry - The study of naturally-occurring, multiply-substituted isotopologues: *Earth and Planetary Science Letters*, v. 262, no. 3–4, p. 309–327, doi: 10.1016/j.epsl.2007.08.020.

Elderfield, H., Yu, J., Anand, P., Kiefer, T., and Nyland, B., 2006, Calibrations for benthic foraminiferal Mg/Ca paleothermometry and the carbonate ion hypothesis: *Earth and Planetary Science Letters*, v. 250, no. 3–4, p. 633–649, doi: 10.1016/j.epsl.2006.07.041.

Elderfield, H., and Ganssen, G., 2000, Past temperature and $\delta^{18}O$ of surface ocean waters inferred from foraminiferal Mg/Ca ratios: *Nature*, v. 705, no. 103, p. 442–445, doi: 10.1038/35013033.

Elsdon, T.S., and Gillanders, B.M., 2004, Fish otolith chemistry influenced by exposure to multiple environmental variables: *Journal of Experimental Marine Biology and Ecology*, v. 313, no. 2, p. 269–284, doi: 10.1016/j.jembe.2004.08.010.

Emiliani, C., 1966, Isotopic Paleotemperatures: *Science*, v. 154, p. 851–857, doi: 10.1126/science.154.3751.851.

Emiliani, C., 1955, Pleistocene temperatures: *Journal of Geology*, v. 63, p. 538–578.

Freitas, P.S., Clarke, L.J., Kennedy, H., Richardson, C. a., and Abrantes, F., 2006, Environmental and biological controls on elemental (Mg/Ca, Sr/Ca and Mn/Ca) ratios in shells of the king scallop *Pecten maximus*: *Geochimica et Cosmochimica Acta*, v. 70, no. 20, p. 5119–5133, doi: 10.1016/j.gca.2006.07.029.

Freitas, P., Clarke, L.J., Kennedy, H., Richardson, C., and Abrantes, F., 2005, Mg/Ca, Sr/Ca, and stable-isotope ($\delta^{18}O$ and $\delta^{13}C$) ratio profiles from the fan mussel *Pinna nobilis*: Seasonal records and temperature relationships: *Geochemistry, Geophysics, Geosystems*, v. 6, no. 4, p. 1–16, doi: 10.1029/2004GC000872.

Füllenbach, C.S., Schöne, B.R., and Mertz-Kraus, R., 2015, Strontium/lithium ratio in aragonitic shells of *Cerastoderma edule* (Bivalvia) - A new potential temperature proxy for brackish environments: *Chemical Geology*, v. 417, p. 341–355, doi: 10.1016/j.chemgeo.2015.10.030.

Gasse, F., 2000, Hydrological changes in the African tropics since the Last Glacial Maximum: *Quaternary Science Reviews*, v. 19, no. 1–5, p. 189–211.

Van der Geest, M., 2013, Multi-trophic interactions within the seagrass beds of Banc d´Arguin, Mauritania: A chemosynthesis-based intertidal ecosystem: PhD-thesis, University of Groningen, 253 p.

Ghosh, P., Adkins, J., Affek, H., Balta, B., Guo, W., Schauble, E. a., Schrag, D., and Eiler, J.M., 2006, ^{13}C–^{18}O bonds in carbonate minerals: A new kind of paleothermometer: *Geochimica et Cosmochimica Acta*, v. 70, no. 6, p. 1439–1456, doi: 10.1016/j.gca.2005.11.014.

Ghosh, P., Eiler, J., Campana, S.E., and Feeney, R., 2007, Calibration of the carbonate "clumped isotope" paleothermometer for otoliths: *Geochimica et Cosmochimica Acta*, v. 71, no. 11, p. 2736–2744, doi: 10.1016/j.gca.2007.03.015.

Gillikin, D.P., Dehairs, F., Lorrain, A., Steenmans, D., Baeyens, W., and André, L., 2006, Barium uptake into the shells of the common mussel (*Mytilus edulis*) and the potential for estuarine paleo-chemistry reconstruction: *Geochimica et Cosmochimica Acta*, v. 70, no. 2, p. 395–407, doi: 10.1016/j.gca.2005.09.015.

Giry, C., Felis, T., Kölling, M., Scholz, D., Wei, W., Lohmann, G., and Scheffers, S., 2012, Mid- to late Holocene changes in tropical Atlantic temperature seasonality and interannual to multidecadal variability documented in southern Caribbean corals: *Earth and Planetary Science Letters*, v. 331–332, p. 187–200, doi: 10.1016/j.epsl.2012.03.019.

Glynn, P.W., 1997, Asessment of the present health of coral reefs in the Eastern Pacific, *in* Grigg, R.W. and Birkeland, C. eds., Status of Coral Reefs in the Pacific, UNIHI Sea Grant CP-98-01, p. 33–40.

Glynn, P.W., and Wellington, G.M., 1983, Corals and coral reefs of the Galápagos Islands: University of California Press, Berkeley and Los Angeles, 330 p.

Glynn, P.W., Wellington, G.M., and Birkeland, C., 1979, Coral reef growth in the Galapagos: Limitation by sea urchins: *Science*, v. 203, no. 14, p. 47–49.

Gonfiantini, R., Stichler, W., and Rozanski, K., 1995, Standards and intercomparison materials distributed by the International Atomic Energy Agency for stable isotope measurements, *in* Reference and intercomparison materials for stable isotopes of light elements, IAEA, Vienna, p. 13–29.

Goodwin, D.H., Flessa, K.W., Schöne, B.R., and Dettman, D.L., 2001, Cross-calibration of daily growth increments, stable isotope variation, and temperature in the Gulf of California bivalve mollusk *Chione cortezi*: Implications for paleoenvironmental analysis: *Palaios*, v. 16, p. 387–398, doi: 10.1669/0883-1351(2001)016.

Goodwin, D.H., Schöne, B.R., and Dettman, D.L., 2003, Resolution and fidelity of oxygen isotopes as paleotemperature proxies in bivalve mollusk shells: Models and observations: *Palaios*, v. 18, p. 110–125, doi: 10.1669/0883-1351(2003)182.0.CO;2.

Gordillo, S., Brey, T., Beyer, K., and Lomovasky, B.J., 2015, Climatic and environmental changes during the middle to late Holocene in southern South America: A sclerochronological approach using the bivalve *Retrotapes exalbidus* (Dillwyn) from the Beagle Channel: *Quaternary International*, v. 377, p. 83–90, doi: 10.1016/j.quaint.2014.12.036.

Gorzelak, P., and Salamon, M.A., 2013, Experimental tumbling of echinoderms - Taphonomic patterns and implications: *Palaeogeography, Palaeoclimatology, Palaeoecology*, v. 386, p. 569–574, doi: 10.1016/j.palaeo.2013.06.023.

Gorzelak, P., Stolarski, J., Małkowski, K., and Meibom, A., 2012, Stable carbon and oxygen isotope compositions of extant crinoidal echinoderm skeletons: *Chemical Geology*, v. 291, p. 132–140, doi: 10.1016/j.chemgeo.2011.10.014.

Goudswaard, P.C., Smaal, A.C., and Wagué, A., 2007, The Ecological implications of exploitation of the bivalve *Venus rosalina* in Mauritanian waters: Report C124B/07. Wareningen IMARES, Wageningen. 132 p.

Grauel, A.-L., 2012, Calibration of the “clumped isotope” thermometer on foraminifera and its application to high-resolution climate reconstruction of the past 2500yr in the Gulf of Taranto (Eastern Mediterranean Sea): PhD-Thesis, ETH Zürich,166 p.

Greenwood, P.J., 1980, Growth, respiration and tentative energy budgets for two populations of the sea urchin *Parechinus angulosus* (Leske): *Estuarine and Coastal Marine Science*, v. 10, no. 4, p. 347–367, doi: 10.1016/S0302-3524(80)80116-2.

Grossman, E.L., 2012, Applying oxygen isotope paleothermometry in deep time: *The Paleontological Society Papers*, v. 18, p. 39–67.

Grossman, E.L., and Ku, T.-L., 1986, Oxygen and carbon isotope fractionation in biogenic aragonite: Temperature effects: *Chemical Geology*, v. 59, p. 59–74, doi: 10.1016/0168-9622(86)90057-6.

Gulland, J.A., and Holt, S.J., 1957, Estimation of growth parameters for data at unequal time intervals: Journal de Conseil Conseil International pour l’Exploration de la Mer, no. 25, p. 3–5, doi: 10.1093/icesjms/25.1.47.

Gutierrez, E., and Morales-Nin, B., 1986, Time series analysis of daily growth in *Dicentrarchus labrax* L. otoliths*: Journal of Experimental Marine Biology and Ecology*, v. 103, no. 1–3, p. 163–179, doi: 10.1016/0022-0981(86)90139-5.

Hallmann, N., Schöne, B.R., Strom, A., and Fiebig, J., 2008, An intractable climate archive - sclerochronological and shell oxygen isotope analyses of the Pacific Geoduck, *Panopea abrupta* (bivalve mollusk) from Protection Island (Washington State, USA): *Palaeogeography, Palaeoclimatology, Palaeoecology*, v. 269, no. 1–2, p. 115–126, doi: 10.1016/j.palaeo.2008.08.010.

Hanebuth, T.J.J., and Henrich, R., 2009, Recurrent decadal-scale dust events over Holocene western Africa and their control on canyon turbidite activity (Mauritania): *Quaternary Science Reviews*, v. 28, no. 3–4, p. 261–270, doi: 10.1016/j.quascirev.2008.09.024.

Hanebuth, T.J.J., and Lantzsch, H., 2008, A Late Quaternary sedimentary shelf system under hyperarid conditions: Unravelling climatic, oceanographic and sea-level controls (Golfe d'Arguin, Mauritania, NW Africa): *Marine Geology*, v. 256, no. 1–4, p. 77–89, doi: 10.1016/j.margeo.2008.10.001.

Hardy, K., Camara, A., Piqué, R., Dioh, E., Guèye, M., Diadhiou, H.D., Faye, M., and Carré, M., 2016, Shellfishing and shell midden construction in the Saloum Delta, Senegal: *Journal of Anthropological Archaeology*, v. 41, p. 19–32, doi: 10.1016/j.jaa.2015.11.001.

Hastorf, C.A., and DeNiro, M.J., 1985, Reconstruction of prehistoric plant production and cooking practises by a new isotopic method: *Nature*, v. 315, p. 489–491.

Henderiks, J., and Bollmann, J., 2004, The *Gephyrocapsa* sea surface palaeothermometer put to the test: Comparison with alkenone and foraminifera proxies off NW Africa: *Marine Micropaleontology*, v. 50, no. 3–4, p. 161–184, doi: 10.1016/S0377-8398(03)00070-7.

Henkes, G. a., Passey, B.H., Wanamaker, A.D., Grossman, E.L., Ambrose, W.G., and Carroll, M.L., 2013, Carbonate clumped isotope compositions of modern marine mollusk and brachiopod shells: *Geochimica et Cosmochimica Acta*, v. 106, p. 307–325, doi: 10.1016/j.gca.2012.12.020.

Hildebrand, A.R., Penfield, G.T., Kring, D. a., Pilkington, M., Camargo Z., A., Jacobsen, S.B., and Boynton, W. V., 1991, Chicxulub Crater: A possible Cretaceous/Tertiary boundary impact crater on the Yucatán Peninsula, Mexico: *Geology*, v. 19, p. 867, doi: 10.1130/0091-7613(1991)019<0867:CCAPCT>2.3.CO;2.

Hobbs, J.A., Lewis, L.S., Ikemiyagi, N., Sommer, T., and Baxter, R.D., 2010, The use of otolith strontium isotopes ($^{87}Sr/^{86}Sr$) to identify nursery habitat for a threatened estuarine fish: *Environmental Biology of Fishes*, v. 89, no. 3, p. 557–569, doi: 10.1007/s10641-010-9672-3.

Høie, H., Andersson, C., Folkvord, A., and Karlsen, Ø., 2004, Precision and accuracy of stable isotope signals in otoliths of pen-reared cod (*Gadus morhua*) when sampled with a high-resolution micromill: *Marine Biology*, v. 144, no. 6, p. 1039–1049, doi: 10.1007/s00227-003-1275-5.

Høie, H., Folkvord, A., and Otterlei, E., 2003, Effect of somatic and otolith growth rate on stable isotopic composition of early juvenile cod (*Gadus morhua* L) otoliths: *Journal of Experimental Marine Biology and Ecology*, v. 289, no. 1, p. 41–58, doi: 10.1016/S0022-0981(03)00034-0.

Holcomb, M., Cohen, A.L., and Mccorkle, D.C., 2013, An evaluation of staining techniques for marking daily growth in scleractinian corals: *Journal of Experimental Marine Biology and Ecology*, v. 440, p. 126–131.

Holz, C., Stuut, J.-B.W., Henrich, R., and Meggers, H., 2007, Variability in terrigenous sedimentation processes off northwest Africa and its relation to climate changes: Inferences from grain-size distributions of a Holocene marine sediment record: *Sedimentary Geology*, v. 202, no. 3, p. 499–508, doi: 10.1016/j.sedgeo.2007.03.015.

Houvenaghel, G.T., 1978, Oceanographic conditions in the Galapagos archipelago and their relationships with life on the islands, *in* Upwelling Ecosystems, Springer Berlin Heidelberg, p. 181–200.

Humphreys, A.F., Halfar, J., Rivera, F., Manzello, D., Reymond, C.E., Westphal, H., and Riegl, B., 2016, Variable El Nino-Southern Oscillation influence on biofacies dynamics of eastern Pacific shallow-water carbonate systems: *Geology*, v. 44, no. 7, p. 571–574, doi: 10.1130/G37745.1.

Huntington, K.W., Budd, D. a., Wernicke, B.P., and Eiler, J.M., 2011, Use of clumped-isotope thermometry to constrain the crystallization temperature of diagenetic calcite: *Journal of Sedimentary Research*, v. 81, no. 9, p. 656–669, doi: 10.2110/jsr.2011.51.

Huntington, K.W., Eiler, J.M., Affek, H.P., Guo, W., Bonifacie, M., Yeung, L.Y., Thiagarajan, N., Passey, B., Tripati, A., Daëron, M., and Came, R., 2009, Methods and limitations of "clumped" CO_2 isotope (Δ_{47}) analysis by gas-source isotope ratiomass spectrometry: *Journal of Mass Spectrometry*, v. 44, no. 9, p. 1318–1329, doi: 10.1002/jms.1614.

Ingram, B.L., and Sloan, D., 1992, Strontium isotopic composition of estuarine sediments as paleosalinity-paleoclimate indicator.: *Science*, v. 255, p. 68–72, doi: 10.1126/science.255.5040.68.

Inoue, M., Suzuki, A., Nohara, M., Hibino, K., and Kawahata, H., 2007, Empirical assessment of coral Sr/Ca and Mg/Ca ratios as climate proxies using colonies grown at different temperatures: *Geophysical Research Letters*, v. 34, no. 12, p. 2–5, doi: 10.1029/2007GL029628.

Johnson, W.S., 1973, Respiration rates of some New Zealand echinoderms: *N.Z. J. Mar. Freshwater Res.*, v. 7, doi: 10.1080/00288330.1973.9515463.

Jones, K.B., Hodgins, G.W.L., Etayo-Cadavid, M.F., and Andrus, C.F.T., 2009, Upwelling signals in radiocarbon from early 20th-century Peruvian Bay Scallop (*Argopecten purpuratus*) shells: *Quaternary Research*, v. 72, no. 3, p. 452–456, doi: 10.1016/j.yqres.2009.07.008.

Kalish, J., 1991, ^{13}C and ^{18}O isotopic disequilibria in fish otoliths: Metabolic and kinetic effects: *Marine Ecology Progress Series*, v. 75, p. 191–203, doi: 10.3354/meps075191.

Kasemann, S.A., Schmidt, D.N., Bijma, J., and Foster, G.L., 2009, *In situ* boron isotope analysis in marine carbonates and its application for foraminifera and palaeo-pH: *Chemical Geology*, v. 260, no. 1–2, p. 138–147, doi: 10.1016/j.chemgeo.2008.12.015.

Kemp, D.B., and Sexton, P.F., 2014, Time-scale uncertainty of abrupt events in the geologic record arising from unsteady sedimentation: *Geology*, v. 42, no. 10, p. 891–894, doi: 10.1130/G35783.1.

Kidwell, Susan, M., and Baumiller, T.K., 1990, Experimental Disintegration of Regular Echinoids: Roles of Temperature, Oxygen, and Decay Thresholds: *Paleobiology*, v. 16, no. 3, p. 247–271.

Kim, J.-H., Meggers, H., Rimbu, N., Lohmann, G., Freudenthal, T., Müller, P.J., and Schneider, R.R., 2007, Impacts of the North Atlantic gyre circulation on Holocene climate off northwest Africa: *Geology*, v. 35, no. 5, p. 387, doi: 10.1130/G23251A.1.

Kim, S.-T., and O'Neil, J., 1997, Equilibrium and nonequilibrium oxygen isotope effects in synthetic carbonates: *Geochimica et Cosmochimica Acta*, v. 61, no. 16, p. 3461–3475, doi: 10.1016/S0016-7037(97)00169-5.

Klein, R.T., Lohmann, K.C., and Thayer, C.W., 1996, Bivalve skeletons record sea-surface temperature and $\delta^{18}O$ via Mg/Ca and $^{18}O/^{16}O$ ratios: *Geology*, v. 24, no. 5, p. 415–418, doi: 10.1130/0091-7613(1996)024<0415.

Klicpera, A., 2014, Carbonate secreting organisms in clastic shelf systems and their potential as environmental archive: PhD-thesis, University of Bremen, 199 p.

Klicpera, A., Michel, J., and Westphal, H., 2015, Facies patterns of a tropical heterozoan carbonate platform under eutrophic conditions: the Banc d'Arguin, Mauritania: *Facies*, doi: 10.1007/s10347-014-0421-5.

Knutson, D.W., Buddemeier, R.W., and Smith, S. V., 1972, Coral chronometers: Seasonal growth bands in reef corals: *Science*, v. 177, no. 4045, p. 270–272, doi: 10.1126/science.177.4045.270.

Kröpelin, S., Verschuren, D., Lézine, a-M., Eggermont, H., Cocquyt, C., Francus, P., Cazet, J.-P., Fagot, M., Rumes, B., Russell, J.M., Darius, F., Conley, D.J., Schuster, M., von Suchodoletz, H., et al., 2008, Climate-driven ecosystem succession in the Sahara: the past 6000 years: *Science*, v. 320, no. 5877, p. 765–8, doi: 10.1126/science.1154913.

Kuhlmann, H., Meggers, H., Freudenthal, T., and Wefer, G., 2004, The transition of the monsoonal and the N Atlantic climate system off NW Africa during the Holocene: *Geophysical Research Letters*, v. 31, no. 22, doi: 10.1029/2004GL021267.

Kutzbach, J.E., and Liu, Z., 1997, Response of the African monsoon to orbital forcing and ocean feedbacks in the middle Holocene: *Science*, v. 278, no. 5337, p. 440–443, doi: 10.1126/science.278.5337.440.

Lamb, H.F., Gasse, F., Benkaddour, A., El Hamouti, N., van der Kaars, S., Perkins, W.T., Pearce, N.J.G., and Roberts, C.N., 1995, Relation between century-scale Holocene arid intervals in tropical and temperate zones: *Nature*, v. 373, no. 12, p. 134–137.

Lamy, F., Arz, H.W., Bond, G.C., Bahr, A., and Pätzold, J., 2006, Multicentennial-scale hydrological changes in the Black Sea and northern Red Sea during the Holocene and the Arctic/North Atlantic Oscillation: *Paleoceanography*, v. 21, no. 1, p. 1–11, doi: 10.1029/2005PA001184.

Larsen, S.C., 2015, Recrystallization of biogenic aragonite shells from archaeological contexts and implications for paleoenvironmental reconstruction: MSc-thesis, Werstern Washington Uuniversity,103 p.

Lavaud, R., Thébault, J., Lorrain, A., van der Geest, M., and Chauvaud, L., 2013, *Senilia senilis* (Linnaeus, 1758), a biogenic archive of environmental conditions on the Banc d'Arguin (Mauritania): *Journal of Sea Research*, v. 76, p. 61–72, doi: 10.1016/j.seares.2012.11.003.

Lavigne, M., Hill, T.M., Sanford, E., Gaylord, B., Russell, A. D., Lenz, E. a., Hosfelt, J.D., and Young, M.K., 2013, The elemental composition of purple sea urchin (*Strongylocentrotus purpuratus*) calcite and potential effects of pCO_2 during early life stages: *Biogeosciences*, v. 10, no. 6, p. 3465–3477, doi: 10.5194/bg-10-3465-2013.

Lazareth, C.E., Vander Putten, E., André, L., and Dehairs, F., 2003, High-resolution trace element profiles in shells of the mangrove bivalve *Isognomon ephippium*: A record of environmental spatio-temporal variations? *Estuarine and Coastal and Shelf Science*, v. 57, no. 5–6, p. 1103–1114, doi: 10.1016/S0272-7714(03)00013-1.

Lear, C.H., Rosenthal, Y., and Slowey, N., 2002, Benthic foraminiferal Mg/Ca-paleothermometry: A revised core-top calibration: *Geochimica et Cosmochimica Acta*, v. 66, no. 19, p. 3375–3387, doi: 10.1016/S0016-7037(02)00941-9.

Liu, Z., Wang, Y., Gallimore, R., Gasse, F., Johnson, T., deMenocal, P., Adkins, J., Notaro, M., Prentice, I.C., Kutzbach, J., Jacob, R., Behling, P., Wang, L., and Ong, E., 2007, Simulating the transient evolution and abrupt change of Northern Africa atmosphere–ocean–terrestrial ecosystem in the Holocene: *Quaternary Science Reviews*, v. 26, no. 13–14, p. 1818–1837, doi: 10.1016/j.quascirev.2007.03.002.

Liu, Y., Xie, L., Morrison, J.M., Kamykowski, D., and Sweet, W. V., 2014, Ocean circulation and water mass characteristics around the Galápagos archipelago simulated by a multiscale nested ocean circulation model: *International Journal of Oceanography*, v. 2014, p. 1–16, doi: 10.1155/2014/198686.

López Correa, M., Montagna, P., Vendrell-Simón, B., McCulloch, M., and Taviani, M., 2010, Stable isotopes ($\delta^{18}O$ and $\delta^{13}C$), trace and minor element compositions of recent scleractinians and last glacial bivalves at the Santa Maria di Leuca deep-water coral province, Ionian Sea: *Deep Sea Research Part II: Topical Studies in Oceanography*, v. 57, no. 5–6, p. 471–486, doi: 10.1016/j.dsr2.2009.08.016.

Lorrain, A., Gillikin, D.P., Paulet, Y.M., Chauvaud, L., Le Mercier, A., Navez, J., and André, L., 2005, Strong kinetic effects on Sr/Ca ratios in the calcitic bivalve *Pecten maximus*: *Geology*, v. 33, no. 12, p. 965–968, doi: 10.1130/G22048.1.

Magdans, U., and Gies, H., 2004, Single crystal structure analysis of sea urchin spine calcites: Systematic investigations of the Ca/Mg distribution as a function of habitat of the sea urchin and the sample location in the spine: *European Journal of Mineralogy*, v. 16, no. 2, p. 261–268, doi: 10.1127/0935-1221/2004/0016-0261.

Maier, E., and Titschack, J., 2010, *Spondylus gaederopus*: A new mediterranean climate archive - based on high-resolution oxygen and carbon isotope analyses: *Palaeogeography, Palaeoclimatology, Palaeoecology*, v. 291, no. 3–4, p. 228–238, doi: 10.1016/j.palaeo.2010.02.032.

Makarewicz, C.A., and Sealy, J., 2015, Dietary reconstruction, mobility, and the analysis of ancient skeletal tissues: Expanding the prospects of stable isotope research in archaeology: *Journal of Archaeological Science*, v. 56, p. 146–158, doi: 10.1016/j.jas.2015.02.035.

Marceniuk, A.P., and Menezes, N.A., 2007, Systematics of the family Ariidae (Ostariophysi, Siluriformes), with a redefinition of the genera (Zootaxa 1416): Magnolia Press, Auckland,126 p.

Markel, K., Kubanek, F., and Willgallis, A., 1971, Polykristalliner Calcit bei Seeigel (Echinodermata: Echinoidea): Z Zellforsch, v. 119, p. 355–377.

Marshall, S.L., and Parker, S.S., 1982, Pattern identification in the microstructure of Sockeye salmon (*Oncorhynchus nerka*) otoliths: *Canadian Journal of Fisheries and Aquatic Sciences*, v. 39, no. 4, p. 542–547, doi: 10.1139/f82-077.

Martin, G.B., and Wuenschel, M.J., 2006, Effect of temperature and salinity on otolith element incorporation in juvenile gray snapper *Lutjanus griseus*: *Marine Ecology Progress Series*, v. 324, p. 229–239, doi: 10.3354/meps324229.

Martinez, P., Bertrand, P., Shimmield, G.B., Cochrane, K., Jorissen, J., Foster, J., and Dignan, M., 1999, Upwelling intensity and ocean productivity changes off Cape Blanc (northwest Africa) during the last 70 , 000 years : geochemical and micropalaeontological evidence: *Marine Geology*, v. 158, p. 57–74.

McConnaughey, T., 1989a, ^{13}C and ^{18}O isotopic disequilibrium in biological carbonates: I. Patterns: *Geochimica et Cosmochimica Acta*, v. 53, no. 1, p. 151–162, doi: 10.1016/0016-7037(89)90282-2.

McConnaughey, T., 1989b, ^{13}C and ^{18}O isotopic disequilibrium in biological carbonates: II. In vitro simulation of kinetic isotope effects: *Geochimica et Cosmochimica Acta*, v. 53, no. 1, p. 163–171, doi: 10.1016/0016-7037(89)90283-4.

McGee, D., deMenocal, P.B., Winckler, G., Stuut, J.B.W., and Bradtmiller, L.I., 2013, The magnitude, timing and abruptness of changes in North African dust deposition over the last 20,000 yr: *Earth and Planetary Science Letters*, v. 371–372, p. 163–176, doi: 10.1016/j.epsl.2013.03.054.

McGurk, M.D., 1984, Ring deposition in the otoliths of larval Pacific Herring, *Clupea harengus pallasi*: *Fishery Bulletin*, v. 82, no. 1, p. 113–120.

McNiven, I.J., and Wright, D., 2008, Ritualized marine midden formation in western Zenadh Kes (Torres Strait), *in* Clark, G. and O'Connor, S. eds., Terra Australis 29; Islands of inquiry: Colonisation, seafaring and the archaeology of maritime landscapes, ANU E Press, Canberra, 510 p.

McPherson, 1968, Feeding and oxygen uptake of the tropical sea urchin *Eucidaris tribuloides* (Lamarck): *Biological Bulletin*, v. 135, no. 2, p. 308–321.

Michel, J., Vicens, G.M., and Westphal, H., 2011, Modern heterozoan carbonates from a eutrophic tropical shelf (Mauritania): *Journal of Sedimentary Research*, v. 81, p. 641–655, doi: 10.2110/jsr.2011.53.

Michel, J., Westphal, H., and Hanebuth, T.J.J., 2009, Sediment partitioning and winnowing in a mixed eolian-marine system (Mauritanian shelf): *Geo-Marine Letters*, v. 29, no. 4, p. 221–232, doi: 10.1007/s00367-009-0136-8.

Milano, S., Prendergast, A.L., and Schöne, B.R., 2016, Effects of cooking on mollusk shell structure and chemistry: Implications for archeology and paleoenvironmental reconstruction: *Journal of Archaeological Science*: Reports, v. 7, p. 14–26, doi: 10.1016/j.jasrep.2016.03.045.

Mitsuguchi, T., Matsumoto, E., and Uchida, T., 2003, Mg/Ca and Sr/Ca ratios of Porites coral skeleton: Evaluation of the effect of skeletal growth rate: *Coral Reefs*, v. 22, no. 4, p. 381–388, doi: 10.1007/s00338-003-0326-1.

Mittelstaedt, E., 1991, The ocean boundary along the northwest African coast: Circulation and oceanographic properties at the sea surface: *Progress in Oceanography*, v. 26, p. 307–355.

Mosegaard, H., Svedäng, H., and Taberman, K., 1988, Uncoupling of somatic and otolith growth rates in Arctic Char (*Salvelinus alpinus*) as an effect of differences in temperature response: *Canadian Journal of Fisheries and Aquatic Sciences*, v. 45, no. 9, p. 1514–1524, doi: 10.1139/f88-180.

Moureaux, C., Pérez-Huerta, A., Compère, P., Zhu, W., Leloup, T., Cusack, M., and Dubois, P., 2010, Structure, composition and mechanical relations to function in sea urchin spine: *Journal of Structural Biology*, v. 170, no. 1, p. 41–49, doi: 10.1016/j.jsb.2010.01.003.

Müller P., Wu, H.C., Barusseau, J.-P., Vernet, R., and Westphal, H. , in prep., Otolith and bivalve isotope records of monsoon precipitation discharge during the mid- to late-Holocene of NW Africa: in preperation for submission to *Geology*.

Müller P., Sraudigel, P.T., Murray, S.T., Vernet, R., Barusseau, J.-P., Westphal, H., and Swart, P.K., under revision, Prehistoric cooking versus paleoclimate proxies in shell-midden constituents: Under revision for resubmission to *Nature Scientific Reports*.

Müller, P., Reymond, C.E., Siegel, P., and Westphal, H., in press, Paleoenvironmental proxies in echinoid spines (*Eucidaris galapagensis*, Döderlein 1887) along a natural water temperature gradient: in press in *Palaeogeography, Palaeoclimatology, Palaeoecology*, doi: 10.1016/j.palaeo.2016.06.024.

Müller, P., Taylor, M.H., Klicpera, A., Wu, H.C., Michel, J., and Westphal, H., 2015a, Food for thought : Mathematical approaches for the conversion of high-resolution sclerochronological oxygen isotope records into sub-annually resolved time series: *Palaeogeography, Palaeoclimatology, Palaeoecology*, v. 440, p. 763–776, doi: 10.1016/j.palaeo.2015.09.032.

Müller, P., Taylor, M.H., Klicpera, A., Wu, H.C., Michel, J., and Westphal, H., 2015b, Supplemental Files: Foods for thought: Mathematical approaches for the conversion of high resolution sclerochronological oxygen isotope records into sub-annually resolved time series: Supplemental Material, doi: 10.6084/m9.figshare.1534694 figshare.

Munro, J.; Pauly, D., 1983, A simple method for comparing the growth of fishes and invertebrates: *Fishbyte*, v. 1, no. 1, p. 5–6.

Murray, S.T., Arienzo, M.M., and Swart, P.K., 2016, Determining the Δ_{47} acid fractionation in dolomites: *Geochimica et Cosmochimica Acta*, v. 174, no. October, p. 42–53, doi: 10.1016/j.gca.2015.10.029.

Nasreddine, K., Benzinou, A., Parisi-Baradad, V., and Fablet, R., 2009, Variational 1D signal registration and shape geodesics for shape classification: Application to marine biological archives, *in* DSP 2009: 16th International Conference on Digital Signal Processing, Proceedings, p. 1–6.

Ndomahina, E.T., 1975, Studies on the habitat, age and growth of the cockle *Senilis* (=*Arca*) *senilis* (L.): BSc-thesis, University of Sierra Leone, 72 p.

Okera, W., 1976, Observations on some population parameters of exploited stocks of *Senilia senilis* (=*Arca senilis*) in Sierra Leone: *Marine Biology*, v. 38, no. 3, p. 217–229, doi: 10.1007/BF00388935.

Paillard, D., Labeyrie, L., and Yiou, P., 1996, Macintosh program performs time-series analysis: Eos, *Transactions American Geophysical Union*, v. 77, no. 39, p. 379, doi: 10.1029/96EO00259.

Pannella, G., 1971, Fish otoliths: daily growth layers and periodical patterns.: *Science*, v. 173, no. 4002, p. 1124–7.

Passey, B.H., and Henkes, G. a., 2012, Carbonate clumped isotope bond reordering and geospeedometry: *Earth and Planetary Science Letters*, v. 351–352, p. 223–236, doi: 10.1016/j.epsl.2012.07.021.

Patterson, W.P., Smith, G.R., and Lohmann, K.C., 1993, Continental paleothermometry and seasonality using the isotopic composition of aragoniteic otoliths of freshwater fishes: *Geophysical Monograph*, v. 78, p. 191–202, doi: 10.1029/GM078p0191.

Pauly, D., and Munro, J.L., 1984, Once more on the comparison of growth in fish and invertebrates: *Fishbyte*, v. 2, p. 21.

Pausata, F.S.R., Messori, G., and Zhang, Q., 2016, Impacts of dust reduction on the northward expansion of the African monsoon during the Green Sahara period: *Earth and Planetary Science Letters*, v. 434, p. 298–307, doi: 10.1016/j.epsl.2015.11.049.

Pelejero, C., Calvo, E., McCulloch, M.T., Marshall, J.F., Gagan, M.K., Lough, J.M., and Opdyke, B.N., 2005, Preindustrial to modern interdecadal variability in coral reef pH: *Science*, v. 309, p. 2204–2207, doi: 10.1126/science.1113692.

Petersen, S. V., and Schrag, D.P., 2014, Clumped isotope measurements of small carbonate samples using a high-efficiency dual-reservoir technique: *Rapid Communications in Mass Spectrometry*, v. 28, no. 21, p. 2371–2381, doi: 10.1002/rcm.7022.

Philippsen, B., 2012, Variability of freshwater reservoir effects: PhD thesis, Aarhus University, 189 p.

Piasecki, A., 2015, Site-specific isotopes in small organic molecules: PhD-thesis, California Institue of Technology, Pasadena, CA, USA, 157 p.

Pörtner, H.O., Berdal, B., Blust, R., Brix, O., Colosimo, A., De Wachter, B., Giuliani, A., Johansen, T., Fischer, T., Knust, R., Lannig, G., Naevdal, G., Nedenes, A., Nyhammer, G., et al., 2001, Climate induced temperature effects on growth performance, fecundity and recruitment in marine fish: Developing a hypothesis for cause and effect relationships in Atlantic cod (*Gadus morhua*) and common eelpout (*Zoarces viviparus*): *Continental Shelf Research*, v. 21, no. 18–19, p. 1975–1997, doi: 10.1016/S0278-4343(01)00038-3.

Poulain, C., Gillikin, D.P., Thébault, J., Munaron, J.M., Bohn, M., Robert, R., Paulet, Y.-M., and Lorrain, A., 2015, An evaluation of Mg/Ca, Sr/Ca, and Ba/Ca ratios as environmental proxies in aragonite bivalve shells: *Chemical Geology*, v. 396, p. 42–50, doi: 10.1016/j.chemgeo.2014.12.019.

Putten, E. Vander, Dehairs, F., Keppens, E., and Baeyens, W., 2000, High resolution distribution of trace elements in the calcite shell layer of modern *Mytilus edulis*: Environmental and biological controls: *Geochimica et Cosmochimica Acta*, v. 64, no. 6, p. 997–1011, doi: 10.1016/S0016-7037(99)00380-4.

Quack, B., Peeken, I., Petrick, G., and Nachtigall, K., 2007, Oceanic distribution and sources of bromoform and dibromomethane in the Mauritanian upwelling: *Journal of Geophysical Research: Oceans*, v. 112, no. 10, doi: 10.1029/2006JC003803.

Rachmayani, R., Prange, M., and Schulz, M., 2015, North African vegetation – precipitation feedback in early and mid-Holocene climate simulations with CCSM3-DGVM: *Climate of the Past*, v. 11, p. 175–185, doi: 10.5194/cp-11-175-2015.

R Development Core Team, 2013, R: A language and environment for statistical computing: R Foundation for Statistical Computing Vienna Austria,.

Reimer, P.J., Bard, E., Bayliss, A., Beck, J.W., Blackwell, P.G., Bronk, C., Caitlin, R., Hai, E.B., and Edwards, R.L., 2013, Intcal13 and Marine13 radiocarbon age calibration curves 0 – 50,000 years cal BP: *Radiocarbon*, v. 55, no. 4, p. 1869–1887.

Renssen, H., Brovkin, V., Fichefet, T., and Goosse, H., 2006, Simulation of the Holocene climate evolution in Northern Africa: The termination of the African Humid Period: *Quaternary International*, v. 150, no. 1, p. 95–102, doi: 10.1016/j.quaint.2005.01.001.

Reymond, C.E., Zihrul, K., Halfar, J., Riegl, B., Humphreys, A., and Westphal, H., 2015, Heterozoan carbonates from the equatorial rocky reefs of the Galápagos Archipelago: *Sedimentology*, doi: 10.1111/sed.12244.

Reynolds, R.W., Rayner, N. a., Smith, T.M., Stokes, D.C., and Wang, W., 2002, An improved in situ and satellite SST analysis for climate: *Journal of Climate*, v. 15, p. 1609–1625, doi: 10.1175/1520-0442(2002)015<1609:AIISAS>2.0.CO;2.

Reynolds, R.W., Smith, T.M., Liu, C., Chelton, D.B., Casey, K.S., and Schlax, M.G., 2007, Daily high-resolution-blended analyses for sea surface temperature: *Journal of Climate*, v. 20, no. 1994, p. 5473–5496, doi: 10.1175/2007JCLI1824.1.

Richards, F.J., 1959, A flexible growth function for empirical use: *Journal of Experimental Botany*, v. 10, no. 29, p. 290–300, doi: 10.1093/jxb/10.2.290.

Richards, M.P., and Hedges, R.E.M., 1999, Stable isotope evidence for similarities in the types of marine foods used by Late Mesolithic humans at sites along the Atlantic coast of Europe: *Journal of Archaeological Science*, v. 26, no. 6, p. 717–722, doi: 10.1006/jasc.1998.0387.

Richards, M.P., Jacobi, R., Cook, J., Pettitt, P.B., and Stringer, C.B., 2005, Isotope evidence for the intensive use of marine foods by Late Upper Palaeolithic humans: *Journal of Human Evolution*, v. 49, no. 3, p. 390–394, doi: 10.1016/j.jhevol.2005.05.002.

Richter, D., and Bruckschen, P., 1998, Geochemistry of recent tests of *Echinocyamus pusillus*: Constraints for temperature and salinity: *Carbonates and Evaporites*, v. 13, no. 2, p. 157–167, doi: 10.1007/BF03176589.

Ries, J.B., 2004, Effect of ambient Mg/Ca ratio on Mg fractionation in calcareous marine invertebrates: A record of the oceanic Mg/Ca ratio over the Phanerozoic: *Geology*, v. 32, no. 11, p. 981–984, doi: 10.1130/G20851.1.

Ritchie, J.C., Eyles, C.H., and Haynes, C.V., 1985, Sediment and pollen evidence for an early to mid-Holocene humid period in the eastern Sahara: *Nature*, v. 314, p. 352–355.

Roberts, N., 2014, The Holocene - An Environmental History: 3rd Edition, Wiley-Blackwell, Oxfrod, 376 p.

Sadler, P.M., 1981, Sediment accumulation rates and the completeness of stratigraphic sections: *The Journal of Geology*, v. 89, no. 5, p. 569–584.

Sakamoto, C.M., Millero, F.J., Yao, W., Friederich, G.E., and Chavez, F.P., 1998, Surface seawater distributions of inorganic carbon and nutrients around the Galapagos Islands: results from the PlumEx experiment using automated chemical mapping: *Deep Sea Research Part II: Topical Studies in Oceanography*, v. 45, no. 6, p. 1055–1071, doi: 10.1016/S0967-0645(98)00013-7.

Santrock, J., Studley, S.A., and Hayes, J.M., 1985, Isotopic analyses based on the mass spectrum of carbon dioxide.: *Analytical Chemistry*, v. 57, no. 12, p. 1444–1448, doi: 10.1021/ac00284a060.

Savin, S.M., 1982, Stable isotopes in climatic reconstructions: *Climate in Earth History: Studies in Geophysics*, p. 164–171.

Schauble, E.A., Ghosh, P., and Eiler, J.M., 2006, Preferential formation of ^{13}C–^{18}O bonds in carbonate minerals, estimated using first-principles lattice dynamics: *Geochimica et Cosmochimica Acta*, v. 70, no. 10, p. 2510–2529, doi: 10.1016/j.gca.2006.02.011.

Schauer, A.J., Kelson, J., Saenger, C., and Huntington, K.W., 2016, Choice of ^{17}O correction affects clumped isotope (Δ_{47}) values of CO_2 measured with mass spectrometry: *Rapid Communications in Mass Spectrometry*, doi: 10.1002/rcm.7743.

Schmid, T.W., and Bernasconi, S.M., 2010, An automated method for "clumped-isotope" measurements on small carbonate samples: *Rapid Communications in Mass Spectrometry*, v. 24, p. 1955–1963, doi: 10.1002/rcm.

Schneider, W., 1990, Field guide to the commercial marine ressources of the Gulf of Guinea: FAO species identification sheets for fisheries purposes, FAO Regional Office for Africa, Rome, FAO, 268 p.

Schöne, B.R., Dunca, E., Fiebig, J., and Pfeiffer, M., 2005a, Mutvei's solution: An ideal agent for resolving microgrowth structures of biogenic carbonates: *Palaeogeography, Palaeoclimatology, Palaeoecology*, v. 228, p. 149–166, doi: 10.1016/j.palaeo.2005.03.054.

Schöne, B.R., Fiebig, J., Pfeiffer, M., Gleß, R., Hickson, J., Johnson, A.L. a, Dreyer, W., and Oschmann, W., 2005b, Climate records from a bivalved Methuselah (*Arctica islandica*, Mollusca; Iceland): *Palaeogeography, Palaeoclimatology, Palaeoecology*, v. 228, p. 130–148, doi: 10.1016/j.palaeo.2005.03.049.

Schöne, B.R., Freyre Castro, A.D., Fiebig, J., Houk, S.D., Oschmann, W., and Kröncke, I., 2004, Sea surface water temperatures over the period 1884-1983 reconstructed from oxygen isotope ratios of a bivalve mollusk shell (*Arctica islandica*, southern North Sea): *Palaeogeography, Palaeoclimatology, Palaeoecology*, v. 212, no. 3–4, p. 215–232, doi: 10.1016/j.palaeo.2004.05.024.

Schöne, B.R., and Gillikin, D.P., 2013, Unraveling environmental histories from skeletal diaries - advances in sclerochronology: *Palaeogeography, Palaeoclimatology, Palaeoecology*, v. 373, p. 1–5, doi: 10.1016/j.palaeo.2012.11.026.

Schöne, B.R., Tanabe, K., Dettman, D.L., and Sato, S., 2003, Environmental controls on shell growth rates and $\delta^{18}O$ of the shallow-marine bivalve mollusk *Phacosoma japonicum* in Japan: *Marine Biology*, v. 142, p. 473–485, doi: 10.1007/s00227-002-0970-y.

Schroeder, J.H., Dwornik, E.J., and Lindsay, J.R., 1968, Compositional and crystallographic aspects of the echinoid skeleton [abs.]: Trans. Geophys. Union, v. 49, p. 2019.

Secor, D.H., and Dean, J.M., 1989, Somatic growth effects on the otolith - fish size relationship in young pond-reared Striped Bass, *Morone saxatilis*: *Canadian Journal of Fisheries and Aquatic Sciences*, v. 46, p. 113–121, doi: 10.1139/f89-015.

Sevrin-Reyssac, J., 1993, Hydrology and underwater climate of the Banc d'Arguin, Mauritania: A review: *Hydrobiologia*, v. 258, p. 1–8, doi: 10.1007/978-94-011-1986-3_1.

Skonieczny, C., Paillou, P., Bory, A., Bayon, G., Biscara, L., Crosta, X., Eynaud, F., Malaizé, B., Revel, M., Aleman, N., Barusseau, J.-P., Vernet, R., Lopez, S., and Grousset, F., 2015, African humid periods triggered the reactivation of a large river system in Western Sahara: *Nature Communications*, v. 6, p. 8751, doi: 10.1038/ncomms9751.

Somers, I.F., 1988, On a seasonally oscillating growth function: *Fishbyte*, v. 6, p. 8–11.

Staudigel, P.T., and Swart, P.K., 2016, Isotopic behavior during the aragonite-calcite transition: Implications for sample preparation and proxy interpretation: *Chemical Geology*, v. 442, no. 2012, p. 130–138, doi: 10.1016/j.chemgeo.2016.09.013.

Stern-Pirlot, A., and Wolff, M., 2006, Population dynamics and fisheries potential of *Anadara tuberculosa* (Bivalvia : Arcidae) along the Pacific coast of Costa Rica: *Revista De Biologia Tropical*, v. 54, p. 87–100.

Stolper, D.A., and Eiler, J.M., 2015, The kinetics of solid-state isotope-exchange reactions for clumped isotopes: A study of inorganic calcites and apatites from natural and experimental samples: American Journal of Science, v. 315, no. 5, p. 363–411, doi: 10.2475/05.2015.01.

Surge, D., Kelly, G., Arnold, W.S., Geiger, S.P., Goewert, a. E., and Walker, K.J., 2008, Isotope sclerochronology of *Mercenaria mercenaria*, *M. Campechiensis*, and their natural hybrid form: Does genotype matter? *Palaios*, v. 23, no. 8, p. 559–565, doi: 10.2110/palo.2007.p07-056r.

Surge, D., Lohmann, K.C., and Dettman, D.L., 2001, Controls on isotopic chemistry of the American oyster, *Crassostrea virginica*: Implications for growth patterns: *Palaeogeography, Palaeoclimatology, Palaeoecology*, v. 172, no. 3–4, p. 283–296, doi: 10.1016/S0031-0182(01)00303-0.

Surge, D., and Walker, K.J., 2005, Oxygen isotope composition of modern and archaeological otoliths from the estuarine hardhead catfish (*Ariopsis felis*) and their potential to record low-latitude climate change: *Palaeogeography, Palaeoclimatology, Palaeoecology*, v. 228, no. 1–2, p. 179–191, doi: 10.1016/j.palaeo.2005.03.051.

Swart, P.K., 1983, Carbon and oxygen isotope fractionation in scleractinian corals: A review: *Earth-Science Reviews*, v. 19, no. 1, p. 51–80, doi: 10.1016/0012-8252(83)90076-4.

Swart, P.K., Burns, S.J., and Leder, J.J., 1991, Fractionation of the stable isotopes of oxygen and carbon in carbon dioxide during the reaction of calcite with phosphoric acid as a function of temperature and technique: *Chemical Geology*, v. 86, no. 2, p. 89–96, doi: 10.1016/0168-9622(91)90055-2.

Swisher, C.C., Grajales-Nishimura, J.M., Montanari, A., Margolis, S. V., Claeys, P., Alvarez, W., Renne, P., Cedillo-Pardoa, E., Maurrasse, F.J.-M.R., Curtis, G.H., Smit, J., and McWilliams, M.O., 1992, Coeval $^{40}Ar/^{39}Ar$ ages of 65.0 million years ago from Chicxulub crater melt rock and Cretaceous-Tertiary boundary tektites: *Science*, v. 257, no. 5072, p. 954–958, doi: 10.1126/science.257.5072.954.

Tanaka, M., 1982, A new growth curve which expresses infinitive increase: *Publ. Amakusa Mar. Biol. Lab.*, v. 6, no. 2, p. 167–177.

Tanaka, M., 1988, Eco-physiological meaning of parametres of ALOG growth curve: *Publ. Amakusa Mar. Biol. Lab.*, v. 9, no. 2, p. 103–106.

Taylor, W.R., 1986, Ariidae, *in* Daget, A.J., Gosse, J.-P., and Thys van den Audenaerde, D.F.E. eds., Checkl-List of the freshwater fishes of Africa (CLOFFA), ORSTOM, Paris, p. 153–159.

Thomas, K.D., 2015a, Molluscs emergent, Part I: Themes and trends in the scientific investigation of mollusc shells as resources for archaeological research: *Journal of Archaeological Science*, v. 56, p. 133–140, doi: 10.1016/j.jas.2015.01.024.

Thomas, K.D., 2015b, Molluscs emergent, part II: Themes and trends in the scientific investigation of molluscs and their shells as past human resources: *Journal of Archaeological Science*, v. 56, p. 159–167, doi: 10.1016/j.jas.2015.01.015.

Thompson, V.D., and Andrus, C.F.T., 2016, Evaluating mobility, monumentality, and feasting at the Sapelo Island shell ring complex: *American Antiquity*, v. 76, no. 2, p. 315–343.

Thompson, L.G., Mosley-thompson, E., Davis, M.E., Henderson, K.A., Brecher, H.H., Zagorodnov, V.S., Mashiotta, T.A., Lin, P., Mikhalenko, V.N., Hardy, D.R., and Beer, J., 2002, Kilimanjaro ice core records: Evidence of Holocene climate change in tropical Africa: *Science*, v. 298, p. 589–593.

Thompson, J.R., Petsios, E., Davidson, E.H., Erkenbrack, E.M., Gao, F., and Bottjer, D.J., 2015, Reorganization of sea urchin gene regulatory networks at least 268 million years ago as revealed by oldest fossil cidaroid echinoid.: *Scientific reports*, v. 5, no. October, p. 15541, doi: 10.1038/srep15541.

Thorrold, S.R., Campana, S.E., Jones, C.M., and Swart, P.K., 1997, Factors determining $\delta^{13}C$ and $\delta^{18}O$ fractionation in aragonitic otoliths of marine fish: *Geochimica et Cosmochimica Acta*, v. 61, no. 14, p. 2909–2919, doi: 10.1016/S0016-7037(97)00141-5.

Tobin, T.S., Wilson, G.P., Eiler, J.M., and Hartman, J.H., 2014, Environmental change across a terrestrial Cretaceous-Paleogene boundary section in eastern Montana, USA, constrained by carbonate clumped isotope paleothermometry: *Geology*, v. 42, no. 4, p. 351–354, doi: 10.1130/G35262.1.

Urey, H.C., 1947, The thermodynumic properties of isotopic substances: *Journal of the Chemical Society*, p. 562–581.

Vakily, J.M., 1992, Determination and comparison of bivalve growth, with emphasis on Thailand and other tropical areas: ICLARM Technical Reports 36, p. 1–121, doi: 10.1007/s13398-014-0173-7.2.

Vanhove, D., Stassen, P., Speijer, R.P., Claeys, P., and Steurbaut, E., 2012, Intra- and intertaxon stable O and C isotope variability of fossil fish otoliths : an early Eocene test case: *Austrian Journal of Earth Sciences*, v. 105/1, p. 200–207.

Vernet, R., 2007, Le golfe d´Arguin de la préhistoire à l'histoire - Littoral et plaines intérieures: Collection PNBA, n 3, Noualchott, 199 p.

Vernet, R., and Tous, P., 2004, Les amas coquilliers de Mauritanie occidentale et leur contexte paléoenvironnemental (VIIe-IIe millénaires BP): *Préhistoire Anthropologie Méditerranéennes*, v. 13, p. 55–69.

Versteegh, E.A.A., Blicher, M.E., Mortensen, J., Rysgaard, S., Als, T.D., and Wanamaker, A.D., 2012, Oxygen isotope ratios in the shell of *Mytilus edulis*: Archives of glacier meltwater in Greenland? *Biogeosciences*, v. 9, no. 12, p. 5231–5241, doi: 10.5194/bg-9-5231-2012.

de Villiers, S., Nelson, B.K., and Chivas, a R., 1995, Biological controls on coral Sr/Ca and $\delta^{18}O$ reconstructions of sea surface temperatures: *Science*, v. 269, no. 5228, p. 1247–1249, doi: 10.1126/science.269.5228.1247.

de Vries, M.C., Gillanders, B.M., and Elsdon, T.S., 2005, Facilitation of barium uptake into fish otoliths: Influence of strontium concentration and salinity: *Geochimica et Cosmochimica Acta*, v. 69, no. 16, p. 4061–4072, doi: 10.1016/j.gca.2005.03.052.

Wacker, U., Fiebig, J., and Schoene, B.R., 2013, Clumped isotope analysis of carbonates: Comparison of two different acid digestion techniques.: *Rapid communications in mass spectrometry*, v. 27, no. 14, p. 1631–42, doi: 10.1002/rcm.6609.

Walker, K.J., and Surge, D., 2006, Developing oxygen isotope proxies from archaeological sources for the study of Late Holocene human-climate interactions in coastal southwest Florida: *Quaternary International*, v. 150, no. 1, p. 3–11, doi: 10.1016/j.quaint.2006.01.022.

Walther, B.D.D., and Rowley, J.L.L., 2013, Drought and flood signals in subtropical estuaries recorded by stable isotope ratios in bivalve shells: *Estuarine and Coastal and Shelf Science*, v. 133, p. 235–243, doi: 10.1016/j.ecss.2013.08.032.

Wang, T., Surge, D., and Walker, K.J., 2013, Seasonal climate change across the Roman Warm Period/Vandal Minimum Transition using isotope sclerochronology in archaeological shells and otoliths, Southwest Florida, USA: *Quaternary International*, v. 308–309, p. 230–241, doi: 10.1016/j.quaint.2012.11.013.

Warburton, K., 1978, Age and growth determination in a marine catfish using an otolith check technique: *Journal of Fish Biology*, v. 13, p. 429–434, doi: 10.1111/j.1095-8649.1978.tb03451.x.

Wardecki, D., Przeniosło, R., and Brunelli, M., 2008, Internal pressure in annealed biogenic aragonite: *The Royal Society of Chemistry*, v. 10, p. 1450–1453, doi: 10.1039/b805508d.

Waselkov, G.A., 1987, Shellfish gathering and shell midden archaeology: *Advances in Archaeological Method and Therory*, v. 10, p. 93–210.

Weber, J.N., 1968, Isotopes of carbon and oxygen in calcareous marine invertebrates - the Asteroidea, Ophiuroidea and Crinoidea: *Geochemica et Cosmochimica Acta*, v. 32, p. 33–70, doi: 10.1016/0016-7037(68)90087-2.

Weber, J.N., 1973, Temperature dependence of magnesium in Echinoid and Asteroid skeletal calcite: A reinterpretation of its significance: *The Journal of Geology*, v. 81, no. 5, p. 543–556.

Weber, J.N., and Raup, D.M., 1966, Fractionation of the stable isotopes of carbon and oxygen in marine calcareous organisms-the Echinoidea. Part I. Environmental and genetic Factors: *Geochemica et Cosmochemica Acta*, v. 30, p. 681–703, doi: 10.1016/0016-7037(66)90097-4.

Wefer, G., Berger, W.H., Bijma, J., and Fischer, G., 1999, Clues to Ocean History: a Brief Overview of Proxies, *in* Fischer, G. and Wefer, G. eds., Use of Proxies in Paleoceanography, Springer Berlin Heidelberg, Berlin, Heidelberg, p. 1–68.

Wei, G., Sun, M., Li, X., and Nie, B., 2000, Mg/Ca, Sr/Ca and U/Ca ratios of a porites coral from Sanya Bay, Hainan Island, South China Sea and their relationships to sea surface temperature: *Palaeogeography, Palaeoclimatology, Palaeoecology*, v. 162, no. 1–2, p. 59–74, doi: 10.1016/S0031-0182(00)00105-X.

Weldeab, S., Lea, D.W., Schneider, R.R., and Andersen, N., 2007, 155,000 years of West African monsoon and ocean thermal evolution: *Science*, v. 316, no. 5829, p. 1303–7, doi: 10.1126/science.1140461.

Wellington, G.M., Dunbar, R.B., and Merlen, G., 1996, Calibration of stable oxygen iostope signatures in Galapagos corals: *Paleoceanography*, v. 11, no. 4, p. 467–480, doi: 10.1029/96PA01023.

Welsh, K., Elliot, M., Tudhope, A., Ayling, B., and Chappell, J., 2011, Giant bivalves (*Tridacna gigas*) as recorders of ENSO variability: *Earth and Planetary Science Letters*, v. 307, no. 3–4, p. 266–270, doi: 10.1016/j.epsl.2011.05.032.

Westphal, H., Beuck, L., Braun, S., Freiwald, A., Hanebuth, T.J.J., Hetzinger, S., Klicpera, A., Kudrass, H.R., Lantzsch, H., Lundälv, T., Vicens, G.M., Preto, N., Reumont, J. v., Schilling, S., et al., 2014, Phaeton - paleoceanographic and paleo-climatic record on the Mauritanian shelf - Cruise No. MSM 16/3 - October 13 - November 20, 2010 - Bremerhaven (Germany) - Mindelo (Cap Verde). MARIA S. MERIAN-Berichte, MSM 13/3. 57 p. doi:10.2312/cr_msm16_3

Westphal, H., Halfar, J., and Freiwald, A., 2010, Heterozoan carbonates in subtropical to tropical settings in the present and past: *International Journal of Earth Sciences*, v. 99, no. S1, p. 153–169, doi: 10.1007/s00531-010-0563-9.

Winsor, C.P., 1932, The Gompertz curve as a growth curve.: *Proceedings of the National Academy of Sciences*, v. 18, no. 1, p. 1–8, doi: 10.1073/pnas.18.1.1.

Wolff, W.J., Gueye, A., Meijboom, A., Piersma, T., and Alassane Sall, M., 1987, Distribution, biomass, recruitment and productivity of *Anadara senilis* (L.) (Mollusca: Bivalvia) on the Banc d`Arguin, Mauritania: *Netherlands Journal of Sea Research*, v. 21, no. 3, p. 243–253.

Yáñez-Arancibia, A., and Lara-Domínguez, A.L., 1988, Ecology of three sea catfishes (Ariidae) in s tropical coastal ecosystem - southern Gulf of Mexico: *Marine Ecology Progress Series*, v. 49, p. 215–230, doi: doi:10.3354/meps049215.

Yu, J., and Elderfield, H., 2008, Mg/Ca in the benthic foraminifera *Cibicidoides wuellerstorfi* and *Cibicidoides mundulus*: Temperature versus carbonate ion saturation: *Earth and Planetary Science Letters*, v. 276, p. 129–139, doi: 10.1016/j.epsl.2008.09.015.

Zhao, M., Haslett, S.K., Jordan, R.W., Sarnthein, M., and Zhang, Z., 2000, Marine and terrestrial biomarker records for the last 35 , 000 years at ODP site 658C off NW Africa: *Organic Geochemistry*, v. 31, p. 919-930.

Zühlsdorff, C., Hanebuth, T.J.J., and Henrich, R., 2008, Persistent quasi-periodic turbidite activity off Saharan Africa and its comparability to orbital and climate cyclicities: *Geo-Marine Letters*, v. 28, no. 2, p. 87–95, doi: 10.1007/s00367-007-0092-0.